EMPIRICAL CORRELATIONS FOR TEMPERATURE, AND OUTPUT POWER OF PHOTOVOLTAIC PANEL UNDER DIFFERENT COOLING CONDITIONS USING POROUS MEDIA

By

ALMASALEHA ISMAIL KHALEEL MOHAMMAD

Thesis Submitted to the School of Graduate Studies, Universiti Putra Malaysia, in Fulfilment of the Requirements for the Degree of Doctorate of Philosophy

January 2024

FK 2024 13

Abstract of thesis presented to the Senate of Universiti Putra Malaysia in fulfillment of the requirement for the degree of Doctor of Philosophy

EMPIRICAL CORRELATIONS FOR TEMPERATURE, AND OUTPUT POWER OF PHOTOVOLTAIC PANEL UNDER DIFFERENT COOLING CONDITIONS USING POROUS MEDIA

By

ALMASALEHA ISMAIL KHALEEL MOHAMMAD

January 2024

Chairman : Siti Ujila binti Masuri, PhD
Faculty : Engineering

Fossil fuels have traditionally been central to global energy generation. However, the depletion of these resources has urged the need for renewable alternatives. This challenge has driven the use of photovoltaics (PV) for electrical energy generation. However, when PV panels are used, their temperature rises, resulting in reduced output energy and electrical efficiency. The primary objectives of this study are to reduce the operating temperature of the PV panel by using porous media cooling. To achieve these objectives, both experimental and numerical studies were undertaken. The experimental work was divided into indoor and outdoor experiments, whereby porosity size ranged from 0.35 to 0.5 and volumetric flow rates ranged from 1 to 4 L/min were considered. These experiments employed a cooling channel mounted on the back of the PV panel. In the numerical studies, a mathematical model was first utilized to evaluate temperature changes and output power using thermal circuit representation. Additionally, ANSYS software was used in the study to investigate the effect of various other parameters involved in PV cooling by porous media. These parameters include the cooling channel height, as well as the shape of the cooling channel which was achieved by varying the channel height at the liquid outlet. Moreover, various types of coolants, which were water, chemical alcohol, engine oil, and different types of porous media, including gravel, marble, flint, and sandstone were further considered in this study. Machine learning (AdaBoost algorithm) was also considered to weigh the parameters influencing PV cooling. Empirical correlations were then developed to predict the temperature and output power of PV panels to complete the study. Based on the indoor experiments, the best-case scenario resulted in a reduced surface temperature of 38.7°C, with an enhanced output power of 19 W, which was achieved with a porosity size of 0.35 and a volumetric flow rate of 2 L/min. For the outdoor test, the optimal results were attained with the same porosity size and volumetric flow rate, with a PV surface temperature of 39.4°C. The comparison between the experimental and mathematical results yielded a maximum error of only 5.6%. For the present study using ANSYS, the PV temperature was reduced to 36.6°C, which was achieved with a cooling channel height of 5 mm at the inlet and 3 mm at the outlet, employing water as the coolant and sandstone as the porous media with a porosity size of 0.35 and a volume flow rate of 2 L/min. Machine learning identified porosity size as the primary parameter influencing the PV cooling efficiency, accounting for 25% of all parameters. Finally, the comparison between the experimental results and empirical correlations produced a maximum error of only 4.7%.

Keywords: Machine learning, output Power, Photovoltaics, and PV cooling.

SDG: GOAL 7: Affordable and clean energy

Abstrak tesis yang dikemukakan kepada Senat Universiti Putra Malaysia sebagai memenuhi keperluan untuk ijazah Doktor Falsafah

KORELASI EMPIRIKAL UNTUK SUHU, DAN KUASA KELUARAN PANEL FOTOVOLTAIK DI BAWAH KEADAAN PENYEJUKAN YANG BERBEZA MENGGUNAKAN MEDIA BERONGGA

Oleh

ALMASALEHA ISMAIL KHALEEL MOHAMMAD

Januari 2024

Pengerusi : Siti Ujila binti Masuri, PhD
Fakulti : Kejuruteraan

Bahan api fosil telah menjadi pusat kepada penghasilan tenaga global secara tradisional. Walaubagaimanapun, pengekalan sumber-sumber ini telah menekankan keperluan untuk alternatif yang boleh diperbaharui. Cabaran ini telah mendorong penggunaan fotovoltan (PV) untuk penghasilan tenaga elektrik. Walau bagaimanapun, apabila panel PV digunakan, suhu mereka meningkat, menyebabkan pengurangan tenaga keluaran dan kecekapan elektrik. Objektif utama kajian ini adalah untuk mengurangkan suhu operasi panel PV dengan menggunakan penyejukan media berliang. Untuk mencapai objektif ini, kedua-dua kajian eksperimen dan berangka telah dijalankan. Kerja eksperimen dibahagikan kepada ujikaji dalaman dan luaran, di mana saiz porositi berkisar dari 0.35 hingga 0.5 dan kadar aliran volumetrik berkisar dari 1 hingga 4 L/min telah dipertimbangkan. Eksperimen ini menggunakan saluran penyejukan yang dipasang di bahagian belakang panel PV. Dalam kajian berangka, model matematik pertama kali digunakan untuk menilai perubahan suhu dan kuasa keluaran menggunakan perwakilan litar terma. Selain itu, perisian ANSYS digunakan dalam kajian untuk menyiasat kesan pelbagai parameter lain yang terlibat dalam penyejukan PV dengan media berliang. Parameter ini termasuk ketinggian saluran penyejukan, serta bentuk saluran penyejukan yang dicapai dengan mengubah ketinggian saluran di bahagian keluaran cecair. Selain itu, pelbagai jenis penyejuk, iaitu air, alkohol kimia, minyak enjin, dan pelbagai jenis media berliang, termasuk kerikil, marmar, flint, dan batu pasir turut dipertimbangkan dalam kajian ini. Pembelajaran mesin (algoritma AdaBoost) juga dipertimbangkan untuk menimbang parameter-parameter yang mempengaruhi penyejukan PV. Korelasi empirik kemudian dibangunkan untuk meramalkan suhu dan kuasa keluaran panel PV untuk menyelesaikan kajian. Berdasarkan eksperimen dalaman, senario terbaik menghasilkan suhu permukaan yang berkurang kepada 38.7°C, dengan kuasa keluaran yang dipertingkatkan sebanyak 19 W, yang dicapai dengan saiz porositi 0.35 dan kadar aliran volumetrik 2 L/min. Bagi ujian luaran, hasil optimum diperoleh dengan saiz porositi dan kadar aliran volumetrik yang sama, dengan suhu permukaan PV sebanyak 39.4°C. Perbandingan antara hasil eksperimen dan matematik memberikan kesilapan maksimum hanya 5.6%. Untuk kajian menggunakan ANSYS, suhu PV berkurang kepada 36.6°C, yang dicapai dengan ketinggian saluran penyejukan 5 mm di bahagian masuk dan 3 mm di bahagian keluar, menggunakan air sebagai penyejuk dan batu pasir sebagai media berliang dengan saiz porositi 0.35 dan kadar aliran volumetrik 2 L/min. Pembelajaran mesin mengenalpasti saiz porositi sebagai parameter utama yang mempengaruhi kecekapan penyejukan PV, merangkumi 25% daripada semua parameter. Akhirnya, perbandingan antara hasil eksperimen dan korelasi empirik menghasilkan kesilapan maksimum hanya 4.7%.

Kata kunci: Fotovoltaik, Kuasa keluaran, Pembelajaran mesin dan penyejukan PV.

SDG: Matlamat 7: Tenaga mampu milik dan bersih

ACKNOWLEDGEMENTS

I am genuinely grateful for the invaluable support and guidance provided by my exceptional supervisors, Associate Prof. Dr. Siti Ujila Binti Masuri, Prof. Dr. Omar Badran, and Prof. Ir. Ts. Dr. Abd. Rahim Abu Talib, and Prof. Ir. Dr. Mohd Khairol Anuar bin Mohd Ariffin. Their expertise, helpfulness, patience, and kindness have been instrumental in shaping the depth and quality of this research. Their deep knowledge and encouragement have enabled me to achieve meaningful results that can contribute to the advancement of renewable energy research on a global scale.

I would like to extend my heartfelt appreciation to all the individuals who have contributed to the success and completion of this research. Whether it was through their direct involvement in the field or their valuable insights and knowledge shared, their contributions have played a pivotal role in this endeavour.

Special thanks are reserved for my parents, wife, and children, whose unwavering support and encouragement have been a constant source of motivation throughout my studies. Their belief in my abilities and understanding during challenging times have been crucial in my academic journey.

To all who have been a part of this research journey, I extend my sincere gratitude for being by my side and sharing the joy of reaching significant milestones. Each of you has left a positive impact, and I am genuinely thankful for the enriching experiences you have shared.

This thesis was submitted to the Senate of Universiti Putra Malaysia and has been accepted as fulfillment of the requirement for the degree of Doctor of Philosophy. The members of the Supervisory Committee were as follows:

Siti Ujila binti Masuri, PhD
Associate Professor
Faculty of Engineering
Universiti Putra Malaysia
(Chairman)

Abd. Rahim bin Abu Talib, PhD
Professor Ir. Ts.
Faculty of Engineering
Universiti Putra Malaysia
(Member)

Mohd Khairol Anuar bin Mohd Ariffin, PhD
Professor Ir.
Faculty of Engineering
Universiti Putra Malaysia
(Member)

Omar Othman Badran, PhD
Professor
Faculty of Engineering Technology
Al-Balqa Applied University
(Member)

____
ZALILAH MOHD SHARIFF, PhD
Professor and Dean
School of Graduate Studies
Universiti Putra Malaysia

Date: 8 August 2024

TABLE OF CONTENTS

LIST OF TABLES

LIST OF FIGURES

NOMENCLATURE

A	Surface area, m^2
Al2O3	Aluminium oxide
BHE	Subsurface heat exchanger
c	Solar cell
$conv$	Convection
$cond$	Conduction
Cp	Specific heat at constant pressure, J/Kg.k
CPV	Concentrator photovoltaic
DC	Direct current, A
dp	Gravel diameter, mm
EVA	Ethyl vinyl acetate
G	Solar intensity, W/m^2
g	Glass
GC-CPCS	Ground central panel cooling system
h	Heat transfer coefficient, W/m^2. k
hr	Radiation heat transfer coefficient, W/m^2. k
I	PV panel output current, A
i	Insulation
I_L	Light generated current, A
$I_{L,ref}$	Light-generated current at stc. W/m^2.k
in	Inlet water
Io, ref	Diode reverse saturation current, A
k	Thermal conductivity, W/m.k
L	Length, m
Nu	Nusselt number
P	Power, W
PCM	Phase change material
PHP	Pulsating heat pipes
PV	Photovoltaic
∇P	The pressure difference, Pa
q''	Heat flux, W/m^2
R	Thermal resistance, K/W

rad	Radiation
Re	Reynolds number (dimensionless)
ref	Reference
RS	Series resistance, Ω
RSref	Series resistance at STC, Ω
UA	Uncertainty of the area
UG	Uncertainty about solar radiation
UP	Uncertainty of the output power
Voc	Open-circuit voltage, V
Emax	Maximum radiation inside solar simulator, W/m^2
Emin	Minimum radiation inside the solar simulator, W/m^2
$T\infty$	Ambient temperature, ^oC
Ts	Surface temperature, ^oC
$Tsur$	Surrounding temperature, ^oC
V	Liquid velocity, m/s
$\forall f$	Fluid volume Liter
$\forall t$	Total volume, Liter
μ	Viscosity of the liquid, $N \cdot s/m^2$
ρf	Liquid density, Kg/m^3
α	Absorptivity
β	Packing factor
τ	Transmissivity
ŋ	Efficiency
ϕ	Porosity size

CHAPTER 1

INTRODUCTION

1.1 Overview

The world's heavy reliance on traditional energy sources like gas and oil has significant economic implications for countries heavily consuming these resources. Developing nations, in particular, face economic challenges due to the high cost of generating power from fossil fuels (Badran et al., 2010). To address this issue and mitigate the impact on their economies, many of these countries are turning towards renewable energy sources as a potential solution. These countries often possess abundant renewable energy resources, especially in regions like the solar belt, where daily solar radiation averages 5-8 hours (Hafith et al., 2013).

Renewable energy is harnessed from natural sources that are continuously replenished, ensuring an inexhaustible supply. This stands in contrast to traditional energy sources such as coal, oil, and gas, which deplete as they are used. Moreover, renewable energy is renowned for being clean and environmentally friendly, as it does not produce harmful emissions like greenhouse gases that contribute to climate change. By adopting renewable energy, countries can make a significant contribution to combating climate change and preserving the environment for future generations.

Beyond its environmental benefits, renewable energy also presents promising economic opportunities. The renewable energy sector and related technology development create new job opportunities, bolstering local economies. Additionally, the costs of producing renewable energy are continually declining, making it increasingly competitive with traditional energy sources. This cost-effectiveness enhances the appeal of renewable energy adoption, facilitating the transition to sustainable energy practices. Furthermore, embracing renewable energy enables countries to achieve greater energy independence and diversification of their energy sources. By relying less on imported fossil fuels, nations can enhance their energy security and reduce vulnerability to fluctuations in global energy markets. This diversification also promotes a more resilient and sustainable energy infrastructure, supporting long-term economic growth and stability.

1.2 Problem statement

Despite the immense potential of solar energy as a clean and renewable energy source (Badran et al., 2010), the main problem in photovoltaic (PV) operation is the loss of electrical power due to the rise in cell temperature, which leads to a decrease in power and electrical efficiency (Ebaid et al., 2018). Elevated temperatures increase the resistance within the solar cells, reducing their ability to convert sunlight into electricity efficiently. This phenomenon, known as the temperature coefficient, results in decreased power output as the temperature rises.

Moreover, high temperatures accelerate the degradation of materials used in PV panels, such as semiconductor materials and encapsulation layers. This degradation can lead to a decrease in the overall performance and lifespan of the solar panels, affecting their reliability and long-term viability (Eitner et al., 2009). Additionally, excessive heat can exacerbate the phenomenon of "hot spots," where localized areas of the panel experience significantly higher temperatures than others. Hot spots can cause irreparable damage to the affected cells, further reducing the overall efficiency of the PV system (Laabab et al., 2022), and the permanent damage caused by hot spots is estimated at 15% (Olalla et al., 2018).

Existing studies by Ahmed et al. (2019) underscore the urgency of implementing efficient cooling methodologies in PV systems. However, previous cooling methods such as water-cooling, air cooling, and single turn pulsating heat pipes suffer from drawbacks such as excessive water consumption, limited sunlight penetration, production costs, and safety concerns (Laabab et al., 2022; Harmailil et al., 2024). Therefore, there is a crucial need for research that focuses on developing improved cooling techniques tailored to the specific requirements of PV panel operation.

In addition to the need for improved cooling methods for PV panels, investigating the optimal configuration for various cooling parameters including the cooling channel height, the shape of the cooling channel, types of coolants, and types of cooling materials to achieve the best PV cooling is equally important (Zhang et al., 2022). Failure to address the limitations of existing research regarding optimal parameter selection can lead to a suboptimal cooling performance decrease and limited applicability, which hinders the design and implementation of efficient cooling systems for diverse applications and operating conditions (Harmailil et al., 2024).

With the complexity of the relationship between various cooling parameters and their effects on PV panel cooling, such a study requires tremendous effort and time when investigated experimentally (Zhang et al., 2023). The main issue then lies in the lack of established experimental relationships that accurately determine the complex relations between these parameters and the changes in temperature and the resulting energy output. Therefore, formulating experimental correlations of temperature and output power under various cooling conditions is vital to establishing a predictive framework (Gholami et al., 2022). Failure to develop these empirical correlations can lead to more expensive experimental work. Addressing these challenges will contribute to enhancing the overall efficiency and effectiveness of PV panel cooling systems.

Given these factors, the research aims to tackle the underlying issues of efficiency decline caused by excessive heat in PV panels. By employing effective cooling techniques, such as those utilizing porous media, the study seeks to solve the above-mentioned problems through both experimental and numerical investigations. This will involve selecting suitable cooling parameters and establishing empirical relationships that accurately predict changes in temperature and power output across various cooling scenarios.

1.3 Objectives

The main aim of the work is to improve the cooling of photovoltaic (PV) panels by using porous media. The specific objectives are as follows:

1. To reduce the operating temperature of the PV panel by using porous media cooling and determine the optimum porosity size and volume flow rates.

2. To investigate the effect of various parameters on PV cooling by porous media using ANSYS. These parameters include the cooling channel height, shape of the cooling channel, types of coolants, and types of porous media.

3. To formulate the empirical correlations for temperature and output power under different cooling conditions using porous media.

1.4 Scope and limitations

- The experimental phase of this research was conducted both indoors and outdoors at the Faculty of Engineering Technology, located at Al-Balqa Applied University in Jordan.

- The indoor experiments provided a controlled setting, allowing for precise measurements and observations while minimizing external influences. This approach ensured accurate data collection and facilitated the study of specific cooling parameters in a controlled environment.

- Conversely, the outdoor experiments offered insights into the cooling system's behaviour in authentic, dynamic environmental conditions. Subjecting the system to natural fluctuations in temperature, solar irradiance, and weather patterns, could assess its performance under real-world operational conditions. Through the outdoor experiments can be provided valuable information on the cooling system's reliability, efficiency, and adaptability to changing weather conditions, which are critical factors for practical applications.

- The combination of indoor and outdoor experiments enabled this research to validate the findings and draw robust conclusions about the cooling system's effectiveness and its potential for practical implementation. Moreover, conducting experiments in Jordan, with its diverse climate and solar radiation patterns, allowed the research to have broader implications for solar energy applications in similar regions around the world.

- The research also incorporated a comprehensive numerical study using cutting-edge software tools to further analyse and optimize the cooling system's performance. The numerical simulations were conducted using ANSYS 2019, MATLAB 2019, and AUTOCAD 2014, which allowed for a detailed investigation of the heat transfer mechanisms and fluid dynamics within the cooling system (Hussien et al., 2023; Bahaidarah et al., 2013).

- Porous media (gravels) has been used in experimental work for photovoltaic cooling.

- A 5 cm thick cooling channel was used in experimental work (Bahaidarah et al., 2013).

- The porosities sizes used were 0.35, 0.40, 0.48 and 0.5. If a porosity size of less than 0.35 is used, it becomes difficult for water to pass through the channel.

- The water volume flow rates used were 1, 1.5, 2, 3, and 4 L/min. Therefore, since the cooling of photovoltaics is affected by changing the flow rate only up to a certain extent, the increase in the flows rates is not significant (Ebaid et al., 2018).

- The indoor experiments were done within 40 days, and each experiment was three hours continuously (Irwan et al., 2015).

- The outdoor experiments were done for 60 consecutive days, and every day for eight consecutive hours, from 9:00 am to 4:00 pm (Ebaid et al., 2018).

- The diameters of the gravel used in this study were chosen based on what is available in the local Jordanian market to avoid additional financial costs. The gravel used was proven to their hard and water-repellent. Also, they are used in construction materials in Jordan.

1.5 Thesis structure

The first chapter outlines the research problem, objectives, and novelty, setting the stage for the study's importance. Chapter 2 focuses on renewable energy, emphasizing photovoltaic cells, components, performance factors, and a comprehensive literature review. This chapter lays the foundation for subsequent methodology and analysis. In the third chapter, the methodology is detailed, including indoor and outdoor tests, numerical studies, ANSYS simulations, mathematical modelling, and machine learning. Chapter 4 presents and analyses results from experiments and numerical approaches. Chapter 5 concludes with key findings, implications, and recommendations, encapsulating the study's potential impact on renewable energy advancement.

CHAPTER 2

LITERATURE REVIEW

2.1 Overview

This chapter highlights the vital role of renewable energy in addressing global sustainability challenges, with a particular focus on photovoltaic cells. These cells have significant potential to transform the energy landscape by harnessing clean solar power, meeting growing electricity needs while reducing carbon emissions. The chapter presents the components of solar systems, emphasizing their collaborative efficiency in converting solar energy into electricity. Additionally, it presents factors influencing photovoltaic cell performance, such as solar irradiance, temperature, shading, and humidity.

This foundational understanding sets the stage for the study's focus on enhancing photovoltaic cell efficiency. The chapter conducts a thorough literature review, analysing cooling techniques to mitigate temperature impacts on solar panels. Various strategies, from passive cooling such as heat sinks to active cooling, were presented, creating a comprehensive perspective on their effects.

2.2 Solar energy description and PV panels

The escalating reliance on fossil fuels, coupled with increasing environmental concerns, necessitates a thorough exploration and adoption of renewable energy sources. Among these alternatives, solar energy emerges as a compelling and sustainable solution, characterized by its abundance, free availability, and perpetual availability. Photovoltaic cells, responsible for directly converting sunlight into electrical power, hold considerable promise in harnessing solar energy for many applications.

An intrinsic advantage of solar energy lies in its environmental cleanliness. Unlike conventional energy sources, photovoltaic cells generate electricity without emitting harmful pollutants, positioning solar energy as an environmentally friendly option. This attribute contributes significantly to reducing greenhouse gas emissions and mitigating air pollution, pivotal factors in the global challenge of climate change.

Furthermore, the low maintenance requirements of photovoltaic cells stand out as a noteworthy benefit. Once installed, these cells demand minimal supervision or regular upkeep, rendering them highly reliable and cost-effective over their lifespan, often exceeding 20 years (Sivaraj et al., 2022). Photovoltaic cells' durability and prolonged service life make them a sound investment for sustainable energy production. The applications of photovoltaic cells span across diverse sectors. They play a pivotal role in powering satellites, illuminating streetlights, and supplying energy to remote power stations situated in coastal and isolated areas. Communication stations extensively rely on photovoltaic cells to ensure uninterrupted electricity supply for essential services. Moreover, solar energy finds application in the transportation sector, where tour vehicles utilize the power of photovoltaic cells to efficiently operate lighting and various onboard systems.

Beyond these applications, solar energy contributes significantly to enhancing public infrastructure and amenities. It powers public parks and gardens, ensuring well-lit and enjoyable outdoor spaces for communities. Additionally, solar energy provides electricity in scout camps, offering renewable energy solutions during outdoor adventures. Photovoltaic cells also play a crucial role in pumping water, contributing to sustainable agricultural practices, and ensuring water supply in remote areas. As the demand for sustainable energy continues to surge, the development and implementation of photovoltaic technology are poised to play a pivotal role in meeting these energy needs. However, further research and advancements are imperative to optimize the efficiency, reliability, and cost-effectiveness of photovoltaic cells. Collaborative efforts, encompassing material scientists, engineers, and policymakers in multidisciplinary approaches, are essential to drive innovation and facilitate a seamless transition to a clean and renewable energy future. The utilization of solar energy, particularly through photovoltaic cells, presents a promising solution to address the challenges posed by conventional energy sources. Its clean and sustainable nature, coupled with its versatility in various applications, positions it as a crucial player in the transition toward a greener and more sustainable future. By prioritizing research, development, and the widespread adoption of photovoltaic technology, we can pave the way for a cleaner, more resilient, and eco-friendly energy landscape.

2.3 The importance of solar energy

Solar energy constitutes a vast and versatile resource, embodying two principal components: thermal energy and photovoltaic energy. These components, each with distinct functionalities, contribute significantly to fostering a sustainable and environmentally friendly future.

The historical utilization of thermal energy spans centuries, finding applications across various facets of daily life. In the agricultural sector, thermal energy plays a pivotal role in drying crops and preserving food products. The exposure of agricultural produce to solar warmth facilitates moisture reduction, extends shelf life, and prevents spoilage, thereby ensuring a consistent food supply throughout the year.

Moreover, thermal energy contributes to the heating of homes and buildings, enhancing comfort and warmth. Solar heating systems capture sunlight, converting it into heat for space heating, particularly in colder months. This not only diminishes reliance on conventional heating methods but also reduces greenhouse gas emissions, thereby promoting environmental cleanliness.

Another critical application of thermal energy lies in water heating for domestic and industrial purposes. Solar water heaters employ sunlight to elevate water temperature, providing an energy-efficient alternative to traditional water heating systems. This technology finds widespread adoption in residential spaces, hotels, and industries, contributing to energy conservation and diminishing electricity consumption.
Solar desalination represents yet another significant application of thermal energy, offering a sustainable solution in regions facing limited access to fresh water. Solar desalination plants utilize solar energy to heat water, inducing evaporation, followed by condensation to obtain fresh water. This process addresses water scarcity issues and fosters water security in arid regions. Conversely, photovoltaic energy stands out as a

groundbreaking technology revolutionizing electrical energy production. Photovoltaic cells, commonly known as solar panels, directly convert sunlight into electricity through the photovoltaic effect, gaining widespread popularity due to their clean and renewable nature. Solar photovoltaic systems are extensively deployed in residential and commercial settings to generate electricity for diverse purposes. They provide a reliable and sustainable energy source, reducing dependence on conventional fossil fuel-based power generation and mitigating associated environmental impacts. Furthermore, photovoltaic energy facilitates the decentralization of energy production, empowering individuals and communities to achieve self-sufficiency in electricity generation. The applications of photovoltaic energy extend beyond terrestrial contexts, playing a crucial role in space exploration. Photovoltaic cells power satellites, space probes, and the International Space Station, ensuring continuous and reliable energy supply for scientific research and communication.

In conclusion, solar energy, with its multifaceted components of thermal and photovoltaic energy, possesses immense potential to revolutionize our lifestyles and address pressing energy and environmental challenges. The combined utilization of thermal energy across diverse applications and photovoltaic energy for clean electricity generation provides a sustainable pathway toward a greener future. By embracing and advancing solar technologies, we can effectively reduce our carbon footprint, enhance energy security, and contribute to building a cleaner and more sustainable world.

2.4 Basic components of photovoltaic systems

The photovoltaic panel system is a complex assembly of critical components that operate synergistically to effectively capture solar energy and transform it into usable electricity. A comprehensive comprehension of the individual roles and functionalities of these components is imperative for a nuanced understanding of the overall efficiency and reliability inherent in solar power systems. The subsequent discourse will provide an in-depth exploration of each constituent part.

2.4.1 Photovoltaic cells

The genesis of photovoltaic technology can be traced back to the early 1950s with the development of silicon-based materials. These materials undergo meticulous fabrication into specific geometric configurations and dimensions, tailored to efficiently convert solar radiation into electrical energy at the predetermined voltage and current levels. The resultant photovoltaic cells function as the fundamental components of solar panels, facilitating the direct conversion of sunlight into usable electricity.

The electrical output of photovoltaic cells, and consequently the overall electrical power generated by the solar panel, is subject to several influential factors. Notably, the area of the solar panel assumes a pivotal role in this regard. Larger solar panels possess an expanded surface area, enhancing their capacity to capture sunlight and consequently elevating their potential for electricity generation. Additionally, external environmental factors such as solar radiation, temperature, humidity, and air velocity significantly impact the performance of photovoltaic cells. These multifaceted considerations collectively contribute to the intricate dynamics governing the electrical output of photovoltaic systems.

2.4.2 Photovoltaic cells work principle

Solar cells are ingenious devices that harness the power of sunlight and transform it into electrical energy through a fascinating phenomenon known as the "photovoltaic effect." This process relies on the interaction of materials within the solar cell with photons, which are tiny particles of light. At the heart of a solar cell lies its traditional structure, typically composed of two essential layers:

Front contact layer: This layer is crafted from highly pure semiconducting silicon and serves as a crucial conductor for the electrical current generated within the cell. It boasts the ability to allow high transmission of sunlight, ensuring that a significant portion of the incoming sunlight can be absorbed and converted into electrical energy. To optimize efficiency, the front contact layer is deliberately made thinner compared to the back layer. Back contact layer: Composed of high-purity semiconducting silicon, the back contact layer plays a pivotal role in the solar cell's operation. It acts as a collector, diligently gathering the electrical current produced within the cell and guiding it for external use. This layer provides a clear pathway for the liberated electrons, enabling the efficient flow of electrical energy for practical applications.

As sunlight reaches the solar cell, its energy-rich photons are absorbed by the semiconducting materials in the front layer. This absorption of light energy causes the electrons within the material to break free from their atoms, setting them loose and allowing them to move freely within the material. Inside the solar cell, an electric field is ingeniously created through the interaction between positive and negative charges. This electric field acts as a guide, steering the liberated electrons in a specific direction, creating order and purpose in their movement. The presence of the back contact layer is absolutely crucial in this process. By skillfully collecting the liberated electrons, this layer ensures that they are directed through external electrical circuits. As these electrons flow through the circuits, they generate an electric current, ready to power electrical devices or charge batteries.

In this awe-inspiring way, solar energy transforms, evolving from the radiance of sunlight to the practicality of electrical energy. This clean and renewable form of energy finds a multitude of applications, from generating electricity for homes and establishments to empowering portable electronic devices.

2.4.3 Types of solar cells made of silicon

Based on Figure 2.1, photovoltaic energy systems utilize three primary types of photovoltaic cells. These classifications are determined by various factors, including efficiency, cost, and suitability for specific climatic conditions. Let's delve deeper into each type:

1. Monocrystalline silicon: Monocrystalline silicon stands out as one of the most widely employed types of photovoltaic cells. Its popularity arises from its exceptional efficiency in generating electrical energy. This high efficiency can be attributed to the use of silicon with remarkably high purity when compared to other cell types. The monocrystalline silicon cells exhibit a uniform crystalline structure,

which enhances their performance under varying sunlight conditions. Although they tend to be relatively pricier than other options, their efficiency and consistent output make them a preferred choice, particularly in areas with ample sunlight and higher energy demands. 2 Polycrystalline silicon: The next type, polycrystalline silicon, is another commonly used option in photovoltaic energy systems. While it may possess slightly lower efficiency compared to monocrystalline silicon cells, it compensates with a more cost-effective production process. These cells are fabricated from multiple silicon fragments, resulting in a less uniform crystalline structure. This structural difference translates into a marginally reduced energy conversion rate. However, the affordability of polycrystalline cells makes them a pragmatic solution for applications where the cost factor is a decisive consideration. Their usage is well-suited for regions with moderate sunlight conditions and where optimal efficiency isn't the sole priority. 3 Thin-film solar cells: Thin-film solar cells constitute the third category of photovoltaic cells, distinguished by their manufacturing process involving the deposition of ultra-thin layers of photovoltaic material. While these cells may not achieve the same levels of efficiency as their crystalline counterparts, they offer a unique set of advantages. Thin-film solar cells possess flexibility, rendering them adaptable to various surfaces and unconventional installations. Additionally, their production process is generally less resource-intensive, contributing to their affordability. These cells find utility in a diverse range of applications and are especially valuable in regions characterized by high temperatures. The flexible nature of thin-film cells allows them to be integrated into structures and objects, providing innovative opportunities for solar energy utilization (Sivaraj et al., 2022).

The selection of a specific photovoltaic cell type depends on careful consideration of factors such as efficiency requirements, budget constraints, and the climatic conditions of the installation site. While monocrystalline and polycrystalline silicon cells prioritize efficiency and cost-effectiveness respectively, thin-film solar cells offer flexibility and versatility. This diversity of options empowers solar energy systems to be tailored to the unique demands of various environments and applications, ultimately contributing to the broader adoption of clean and sustainable energy sources.

Figure 2.1: Types of solar cells
(Sivaraj et al., 2022)

2.5 External influences that affect solar cells

Many influences affect solar cells' production of electrical energy, efficiency, and others, including the amount of solar radiation, the temperature of the solar cell, humidity, dust, and air velocity.

2.5.1 Solar radiation

The generation of electrical power through solar cells hinges upon the interplay between voltage and current intensity, particularly in the face of varying solar intensities. This relationship is eloquently illustrated in Figure 2.2, a graphical representation showcasing the dynamic interdependence between current intensity and voltage across shifting levels of solar radiation.

As portrayed in this illustrative graph, a compelling trend comes to the fore: the correlation between radiation intensity and current intensity is notably direct and proportionate. In simpler terms, as solar radiation escalates, the concurrent surge in current intensity becomes palpable. This phenomenon underscores the solar cells' ability to promptly respond to heightened sunlight exposure by generating more electrical current.

Conversely, the behaviour of voltage across these changing radiation levels exhibits a more nuanced demeanour. While it experiences fluctuations, these alterations are comparatively modest about the more pronounced variations witnessed in current intensity. This observation aligns with the findings established by Jakhrani et al. (2014) whose research underscores the slight variations in voltage in response to escalating solar radiation.

This interplay between current and voltage attests to the agreement between solar cells and the radiant energy they harness. The harmonious partnership between these two vital factors holds the key to effective energy conversion, enabling solar cells to seamlessly adjust to the ebb and flow of solar radiation. Such insights into the behaviour of solar cells in response to varying radiation intensities are instrumental in optimizing their performance and enhancing the overall efficiency of solar energy systems.

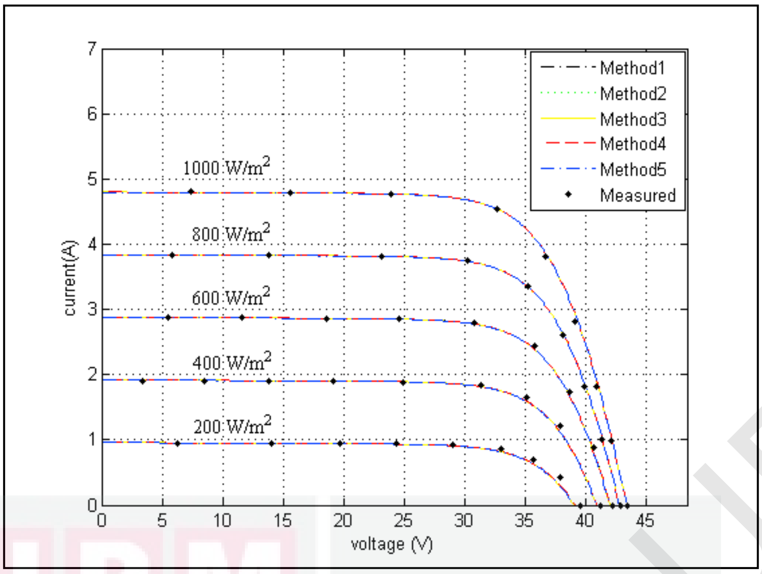

Figure 2.2: I-V curve at different solar radiation
(Jakhrani et al., 2014)

2.5.2 PV temperature

Figure 2.3 provides valuable insights into the relationship between solar cell temperature and its electrical performance. As the temperature of the solar cell rises, a direct impact on the voltage becomes evident. Specifically, with an increase in temperature, the voltage experiences a decrease. This phenomenon poses significant implications for the overall power production and electrical efficiency of the solar cell.

The reduction in voltage was due to elevated temperatures translated into a decrease in the amount of electrical power generated by the solar cell. Consequently, the overall electrical efficiency of the cell will be reduced. It becomes evident that the effect of temperature on voltage is adverse, leading to a less efficient energy conversion process. However, it is noteworthy that an increase in temperature does have a slight positive effect on the current intensity within the solar cell. This means that a higher temperature causes a minor increase in the flow of electric current. However, this increase does not adequately compensate for the substantial loss in voltage, resulting in an overall reduction in the power output.

These findings are supported by the research conducted by Amelia et al. (2016), which highlights the relationship between temperature, voltage, and electrical efficiency in solar cells. They emphasized that the critical importance of thermal management is for mitigating the adverse effects of temperature on solar cell performance.

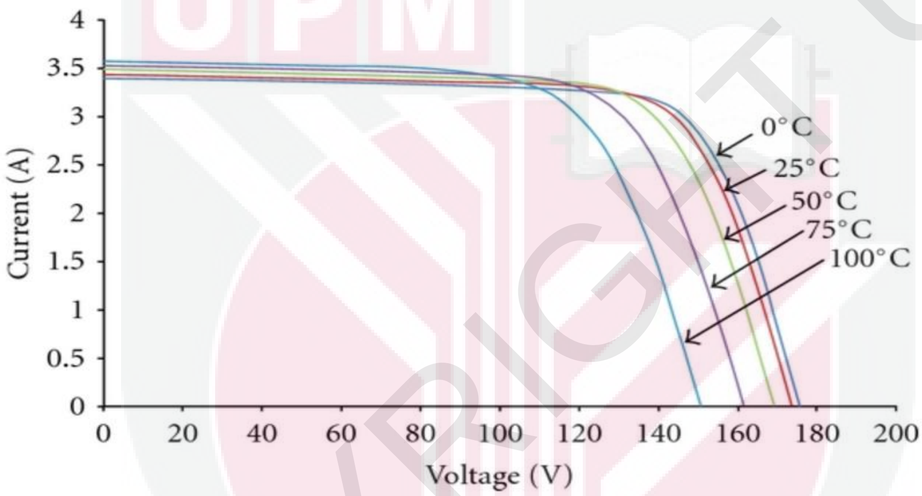

Figure 2.3: I-V curve at different temperatures
(Amelia et al., 2016)

Not addressing the problem of excessive heat in solar panels can have several consequences, ranging from reduced energy output and financial losses to long-term damage and decreased system reliability:

1. Reduced energy output: Excessive heat can lead to a decrease in the efficiency of solar panels, resulting in lower energy production. When solar cells operate at elevated temperatures, their electrical performance tends to degrade, leading to

reduced conversion of sunlight into electricity. This reduction in energy output directly impacts the overall productivity and profitability of solar installations.

2. Financial losses: Lower energy output due to temperature-induced efficiency losses translates into financial losses for solar system owners and operators. Reduced energy generation means lower revenue from electricity sales or decreased savings from offsetting conventional energy consumption. Additionally, if solar panels underperform or fail prematurely due to overheating, it may result in warranty claims, repair costs, or even complete system replacements, further exacerbating financial losses.

3. Long-term damage: Prolonged exposure to high temperatures can cause long-term damage to solar panels and associated components. Excessive heat accelerates the degradation of materials used in solar cells, such as semiconductor materials and encapsulants. This degradation can manifest as increased cell cracking, delamination, or corrosion, ultimately compromising the structural integrity and reliability of the entire photovoltaic system.

4. Decreased system reliability: Overheating can reduce the overall reliability of solar energy systems, leading to potential operational disruptions and maintenance challenges. High temperatures exacerbate the aging processes of electronic components, such as inverters, charge controllers, and wiring, increasing the likelihood of component failures or malfunctions. Additionally, thermal stress on mounting structures and support systems may result in mechanical failures or reduced system stability over time.

Excessive heat in solar panels primarily leads to efficiency loss through several mechanisms:

1. Increased resistance: Elevated temperatures cause an increase in the electrical resistance of semiconductor materials within solar cells. Higher resistance leads to greater losses in electrical current flow, reducing the overall efficiency of energy conversion.

2. Reduced voltage: Temperature-related changes in semiconductor properties can result in a decrease in the open-circuit voltage of solar cells. Lower voltage output diminishes the power output of individual cells and modules, contributing to overall efficiency losses in the system.

3. Carrier recombination: High temperatures promote carrier recombination within semiconductor materials, where electrons and holes recombine instead of contributing to electrical current. This phenomenon reduces the efficiency of charge separation and collection, limiting the solar cell's ability to convert sunlight into electricity.

2.5.3 Humidity effect

Based on the insights provided by Figure 2.4, it becomes evident that humidity plays a significant role in diminishing the power output of photovoltaic cells. This intriguing phenomenon can be attributed to the presence of water vapor within the atmosphere, which effectively absorbs a portion of the incident solar radiation. As this vapor absorbs sunlight, it detracts from the energy that would otherwise be harnessed by the photovoltaic cells, thereby leading to a reduction in their overall power generation capacity.

However, the influence of humidity doesn't stop there. Nature's agreement continues, as the moisture-laden environment facilitates the growth of certain algae. These tiny organisms, taking advantage of increased humidity, might colonize the surface of solar cells. Over time, they can form a layer that acts as an impediment to the direct entry of solar radiation. As a consequence, the efficiency of energy conversion is hindered, further contributing to the decline in power production.

Moreover, the very moisture responsible for nurturing these potential algae colonies contributes to another layer of complexity. It accumulates as a film atop the glass surface that encapsulates the solar cells. This damp layer serves as an additional barrier, obstructing the unfettered passage of solar radiation into the photovoltaic cells. This dual effect, from both the presence of algae and the moisture layer, compounds the challenges faced by solar cells, resulting in a discernible reduction in their ability to generate electrical energy.

Quantitatively speaking, the impact of humidity on photovoltaic panel performance is noteworthy. Studies, such as the research conducted by Panjwani & Narejo (2014), underscore that when photovoltaic panels are exposed to high-humidity environments, their power production potential can experience a decline ranging from 15% to as much as 30%. This statistic underscores the substantial role humidity plays in dictating the energy output of solar cells in real-world conditions.

In summary, the complex interplay between humidity, solar cells, and their environment paints a vivid picture of the multifaceted challenges faced in the realm of solar energy. As humidity exerts its influence through radiation absorption, algae growth, and moisture accumulation, the consequence is a discernible reduction in power generation potential.

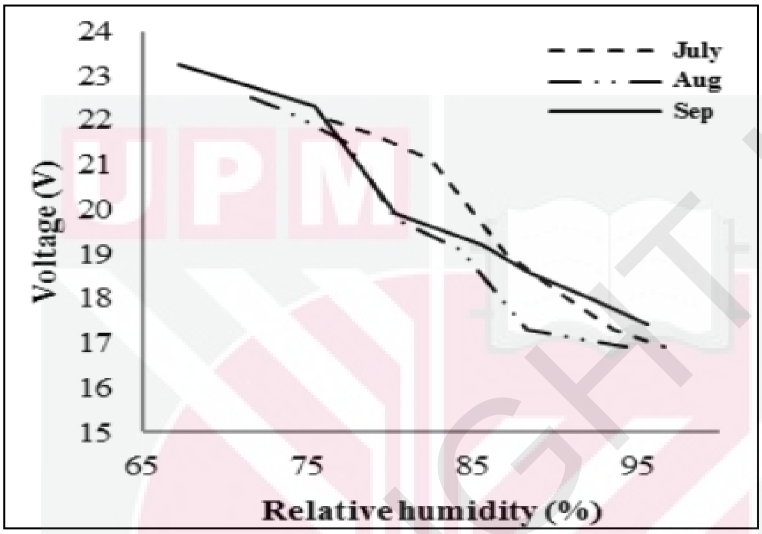

Figure 2.4: Humidity effect
(Panjwani & Narejo, 2014)

2.5.4 Dust effect

The detrimental impact of dust accumulation on solar cells poses a significant challenge to the efficient production of electrical energy. This concern stems from the undeniable fact that the presence of dust particles translates directly into a tangible loss in energy generation. The investigation unveils a cascade of effects wherein these minuscule particles disperse across the surface of the solar cells, creating an obstructive layer that restricts the unfettered penetration of solar radiation.

Within this context, the plight of solar cells becomes increasingly apparent. As a layer of dust gradually envelops the photovoltaic cells, the once-pristine surface transforms into an arena of reduced energy conversion. The obstruction caused by the dust particles diminishes the solar radiation that can be captured, thereby inhibiting the full utilization of the cells' photovoltaic capabilities. Amidst the discourse on the influence of dust on solar energy systems, a myriad of scholarly investigations have sought to unravel the nuances of this challenge. Notably, the comprehensive study conducted by Saidan et al. (2016) stands as a testament to the accurate exploration of dust's effects on photovoltaic cell performance. Their research not only contributes to our understanding of the issue but also underscores the importance of devising strategies to mitigate the impact of dust accumulation.

It is crucial to recognize that the adverse consequences of dust are not confined solely to energy loss. Over time, the cumulative effects of dust can lead to a gradual degradation of the photovoltaic cells themselves. As these particles settle and become ingrained, they might exacerbate temperature imbalances, moisture retention, and potential chemical reactions, all of which could compromise the cells' longevity and overall efficiency.

The multifaceted nature of the dust dilemma beckons for innovative solutions. Researchers and engineers are continuously engaged in developing novel cleaning mechanisms, surface treatments, and protective coatings that can counteract the deleterious effects of dust. The integration of self-cleaning technologies, such as hydrophobic coatings that repel both water and dust, showcases the industry's dedication to ensuring sustained energy production and maximizing the lifespan of solar cells.

2.6 PV panels

This section delves into the pivotal attributes of photovoltaic (PV) modules, casting a spotlight on their defining features. As elucidated in Figure 2.5, an array of visuals paints a vivid picture of the evolution from individual solar cells to a comprehensive PV array. Each step in this progression underscores the multifaceted nature of solar energy systems. In Figure 2.5 (a), a singular solar cell takes centre stage, its composition characterized by crystalline silicon (c-Si). This fundamental building block serves as the elemental unit, embodying the essence of solar energy conversion. Progressing forward, the subsequent depiction in Figure 2.5 (b) seamlessly weaves these individual solar cells into the fabric of a PV module. This union of cells within a module forms the bedrock upon which solar energy systems are constructed. Notably, the terms "PV module" and "solar module" are often wielded interchangeably, underscoring the interconnectedness of these entities. Expanding the perspective further, Figure 2.5 (c) unveils the collaboration of PV modules within a solar panel.

This higher-level amalgamation sees multiple PV modules harmoniously electrically linked and poised atop a singular supporting structure. This arrangement not only facilitates efficient energy capture but also illustrates the synergy achieved when individual units coalesce into a cohesive whole. Finally, Figure 2.5 (d) introduces us to the pinnacle of this hierarchical journey: the PV array. This culmination embodies the grand vision of solar power generation. Comprising a symphony of solar panels, each populated with interconnected PV modules, the array is a testament to the scale and ambition of modern solar energy systems. Here, the sum is truly greater than its parts.

To delve even deeper, it's worth acknowledging that the deployment of PV arrays isn't just about amassing solar panels. Each array configuration, such as the one in Figure 2.5 (d), strategically strings together series-connected pairs of solar panels. This accurate arrangement optimizes the electrical output of the system, ensuring a seamless and synchronized flow of energy.

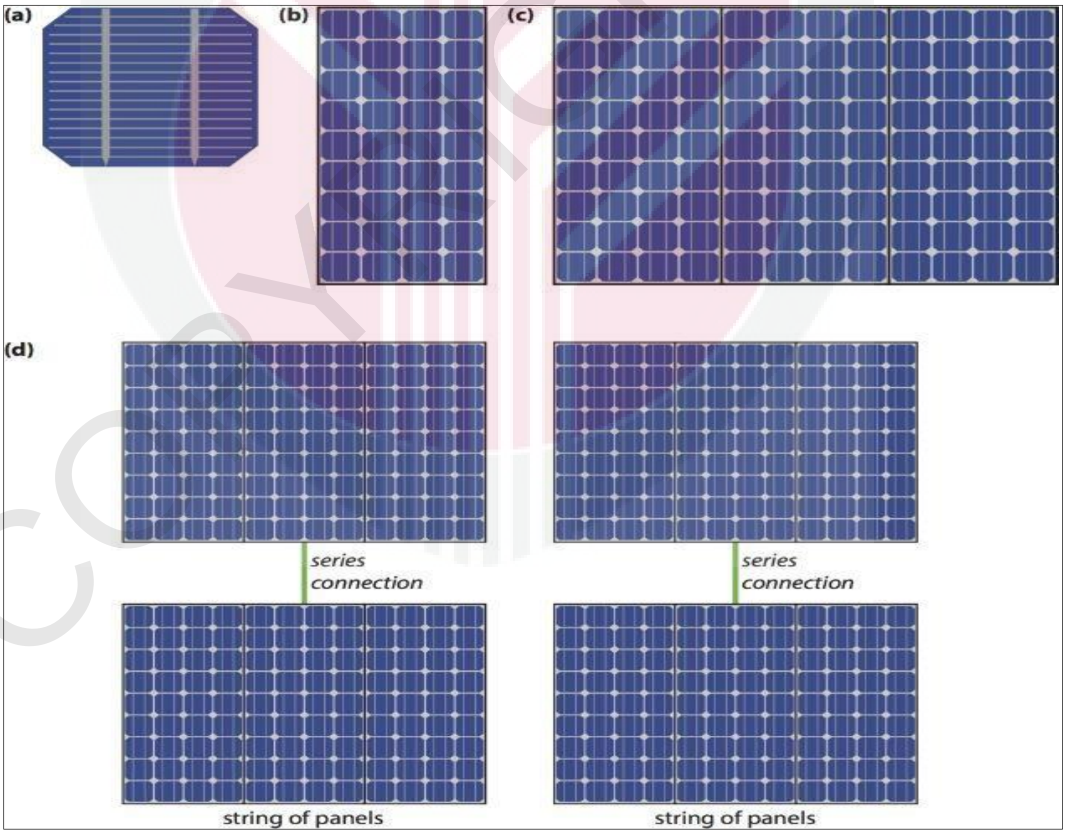

Figure 2.5: (a) solar cell (b) PV module (module panels (d) arrays in series
(Smets et al., 2016)

2.7 PV module components

The manufacture of PV modules involves the consideration of various factors to ensure their service for at least 25 years. The use of carefully selected components is crucial to this end, and Figure 2.6 presents the typical components of a crystalline silicon PV module. The specific media used in the layer stack may vary depending on the manufacturer. The primary components are as follows:

- A soda-lime glass layer several millimetres thick provides mechanical stability and transparency for incoming light. The glass must have low iron content to prevent light absorption and resulting losses. It is also tempered to increase its impact resistance.

- To protect the solar cell when used and to facilitate its transportation, it is placed between two layers of ethylene-vinyl acetate (EVA).

- To protect the solar panel from moisture, rain, and other natural factors, a Tedlar backing is applied.

- An aluminium frame is placed around the photovoltaic panel for more stability and for fixing this panel in the installation places. Aluminium is a good choice because it is light in weight and does not rust over time.

- The electrical junction box, which is installed at the back of the photovoltaic panel to protect it from rain, is used for electrical connections to the system.

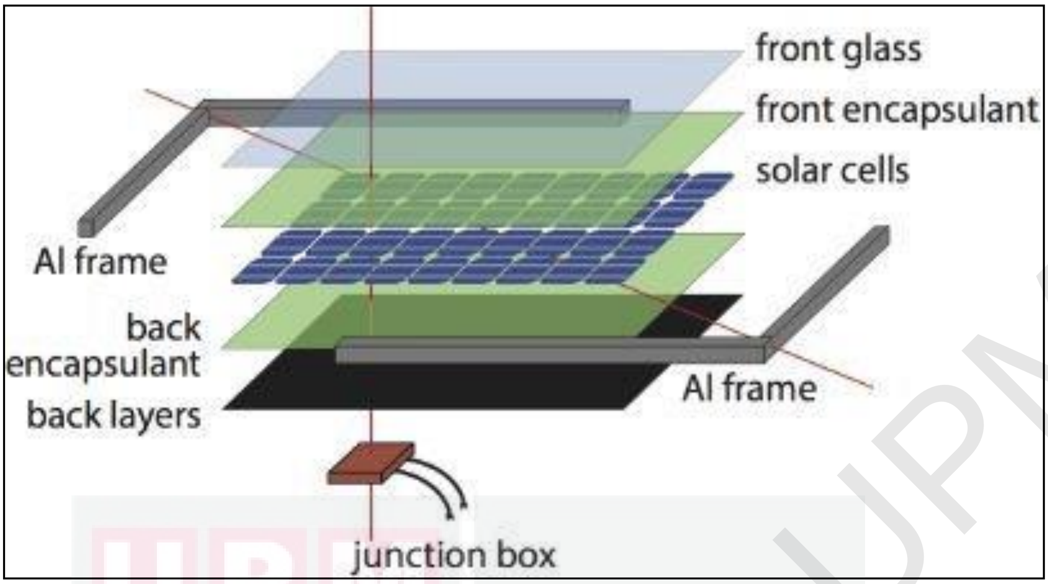

Figure 2.6: PV module components
(Smets et al., 2016)

2.8 PV systems

Photovoltaic systems vary in size and complexity, starting from small and direct equipment that contains only the load and the photovoltaic panel. There are many examples of this, including the photovoltaic unit that is used for street or farm lighting and water pumping that operates during the day, huge photovoltaic power stations are producing high quantities of electricity, which are widespread these days due to the high prices of fossil fuels.

Many solar energy systems are being installed for use in residential homes. However, sometimes it is necessary to install supportive systems for solar stations, such as generators. There are three basic types of photovoltaic systems, the first type is self-contained, the second is connected to the public electrical network, and the third type is mixed mode, and with the difference between these three types, the principle of producing electrical energy is similar.

2.8.1 Stand-alone PV systems

The versatility of photovoltaic solar energy finds its niche even in the far-flung corners of our world, where access to conventional electricity stations remains but a distant dream. In these remote expanses, an ingenious solution takes centre stage: the independent photovoltaic system, often referred to as an off-grid system. This technological marvel stands as a testament to human innovation, bridging the chasm between energy demands and geographical isolation.

The essence of these off-grid systems lies in their self-sufficiency. Devoid of umbilical cords to traditional power grids, they operate as self-contained powerhouses, harnessing the boundless energy of the sun to serve the energy needs of their surroundings. A symphony of photovoltaic components converge in a choreography, each element playing its part to ensure that energy flows seamlessly from sun to socket. One of the fascinating facets of these systems is their inherent adaptability. In certain scenarios, energy generated by photovoltaic arrays can be channelled directly to the intended load, obviating the need for energy storage batteries. This direct pathway of energy is exemplified by applications like solar-powered water pumps. In the sun-drenched embrace of daylight, these pumps spring to life, propelled by the very photons that harmony upon their solar panels. It's a direct communion between sunlight and utility, a testament to harnessing energy at the source.

However, as the sun extinguishes its radiance and the moon ascends, a new challenge emerges. The energy generated during the day must be preserved and doled out judiciously when darkness cloaks the land. Enter the stalwart companions of these systems - batteries. These unassuming powerhouses take on the mantle of energy guardians, storing excess daytime energy for nocturnal use. They stand as sentinels of resilience, ensuring that the rhythm of energy sustains even when the sun momentarily bows out.

Figure 2.7, a visual representation etched with clarity, unveils the simplicity of a system reliant solely on direct energy transfer without batteries. It's a testament to the efficiency of photovoltaic energy in powering applications that harmonize with daylight hours. Meanwhile, Figure 2.8 ushers in the realm of energy storage, illustrating the integration of batteries into the photovoltaic ecosystem. This is the embodiment of foresight, where energy's ebb and flow are deftly managed, transforming sunlight into an everlasting reservoir of power.

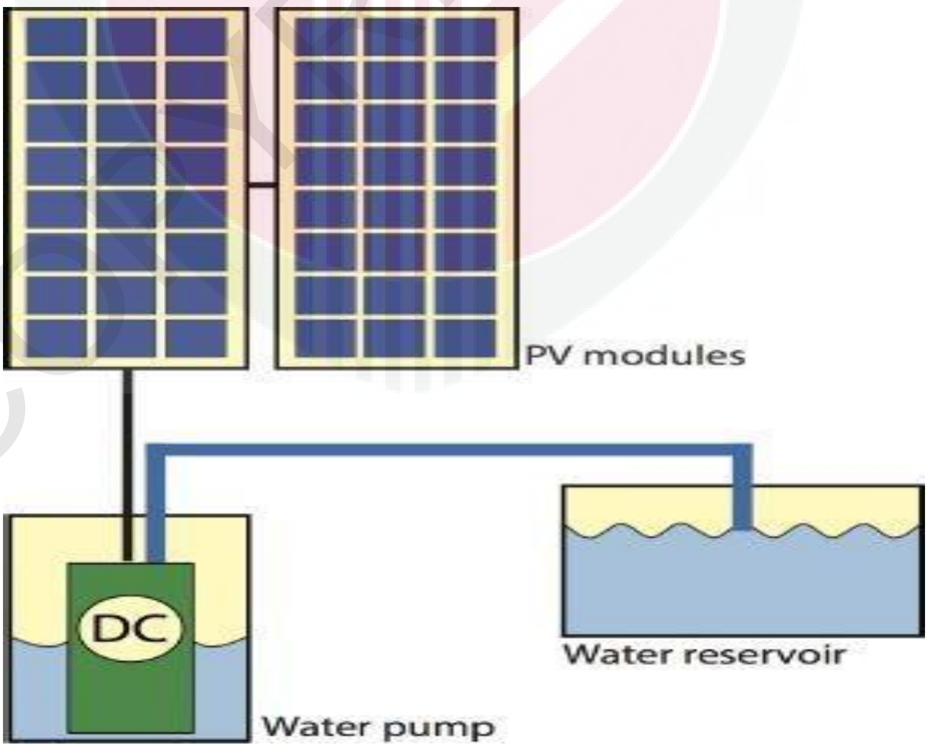

Figure 2.7: Solar system for pumping water
(Smets et al., 2016)

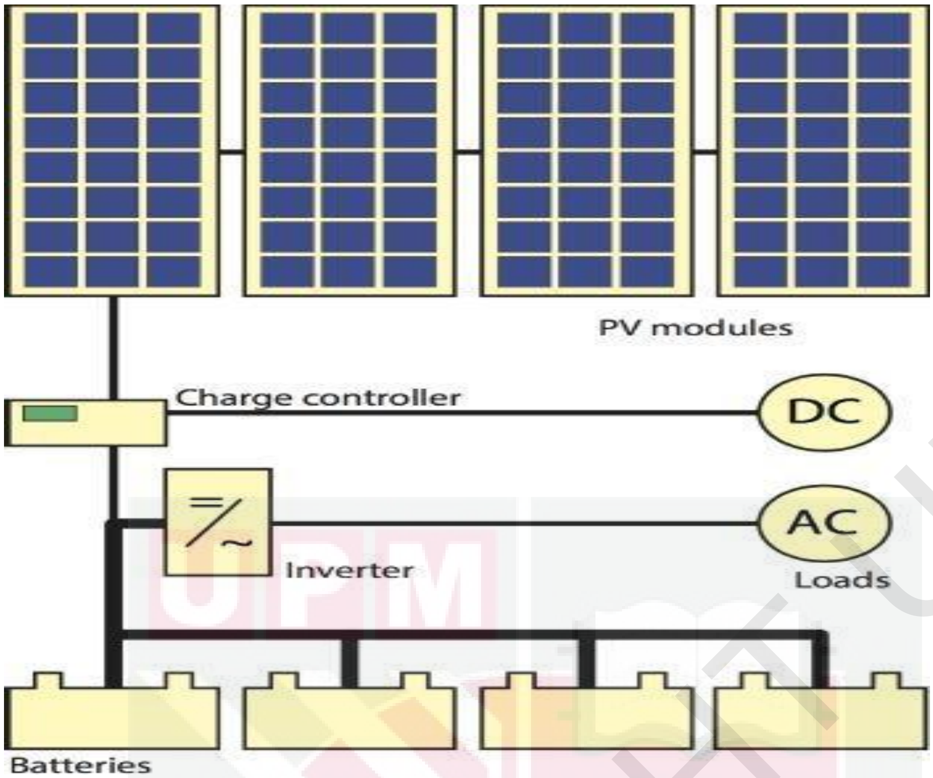

Figure 2.8: PV system with both DC and AC loads
(Smets et al., 2016)

2.8.2 Grid-connected

Figure 2.9 illustrates the use of grid-connected PV systems in the built environment, which have gained popularity over time. These systems are linked to the grid via inverters and meters in and out, which convert DC power into AC electricity. In residential homes, the inverter is connected to the distribution board, enabling the transfer of PV-generated power to the grid or AC appliances within the house. These systems typically do not require batteries as the grid serves as a buffer for excess electricity generated by the PV system and supplies electricity to the home when there is insufficient power generation. However, to increase the self-consumption of PV-generated electricity, more grid-connected systems now incorporate batteries (Marion et al., 2013)

2.8.3 Hybrid system

Photovoltaic units stand resolute as potent generators of electrical energy, assuming their place among a diverse tapestry of energy sources. In a symphony of power production, they share the stage with counterparts such as diesel engines, gas engines, and wind energy-based electricity generators. This collective effort paints a vibrant tableau of energy diversity, ensuring a continuous and dependable supply to meet the voracious appetite of modern society.

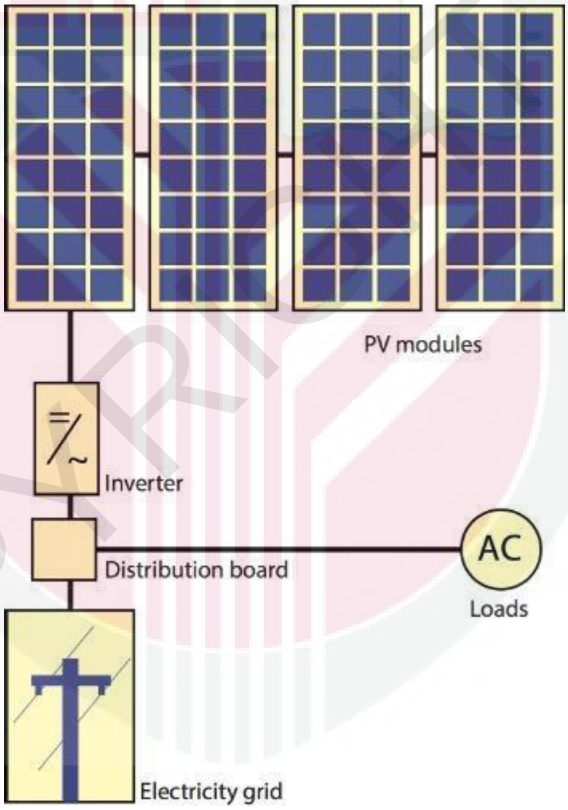

Figure 2.9: Grid-connected PV systems
(Smets et al., 2016)

Yet, in the ever-fluctuating theatre of energy dynamics, there emerge moments when the spotlight must shift. Circumstances unfold where the radiant embrace of the sun is obscured by clouds or the deep shroud of night descends, casting a temporary shadow over photovoltaic units. In these instances, an energy ecosystem characterized by resilience and adaptability comes into play. It's a concept that calls for the symbiotic union of energy sources, a fusion of technologies working harmoniously to sustain the flow of power even when one takes a brief bow.

This harmonization of energies finds its embodiment in the hybrid system. Akin to a conductor orchestrating a symphony, the hybrid system seamlessly intertwines diverse energy sources to create an unbroken cadence of electrical power. Under this banner, photovoltaic units coalesce with other energy stalwarts, acting as an ensemble that delivers consistent performance, unfazed by the unpredictable rhythms of nature. Figure 2.10, etched with illustrative precision, provides a visual entrée into this hybrid reality. It showcases the web of interconnections, where photovoltaic units unite with alternate sources like diesel engines, gas engines, or wind energy turbines. Together, they form a robust ensemble that can elegantly traverse the realms of day and night, inclement weather, and fluctuations in solar energy availability.

This synergy is underpinned by a fundamental premise: the seamless transition between energy sources must be accomplished with finesse. Smart controls and algorithms, akin to musical notes on a conductor's sheet, dictate when each energy source should take the lead, ensuring a harmonious and uninterrupted flow of electricity. This harmony of energy resources optimizes not only power generation but also resource utilization, contributing to a more sustainable and efficient energy landscape.

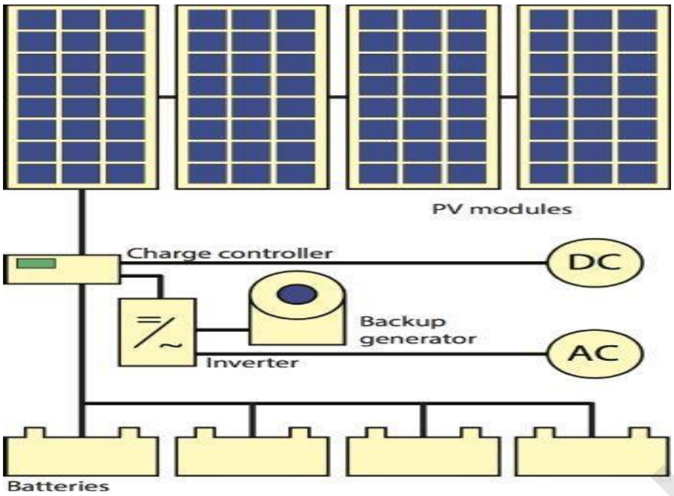

Figure 2.10: Hybrid system
(Smets et al., 2016)

2.8.4 PV system components

Solar cells have limited output power under fixed current and voltage conditions that are impractical for most applications due to their small size. To use electricity from solar panels for practical devices that require a specific voltage and/or current, several solar cells need to be linked together to create a solar module, also known as a PV module. Solar panels are the fundamental component of a PV system, but additional components are required to create a functional system. These components are referred to as the balance of system (BOS) and differ in operation, depending on whether the system is connected to the electricity grid or a standalone system.

- There must be a structure that is usually made of galvanized iron to avoid rusting over time. This structure aims to install photovoltaic panels, and it is oriented in the right direction and at the right angle based on the area.

- Batteries: Sometimes photovoltaic energy is used during the night, so there must be batteries to store this energy.

- Inverters: They are used to convert current from direct current to alternating current.

- In the off-grid systems, charge control devices must be present to prevent the batteries from being overcharged or excessively discharged, and to protect the photovoltaic cells from back current during the night.

- There must be cables to connect the electrical systems and connect the loads with the electrical systems. The electric load, which includes all connected electric appliances, must also be considered during the planning phase, along with whether the loads are AC or DC. Figure 2.11 presents the different components of a PV system.

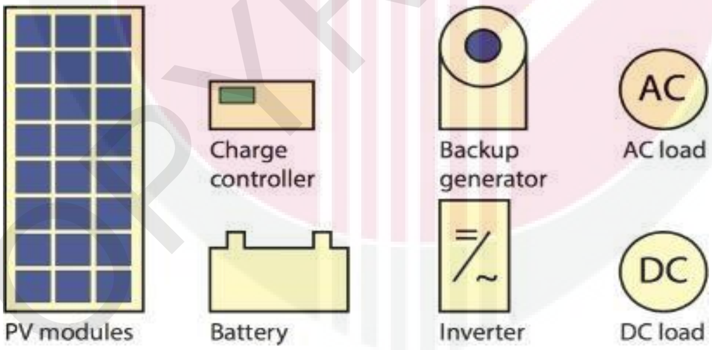

Figure 2.11: PV system components
(Smets et al., 2016)

2.8.5 PV lifetime

Photovoltaic systems, with many now surpassing the three-decade mark, underscore the need for a comprehensive and integrated maintenance approach. Such a system must encompass all components, with a particular focus on the vital photovoltaic panels. Effective maintenance is pivotal not only in extending the system's operational life but also in optimizing its energy production potential well into the future.

Strategically conducted maintenance, rooted in precise engineering methodologies, holds the key to unlocking sustained performance. By adhering to accurate maintenance practices, a photovoltaic system can defy the passage of time and continue generating optimal energy outputs even after a quarter-century. Remarkably, research by Marion et al. (2013), reveals that such well-maintained systems can consistently yield energy levels ranging from 80% to 90% of their initial capacities. This steadfast energy production becomes the enduring hallmark of an accurately cared-for photovoltaic system.

However, the journey towards enduring energy production is not without its challenges. Photovoltaic panels, steadfast sentinels of solar energy conversion, stand exposed to an array of environmental factors that invariably influence their performance. The ceaseless cycle of temperature fluctuations between summer and winter, as well as the diurnal rhythm of day and night, exerts continuous stress on these panels. Beyond thermal dynamics, a medley of other influences emerges, including the erosive effects of moisture, the abrasive impact of sand particles, the frigid touch of frost, and even the unwanted presence of certain types of radiation.

To ensure that these panels consistently deliver their potential, a regime of continuous and vigilant maintenance is non-negotiable. This commitment encompasses both routine assessments and proactive interventions. Regular cleaning routines can stave off the buildup of dust, sand, or other detritus that might dim the panel's capacity to convert sunlight into electrical energy. Inspections can uncover potential issues like moisture ingress or frost damage, and expedite their rectification. Even as the panel ages, diligent maintenance can forestall the encroachment of efficiency-draining factors, guaranteeing the panel's prolonged vitality.

In the grand tapestry of renewable energy, photovoltaic systems stand as stalwart protagonists. Their longevity and unwavering contribution hinge on the bedrock of attentive and systematic maintenance. With each accurately conducted check, each conscientious cleaning, and each targeted intervention, the path toward enduring energy production becomes clearer. This ongoing commitment to maintenance ensures that the promise of photovoltaic technology isn't just realized in the initial years, but sustains as an enduring force well into the future, weaving a cleaner, more sustainable for the world's energy landscape.

2.9 Previous studies on PV cooling

In this section, a thorough survey of prior studies on photovoltaic (PV) cooling was conducted. The captivating field of PV cooling has attracted global attention, leading to a diverse range of cooling technologies for PV systems. The survey of various cooling techniques aimed at optimizing PV panel performance. Passive methods utilize natural convection and radiation, while active techniques employ mechanical systems like pumps, fans, and heat exchangers. Innovative mediums like nanofluids and phase change materials were also explored. This comprehensive survey provides valuable insights for ongoing research, prioritizing effective, eco-friendly, and sustainable cooling solutions to enhance PV panel performance while avoiding unintended negative effects. Numerous researchers have contributed to the understanding of PV systems and cooling techniques.

2.9.1 Air coolant

Based on Figure 2.12 a porous medium, a direct current (DC) fan, and a glass cover were used in the study done by Ahmed et al. (2019) to increase the performance of a hybrid photovoltaic thermal wall (PV/TW) system. When combined with a glass cover, the porous medium with a DC fan enhanced thermal efficiency by 20% and electrical efficiency by 0.5 percent. The porous medium with a DC fan boosted thermal efficiency by 13% and electrical efficiency by 4%. Patil et al. (2023) investigated the effect of air cooling on the energy conversion efficiency of PV/T panels. The results showed that air cooling effectively reduced the panel's temperature, leading to increased energy conversion efficiency. The study indicated that air cooling could be a practical and efficient cooling method for PV/T panels. Ebrahimi et al. (2015) used a novel method of cooling a photovoltaic cell utilizing natural vapor as a coolant was being investigated. On a fake sun, the solar cell's performance was evaluated. The natural vapor came into contact with the PV cell's backside vertically, and it did so in a variety of distributions and mass flow rates. The impact of natural vapor temperature on cooling effectiveness was also studied. The temperature of the PV cell dramatically reduces as the mass flow rate of natural vapor increases, according to the results. In further detail, the when flow rate reaches 1.6 to 5 gr min^{-1}, the PV cell temperature drops by roughly 7 to 16°C. Electrical efficiency rises by around 12.12% to 22.9% as a high salt. A high natural vapor flow rate, low natural vapor temperature, and optimal distribution conditions were necessary for the PV cell to work at its best.

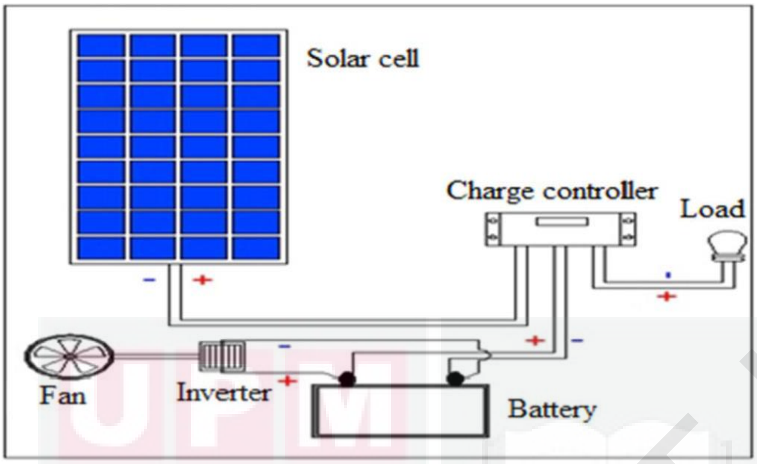

Figure 2.12: Schematic diagram
(Ahmed et al., 2019)

A passive evaporative cooling strategy to enhance the electricity production of a hybrid PV-STEG system was done by Gao et al. (2023). This study investigated a passive evaporative cooling approach for a hybrid PV-STEG system. The researchers found that incorporating passive evaporative cooling can effectively lower the operating temperature of the PV panels, leading to enhanced electricity production. This cooling strategy offers a cost-effective and sustainable method to boost the overall performance of hybrid PV-STEG systems. Experimental and numerical investigation for PV cooling by forced convection done by Hussien et al. (2023). In this research, both experimental and numerical methods were employed to study the impact of forced convection cooling on PV panels. The findings revealed that forced convection cooling significantly reduced the panel's temperature, leading to increased power generation and improved overall efficiency. The study emphasized the importance of optimizing the cooling airflow rate to achieve the best cooling performance. Experimental study of solar PV/T panel to increase the energy conversion efficiency by air cooling.

Modelling of a PV system by a back-mounted spray cooling section for performance improvement done by Herez et al. (2020). This study proposed a modelling approach for a PV system with a back-mounted spray cooling section. The researchers found that incorporating a spray cooling section improved the overall performance of the PV system, leading to higher energy conversion efficiency and better temperature control. Bahaidarah (2016) investigated the impact jet cooling efficacy of photovoltaic panels exposed to weather conditions verified in the Dhahran region of Saudi Arabia. For two configurations, an impingement-cooled PV system and an uncooled PV system, experimental and numerical performance evaluations were done. The whole cooling model includes an optical, radiation, thermal, geometric, and electrical model to analyse the PV system's entire performance. To perform the heat transfer study for a single nozzle to analyse the cell temperature, power output, and conversion efficiency of PV strings, a jet impingement geometric model for PV was created. A seven-parameter electrical model was used to estimate PV cell performance precisely, while an isotropic sky model was used to calculate absorbed radiation. According to temperature measurements, the cell temperature for an uncooled system in June and December 2015 was as high as 69.7°C, and 47.6°C, respectively. The average cell temperature was lowered to 36.6°C for June, and 31.1°C for December, by using jet cooling. By using jet cooling in June, the power production and conversion efficiency were increased by 51.6% and 66.6%, respectively. Similar to this, December's statistics showed a 49.6% increase in power production and an 82.6% increase in conversion efficiency. A simulation shows that using jet cooling with the best settings considerably improved electrical power production and cell efficiency as well as reduced cell temperature while maintaining uniformity for each cell. This study develops a straightforward passive cooling mechanism for freestanding flat PV modules using cotton wick architectures. Elnozahy et al. (2015) evaluated the performance of a Photovoltaic (PV) module with automated cooling and surface cleaning installed on the roof of a building in a hot, dry environment to that of a module without those features. To keep the PV module surface temperature consistently near the ambient temperature, the module cooling was automatically adjusted by the back side temperature by rejecting unconverted solar energy to the ambient. This mechanism also regulates how often the front surface of the module is cleaned. According to the results, the temperature of the module was reduced by around 45.5% and 39% at the front and back sides, respectively. As a consequence, the cooling and surface cleaning module was 11.7% more efficient than the module without cooling and cleaning, where 9%. Furthermore, compared to the uncooled and uncleaned module, the cooled and cleaned module generates an output power of 89.4 W compared to 68.4 W for the uncooled and uncleaned module. Based on Figure 2.13, it was found that the use of cooling in photovoltaic panels gives positive and effective results in increasing electrical efficiency and power. This study incorporated three different passive cooling methods: conductive cooling, and air-passive cooling, Jamali et al. (2018) suggested a revolutionary solar chimney method to cool a semitransparent PV (STPV) system. The STPV serves as the solar chimney's roof and is cooled by the airflow produced by the solar chimney. A theoretical model was created for the suggested system based on the energy balance for its three primary components the earth, (the air, and the STPV). Convection heat transfer coefficients were carefully computed for the heat transfers occurring in the system, and the solar chimney findings were compared to the experimental data. The results of the suggested model correspond well with the earlier data. It was demonstrated that for each radiation intensity, there was an ideal packing factor that optimizes produced power. It has been shown that both the structural characteristics and the radiation intensity affect the system's operation. The suggested approach can lower the STPV's typical temperature by up to 15°C. It was determined that an increase in output power of roughly 29% may be achieved by cooling the STPV power plant with the solar chimney for solar radiation of 500 W/m^2.

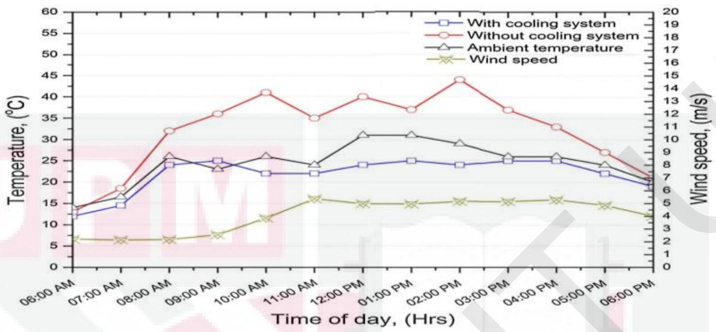

Figure 2.13: PV temperature with time
(Elnozahy et al., 2015)

Wu & Xiong (2014) concede cost-effectiveness, design viability, and low energy usage as the key design considerations for cooling systems, according to their paper evaluation of earlier research on cooling PV cells. These factors led to the development of the passive cooling technique described in their study, which uses rainwater as the cooling medium and a gas expansion mechanism to disperse it. The quantity of water that the gas pushes to flow across the PV cells was proportional to the amount of solar energy that it received since the gas was thermally expanded from receiving solar radiation. The design and modelling of such a system for a residential dwelling application were reported. An investigation of the link between the gas chamber size, solar radiation, and gas expansion volume, as well as the fluctuation in gas temperature and the quantity of rainwater utilized for cooling, was done in their work. The efficiency of the cooling provided by this passive device to the cells was assessed using a heat transfer model. The findings indicated that the passive cooling system lowers the cells' temperature and boosts the PV panel's electrical efficiency by 8.3%. Golzari et al. (2018) investigated experimentally verified photovoltaic cooling Active cooling has been used in the photovoltaic cell, a uniform airflow duct connected to photovoltaic panels that ultimately lowers the temperature and increases efficiency by 12.14%. Many researchers used air to cool photovoltaic cells, including, Lin et al. (2019) compared two cells, one without cooling and the other one with air cooling. gave examples of natural cooling such as the use of fins installed on the back of the solar panels. One of the benefits of this method is that it does not need equipment that consumes energy, but it does not give high efficiency during cooling. The other method of cooling was forced air cooling, which was the active method. In this method, mechanical and electrical equipment was used, and it consumes energy but gives higher efficiency than the natural cooling method. Popovici et al. (2016) used air to cool the photovoltaic panels to improve their efficiency by making heat sinks as a curved wall that can absorb heat from the photovoltaic panels, and it can be identified by high thermophysical phenomenon media through this experiment. The increase in output power and electrical efficiency was due to the reduction in the temperature of this panel. Bilen & Erdoğan (2023) investigated this comprehensive review highlights the importance of cooling in PV/T solar panels and its impact on performance. The researchers analysed various cooling techniques, such as liquid cooling, air cooling, and phase-change materials, and assessed their effects on power generation and efficiency. The study emphasized that effective cooling methods contribute to reducing operating temperatures, thereby enhancing the overall efficiency and prolonging the lifespan of PV/T systems.

Simulation of air-cooled PV/T air conditioning system for cooling and power cogeneration" done by (Fan et al., 2023). In this simulation-based study, researchers developed a novel air-cooled PV/T air conditioning system that effectively utilizes waste heat from PV panels to generate electricity and provide cooling. The research demonstrated that this integrated system not only generates electricity but also cools the space efficiently, making it a promising solution for sustainable energy and cooling needs. Özakin & Kaya (2019) investigated their air-based PVT system's energy and exergy analyses. Additionally, ANSYS Fluent was used to investigate the temperature distribution of the panel surface and the air velocity distribution of the cooling channel and compared the results to the experimental data. For the fin status of empty, frequent, and sparse fins, experiments were conducted. The exergy efficiency of the polycrystal and monocrystal panels was roughly raised by 70% and 30%, respectively, by employing the sparse and frequent fins as opposed to the empty condition. Their thermal efficiency enhanced by around 55% and 70%, respectively. All configurations' panel surface temperatures have lowered by around 10 to 15°C, according to their observations. The temperature contour pictures produced by ANSYS Fluent matched the values acquired during experimentation. Due to the frictional and viscous forces, the air moves more slowly in the areas close to the fins than it does at the entrance and exit of the air channel and in the spaces between the fins. Ahmed & Mohammed (2017) used porous media to find out the effect of different parameters such as pressure drop, fluid flow rate, and PV cell cooling, their tests showed that the cooling with porous media increased the output power by 80.23% and without it by 51.2% which means that the porous media an effective way to increase the thermal efficiency in PV system. In many heating and cooling systems, air was used as a heat transfer medium to reduce the temperature. Air is less effective than liquids in transferring heat, but it has many benefits as it is cheap and inexpensive. There are two ways of cooling using air, natural cooling, that is, without using any electrical or mechanical equipment. El Mays et al. (2017) investigated an experimental study that showed that the electrical efficiency was improved by 1.77%, and the temperature was reduced by 7.2%, the maximum output power was about 19.2 W when the temperature was 49 56°C. With Cooling, the output power was 17.2 W and the temperature was 56°C. Tang et al. (2010) conducted an experimental study to verify the performance of air as a cooling medium, where a small heat pipe was used to cool the photovoltaic cells, and the cooling was under natural air cooling without the use of electrical or mechanical equipment. In comparison to the photovoltaic cells, the temperature was reduced by about 4.7°C, and the output electrical energy increased by about 8%.

Buker et al. (2015) investigated the use of dewdrops were used to cool the photovoltaic cells as the cooling rings were made of polyethylene. Desiccant and liquid desiccant units have been installed to condense the evaporative air, an innovative new method of photovoltaic cooling. To examine the effectiveness of the suggested system and the effects of several parameters including weather, airflow, and regeneration temperature, a pilot-size experimental setup was created and evaluated. Underneath the PV panels, a simple, affordable polyethylene heat exchanger loop was used to generate heat. In addition, a liquid desiccant to improve the dew point cooling unit was used to offer air conditioning by the indirect evaporative cooling and dehumidification of humid air. According to the experimental findings, the suggested tri-generation system can generate around 10.3MWh of electricity per year, 5.2 kWh of cooling power, and 3kWh of heating power, respectively. The results demonstrate the technology's potential and clarify specific recommendations for using such systems. Tonui &

Tripanagnostopoulos (2007) used Air as the main source of cooling the photovoltaic panels in this experiment, giving some new features as it is inexpensive and available, Metal sheets were placed in the middle of the air channel, and this method reduces the temperature and increases the performance of the photovoltaic panel, and based on the results and testing there was an increase in thermal efficiency by 13-18%. Beccali et al. (2009), used glazed air and photovoltaic to achieve primary energy saving and to enable the simultaneous production of electricity and heat, they did not use any heat storage, and the percentage of energy saving was increased to 5.5%, and economic performance around 30%.

2.9.2 Water coolant

Kabeel et al. (2019) identified an optimization cooling technology for raising PV modules with reflector performance under Egyptian circumstances. Three different cooling techniques were experimentally studied to determine the best cooling technology to improve the performance of the PV module with reflectors: using forced-air cooling in the presence of reflectors (case I), using water cooling in the presence of reflectors (case II), and combining forced-air and water cooling in the presence of reflectors (case-III). To determine the optimal cooling method to utilize to boost the performance of the PV module with reflectors, the results of cases I, II, and III were compared to those of the standard PV module. Based on Figure 2.14, the temperature of the PV panels decreased. The economic analysis was studied. The findings indicated that the optimal technology for PV modules was the use of water cooling in the presence of reflectors. For cases, I, II, and III, the net output of electricity was 912, 1077, and 1010 Wh/day, respectively. However, the standard PV module's daily power production was 832 Wh/day. In comparison to the typical example, case-I, case-II, and case-III, showed gains in net production electricity of 80, 245, and 178 Wh/day, respectively when utilizing reflectors and a cooling strategy.

By AL-Musawi et al. (2019) studied the effect of using nanofluids and phase change materials on the performance of photovoltaic thermal (PVT) systems was analyzed. The study aims to enhance the efficiency of these systems by exploiting the unique properties of nanofluids and phase change materials to improve heat exchange and reduce the temperature rise of solar cells, leading to increased electrical and thermal efficiency. The results show that applying these materials can significantly improve the overall performance of PVT systems, making them more efficient and sustainable for solar power generation.

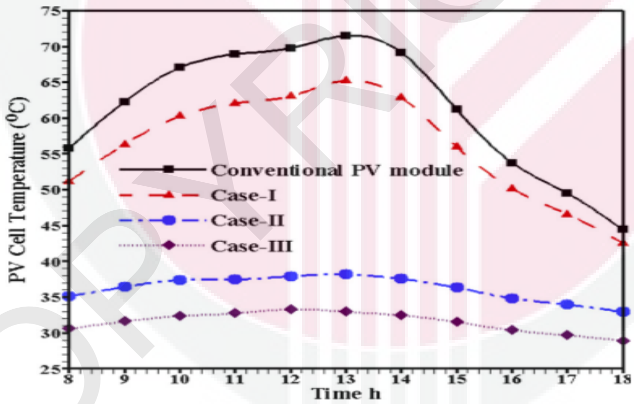

Figure 2.14: PV temperature with time
(Kabeel et al., 2019)

Seasonal analysis of a desiccant air-conditioning system supported by water-cooled PV/T units done by Olmuş et al. (2023). This study conducted a seasonal analysis of a desiccant air-conditioning system integrated with water-cooled PV/T units. The research demonstrated that utilizing water-cooled PV/T units in the system contributed to better temperature control and improved energy efficiency during different seasons.

The results suggested that this integrated approach could effectively address cooling demands while reducing energy consumption. Elminshawy et al. (2019) conducted experimental research on an integrated PV panel cooling system with a subsurface heat exchanger (BHE). The study employed forced atmospheric air at flow rates of 0.0228 m^3/s, 0.0248 m^3/s, and 0.0268 m^3/s, along with temperatures of 35°C, 40°C, and 45°C. The research revealed an increase in electrical efficiency from 12% to 14%.

In another investigation, submerged water heat exchangers were utilized for both experimental and computational tests. The outcomes indicated improvements in output power, electrical efficiency, and thermal efficiency. A three-dimensional cooling channel model was developed to analyse the impact of cooling on photovoltaic cells. Water-passive cooling was done by Idoko et al. (2018). The experiment setup was two 250watt solar panels, each installed at a height of 37 cm to allow for air cooling. Water cooling was then applied to one of the PV modules' surfaces to lower the surface temperature to 20^{o}C. A heat sink made of aluminium, was mounted to the back of the same module. The other module was installed without an aluminium heat sink connection and water cooling. The heat sink used was completely made of aluminium material in the form of fins distributed on the back surface of the photovoltaic panel, and water was used to cool it, and also the water temperature was significantly lowered because of the ice inside it, which led to a reduction in temperature to more than 80% and an increase in the electrical efficiency more than 3%, and the output power increased by 20.96 W, which makes the photovoltaic panels more efficient. Odeh & Behnia (2009), examined cooling PV panels by water making drops of water on the upper surface of the panel. So, the heat loss occurs by convection, and the output power was increased by 5% on delivered energy and (4 – 10) % in system output. Zhu et al.

(2011) conducted a study where they employed a water immersion method to prevent the overheating of photovoltaic (PV) panels. This innovative approach resulted in significant improvements in both the performance and temperature regulation of the PV cells. By immersing the panels in water, they were able to achieve a notable reduction in temperature, with a decrease of up to 8%. This reduction in temperature not only enhanced the efficiency of the PV cells but also contributed to their overall longevity and reliability. The study highlights the effectiveness of water immersion as a cooling technique for maintaining optimal operating conditions for PV panels. Liu et al. (2021) explored the influence of total flow rates, differences in solar radiation, water temperature upon entry to the cooling channel, and cooling channel height. The model provided insights into electrical efficiency, power, panel temperature, and Nusselt number calculations for the upper and lower surfaces of the cooling channel. The study indicated concurrence between the upper and lower surface results. Optimal thermal and electrical efficiency was observed when the channel height was 5 mm and the water mass flow rate was 0.03 kg/sec.

In an experimental study, Gomaa et al. (2020) employed two distinct cooling methods: passive cooling with well-fixed fins on the back of the photovoltaic cell, and active cooling using water directly. A spare PV module without cooling served as a reference. Experimental measurements were conducted on three different PV modules. Results indicated a significant reduction in photovoltaic panel temperature for the cooled panels. Maximum temperatures were 38°C, 55°C, and 58°C for water-cooling, fins-cooling, and non-cooling modules, respectively. Cooling systems enhanced PV module performance, with backwater cooling and fins cooling modules showing daily energy capture increases of 10.2% and 7%, respectively, compared to the non-cooling module. Performance ratios improved by up to 84% for the water-cooling module and 81% for the fins-cooling module, as opposed to 77% for the non-cooling module during the same period.

Kong et al. (2020) investigated the photovoltaic panels that have been cooled and a heat pump has been designed that provides a capacity of about 7 Kilowatts of cooling, heat, and electricity. The method might improve the thermal performance of heat pumps for cold water below 17°C and hot water 80-90°C production, as well as the electrical performance of PV/T modules. The heat pump's cold water was utilized in part to lower the temperature of the PV/T modules and boost their ability to produce electricity. Additionally, the heat from the PV/T added to the heat pump's cooling load, which allowed it to boost both its cooling and heating capabilities. A hot water electrical heating system and a vapor-compression chilled water system were replaced with the new equipment. The innovative device might greatly reduce grid electrical usage by using the electrical power produced by a set of PV/T modules. Economic analysis with a 10-hour daily operation period 7:00-17:00 revealed that seven PV/T modules, each with a peak power of 200 Wp, were the ideal number. Additionally, it was discovered that a total of 23.76 x 103 kWh of electrical energy from the grid was saved per year, and the unit's payback period was 7.87 years.

Aldossary et al. (2016) conducted this research in Saudi Arabia twitches were considered one of the hot regions in Asia, especially in the summer, and the temperature can reach 50°C, as photovoltaic cells have been used extensively in Saudi Arabia recently. Therefore, a good way to cool photovoltaic cells must be found. Two methods were used for cooling, which were passive and active. The simulation was used to compare the results from the centralized heat sink with a circular path and the heat sink with fins, and the results showed that the temperature of the photovoltaic cell was 80°C, while with water cooling, the temperature was reduced to 60°C, and maintained good electrical efficiency. The average cooling water temperature of the single and multiple concentrator photovoltaic (CPV) pumps was also measured, and the results showed that installing 14 single CPV units above the cooling duct will increase the temperature. This allows connection to a single-stage absorptive heat pump for cooling needs. This research assessed the efficiency of a V-trough PV concentrator coupled with a buried heat exchanger (BHE) cooling system done by Elminshawy et al. (2019). A unique test rig was built and put to the test in Egypt, Port Said. The impact of cooling water was investigated at flow rates between 0.01 kg/s and 0.04 kg/s. At water cooling flow rates of 0.04 kg/s, the cooling system with a BHE successfully lowered the maximum panel surface temperature below 39.3°C. In comparison to that of the uncooled panel. As water mass flow rates increase, so does the electrical and thermal efficiency. To assess the cost of power per unit, an economic analysis was conducted. The suggested cooling system helped lower the world average CO_2 emissions by around 49,209 g CO_2/summer season, according to the data, which also indicated a 12.20% improvement in the relative levelled cost of energy.

Irwan et al. (2015) improved photovoltaic (PV) panel electrical efficiency in indoor tests. Solar radiation and operating temperature are two environmental parameters that affect how well a PV panel performs. Due to an increase in operating temperature, these climatic conditions will reduce the electrical efficiency of PV panels. The halogen lamp bulbs were raised using the solar simulator, which was mounted on a steel frame. Such as natural sunshine, the halogen lamp bulbs simulate it. At the test surface of the solar simulator, four sets of average solar radiation were recorded as 413, 620, 821, and 1016 W/m^2. To solve the issue of water flowing over the PV panel's front surface and low efficiency, a DC water pump was employed. One way to increase the effectiveness of a PV panel in maintaining a low operating temperature throughout its operation was through the use of a water-cooling mechanism. According to these experimental findings, using a water-cooling system and a variety of fixed solar radiation, a PV panel's working temperature may be reduced while its power production can be increased. Heat on the front of the PV panel can be minimized by reducing the water spraying.

The alternate cooling method for photovoltaic (PV) panels described in the study of Nižetić et al. (2016) involves misting water onto the panels' surfaces. To evaluate the entire water spray cooling effect on the PV panel performance under conditions of peak solar irradiation levels, an alternate cooling approach was used to concurrently cool both sides of the PV panel. The devised cooling solution for the PV panel was tested in a place with a typical Mediterranean environment after a special testing setup was carefully installed. According to their experimental findings, utilizing the suggested cooling strategy under conditions of peak solar irradiation can result in maximum overall increases of 16.3% effective 7.7% in electricity power production and 14.1% effective 5.9% in PV panel electrical efficiency. Furthermore, it was also able to lower panel temperature in the event of simultaneous front and backside PV panel cooling from an average of 54°C (non-cooled PV panel) to 24°C (cooled PV panel). The suggested water spray cooling method's economic viability was also evaluated. The major benefit of the examined cooling method was related to the PV panel's surface and its self-cleaning effect, which also serves as a boost to the average provided electricity.

Rahimi et al. (2014) investigated how coolant flow distribution affects PV cell cooling. This was accomplished by contrasting the cooling capabilities of two alternative PV cell-integrated microchannel systems. A single-header and a multi-header microchannel with an equal hydraulic diameter of 0.667 mm were used. Water was employed as a working fluid for cooling and using a range of coolant flow rates. The heat removed by the multi-header microchannel was around to be 19% more than that of the single-header microchannel when the heat transfer enhancement from these layouts was evaluated. Additionally, the results demonstrated a 28% increase in electrical power generation for the multi-header microchannel compared to the single-header microchannel. The overall findings support the impact of coolant distribution on the efficiency of PV cell cooling.

Soliman & Hassan (2019) conducted an analysis using ANSYS, where a three-dimensional model for the cooling of photovoltaic cells was constructed. Increasing the cooling results in increased electrical efficiency, output power, and a significant reduction in temperature. Increasing the variety of ratios from 1 to 7 enhances the net photovoltaic energy by approximately 100.6%, 83.2%, and 58.1% for four-pass, two-pass, and parallel flow meters, respectively, at Re of 5. The maximum photovoltaic temperature was reduced, the temperature difference on the photovoltaic surface was increased, and the photovoltaic efficiency was increased when using SiC nanoparticles with the cooling water inside MICs. When used in parallel flow, the nanoparticles increase the net photovoltaic energy compared to water without SiC particles by approximately 9.2% and 2.6%.

Stropnik & Stritih (2016) used numerical methods to investigate how the mass flow rate, channel height, inlet water temperature, and solar radiation intensity affect the heat transfer properties of the cooling channel and the overall system performance. A 3D model was created for a water-cooled PV/T system with a cooling channel, where the photovoltaic panel was positioned on top of the channel. The energy and exergy efficiencies of the PV/T system were computed, in addition to the Nusselt numbers for the upper and lower surfaces of the cooling channel. The results showed that heat transfer by thermal conduction from the bottom surface consistently outperformed the top surface, and a reverse correlation was observed between the Nusselt numbers for the bottom and top surfaces along the flow direction. Royne & Dey (2007) used jet impingement in their study with a cooling device on it under high concentration, by using water in a normal way to the surface. This test was used in Australia, and the results showed an increased efficiency by 1 and 3.1% at a temperature difference of 50. Kordzadeh (2010) increased the electrical efficiency by reducing the operating temperature, through the use of a thin layer of water that is produced directly from the pump, and this layer is on the top surface of the photovoltaic panel. Barrau et al. (2011) used hybrid jet microchannel cooling with high concentration, this way reduced op pressure in hyper design and was more efficient than micro design. Ibrahim et al. (2023) introduced the natural convection method depending on numerical approaches. According to cooling the PV panels using the proposed model the gap of wide air in PV increased from 5 cm to 70 cm to achieve significant progress, the results showed an increase the efficiency of about 9 – 12%. Bahaidarah et al. (2013) tested the performance of PV installed in hot spots such as Dhahran in Saudi Arabia. It introduced water cooling by a heat exchanger on its shallow surface. The study resulted in a 9% increase in efficiency and a 20% reduction in temperature.

Chandrasekar et al. (2013) used a cotton wick structure to develop for PV standalone by using passive cooling, its benefits were reducing the temperature, and thermal degradation. This technique was used in the middle of the operation. The efficiency was 9.5-9.7% using a wick structure with Al_2O_3 and reached 10.4% when using wick and water. The temperature range was 37-65°C, Hamdan et al. (2017) conducted a water application for solar panel cooling using sprinklers to start cooling the panels when they reached the highest temperature reducing their electrical power. In their experimental result temperature reduction by 10°C when operated for 5 minutes, increasing the efficiency by 12.5%. Najafi & Woodbury (2013) used a new photovoltaic cooling design which is Peltier which is a thermocouple attached to the back of the photocell, which gave good control over the temperature of the photocell. Their result showed an energy increase of about 80% when the cell temperature was 298 K instead of 360 K which showed the benefit of photovoltaic cooling.

Zhao & Tan (2014) investigated Photovoltaic cells cooled by thermoelectricity have many advantages such as low weight, high reliability, and temperature difference of about 20°C. Alizadeh et al. (2018) used the heat exchanger to maintain the temperature of PV cells, and it was attached to the rear face of PV panels. The enclosure has an outlet and inlet in which fluid flows in it, this will increase output power by 12-20% and increase electric performance by 9%. Aldihani et al. (2014) conducted in Kuwait, which suffers from dust and storms, used silicon cells of PV panels and cooled them with water, this method reduced the temperature by 20K and increased the output power from 150 W to171 W. Abdulgafar et al. (2007) used water immersion method to cool and improve the efficiency of the polycrystalline solar panels, and they showed an increase in efficiency to about 11% at a depth of 6 cm of water.

2.9.3 Nanofluid

Karami & Rahimi (2014) carried out experimental work to determine how well water-based nanofluid containing trace amounts of nanoparticles cooled the channels. Straight and helical channels were both used in the fabrication of the channels. The straight channel was made up of 23 parallel rectangular channels, each measuring 24.5 cm in length, 5 mm in width, and 3.5 mm in depth. The hydraulic diameter of the straight channel was 4.1 mm. The plate was separated into four symmetrical pieces for the helical arrangement, each of which has a helical channel with dimensions of 5 mm in width, 3.5 mm in depth, and 4.1 mm in hydraulic diameter. Nanofluid cooling performance was examined and the findings were obtained for the average temperature and electrical output of the PV cell. It was found that the average PV cell temperature reduced more dramatically as a result of the nanofluid than it did as a result of ter. For 0.1 weight percent (the best scenario), there were around 39.70% and 53.76% for the helical and straight channels, respectively, at a flow rate of 80 mL/min. Furthermore, with nanofluid concentrations of 0.1 weight percent in both channels, the greatest drop in average temperature about the reference temperature was noted. This resulted in the maximum electrical efficiency of approximately 20.57% and 37.67% for the straight and helical channels respectively. To compare the effectiveness of the channels under study, power-hydraulic performance was also specified. The outcomes demonstrated that the helical channel operates more effectively than the straight one.

Ebaid et al. (2018) employed a nanofluid cooling system in conjunction with the photovoltaic back-surface cooling channel. The tests used two distinct aluminium oxide Al_2O_3 nanofluid concentrations (i.e. 0.05 wt% and 0.1 wt%) in cooling channels with a height of 5 cm. Amphoteric aluminium oxide was a white, doorless powder that was employed in several chemical, commercial, and industrial applications. The experiments have been made for three different volumetric flow rates (i.e. 1 L/min, 1.5 L/min, and 2 L/min). A nanofluid cooling system's potential to boost solar panels' efficiency has been studied. To enhance the cooling performance of the PV modules, experiments have been conducted under various circumstances. The greatest photovoltaic efficiency was demonstrated by the cooling channel with 0.1 weight percent aluminium oxide and a volumetric flow rate of 2 L/min. The highest temperature that the uncooled PV module experienced was 67°C. Thus, utilizing the nanofluid coolant resulted in a 38% drop in temperature and an increase of 9.6% in power production. Radwan et al. (2016) established a new cooling method for low-concentration thermal photovoltaic (LCPV/T) systems. By utilizing a microchannel and nanofluid heat sink. The cooling mediums utilized in their work were nanofluids made of silicon carbide (SiC) and aluminium oxide (Al_2O_3) with varying volume percentages. At various concentration ratios, the effects of cooling mass flow rate and nanoparticle volume fractions on the functionality of the LCPV/T system were examined. A complete model was created that combines a thermodynamic two-phase flow model of the microchannel heat sink with a thermal model for the photovoltaic layers. To calculate performance factors such as the temperature of the solar cells and their electrical and thermal efficiency, the model was numerically simulated. Results showed that employing nanofluid s rather than water alone results in a considerable reduction in solar cell temperature, especially at high concentration ratios. The SiC-water nanofluid reduces the temperature of the cell more effectively than the Al_2O_3-water nanofluid. Both SiC-water and Al_2O_3-water nanofluid significantly lower cell temperature by increasing the volume percentage of nanoparticles. As a result, using nanofluid s increases the electrical efficiency of solar cells, especially at lower Reynolds numbers (Re) and greater concentration ratios. The concentration ratio affects how much a nanofluid affects thermal efficiency. Additionally, when the Reynolds number and nanoparticle volume percentage rise, they increase the friction power. The net electrical power rises at high concentration ratios as the volume percentage of the nanoparticle grows, but the thermal power falls. According to their study, using nanofluid s as a cooling approach was beneficial, especially at high sun concentration ratios when the temperature of the solar cell drops to 38°C and electrical efficiency increases by up to 19%. Xu & Kleinstreuer (2014), used nanofluids for cooling and heating PV systems because this technology can increase the efficiency and electrical power by diluting nanoparticles that stay in the liquids which will increase the overall efficiency and maintain the 70% of energy if the outlet temperature was set up to 62^{o}C.

2.9.4 Other coolants

Bayrak et al. (2020) investigated experimental studies of several photovoltaic (PV) panel cooling techniques were done. The cooling techniques used were phase change material (PCM), thermoelectric (TE), and aluminium One which was frequently used for cooling PVs. While the other PCM has a melting point that was higher than the surface temperature of the PV panel. Surface temperatures and output powers of PV panels were tested utilizing TE material in varied numbers 6, 8, and 12 and aluminium fins in different patterns. It has been noted that improperly chosen PCMs have insulating features that increase the temperature of the PV panel and reduce the output power. The PV with fin system provided the maximum output power of 47.88 W when the most effective cooling techniques were evaluated in the same climatic circumstances, while the PV with PCM and TEM generated the lowest power production of 44.26 W. Verified by Hasan et al. (2016) a method for using the thermal energy that was stored in the PCM behind the PV for applications including household water heating. To provide heat during peak water heating demand hours, the system was tested in the UAE's winter climate. The suggested system recovered 41% of the thermal energy relative to the incoming solar radiation and increased PV electrical conversion efficiency by 1.3%.

Bai et al. (2016) compared the monocrystalline solar modules with and without cooling. This research focuses on the effects of cooling techniques for photovoltaic modules that employ coolant and sprinklers on real performance, cooling time, and cooling impact speed. The resulting results were examined from both a technical and an economic perspective. Based on the characteristics of the regression model employed in the study of 0.61, it can be shown that air temperature in the investigated range of 18-29^{o}C enhances real performance by 1.58 W, and cooling was likely required at higher temperatures. The projected performance was 9.8 W lower on average (P of 0.001) on days with greater clouds.

Rahimi et al. (2015) proposed a combination of solar and wind energy as renewable energy sources for more effective electrical energy production. To cool down a photovoltaic (PV) cell, a lab-scale cooling mechanism based on a conic wind-collecting tunnel was created. Two methods were served by the conic wind tunnel together; the first was to serve as a cooling for solar cells. Second, it was used to create electrical energy using a specially-made turbine. This study focuses on the enormous potential of the suggested cooling system on PV cell performance. According to the data, both the electrical energy generation from PV cells and turbines boosted the overall output power by 36%. CFD simulation based on the moving reference of the frame the (MRF) computational fluid mechanics approach was used to explain the reported results. To assess the impact of the turbine blade in terms of the airflow redirected to the PV cell, the flow distributions in two modes (with and without the turbine) were compared. Micheli et al. (2015) studied state-of-the-art micro-fin research. According to his findings, the micro-fins can reduce system weight while also providing better thermal performance than a traditional heat sink. Because they lessen the stress on the tracker, they were especially advantageous for tracked systems such as constricting photovoltaic (CPV). The performance of a micro-finned CPV system in natural convection was predicted using the heat transfer coefficients obtained from an experimental setup; it was discovered that an optimized fin array may increase mass-specific power by up to 50% compared to an unfanned surface.

Mojumder et al. (2016) investigated experimental work using a PV/T air-based collector system with several thin rectangular fins installed to dissipate heat from the solar panel. The system was operated under natural weather conditions, and temperatures were measured at various locations on the top and back of the solar panel.

A mathematical model was developed using these results to calculate the thermal and electrical efficiency of the proposed PV/T system. For different fins, the highest thermal efficiency and photovoltaic efficiency were about 56.19% and 13.75%, respectively, at a mass flow rate of 0.14 kg/s and solar radiation intensity of 700 W/m^2. Along with discussing uncertainty figures, the squared percentage of the root mean deviation and the correlation coefficient as also used to verify the validity of the result. Moradgholi et al. (2014) presented in their work, a (PV/T) hybrid system by choosing a heat pipe (thermosyphon type) to absorb isothermally the extra heat from solar PV cells. Both spring and summer seasons were used to research photovoltaic/thermal systems. In the spring, the systems were set at a 30° angle, and methanol was utilized as the thermosyphons' working fluid. During the testing, the photovoltaic/thermal system produced 5.67% more electrical power than the ordinary photovoltaic system. Furthermore, the thermal efficiency of the photovoltaic/thermal system was 16.35% higher on average. Acetone was employed as the working fluid and the systems were installed at a 40° angle in the summer. The photovoltaic/thermal system produced 7.7% more electricity on average throughout the testing than the solar system alone, and its approximate thermal efficiency was 45.14 percent. The panel temperature reduced significantly up to 15°C as a result of the suggested state-of-the-art, and more electrical power was produced. The results of their experimental investigation provided credence to the notion of applying heat pipe technology to solar power generation to increase efficiency and obtain thermal energy. It was uncommon to employ cylindrical pin fin heat sinks to cool a panel,

Rajput & Yang (2018) conducted this study and compared the results to those of a conventional single-channel PV/T collector. In his investigation, an older 20-watt polycrystalline solar cell photovoltaic panel with a typical efficiency of 11.7% was heated up by an interior halogen light with an intensity of 1378.4 W/m^2. A cylindrical pin fin heat sink was used to reduce the temperature from 81 to 72°C temperature at the front and 88.6°C. The collector arrangement was a channel with an aspect ratio of α* of 0.08 that was fastened to the back of the panel. Temperatures declined to 47.9°C while using the collector and 58.4°C when utilizing the heat sink. According to his investigation, the heat sink and PV/T collector naturally increase the heat flow of 667.2 W/m^2 at the back of the panel with no cooling by 30 to 41.5%. He highly advised doing investigations of cooling the panel in the presence of no wind and utilizing cylindrical pin heat sinks. Sahay et al. (2015) in Bhopal, India, studied the Ground-Coupled Central Panel Cooling Technology (GC-CPCS), using a novel system for cooling solar PV panels. This study examines the performance of the recently developed Ground-Coupled Central Panel Cooling System and other Solar PV panel cooling systems (GC-CPCS). The research was distinctive in three respects. The idea of central cooling for solar PV panels was first introduced. Second, a Ground Coupled Heat Exchanger was employed in a Solar PV Panel Cooling System for the first time. Third, the testing was carried out in real-world conditions with sun irradiation.

Wu et al. (2018) conducted a cooling medium with a temperature lower than the ambient temperature, allowing for greater and reverse heat transfer where heat was transferred to the cooling medium. Comparing thermal efficiency and electrical efficiency, both thermal and electrical efficiency undergo larger changes when the channel height was 5mm and the mass flow rate was 0.003 kg/s. The overall energy efficiency of the system reached its highest level. Additionally, the performance of the current system was evaluated with cooling and compared to the previous system without cooling, leading to some outstanding results. Chandrasekar & Senthilkumar (2015) used a new way in this study by applying moist cotton wicks to PV panels for cooling. It was used in India, and it showed a reduction in temperature by 12% and increasing the electrical yield by 14%. This study was done in India. (Ma et al., 2015), this study helped with increasing the efficiency of PV using thermal regulation, by using PCM in the solar thermal system. This system can be used to absorb heat from PV panels and discharge that PCM stored heat. This test gave enhancement in output electricity by 9% and an increase in thermal efficiency by 12%, this experiment was conducted in China.

2.9.5 Machine learning

This collection of studies encompasses various aspects of predictive modelling, machine learning, and forecasting techniques applied to diverse domains, particularly in the context of renewable energy, with a specific focus on photovoltaic (PV) systems. Fawaz et al. (2019) presented a comprehensive review of deep learning for time series classification, offering a broader understanding of the applications of deep learning techniques in handling temporal data. Bongiorno et al. (2022) explored the use of machine learning for interpreting electrochemical impedance spectroscopy data. Although the focus is on a different application, the evaluation of training dataset size provides valuable insights applicable to machine learning studies.

Moving into the realm of PV systems, Guo et al. (2024) evaluated probabilistic methods, including bootstrap and quantile regression, for quantifying PV power point forecast uncertainty. This study contributes to understanding and improving the accuracy of PV power forecasting. Markovics et al. (2022) introduced a comparison of machine learning methods for photovoltaic power forecasting based on numerical weather prediction is conducted. The study focuses on assessing the performance of different machine-learning techniques for PV power forecasting.

Eseye et al. (2018) introduced a short-term PV power forecasting technique using a hybrid GA-SVM (Genetic Algorithm-Support Vector Machine) approach. This hybrid technique aims to enhance the accuracy of short-term PV power predictions. Carriere et al. (2019) proposed a novel approach for seamless probabilistic photovoltaic power forecasting covering multiple time frames. This approach contributes to the development of more robust and accurate forecasting methods for varying time horizons. In summary, these studies collectively contribute to advancing the understanding and application of predictive modelling, machine learning, and forecasting techniques in diverse domains, with a specific emphasis on enhancing the efficiency and accuracy of photovoltaic power forecasting.

2.9.6 Summary of the previous studies

In this comprehensive section, were delved into an extensive exploration and survey of various cooling options available for solar panels. The insights drawn from a thorough review of previous literature shed light on the effectiveness and feasibility of different cooling approaches, encompassing water, oil, gases, phase change materials, and nanofluids. A critical scientific analysis of these options has been accurately conducted, enabling us to discern their strengths and limitations. The papers referenced cover a wide range of research topics related to the cooling and performance enhancement of photovoltaic (PV) systems. Some common themes and findings can be observed across these studies:

Cooling Techniques: Various cooling techniques have been explored, including passive cooling methods such as natural convection, forced convection, and jet impingement, as well as active cooling methods utilizing heat pipes and phase-change materials. These methods aim to reduce PV cell temperatures, improve electrical efficiency, and extend the lifespan of PV modules.

Nanofluids and PCM: Several studies investigate the use of nanofluids (fluids with nanoparticles) and phase-change materials (PCMs) to enhance heat transfer and cooling performance. Nanofluids show promise in improving the thermal conductivity of cooling fluids, while PCM can absorb and release latent heat to regulate PV cell temperatures. PV/T Systems: Some research focuses on combined PV/thermal (PV/T) systems that integrate PV modules with solar thermal collectors. These systems allow for simultaneous electricity and thermal energy generation, providing more efficient use of solar energy.

Simulation and Modelling: Computational simulations and mathematical modelling are widely used to analyse and optimize cooling strategies. Techniques such as Computational Fluid Dynamics (CFD) are employed to study fluid flow and temperature distribution on the PV surface. Experimental Studies: Many papers include experimental investigations to validate theoretical results and assess the performance of cooling methods under real-world conditions. Outdoor testing and field studies are common to evaluate cooling efficiency in varying climates. Overall, the research in this area aims to optimize PV system performance, increase electrical efficiency, and extend the lifespan of PV modules through innovative cooling methods. By addressing the thermal challenges associated with PV systems, these studies contribute to advancing the integration of renewable energy sources into the global energy mix. Cooling systems for solar panels are broadly categorized into two main approaches: passive and active cooling. The passive cooling method involves utilizing natural convection and radiation to dissipate heat from the solar panels without the need for external mechanical devices.

Moreover, passive cooling involves circulating a fluid (liquid or gas) without the need for mechanical or electrical equipment. Techniques like air-cooling using fins and phase change materials (PCM) were examples of passive cooling methods. However, passive cooling had limitations in its ability to remove a significant amount of heat efficiently.

On the other hand, active cooling utilizes mechanical or electrical equipment, such as pumps or fans, to circulate the cooling fluid. This method proved highly effective in removing a considerable amount of heat, and the associated equipment was relatively affordable. A variety of active cooling methods were identified, including air cooling, immersion, heat pipes, water spray, solar chimneys, and the use of nanofluids.

Water emerged as an excellent cooling medium due to its thermophysical properties, including strong thermal transmittance coefficients with metals, and its cost-effectiveness. Employing a water-cooling system helped reduce the temperature of photovoltaic cells, resulting in higher overall efficiency. Oils were also commonly used as coolants due to their ability to function over a wide range of temperatures and low-pressure conditions. However, their flammability posed a significant disadvantage. Gases, although suitable for cooling in high-temperature and high-pressure environments, had relatively low heat capacity and required substantial energy to circulate effectively. Air, another cooling option, was not as efficient as water, often requiring additional techniques like cooling fins for optimal performance. Air-cooling could be achieved through forced or natural convection, with fans used for forced convection and fins for free convection. While air cooling reduced the temperature modestly, using phase change materials (PCM) could achieve a more substantial reduction of up however, the performance of PCM cooling was limited in high-temperature environments.

The immersion method proved highly effective in reducing the temperature by over 20 degrees Celsius. Still, it did have some drawbacks, such as issues with the refraction of radiation and challenges in reaching the solar cell. Additionally, water evaporation during the immersion process was a significant concern. Spraying water on the front surface of the solar panel was found to significantly reduce the temperature, but it led to substantial water evaporation. Cooling with nanofluids was more effective than water alone, but it came at a higher cost. Notably, porous media emerged as a significant technology for cooling in general, showing effectiveness in reducing temperatures when compared to cooling with air alone.

After conducting an extensive literature review, it is evident that the choice of cooling fluid and method plays a crucial role in enhancing the efficiency and performance of solar panels. The exploration of innovative cooling solutions, such as porous media, holds promise for even greater advancements in solar panel cooling and renewable energy utilization as a whole.

2.9.7 Disadvantages of cooling methods

The current cooling methods employed for photovoltaic (PV) systems, including cooling by spraying water on the front surface, the immersion method, the use of phase change materials (PCMs), nanofluids, and the use of flammable materials such as oils, exhibit several disadvantages. Here are the drawbacks associated with each of these cooling methods:

2.9.7.1 Cooling by spraying water on the front surface

Water Evaporation: One of the primary drawbacks of this method is water evaporation, which can lead to the consumption of significant amounts of water, especially in arid regions. This not only adds to water usage but also necessitates regular refilling of water reservoirs, increasing maintenance efforts and costs. Potential for Panel Damage: Continuous exposure to water can pose risks of damage to the surface of solar panels over time, potentially affecting their efficiency and longevity. Challenges in Water Management: Managing water flow and distribution across the surface of solar panels can be challenging, particularly in large-scale PV installations. Uneven distribution or excess water accumulation may result in inefficient cooling and potential water wastage.

2.9.7.2 Immersion method

Refraction of Radiation: Immersing solar panels in water may lead to issues with the refraction of solar radiation, affecting the amount of sunlight reaching the photovoltaic cells. This can result in reduced energy output and overall efficiency of the PV system. Water Evaporation and Loss: Similar to spraying water on the front surface, the immersion method also suffers from water evaporation, leading to water loss and the need for regular replenishment. This can be particularly challenging in regions with limited water resources.

2.9.7.3 Nanofluids cooling

Using nanofluids as cooling fluids for photovoltaic cells may face some drawbacks and challenges, including production and Material Costs: Nanofluids can be costly to produce and use compared to traditional cooling fluids. Specialized nanomaterials and advanced production processes may incur additional costs, raising the overall operating expenses of the photovoltaic system. Resource availability and sustainability some nanomaterials required for producing nanofluids may be rare or not available in sufficient quantities, which can affect the sustainability of the process and its ability to meet the growing demand for that technology. Cooling effectiveness and performance stability, nanofluids may encounter challenges in cooling effectiveness and long-term performance stability. The actual cooling impact of nanofluids may not be guaranteed, and some types may experience performance degradation over time or under certain operating conditions. Environmental and safety concerns, the use of nanofluids may raise issues related to environmental and health safety, especially concerning the disposal or discharge of the used fluids into the environment. Some nanomaterials may possess potential toxicity, and their environmental impact may not be sufficiently understood.

Selection of suitable nanomaterials, choosing the appropriate nanomaterials for cooling photovoltaic cells requires extensive studies to verify the effectiveness and safety of those materials. Chemical reactions between nanofluids and other materials in the system may pose an additional challenge that needs to be considered. Environmental conditions impact, environmental factors such as temperature and humidity can significantly affect the effectiveness of nanofluids as a cooling medium, making their use unsuitable in some extreme environmental conditions. Nanoparticle effects, nanoparticles used in nanofluid formulations may raise concerns about health and environmental safety, as these particles may leak into the environment or react undesirably with other substances.

2.9.7.4 Flammable materials

Use of Flammable Materials such as oils, commonly used as coolants for their ability to function over a wide range of temperatures, pose safety risks due to their flammability. Accidental leaks or spills of oil-based cooling systems can lead to fire hazards and environmental contamination. Maintenance Challenges: Managing and maintaining oil-based cooling systems requires careful monitoring to prevent leaks and ensure proper functioning. This can entail additional costs and resources for inspection, maintenance, and cleanup efforts.

In addition to the specific drawbacks outlined above, all cooling methods for PV systems may face common challenges such as energy consumption, space constraints, installation complexity, and performance limitations under extreme environmental conditions. Overcoming these disadvantages request.

2.9.7.5 Cotton wick structures

The use of cotton wick structures for cooling photovoltaic (PV) systems may pose several shortcomings, limited heat transfer efficiency, cotton wick structures may have limited heat transfer efficiency compared to other cooling methods. While they can absorb and transport water through capillary action, their ability to effectively dissipate heat from PV panels may be constrained, leading to suboptimal cooling performance. 2. Susceptibility to environmental conditions, cotton wick structures may be susceptible to environmental factors such as temperature fluctuations, humidity levels, and exposure to sunlight. Extreme conditions could degrade the structural integrity of cotton wicks over time, reducing their cooling effectiveness and lifespan. Potential for Contamination: Cotton wick structures may accumulate dirt, dust, and other contaminants over time, which can hinder their ability to absorb and transport water effectively. Contaminants could clog the capillaries within the cotton wicks, impeding water flow and compromising cooling efficiency. Maintenance Requirements: Maintaining cotton wick structures may require regular cleaning and replacement to ensure optimal performance. Periodic maintenance tasks could add to the overall operational costs and labor requirements of PV systems employing this cooling method. Limited scalability, scaling up the use of cotton wick structures for cooling large-scale PV installations may present logistical challenges. Ensuring uniform water distribution and consistent cooling across a large surface area could be difficult to achieve with cotton wick-based cooling systems. Evaporation Losses: Water absorbed by cotton wick structures may be subject to evaporation losses, especially in hot and dry climates. Evaporation can lead to a reduction in the amount of water available for cooling, potentially diminishing the cooling efficiency of the system. Compatibility with PV Panel design, integrating cotton wick structures into the design of PV panels may require modifications or additional components, which could impact the overall aesthetics, functionality, and cost-effectiveness of the solar installation. Long-term durability, the long-term durability of cotton wick structures in outdoor environments, exposed to sunlight, moisture, and temperature variations, may be a concern. Degradation of the cotton material over time could affect its performance and longevity as a cooling solution for PV systems.

2.9.7.6 Phase change materials (PCMs)

The utilization of phase change materials (PCMs) for cooling photovoltaic (PV) systems presents several shortcomings: 1. Limited temperature range, phase change materials have specific phase transition temperatures at which they absorb or release latent heat. This restricts their effectiveness to a narrow temperature range around the phase transition temperature. Outside of this range, their cooling capacity diminishes, limiting their applicability in environments with fluctuating or extreme temperatures. 2. Thermal conductivity, while phase change materials have high latent heat storage capacity, their thermal conductivity may be relatively low compared to other cooling fluids. This can result in slower heat transfer rates, especially during the phase transition process, leading to longer cooling times and reduced efficiency in dissipating heat from PV panels. 3. Volume expansion, phase change materials undergo volume expansion upon transitioning from solid to liquid state, which can pose challenges in system design and integration. Accommodating this expansion requires additional space within the cooling system, increasing complexity and potentially limiting the scalability of PCM-based cooling solutions. 4. Limited reusability, repeated cycling between solid and liquid states can degrade the physical properties of phase change materials over time, reducing their effectiveness and lifespan. Degradation mechanisms such as phase separation, crystallization, and thermal degradation may occur, leading to diminished performance and the need for periodic replacement of PCMs. 5. Sensitivity to ambient conditions, the performance of phase change materials is influenced by ambient temperature, humidity, and solar radiation levels. Variations in these environmental factors can affect the phase transition behaviour and thermal properties of PCMs, impacting their cooling efficiency and reliability in different operating conditions. 6. Compatibility with system components, integrating phase change materials into PV cooling systems requires compatibility with system components such as heat exchangers, pumps, and storage tanks. Selecting materials that are chemically and mechanically compatible with PCMs is essential to prevent corrosion, leakage, or other system failures. 7. Cost and availability, the cost of phase change materials, especially high-performance PCMs with tailored thermal properties, may be relatively high compared to conventional cooling fluids. Additionally, the availability of suitable PCMs in large quantities for commercial applications may be limited, restricting their widespread adoption in PV cooling systems.

2.9.7.7 Single-turn pulsating heat pipes (PHPs)

The utilization of single-turn pulsating heat pipes (PHPs) for cooling photovoltaic (PV) systems presents several shortcomings: 1. Limited heat transfer capacity, single-turn PHPs may have limited heat transfer capacity compared to other cooling methods such as water-based systems or heat pipes with multiple turns. This limitation can restrict their ability to effectively dissipate heat from PV panels, especially in high-temperature or high-power-density applications. 2. Sensitivity to orientation: single-turn PHPs are sensitive to orientation, and their performance may vary depending on the PV panel's orientation relative to the gravitational field. This orientation dependency can lead to uneven heat distribution and cooling inefficiencies, particularly in installations with non-horizontal panel orientations or variable tilt angles. 3. Operational instability: single-turn PHPs may exhibit operational instability, characterized by intermittent fluid flow and vapor blockage phenomena. These instabilities can disrupt heat transfer within the PHP, leading to temperature fluctuations and reduced cooling performance. Achieving stable and reliable operation of single-turn PHPs under varying operating conditions can be challenging. 4. Limited scalability: the scalability of single-turn PHPs may be limited due to their compact design and single-loop configuration. Scaling up PHP-based cooling systems to accommodate larger PV arrays or higher heat dissipation requirements may require multiple PHP units, increasing system complexity, cost, and space requirements.

2.9.7.8 Air cooling

Air cooling, while widely used due to its simplicity and relatively low cost, presents several shortcomings when employed as the primary cooling method for photovoltaic

(PV) systems: 1. Limited heat dissipation efficiency: air has lower thermal conductivity compared to other cooling fluids like water or oils. As a result, air cooling may not efficiently dissipate heat generated by PV panels, especially under high solar radiation or ambient temperature conditions. This can lead to increased operating temperatures of the PV cells, potentially reducing their efficiency and lifespan. 2. Ineffectiveness in high ambient temperatures: in regions with high ambient temperatures, air cooling may struggle to sufficiently lower the temperature of PV panels to optimal levels. This is particularly problematic during peak sunlight hours when solar irradiance is highest, exacerbating heat buildup on the panel surfaces. As a consequence, the performance of the PV system may be compromised, and the risk of thermal degradation of solar cells increases. 3. Dependency on natural convection: air cooling systems typically rely on natural convection for heat transfer, which may be insufficient to remove heat efficiently, especially in stagnant or low airflow conditions. Without adequate airflow, the convective heat transfer coefficient decreases, impeding the cooling process and leading to higher operating temperatures of the PV modules.

Table 2.1 provides a comprehensive overview of various cooling strategies that have been rigorously explored and applied in the context of photovoltaic cell cooling. This compilation represents a summary of extensive research efforts conducted by experts and scientists in the field. The quest for efficient cooling solutions for photovoltaic cells has been driven by the crucial need to maintain optimal cell performance, improve energy conversion efficiency, and extend the overall lifespan of solar panels. The strategies enlisted in Table 2.1 encompass a wide spectrum of cooling techniques, each tailored to address specific challenges and environmental conditions.

2.9.8 Summary of methodology of previous studies

The reviewed works use a variety of methodologies to investigate the cooling methods used or the shortcomings of current cooling methods for PV systems. The methodologies can be summarized as follows:

1. Literature review: the studies began with a comprehensive review of the existing literature on cooling technologies for PV systems. This includes examining previous research, case studies, and experimental data to identify common challenges and limitations associated with current cooling methods.

2. Experimental studies: many of the works reviewed involve experimental investigations conducted in laboratory settings or real-world environments. These experiments involve testing different cooling system strategies, materials, and configurations to evaluate their effectiveness in reducing photovoltaic cell temperatures and improving energy production.

3. Simulation and modelling: computer simulations and mathematical modelling are widely used to analyse the thermal behaviour of solar panels and evaluate the performance of cooling solutions. Techniques such as computational fluid dynamics (CFD) and finite element analysis (FEA) are used to simulate heat transfer, fluid flow, and temperature distribution inside PV modules.

4. Performance evaluation: the performance of cooling methods is evaluated based on various metrics, including temperature reduction, energy production, efficiency

improvement, and system reliability. Experimental data and simulation results are analysed to determine the effect of cooling on the overall performance of PV systems.

5. Comparative analysis: many studies conduct comparative analyses to compare different cooling technologies or materials. This includes evaluating the drawbacks of each method in terms of cost, energy saving, environmental impact, and practical feasibility.

6. Verification and verification: to ensure the validity and reliability of the results, verification and validation procedures are often used. This may include comparing experimental data to theoretical predictions, validating simulation models with experimental data, and performing sensitivity analyses to evaluate model accuracy.

Table 2.1: A comprehensive overview of the different cooling strategies

Researcher	Cooling Method	Liquid Used	Results
Bilen & Erdoğan (2023)	Comprehensive review	-	Effects of cooling on the performance of PV/T solar panels
Gao et al. (2023)	Passive evaporative cooling	-	Passive evaporative cooling strategy to enhance electricity production in hybrid PV-STEG system
Hussien et al. (2023)	Experimental and numerical investigation	-	Experimental and numerical investigation for PV cooling by forced convection
Zhang et al. (2022)	Modelling	Back-mounted spray cooling	Modelling of a PV system by a back-mounted spray cooling section for performance improvement.

Table 2.1: Continued

Wu & Xioang (2014)	Water-cooled PV/T system	Water	Studied heat transfer characteristics and performance of a water-cooled PV/T system.
El Mays et al. (2017)	air-cooled PV/T system	Air	Improving Photovoltaic Panel Using Finned Plate of Aluminum. The primary objective of the study was to improve the efficiency of photovoltaic panels by increasing effective cooling and reducing operating temperature.
Elminshawy et al. (2019)	Buried water heat exchanger	Water	Experimental investigation of a V-trough PV concentrator integrated with a buried water heat exchanger.
Elminshawy et al. (2019)	Buried heat exchanger	Water	Performance of a buried heat exchanger system for PV panel cooling under elevated air temperatures.
Wu et al. (2018)	Heat sink and water type PV/T collector	Water	Compared heat sink and water type PV/T collector for cooling a PV panel.
Golzari et al. (2018)	Corona Wind	Air	Experimental investigation of the effects of corona wind on the performance of an air-cooled PV/T.
Alizadeh et al. (2018)	Single turn pulsating heat pipe	Water	Numerical simulation of PV cooling using a single turn pulsating heat pipe.
Al-Musawi et al. (2019)	Nanofluids and phase-change materials	Nanofluids	Numerical study of the effects of nanofluids and phase-change on PV

Table 2.1: Continued

Ma et al. (2015)	Phase change materials	Phase change materials	Using phase change materials in PV systems for thermal regulation and electrical efficiency improvement.
Özakin & Kaya (2019)	PV-heat spreader-microchannels system	Nanofluids	Evaluated the effect of heat spreader size, microchannel configuration, and nanoparticles on PV performance.
Micheli et al. (2015)	Plate micro-fins in natural convection	Air, Water	Investigated passive concentrating PV cooling using plate micro-fins.
Nižetić et al. (2016)	Water spray cooling	Water	Investigated the performance response of water spray cooling applied to a photovoltaic panel.
Sahay et al. (2015)	Ground-coupled central panel cooling system	Water, Air	Reviewed solar PV panel cooling systems with a ground-coupled central panel cooling system.
Krauter (2004)	Water flow over the front of photovoltaic panels	Water	Increased electrical yield via water flow over the front of photovoltaic panels.
Hasan et al. (2016)	Phase change materials	Phase change materials	Energy efficiency enhancement of photovoltaics by phase change materials through thermal energy recovery.
Badran et al. (2010)	Solar Electric Power Technologies	-	Evaluation of Solar Electric Power Technologies in Jordan. And increase outpower and electrical efficiency improvement

Table 2.1: Continued

Kabeel et al. (2019)	Reflector	-	Investigated the optimization cooling technique for improving PV module performance with reflectors.
Hafith et al. (2013)	Residential grid-connected PV system	-	Evaluated the feasibility of a residential grid-connected PV system under the Jordanian net metering law.
Chandrasekar et al. (2013)	Cotton wick structures	Water	Passive cooling of standalone flat PV module with cotton wick structures.
Bai et al. (2016)	Active and passive cooling techniques	Water	Investigated technical and economic effects of cooling PV modules under Hungarian conditions.
Mazón-Hernández et al. (2013)	Induced or forced air stream	Air	Improved electrical parameters of a photovoltaic panel using an induced or forced air stream.
Ebrahimi et al. (2015)	Natural vaporization	-	Experimented with natural vaporization for cooling a PV cell.
Bai et al. (2016)	Active and passive cooling techniques	Water	Investigated technical and economic effects of cooling PV modules under Hungarian conditions.

Table 2.2 presents a comprehensive comparison of various PV cooling methods, focusing on their respective effectiveness in reducing temperature and the resulting increase in output power. This table serves as a valuable reference, providing a clear

and concise overview of the performance of different cooling techniques for photovoltaic cells. Each method's ability to reduce the temperature of the solar panels is assessed, and the corresponding rate of increase in output power is quantified.

Table 2.2: Summary of a group of different types of PV cooling

Authors	Coolant	Reduction of temperature (°C)	Increase of output power %
El Mays et al. (2017)	Air	6	-
Lin et al. (2019)	Air	4	7
Tang et al. (2010)	Air	4.7	8
Mazón-Hernández et al. (2013)	Air	22	-
Micheli et al. (2015)	Air	13	7.7
Wu et al. (2018)	Air	12.5	-
Ebrahimi et al. (2015)	Air	20	
Amori and Al-Najjar (2012)	Air	16	
Herez et al. (2020)	Heat pipe cooling	14	--
Moradgholi et al. (2014)	Methanol	13	5
Karami & Rahimi (2014)	Nanofluids	18	
Al-Musawi et al. (2019)	Nanofluids	19	
Ebaid et al. (2018)	Nanofluied	20	9
Smith et al. (2014)	Water	11	6
Hasan et al. (2016)	PCM/ water	19	6
Bahaidarah et al. (2013)	Water	17	-
Rahimi et al. (2014)	Water	26	-

Table 2.2: Continued

Baloch et al. (2015)	Water	12	
Hachicha et al. (2015)	Water	7.7	
Irwan et al. (2015)	Water	15	
Wu & Xioang (2014)	Water	18.5	
Barrau et al. (2011)	Water	2	

2.9.9 Connection of literature to objectives

Objective 1: To reduce the operating temperature of the PV panel by using porous media cooling. Contributions from Kabeel et al. (2019): Investigated various cooling technologies, including forced-air cooling, water cooling, and combined forced-air and water cooling. Identified water cooling in the presence of reflectors as the optimal technology for lowering PV panel temperature. Provided quantitative results showing temperature reduction and increased electrical efficiency. To find the best porosity size and volume flow rates. Contributions from Liu et al. (2021): Explored the influence of total flow rates and cooling channel height on electrical efficiency, power, panel temperature, and Nusselt number. Offered insights into optimal thermal and electrical efficiency with specific channel height and water mass flow rate (5 mm and 0.03 kg/sec, respectively).

Objective 2: To investigate the effect of various parameters in PV cooling by porous media. Contributions from Stropnik & Stritih (2016): Utilized numerical methods to study the impact of mass flow rate, channel height, inlet water temperature, and solar radiation on the cooling channel. Analysed energy and exergy efficiencies of the PV/T system, providing valuable insights into parameter dependencies. To find quick and adequate results for PV temperature and output power. Contributions from Idoko et al. (2018): Demonstrated the rapid cooling effects of water on PV panels, achieving a reduction in temperature by more than 20%. Showed an increase in electrical efficiency by more than 3% and output power by 20.96W.

Objective 3: To formulate the empirical correlation for temperature and output power under different cooling conditions using porous media. Contributions from Soliman, and Hassan (2019): Conducted a numerical study using ANSYS to model the cooling of photovoltaic cells with various cooling ratios. Established correlations between cooling conditions and increased electrical efficiency, output power, and temperature reduction.

Additional Contributions: Contributions from Rahimi et al. (2015): Suggested the use of a multi-header microchannel design for enhanced PV panel cooling. Demonstrated an improvement of 28% in electrical power and a significant reduction in panel temperature. Contributions from Irwan et al. (2015): Introduced a unique method of using halogen lamps and water cooling to increase electrical efficiency. Showed a decrease in temperature and an increase in output power by 9-22%. Contributions from Sahay et al. (2015): Presented a low-cost ground central panel cooling system in India, contributing to increased PV panel efficiency. Overall Contribution:

The cited literature contributes to the thesis objectives by providing valuable insights, experimental results, and methodologies related to cooling technologies for photovoltaic panels. The studies cover a wide range of cooling methods, parameters, and their impacts on PV panel performance, aligning with the objectives outlined for porous media cooling. The findings from these sources contribute to the theoretical foundation and practical understanding needed to achieve the goals of the thesis.

2.10 Theory

This section delves into a comprehensive overview of heat transfer rates and porosity size calculations, which play a critical role in various engineering and scientific disciplines. Heat transfer rates are fundamental in understanding the flow of thermal energy between different mediums or surfaces. The ability to quantify how heat moves from one object to another is crucial in designing efficient thermal management systems, optimizing energy utilization, and ensuring the reliability and performance of various devices and processes.

Porosity size calculations are equally significant, particularly in porous materials and composite structures. Porosity size refers to the volume fraction of voids or pores within a material. It is a critical parameter that influences the material's thermal conductivity, mechanical strength, and overall performance. Porosity size calculations play a pivotal role in diverse applications, such as porous media heat exchangers, catalytic reactors, and filtration systems. Engineers utilize porosity size data to design and analyse the behaviour of porous materials under different thermal and mechanical conditions.

2.10.1 Heat transfer mechanism

Figure 2.15 provides valuable insights into the different mechanisms of heat transfer, showcasing three primary types: conduction, convection, and radiation. Each method plays a crucial role in the way heat is transferred between solid objects, liquids, and fluids.

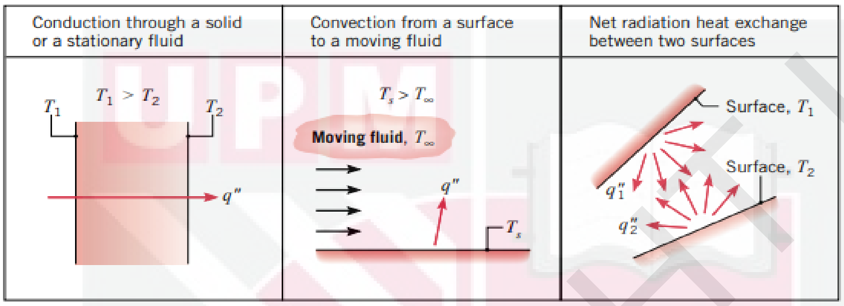

Figure 2.15: Conduction, convection, and radiation heat transfer
(Incropera & DeWitt, 2007)

2.10.1.1 Conduction heat transfer

The first mode of heat transfer is conduction, which occurs when heat is transmitted through a medium without any significant movement of the medium itself. This process is prevalent in solids, where thermal energy travels from one molecule to another through direct physical contact. Conduction is responsible for heat distribution within solid materials and plays a key role in maintaining temperature equilibrium. Through Fourier's law, it becomes possible to quantitatively calculate the energy transferred via thermal conduction, a fundamental process in heat transfer. This law is encapsulated in Equation 2.1, as introduced by (Incropera & DeWitt, 2007).

Equation 2.1 is a powerful tool that allows researchers and engineers to analyse and predict the rate at which thermal energy flows between two bodies in contact. The equation takes into account important parameters such as the temperature gradient (dT/dx) and the thermal conductivity (k) of the material through which the heat is being conducted. The temperature gradient represents the change in temperature per unit length, while thermal conductivity reflects a material's ability to conduct heat. By leveraging Equation 2.1 (Incropera & DeWitt, 2007), researchers can gain deeper insights into the mechanisms of thermal conduction, enabling them to optimize cooling systems for various applications. For instance, in the context of photovoltaic cells, understanding how heat is conducted within the materials helps in designing effective cooling mechanisms to dissipate excess heat and maintain optimal operating temperatures. This, in turn, enhances the overall efficiency and longevity of the solar cells.

$$\frac{\partial}{\partial x}\left(k\frac{\partial T}{\partial x}\right)+\frac{\partial}{\partial y}\left(k\frac{\partial T}{\partial y}+\right)+\frac{\partial}{\partial z}\left(k\frac{\partial T}{\partial z}\right)+q_v=\rho C_P\frac{\partial T}{\partial t} \quad 2.1$$

When the heat transfer is in one direction, the equation is written as follows:

$$q''_{cond}=-k\frac{dT}{dy}=k\frac{T_1-T_s}{L} \quad 2.2$$

The heat flux q'', k is the thermal conductivity of the material for which the retransfer will be calculated and L is the thickness of the material.

2.10.1.2 Convection heat transfer

The second mode, convection, involves the transfer of heat between a solid surface and a fluid that is in motion. This motion facilitates the movement of heated particles away from the solid surface, replacing them with cooler particles. Convection is commonly observed in liquids and gases, such as air currents carrying warmth from a heated surface to the surrounding environment (Incropera & DeWitt, 2007).

Equation 2.3 represents a pivotal tool for quantifying convective heat transfer, a fundamental process in the transfer of thermal energy. With this equation at our disposal, we gain the ability to analyse and predict the rate at which heat is exchanged between a solid surface and a moving fluid, such as air or water.

In Equation 2.3 (Incropera & DeWitt, 2007), key parameters come into play to determine the convective heat transfer coefficient (h). This coefficient encapsulates the efficiency of heat transfer between the solid surface and the fluid, taking into account crucial factors like fluid velocity, thermal properties, and the characteristic length of the solid surface.

$$q''_{conv} = h\mathrm{dT} = h(T_s - T_\infty) \qquad \textbf{2.3}$$

where h is the convective heat transfer coefficient, and T_s is the surface temperature and T_∞ is the ambient temperature. Through Equation 2.4, the radiation heat transfer can be calculated.

2.10.1.3 Radiation heat transfer

The third mode, radiation, is distinct from the other two as it involves the emission of electromagnetic waves from a hot body. This form of heat transfer does not rely on a medium to propagate, making it possible for thermal energy to traverse the vacuum of space. Each body emits radiation based on its temperature, with the intensity of emitted energy increasing with higher temperatures. Understanding these diverse mechanisms of heat transfer is essential for designing effective cooling strategies for photovoltaic cells and other technological applications. By harnessing the principles of conduction, convection, and radiation, researchers and engineers can develop innovative cooling systems to mitigate the impact of excessive heat on photovoltaic cell performance. Through Equation 2.4, the radiation heat transfer can be calculated. Radiation is a phenomenon wherein energy is emitted from an object that possesses a non-zero temperature. This energy transmission occurs through electromagnetic waves and plays a significant role in heat transfer processes. However, an essential condition for radiation heat transfer to take place is the presence of space for these electromagnetic waves to propagate.

In this context, Equation 2.4 (Incropera & DeWitt, 2007) serves as a crucial tool for quantifying radiation heat transfer. This equation enables researchers and engineers to calculate the rate at which energy is radiated from a hot body to its surroundings. The equation incorporates key parameters such as the Stefan-Boltzmann constant (σ), which characterizes the emissivity of the object's surface and the absolute temperature (T) of the emitting body. Equation 2.5 (Incropera & DeWitt, 2007) is used to find the radiation heat transfer coefficient.

$$q''_{Rad} = \varepsilon\sigma(T_s^4 - T_{sur}^4) = h_r(T_s - T_{sur}) \qquad \textbf{2.4}$$

$$h_r = \varepsilon\sigma(T_s + T_{sur})(T_s^2 + T_{sur}^2) \qquad \textbf{2.5}$$

where h_r is the radiation heat transfer coefficient, and T_s is the surface temperature and T_{sur} is the surrounding temperature.

2.10.2 Thermal resistance method

In heat transfer, thermal resistance can be defined as the ratio of a driving potential (such as temperature difference) to the corresponding transfer rate (such as heat flow rate). It quantifies how much opposition heat encounters as it moves through a material or a system. The concept of thermal resistance is analogous to electrical resistance in electrical circuits, where the flow of current is impeded by resistance. Thermal resistance is an important parameter in various heat transfer processes and systems. It characterizes the efficiency with which heat is transferred from one medium to another, and understanding it is essential for optimizing heat transfer and energy efficiency.

$$q''_{cond} = k\frac{T_1 - T_2}{L} = \frac{T_1 - T_2}{R_{cond}} \quad \textbf{2.6}$$

$$q''_{conv} = h(T_s - T_\infty) = \frac{(T_s - T_\infty)}{R_{conv}} \quad \textbf{2.7}$$

$$q''_{rad} = h_r(T_s - T_{sur}) = \frac{(T_s - T_{sur})}{R_{rad}} \quad \textbf{2.8}$$

Through Equations, 2.9 to 2.11, (Incropera & DeWitt, 2007) thermal resistances for conduction, convection, and radiation are calculated.

$$R_{cond} = \frac{L}{k} \quad \textbf{2.9}$$

In the realm of heat transfer, thermal resistance for conduction (denoted as R_{cond}) is a critical parameter that plays a significant role in determining the efficiency of heat flow through a material. This essential factor reflects the relationship between the thickness of a material and its thermal conductivity.

Thermal conductivity refers to a material's ability to conduct heat, while material thickness represents the physical distance through which heat must travel. Consequently, R_{conv} is a measure of how much resistance the material poses to the flow of thermal energy. A high thermal resistance indicates that heat encounters more obstacles as it traverses through the material, resulting in a slower rate of heat transfer.

$$\boldsymbol{R_{conv} = \frac{1}{h}} \qquad \textbf{2.10}$$

In the domain of heat transfer, thermal resistance for convection (referred to as R_{conv}) is a crucial parameter that plays a pivotal role in assessing the efficiency of heat transfer between a solid surface and a fluid medium. This essential factor is directly associated with the convection heat transfer coefficient.

$$\boldsymbol{R_{rad} = \frac{1}{h_r}} \qquad \textbf{2.11}$$

In the realm of heat transfer, thermal resistance to radiation (referred to as R_{rad}) is a vital parameter that governs the efficiency of heat exchange through thermal radiation. This fundamental factor is closely associated with the radiation heat transfer coefficient, which characterizes the ability of a surface to emit and absorb thermal radiation.

R_{rad} quantifies the resistance encountered by thermal energy as it is radiated from one surface to another. This parameter is particularly crucial in scenarios where conventional methods of heat transfer, such as conduction and convection, are limited or negligible. Unlike conduction and convection, thermal radiation does not require a physical medium for heat transfer, making it essential for applications involving vacuum or space environments.

2.10.3 Porous media

Terrestrial porosity size is an essential property related to the ability of soil or rock to absorb and store liquids, such as water, oil, and gas, within small spaces known as pores. Porosity size is one of the primary factors influencing the behaviour and properties of rocks and soils concerning preservation and fluid transport.

Porosity size occurs as a result of the interlocking of the grains (small particles) that constitute rock or soil. If the distances between the grains are substantial and continuous, the porosity size is high, facilitating fluid movement within the rock or soil. Conversely, if the voids are small and discontinuous, the porosity size is low, making it more challenging for liquids to penetrate. Porous media play a crucial role in heat transfer due to their unique properties that enable efficient heat exchange. There are many advantages to using porous media for heat transfer. In certain applications, porous media are used to dissipate heat. When an object is exposed to heat, porous media can help disperse the heat and facilitate its dissipation away from the hot surface, lowering the body's temperature. Porous media can also be utilized in water evaporative cooling systems. When air is passed through porous media saturated with water, the water is evaporated, drawing heat from the air and cooling the surroundings.

In technical applications, porous media can evenly distribute heat over a larger area. When hot liquids pass through porous media, heat is distributed across the inner surfaces of the material, enabling better heat distribution. Other applications of porous media in heat transfer include cooling and heating systems, thermal engineering applications, biotechnology, and the chemical and petroleum industries. Porous media offer innovative opportunities for multiple applications aimed at improving heat efficiency and control in various industries.

Porosity size is determined based on the volume of voids between the gravel grains and the total volume. The total volume of water inside the cooling channel is calculated before gravel is placed inside it. After placing the gravel and adding water to the channel, the void volume is known, and porosity size is calculated using Equation 2.12 (Ramadan et al., 2007).

$$\boldsymbol{\phi = 1 - \frac{\forall_f}{\forall_t}} \qquad \textbf{2.12}$$

Where ϕ is the porosity size, $\forall_f$ fluid volume, and $\forall_t$ is the total volume.

2.10.4 Gravel

Gravel stands out as a highly effective porous material for cooling photovoltaic cells, owing to its unique and valuable characteristics. Let's delve further into why gravel is essential for utilization in porous media cooling:

- Good thermal conductivity: gravel possesses impressive thermal conductivity, facilitating the rapid transfer of heat from the photovoltaic cells to the cooling medium. As a result, it efficiently dissipates the excess heat generated by the cells, ensuring they operate at optimal temperatures.

- Resilience and corrosion resistance: the robust nature of gravel allows it to withstand harsh operating conditions and makes it highly resistant to corrosion. This attribute ensures that it can function effectively even in outdoor environments exposed to various weather conditions, enhancing its reliability in long-term applications.

- Cost-effectiveness: gravel's affordability is a significant advantage, making it easily accessible and well-suited for widespread use in cooling systems for photovoltaic cells. Its cost-effectiveness also makes renewable energy technologies more accessible and economically viable.

- Environmental sustainability: one of the key benefits of using gravel as a cooling medium is its ability to be reused over extended periods. This eco-friendly characteristic reduces waste and promotes sustainability, contributing to a greener approach to cooling technology.

- Abundant availability: gravel can be readily sourced from natural deposits or industrial sources, ensuring a steady and abundant supply for practical implementation. Its easy accessibility makes it a convenient choice for large-scale cooling applications in the solar energy industry.

Collectively, these features elevate the performance and cost-effectiveness of gravel as an efficient cooling medium for photovoltaic cells. By leveraging its thermal conductivity, resilience, affordability, and sustainability, gravel emerges as an ideal and dependable choice for optimizing the performance of solar panels and advancing the adoption of renewable energy solutions.

CHAPTER 3

RESEARCH METHODOLOGY

3.1 Overview

The pursuit of reducing solar cell temperatures is of paramount importance in today's world, as it holds the key to unlocking significant advancements in renewable energy technologies. By effectively mitigating the adverse effects of excessive heat through the implementation of a cutting-edge cooling system for solar panels. The implications of successfully regulating the temperature of solar cells are profound. Enhanced electric power efficiency translates to higher energy yields, contributing to a more sustainable and environmentally friendly energy generation process. Additionally, prolonging the life of solar panels not only optimizes their economic viability but also reduces electronic waste and promotes a circular economy approach, aligning with the principles of responsible consumption and production.

The flowchart depicted in Figure 3.1 provides a visual representation of the well-thought-of research methodology, where the study is thoughtfully divided into two main categories: experimental and numerical procedures. This approach not only ensures a comprehensive understanding of the system's behaviour but also fosters a holistic analysis of the solar panel's performance under various conditions.

The experimental phase's real-world testing and data collection enables the researchers to directly observe how the solar panels respond to different environmental scenarios. This hands-on approach reinforces the credibility of the findings and allows for valuable insights into the system's behaviour under practical conditions. On the other hand, the integration of numerical simulations, powered by sophisticated software, facilitates the exploration of heat transfer mechanisms within the solar panel system. Such. numerical analyses offer a level of detail and precision that would be difficult to achieve through physical experiments alone. The interplay between the cooling system and the solar panel's performance will be elucidated, shedding light on the fundamental factors that influence electric power efficiency. Furthermore, the strategies proposed to counteract the detrimental effects of high heat will open doors to new possibilities for improved solar energy utilization.

This comprehensive approach is not confined to the laboratory; instead, it aims to make a substantial impact in the real world. By advancing our knowledge of solar panel behaviour and checking their performance through cooling systems, this research endeavours to pave the way for more sustainable and efficient solar power generation. The insights gained from this study hold the potential to drive further innovation, influencing the design and operation of solar energy systems worldwide.

3.2 Experimental work

Recognizing the pivotal importance of experimental research, a comprehensive study was undertaken to explore the cooling dynamics of photovoltaic cells. This research endeavour unfolded through a dual approach, divided into internal testing and external testing phases. To facilitate these experiments, purpose-built experimental facilities have been established within the boundaries of the Faculty of Engineering Technology (FET) at Balqa Applied University (BAU) in Amman.

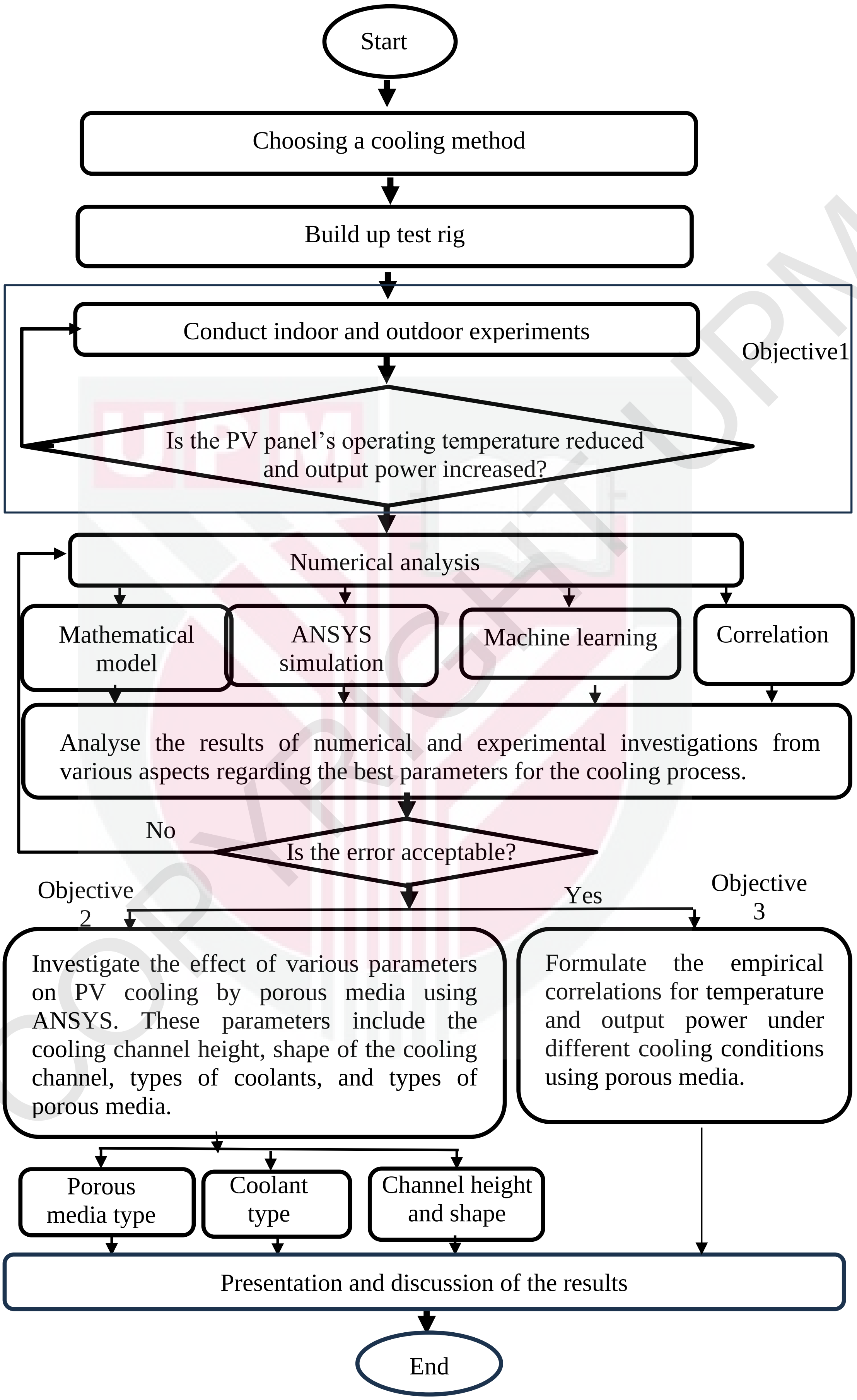

Figure 3.1: Flowchart of research activities

The first section of this experiment was revealed inside the solar energy laboratory, which is a controlled environment in which all variables, including solar radiation, wind speed, humidity, and others, are kept constant. For outdoor testing under extended skies, the photovoltaics were subjected to natural sunlight, a world in which cooling mechanisms were subject to a full range of environmental variables. In both experiments, 30 W polycrystalline photovoltaics were used. In Table 3.1, the specifications of the photovoltaic panels that were used in the practical experiments are listed.

Under the panel, a cooling channel towered a height of 5 cm, a corridor through which the currents of cooling flowed. The channel was well insulated, safeguarding against extraneous influences. Within this channel, a realm of porous media awaited, each with distinct porosities. The material of choice is gravel because of its availability and thermal conductivity shown in Table 3.2.

The photovoltaic system shown in Figure 3.2 was used to reduce the temperature of the photovoltaic panel absorbed by the water passing through the cooling channel. Two tanks of water were used, each with a capacity of one cubic meter, the first tank was used for cold water supplying the cooling channel, and the second tank for water discharge from the cooling channel in order not to mix cold water with hot water. Figure 3.3 shows the cooling channel installed underneath the photovoltaic panel for cooling purposes. The channel size was matching the size of the photovoltaic panel, and it has been confirmed that there was no water leakage from the channel. The K-type thermocouples were installed in various places on the photocell to measure the temperature of the water entering and leaving the cooling channel and measure the ambient temperature as well. Various measuring devices were used to measure the intensity of solar radiation, temperatures, voltage, current, flow meter, and pressure gauge as shown in Figure 3.4. A pump was used to circulate water.

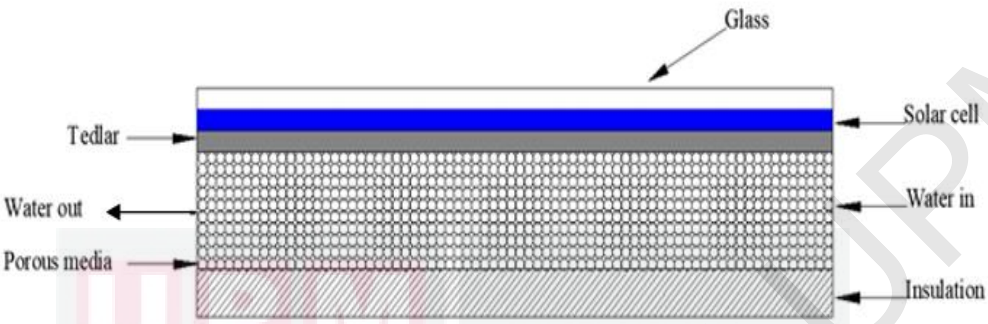

Figure 3.2: Photovoltaic system

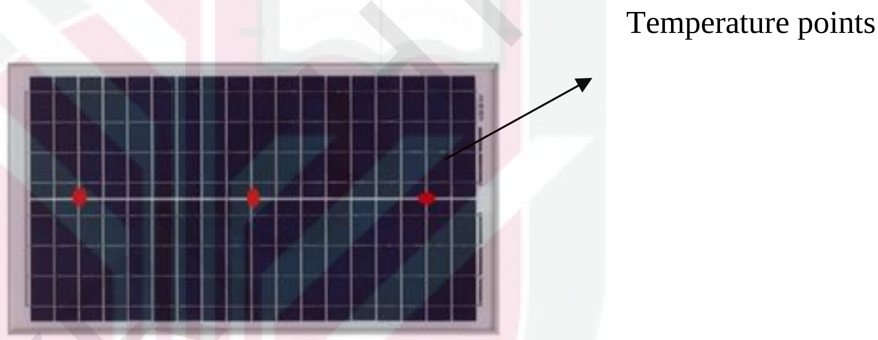

a) PV panel

b) Cooling channel

c) PV is installed on the cooling channel

Figure 3.3: PV panel and cooling channel

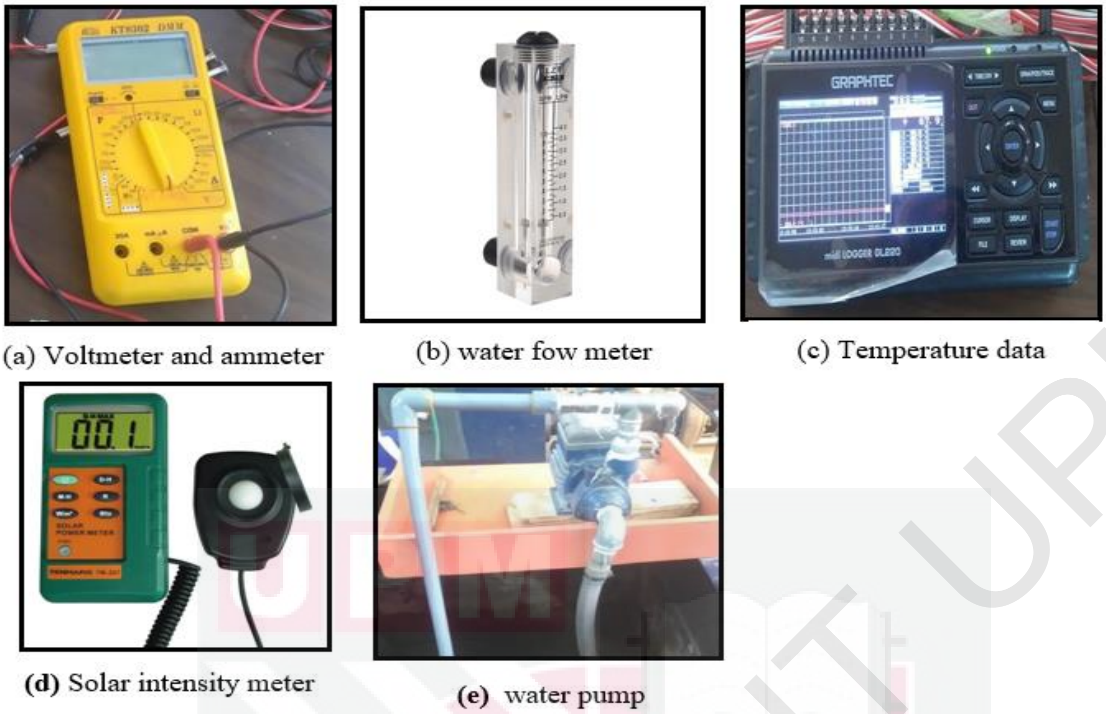

Figure 3.4: Experimental instruments for PV cooling

Table 3.1: Photovoltaic panel specifications

Solar PV module parameter	Value at AM 1.5 spectra STC
Maximum power, P_{max}	30 W
Open-circuit voltage, V_{oc}	22 V
Short-circuit current, I_{sc}	1.84 A
Voltage at P_{max}	18 V
Current at P_{max}	1.67 A
Operating temperature	-40°C to +85°C
Solar intensity, G	1000 W/m^2

To reveal the relationship between the decrease in temperature and also the increase in energy resulting from cooling solar panels through the use of porous media, two basic equations 3.1 and 3.2 were used as explained by (Ebaid et al., 2018). They serve as tools that connect areas of theoretical understanding and practical application and guide us to a field where ideas are extracted and transformed into tangible results. Within the first equation, the temperature reduction is known. It holds promise for measuring the extent to which cooling by porous media can mitigate the PV overheating experienced by solar panels.

In tandem, the second equation reveals enhanced electrical production capacity. Through this equation, it becomes possible to know the increase in energy production. It provides a means by which to examine the effect of cooling on the conversion efficiency of photovoltaics, providing insight into the tangible benefits of using porous media as a cooling mechanism.

$$\%\mathbf{T}_{\mathbf{max,\,decrease}} = \frac{\mathbf{T}_{\mathbf{withoutcooling}} - \mathbf{T}_{\mathbf{cooling}}}{\mathbf{T}_{\mathbf{withoutcooling}}}\ \mathbf{X\ 100}\% \qquad \mathbf{3.1}$$

$$\%\mathbf{P}_{\mathbf{max,\,increase}} = \frac{\mathbf{P}_{\mathbf{cooling}} - \mathbf{P}_{\mathbf{withoutcooling}}}{\mathbf{P}_{\mathbf{withoutcooling}}}\ \mathbf{X100}\% \qquad \mathbf{3.2}$$

3.2.1 Indoor test

The pursuit of comprehending the dynamics underlying photovoltaic panel cooling necessitates a rigorously controlled and methodologically precise approach. To mitigate extraneous influences and secure the fidelity of outcomes, a series of designed indoor tests were conducted within the confines of the solar energy laboratory, a sanctum of scientific inquiry, situated within the esteemed precincts of the Faculty of Engineering Technology.

This controlled environment became the crucible within which a comprehensive spectrum of ambient conditions was carefully established, mirroring the interplay of factors in the photovoltaic panel behaviour. The solar radiation, that cascading torrent of energy-bearing photons, was vigilantly measured and adeptly controlled to ensure a stable baseline. Simultaneously, ambient temperature, a critical harbinger of thermal dynamics, underwent a regulated regimen. The undulating currents of air velocity, instrumental in energy transport, were with deliberate precision. Even the delicate flux of water, underwent quantification, heralding the imperative flow in the realm of cooling experimentation.

This controlled laboratory environment is paramount in the relentless pursuit of scientific precision. By methodically isolating the cooling effect from the vicissitudes of external interferences. A solar simulator is a device that was used inside the solar laboratory in FET. It produces radiation that approximates the characteristics of natural solar radiation. This device works under certain conditions and was installed based on the purpose of the experiment. It was difficult to stabilize solar radiation in ambient conditions, since its value changes with the change of time. Successive days and months during the year, sometimes there was no solar radiation due to the clouds in the sky. Therefore, the presence of solar simulation was very helpful for research on PV systems.

The solar simulation was calibrated according to the specifications of the American Standards for Testing and Media (ASTM, E927,2005) based on this standard, there are three classes A, B, and C where spatial non-uniformity of Irradiance and temporal Instability of Irradiance 2%, 5%, and 10%, class A, class B, and class C respectively.

The value of solar radiation was set constant during the indoor experimental period, which lasted three hours continuously without any interruption. Figure 3.5 shows the solar simulation, which contains fifty bulbs made of halogen because this type of bulb gives radiation with heat, unlike LED bulbs, which only give radiation. These lamps have a capacity of 50 W each and 220 V. Each bulb was controlled separately to reach the desired homogenous radiation above the photovoltaic panel. The photovoltaic panel was 51 cm below the bulbs to reach an average solar radiation of 1600 W/m^2. The percentage of thermal inhomogeneity was 1.7% and it was of Class A based on ASTM standards, and calculations based on Equation 3.3 (Meng et al., 2011) and the percentage of solar radiation heterogeneity was 3.5% and it was of Class B based on Equation 3.4 (Meng et al., 2011)

$$\textbf{Non-uniformity}\ (\%) = \frac{\mathbf{T_{max} - T_{min}}}{\mathbf{T_{max} + T_{min}}}\ \mathbf{*100\%} \qquad \mathbf{3.3}$$

$$\textbf{Non-uniformity}\ (\%) = \frac{\mathbf{E_{max} - E_{min}}}{\mathbf{E_{max} + E_{min}}}\ \mathbf{*100\%} \qquad \mathbf{3.4}$$

where $T_{\max}$ and $T_{\min}$ are the maximum and minimum temperatures at different points of the PV panel, *and* $E_{\max}$ *and* $E_{\min}$ are the maximum and minimum radiation at different points of the PV panel.

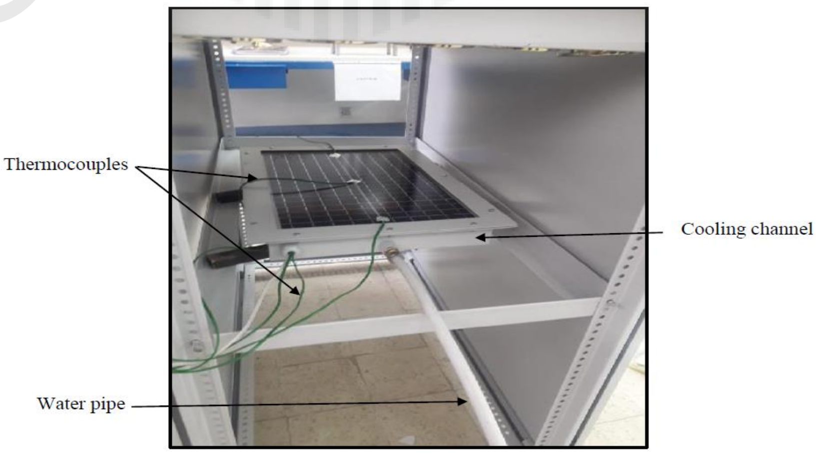

Figure 3.5: Solar simulator

3.2.1.1 Setup of the experiment

Figure 3.6 illustrates the schematic diagram of the PV cooling system. The setup incorporates a cold-water tank with a one-cubic-meter capacity, serving as a reservoir for supplying water to the system during the cooling process. Subsequently, the water is directed to a pump, which then feeds it into the cooling channel. To regulate the flow rate, the water passes through a flow meter.

Following this, the cold water enters the cooling channel situated beneath the photovoltaic panel, within which porous media (gravel) is contained. In this arrangement, the cold water serves to absorb the elevated temperature from the photovoltaic panel, which has been subjected to increased temperatures due to the incident light source. After this heat absorption process, the water proceeds to another hot tank, boasting a one-cubic-meter capacity. The solar radiation inside the solar simulator was set to be 1600W/m^2 (Irwan et al., 2015).

This channel was filled with porous media which is (gravel). The gravel properties are presented in Table 3.2. Of different porosities (0.35, 0.40, 0.4, and 0.5). Furthermore, the porosities of (0.35, 0.4, 0.48, and 0.5) were tested on different water volume flow rates (1, 1.5, 2, 3, and 4 L/min) to find out the best porosity size that performs the best cooling as explained in detail in Chapter 2.

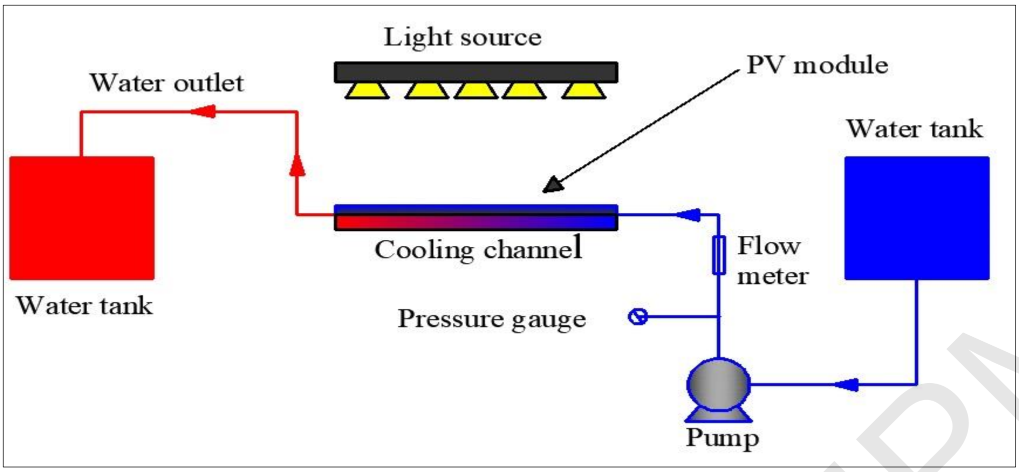

Figure 3.6: PV cooling schematic diagram

Table 3.2 presents the properties of gravel such as particle diameter density, porosity size, specific heat, and thermal conductivity, which were found experimentally in the civil engineering laboratory and the heat transfer laboratory in the Department of Mechanical Engineering. The diameters of the gravel used in this study were chosen based on what is available in the local Jordanian market to avoid additional financial costs. The gravel used was proven to their hard and water-repellent.

Table 3.2: Gravel properties

d_m (mm)	ϕ	$\forall_t$ (Liter)	$\forall_f$ (Liter)	ρ (kg/m³)	k (W/m².K)	C_P (J/kg.K)
2	0.35	9.18	5.96	2630	1.19	900
5	0.4	9.18	5.5	2630	1.19	900
10	0.48	9.81	4.77	2630	1.19	900
11	0.5	9.18	4.59	2630	1.19	900

Table 3.3 provides a comprehensive overview of the porous media utilized in this study, along with their respective properties. Porous media are materials that contain

void spaces or pores, allowing the flow of fluids or gases through them. These materials are of significant interest in various fields, including heat transfer, fluid dynamics, and filtration processes. The choice of porous media is crucial in conducting experiments and simulations related to fluid flow and heat transfer. Different porous materials exhibit varying permeability, porosity size, and thermal conductivity, which directly impact the flow characteristics and heat transfer rates within the medium.

In this study, a range of porous media was carefully selected to investigate their behaviour under specific conditions. The properties of these media were thoroughly analysed to understand their influence on fluid flow patterns, heat transfer rates, and other relevant phenomena.

Table 3.3: Material properties

Material name	**ρ (kg/m³)**	**k (W/m². K)**	**C_P (J/kg.K)**
Gravel	2630	1.19	900
Flint (Sun, 2017)	2600	3.5	740
Marble (Čáchová et al., 2016)	2700	3	800
Sandston (Sun, 2017)	2800	5	1000

3.2.2 Outdoor test

In this study, an exhaustive investigation into the dynamics of cooling photovoltaic panels in an outdoor setting was undertaken. The experimental approach followed a systematic and planned regimen to elucidate the interrelationships between various cooling techniques and the resulting performance of photovoltaic systems. This investigation utilized four distinct photovoltaic panels, each serving as a critical conduit for experimental analysis. The experimental setup, outlined in Figure 3.7, demonstrated the careful array of instruments deployed to unravel the intricacies of photovoltaic panel cooling. The outdoor experimental campaign was conducted on the rooftop premises of the Department of Mechanical Engineering, situated within the Faculty of Engineering Technology at Al-Balqa Applied University.

(a) setup

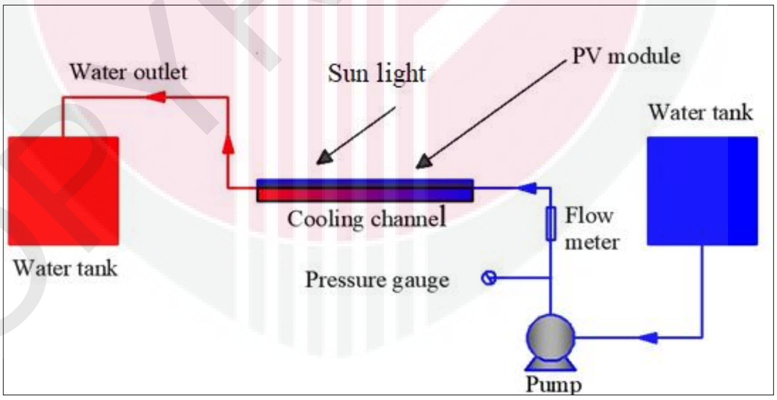

(b) Schematic diagram

Figure 3.7: Experimental setup and schematic diagram for outdoor test

Methodological rigor was upheld by maintaining consistent environmental conditions across each experimental iteration. Key parameters including solar radiation, air velocity, and ambient temperature were accurately measured to establish a uniform foundation for comparative evaluations. This harmonization of variables created a controlled backdrop against which the cooling dynamics of photovoltaic panels could be systematically explored. The experimental experimentation was structured within a three-part framework, each segment tailored to distinct dimensions of cooling effectiveness.

- Case I, a comparative analysis was conducted, contrasting the cooling dynamics facilitated by porous media with those enabled by water cooling and the absence of cooling.
- Case II delved into the realm of optimal design parameters, with a particular focus on porosity size. Through a rigorous iteration process, the delicate equilibrium where cooling efficiency aligns with photovoltaic performance was systematically probed. In this endeavour, experimental observations were seamlessly integrated with scientific inquiry, resulting in a deeper understanding of the underlying interplay that governs optimal cooling design.
- The final phase, Case III, directed its attention to volume flow rates, investigating the relationship between fluid dynamics and cooling efficiency. Employing a controlled range of volume flow rates, this phase revealed the optimal point that signifies the most efficient cooling performance.

3.2.2.1 Comparisons between cooling with and without porous media

The experimental investigation encompassed an accurate exploration across three distinct photovoltaic panels, each representing a different cooling scenario. The first panel remained unaided, without any cooling mechanism. The second panel experienced cooling solely through the medium of water circulation. Meanwhile, the third panel was subjected to a cooling regimen involving water circulation intertwined with a porous material, characterized by a porosity size of 0.35. The parameters of this material were accurately selected to usher forth an intriguing interplay of cooling dynamics. Moreover, the study delved into the effect of altering the water flow volume, dissecting the influence of varying rates of 1 L/min, 1.5 L/min, and 2 L/min.

This experimental expedition was conducted over three consecutive days, followed by a replication spanning another set of six days. This duplication was undertaken as a means of fortifying the robustness and credibility of the findings, ensuring that the results garnered are resilient against potential aberrations or anomalies. These nine days of relentless inquiry bore testimony to the rigor with which the study was pursued, aiming to derive a comprehensive comprehension of the cooling phenomena at play.

The overarching objective of this experimental endeavour was multifaceted. The principal impetus lay in conducting a comparative analysis, of the efficacy of cooling facilitated by porous media against the cooling effect induced solely by the circulation of water. This comparative assessment aimed to provide experimental clarity regarding the potential of porous media-based cooling in contrast to conventional water-based cooling mechanisms. Moreover, the inquiry extended toward ascertaining the optimal volume flow rate that could yield the maximum cooling benefit. This entailed an accurate exploration of varying flow rates, with the ultimate aim of unravelling the critical threshold that engenders the pinnacle of cooling efficiency.

In summary, this comprehensive experimental exploration unfurled over a landscape of cooling dynamics. It dissected diverse cooling methodologies, delineating their respective impacts on photovoltaic panel performance. Through subjecting these mechanisms to controlled scrutiny, also the study sought to unravel the nuances of cooling efficacy and ultimately chart a course toward enhancing the overall energy efficiency and performance of photovoltaic panels.

3.2.2.2 The best possible porosity size for the best cooling

The exploration of this specific case is upon experimentation work, accurately conducted across three distinct photovoltaic panels. Within this framework, the panels were installed up cooling channels that were accurately populated with varying porous media. Each channel, serving as a conduit for cooling dynamics, was characterized by a distinct porosity size, carefully selected to unravel the nuanced interplay between porosity size and cooling efficacy. The first channel embraced a porosity size of 0.35, the second channel an embodiment of 0.40, and the third channel with a distinct porosity size of 0.48. This dynamic interplay of porosity sizes formed the foundational cornerstone of the experimental exploration.

The inquiry was further enriched through the introduction of a dynamic variable, the volume flow rate. Each channel, endowed with a unique porosity size, underwent alterations in the volume flow rate, spanning the spectrum of 1 L/min. 2 L/min, and 3 L/min. These variable flow rates emerged as a central tenet of the experimental design, aiming to dissect the interdependence between porosity size, flow rate, and the consequent cooling impact.

The experimental work was executed over three days, ensuring an encompassing scope for experimental observation. In the relentless pursuit of scientific rigor, the experiments were replicated over an additional six-day period. This deliberate replication underscored the unwavering commitment to the fidelity of results, guarding against the spectre of transient anomalies or deviations.

At the heart of this accurate series of experiments lay a central objective to discern the most optimal porosity size conducive to facilitating the most effective cooling. This is for an optimal equilibrium engaged with the diverse spectrum of porosities, ascertaining the porosity size that best engenders cooling efficiency. By accurately observing the interaction between varying porosities and flow rates, the study endeavoured to chart a course toward enhancing the overall cooling efficiency of photovoltaic panels.

This study showed the agreement between porous media, porosity size, and cooling efficacy. The systematic manipulation of these variables within a controlled experimental framework offered a unique vantage point into the realm of optimized cooling. Through careful experimental observation, accurate replication, and methodological precision, the study endeavoured to carve a path toward unlocking the most effective porosity size capable of ushering forth enhanced photovoltaic panel cooling performance.

3.2.2.3 The best volume flow rate fit for the best cooling

The tapestry of experimental exploration in pursuit of the best photovoltaic panel cooling unfurled across a triad of interconnected cases. These experimental endeavours, which comprised a pivotal chapter of scientific inquiry, were accurately executed across four distinct photovoltaic panels. A single panel stood as a sentinel, exposed to the ambient environment without the influence of cooling mechanisms. In contrast, the second case emerged as a controlled arena for investigating cooling efficiency facilitated through the interplay of porous media. The panel, ensconced within a cooling channel filled with porous media featuring a porosity size of 0.35, became the epicentre of experimental exploration. This specific porous composition was accurately chosen to engender a robust dialogue between porosity size and cooling efficacy. However, the dynamic variation in the water flow volume introduced a quintessential variable that endowed flow rates: 1 L/min, 2 L/min, and 3 L/min. This dynamic spectrum of flow rates yielded experimental data, each resonating with the interplay between porosity size, flow rate, and cooling efficiency.

This experiment progressed through a calculated temporal cadence. Each experiment extended over a single day, serving as a portal into the dynamics of cooling within the porous media. This pivotal observation phase was followed by accurate replication, an encore that spanned two successive days. The purpose of this duplication is the robust validation of findings, cementing the veracity of experimental results and safeguarding them from transient aberrations.

The overarching goal of this experimental tour de force was clear: to discern the optimal volume flow rate within the framework of a porous media-infused cooling mechanism, characterized by a porosity size of 0.35. This pursuit of optimized volume flow rate, and the symphonic harmony between water dynamics and porous media, forged the essence of this exploration.

In essence, these experimental triads, entwining porous media, porosity size, and water flow rate, extended an invitation to engage with the subtleties of cooling dynamics. Through this accurately designed series of experiments, an unfolded to pinpoint the volume flow rate that optimally complements the porosity size, resonating harmoniously to the most efficient cooling for photovoltaic panels. This accurate pursuit was emblematic of scientific inquiry at its zenith, a study of variables accurately choreographed to illuminate the path toward enhanced energy efficiency and performance.

3.3 Measurement setting and uncertainty of measurements

The instrumentation ensemble included an array of thermocouple sensors, accurately arrayed across the photovoltaic panel's expanse. These sensors, diligently measured temperatures at distinct locales, unveiling the thermal transpiring across the panel's surface. Concurrently, temperatures of the inflowing and outflowing water within the cooling channel were accurately gauged, offering a window into the interplay between cooling agents and photovoltaic panel temperature modulation. The ambient temperature, serving as a backdrop for the choreography of cooling dynamics, was an essential metric woven into the fabric of experimental observation.

The ensemble further extended to incorporate a voltmeter and an ammeter, their roles expanding beyond mere measurement to encapsulate the energetic essence of the photovoltaic panel. These instruments stood as sentinels at the confluence of current and voltage, their measurements encapsulating the heart of photovoltaic electrical output. While each instrument played a pivotal role in the experimental tableau, it was imperative to acknowledge that each possessed a distinct realm of accuracy, as delineated in Table 3.4. By the tenets of scientific rigor, the calibration process assumed centre stage, unfurling as a vehicle to assess uncertainties with accuracy and precision. The quantification of uncertainty rested upon the scaffolding of mathematical equations, a testament to the fusion of experimental observation and scientific analysis. Central to this was Equation 3.5, a veritable cornerstone upon which the edifice of uncertainty evaluation was erected. This mathematical construct, akin to a compass guiding the experimental journey, enabled the calculation of uncertainties with methodical rigor.

The culmination of these systematic calculations unveiled a tapestry of insights, each thread accurately woven through the prism of uncertainty analysis. The experimental expedition stood as a testament to the integration of multifaceted disciplines, the seamless fusion of instrumentation, mathematical rigor, and experimental observation. The uncertainty of output power, efficiency and area are calculated based on Equations 3.5 to 3.7 (Elminshawy et al., 2019).

$$\frac{\mathbf{UP}}{\mathbf{P}} = \sqrt{\left(\frac{\mathbf{UI}}{\mathbf{I}}\right)^{2} + \left(\frac{\mathbf{UV}}{\mathbf{V}}\right)^{2}} \qquad \mathbf{3.5}$$

where I is the current and V is the voltage. Based on Equation 3.6, the uncertainty of the area of 0.17% was calculated.

$$\frac{\mathbf{UA}}{\mathbf{A}} = \sqrt{\left(\frac{\mathbf{UW}}{\mathbf{W}}\right)^{2} + \left(\frac{\mathbf{UL}}{\mathbf{L}}\right)^{2}} \qquad \mathbf{3.6}$$

where w and L are the width and length of the cooling channel. Meanwhile based on Equation 3.5, the uncertainty of the electrical efficiency of 0.2%

$$\frac{\mathbf{U\eta}}{\boldsymbol{\eta}} = \sqrt{\left(\frac{\mathbf{UP}}{\mathbf{P}}\right)^{2} + \left(\frac{\mathbf{UA}}{\mathbf{A}}\right)^{2} + \left(\frac{\mathbf{UG}}{\mathbf{Grad}}\right)^{2}} \qquad \mathbf{3.7}$$

where P is the output power, UP is the uncertainty of the output power, A is the PV panel area, UA uncertainty of the area, Grad is the solar radiation, and UG uncertainty of the solar radiation. The accuracy were taken directly from the devices used such as temperature, current, and voltage while the uncertainties for power and efficiency were calculated through equations (3.5 and 3.7).

Table 3.4: Uncertainty of the equipment that was used in the experiment

Instrument	Measured parameters	Accuracy	Range	Uncertainty
Solar power meter	intensity of solar radiation	$\pm$1 W/m^2	0-2000 W/m^2	10 W/m^2
Ammeter	current	$\pm$1 m A	0-10 A	1% +3
Voltmeter	voltage	$\pm$1 mV	0-200 V	0.5% +2
Thermocouple	Temperature	$\pm$0.1^{o}C	-210 to 200^{o}C	0.57x10^{-3o}C

3.4 Numerical studies

A numerical study was conducted for cooling the photovoltaic panel to find the temperature and output power of the PV panel. The numerical studies do not require a long time or high financial cost to obtain results, it was possible to do many numerical studies by changing some of the influencing factors such as solar radiation, air speed, ambient temperature, water flow rates, porosity sizes, and others. These numerical results were validated by the experimental results, and are compared for finding the deviation if there was any, and this will be explained in detail in the next chapter. The numerical study was divided into four scenarios: The first scenario was mathematical, the second was numerical simulation using ANSYS, the third was machine learning, and the fourth scenario was a correlation.

3.4.1 Mathematical modelling

Mathematical modelling is a crucial tool to understand the thermal behaviour of PV systems and evaluate the effectiveness of different cooling technologies. The mathematical modelling approach used in this study involves the use of heat transfer equations and numerical simulations to predict temperature distribution, heat fluxes, and energy conversion efficiencies within PV modules. The mathematical model aims to understand the effect of solar radiation, flow volume, porosity, heat transfer mechanisms (conduction, convection, and radiation), and cooling methods used to mitigate temperature rise in photovoltaic cells. The model takes into account the physical properties of the PV materials, such as thermal conductivity, absorption, and emissivity, as well as the properties of the cooling fluids or materials used in the system. A mathematical formulation was used to find out the following; the temperature of the PV panel, the output power, the electrical efficiency, the open voltage, the current, the difference in water pressure, the effect of the porosity size, the velocity of the water, the Nusselt number and its relationship to the Reynolds number, the Prandl number, the effect of porosity size, the volume of the water flow rate, and the size of the porous media that affect the cooling of the solar panels.

3.4.1.1 Thermal system modelling

Based on Figure 3.8, a mathematical model was built to find the temperature of the solar panel based on previous studies (Ahmed et al., 2019) the following assumptions were made;

1- The cooling channel was isolated in all directions except for the upper direction where the solar panel was attached
2- There was no water leakage except for the water entrance and the exit from the channel
3- The system operates in a constant flow rate of water throughout the experimental period
4- The difference in the temperature of the solar panel was along the solar panel.

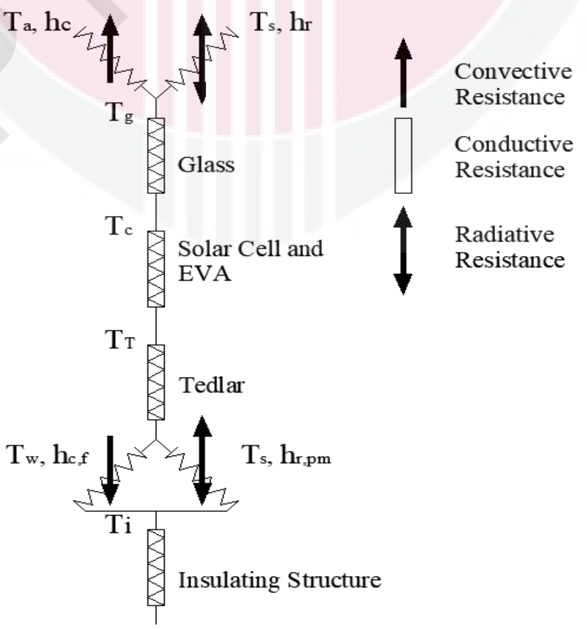

Figure 3.8: Thermal resistance

3.4.1.1.1 PV panel energy analysis

Photovoltaic panels receive solar radiation, it is difficult to convert all this radiation into electrical power, as part of this radiation turns into heat and leads to an increase in the temperature of the solar panel. Based on Equation 3.8, the total heat transfer is calculated (Incropera & DeWitt, 2007).

$$q''_t = q''_{cond} + q''_{conv} + q''_{Rad} = \frac{T_g - T_f}{R_1} + \frac{(T_g - T_\infty)}{R_{conv}} + \frac{(T_g - T_{sur})}{R_{rad}} \qquad 3.8$$

The thermal resistances can be found through the following Equations 3.9 to 3.11(Incropera & DeWitt, 2007).

$$R_1 = \frac{L_g}{k_g} + \frac{L_{EVA}}{k_{EVA}} + \frac{L_c}{k_c} + \frac{L_{EVA}}{k_{EVA}} + \frac{L_T}{k_T} + \frac{1}{h_{r,pm} + h_{c,f}} \qquad 3.9$$

$$R_{conv} = \frac{1}{h_c} \qquad 3.10$$

$$R_{rad} = \frac{1}{h_r} \qquad 3.11$$

where R_{cond} is thermal resistances for conduction, R_{conv} is thermal resistances for convection, R_{rad} is thermal resistances for radiation, k_g denotes thermal conductivity of glass, h_c is Convective heat transfer coefficient, h_r is radiant heat transfer coefficient, the values of the coefficients. Equation 3.12 combines the thermal resistance of convection and radiation. Equation 3.13 use to find total coefficient of heat transfer.

$$\sum R_{c,r} = \frac{R_{conv}\ R_{rad}}{R_{conv} + R_{rad}},\ U_{c,r} = \left[\sum R_{c,r}\right]^{-1} \qquad 3.12$$

$$U_1 = \left[\sum R_1\right]^{-1} \qquad 3.13$$

where R_t is the total thermal resistances for conduction and $U_{c,r}$ is the coefficient of heat transfer between the PV cell and the surrounding environment. The temperature of the solar panel can be calculated based on the Equation 3.14 (Ahmed et al., 2019).

$$\boldsymbol{G.\alpha_c = E + U_{c,r}(T_g - T_a) + U_1 (T_g - T_f)} \qquad \textbf{3.14}$$

where T_f expresses the temperature of the fluid, and the temperature of the solar panel from the front is symbolized by T_g. The temperature of the surrounding air is symbolized by T_a. G is the solar radiation and E is the electric power coming out of the solar panel, and finally, it indicates the absorbance, where U_1 is the overall heat transfer coefficient for glass to water. After rearranging Equation 3.14, the temperature of the photovoltaic cell can be calculated using Equation 3.15 as follows;

$$\boldsymbol{T_g = \frac{G.\alpha_c - E + U_{c,r}T_a + U_1 T_f}{U_{c,r} + U_1}} \qquad \textbf{3.15}$$

U_c is the coefficient of heat transfer between the PV glass and the surrounding environment, and it can be calculated based on the Equation 3.16 (Ramadan et al., 2007).

$$\boldsymbol{U_{c,r} = \left[\frac{1}{h_c + h_r}\right]^{-1}} \qquad \textbf{3.16}$$

Convective heat transfer coefficient, and radiation heat transfer coefficient, the values of the coefficients can be found in Equations 3.17 and 3.18 (Ramadan et al., 2007), respectively this equation indicates that the convective heat transfer coefficient is affected by the flow velocity of the surrounding fluid. As the wind speed increases, the convective heat transfer coefficient increases accordingly, indicating a higher heat transfer rate between the photovoltaic cell and the surrounding air due to enhanced fluid movement. This is consistent with the physical intuition that higher wind speeds lead to more efficient cooling of the photovoltaic cell by increasing the rate of heat removal through convection.

$$h_c = 5.7 + 3.8V \quad 3.17$$

where V is the velocity of the surrounding air around the PV cells. Radiation heat transfer coefficient the equation indicates that the radiation heat transfer coefficient is influenced by the emissivity of the surfaces and the temperature difference between the PV cell and the surroundings. A higher temperature difference and higher emissivity result in a higher radiation heat transfer coefficient, indicating a higher rate of heat transfer between the surfaces due to thermal radiation.

$$h_r = \varepsilon\,\sigma\left(T_g{}^2 + T_a{}^2\right)\left(T_g + T_a\right) \quad 3.18$$

where ε is emissivity and σ is the Stefan-Boltzmann constant

$$U_1 = \left[\frac{L_g}{k_g} + \frac{L_{EVA}}{k_{EVA}} + \frac{L_c}{k_c} + \frac{L_{EVA}}{k_{EVA}} + \frac{L_T}{k_T} + \frac{1}{h_{r,pm} + h_{c,f}}\right]^{-1} \quad 3.19$$

where L_g and k_g are the thickness and thermal conductivity of glass, *and* L_{EVA}, and k_{EVA} are the thickness and thermal conductivity of EVA. L_T *and* k_T are the thickness and thermal conductivity of Tedlar (Ramadan et al., 2007).

$$G.\alpha_c = U_{front2}(T_T - T_a) + h_{c,f}\left(T_T - T_f\right) + h_{r,pm}\left(T_T - T_{pm}\right) \quad 3.20$$

Through Equations 3.20 and 3.21, the temperature of the solar panel from the back. Based on Equation 3.22 can find overall heat transfer coefficient from glass to bottom Tedlar.

$$T_T = \frac{U_2 T_g + h_{c,f} T_f + h_{r,pm} T_{pm}}{h_{c,f} + h_{r,pm} + U_2} \quad 3.21$$

$$U_2 = \left[\frac{L_g}{k_g} + \frac{L_{EVA}}{k_{EVA}} + \frac{L_c}{k_c} + \frac{L_{EVA}}{k_{EVA}} + \frac{L_T}{k_T}\right]^{-1} \quad 3.22$$

where U_2 is the overall heat transfer coefficient from glass to bottom Tedlar, $h_{c,f}$ is the convective heat transfer coefficient for water flowing channel filled with porous medium can be calculated from Equation 3.23. Based on Equations 3.23 to 3.26

(Ramadan et al., 2007), can find thermal conductivity, Nusselt number, Prandtl number and Reynolds number

$$\boldsymbol{h_{c,f}} = \left[\frac{\boldsymbol{D_{hd}}}{\boldsymbol{Nu_{pm-f}.k_e}}\right]^{-1} \qquad 3.23$$

$$\boldsymbol{k_e} = \boldsymbol{\phi k_{s+}} (1-\boldsymbol{\phi})\boldsymbol{k_f} \qquad 3.24$$

where ke is the thermal conductivity and ϕ is the porosity size.

$$\boldsymbol{Nu_{pm-f}} = \left(\frac{\boldsymbol{0.255}}{\boldsymbol{\phi}}\right)\boldsymbol{Re_{pm}^{\frac{2}{3}}.Pr_f^{1/3}} \qquad 3.25$$

Nu_{pm-f} is the Nusselt number; the physical meaning of the Nusselt number lies in its ability to quantify how well a fluid conducts heat through convection, Pr_f is the Prandtl number, Re_{pm} is Reynolds number (Ramadan et al., 2007). The physical meaning of the Reynolds number lies in its ability to predict the flow regime of a fluid. The value of the Reynolds number helps determine whether the flow is laminar, turbulent, or in a transitional state.

$$\boldsymbol{Re_{pm}} = \frac{\boldsymbol{\rho_f} \mathbf{V}\ \boldsymbol{d_{pm}}}{\mu(\mathbf{1}-\boldsymbol{\phi})} \qquad 3.26$$

where ρ_f is fluid density, V is inlet fluid velocity, $h_{r,pm}$ is the radiation heat transfer coefficient from Tedlar to the porous medium, which can be calculated based on the Equation 3.27 (Ramadan et al., 2007).

$$\boldsymbol{h_{r,pm}} = \varepsilon\boldsymbol{\sigma}(\boldsymbol{T_T} + \boldsymbol{T_{pm}})(\boldsymbol{T_T}^2 + \boldsymbol{T_{pm}}^2) \qquad 3.27$$

The pressure difference in porous media is found in Equation 3.28 (Ramadan et al., 2007). the equation describes how the pressure gradient along the flow direction is influenced by various factors such as fluid velocity, viscosity, void fraction, dispersed phase diameter, and fluid density. It provides insights into the balance between viscous and inertial forces in two-phase flow systems.

$$\frac{\nabla P}{\nabla L} = \frac{150V\mu(1-\phi^2)}{d_p\phi^3} + \frac{1.75V^2\rho_f(1-\phi)}{d_p\phi^3} \quad 3.28$$

where ∇P *is* the pressure difference in porous media, ρ_f is liquid density, V is liquid velocity, μ viscosity of the liquid, d_p is gravel diameter and ϕ is the porosity size.

3.4.1.2 Mathematical model of an electrical system

Figure 3.9 shows the equivalent circuit for a photocell. As mentioned earlier, the output of electric power is affected by PV back temperature, and solar radiation, because the high temperature directly affects the voltage and the current (Bahaidarah et al., 2013).

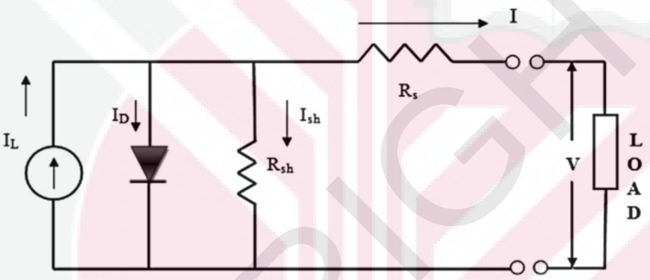

Figure 3.9: The equivalent circuit for PV cell
(Bahaidarah et al., 2013)

Table 3.5 expresses the value of the I-V curve, when the value of the open voltage is the highest, the current value is zero.

Table 3.5: I-V specific for PV panel
(Bahaidarah et al., 2013)

Point	Conditions
Short circuit current	$I = I_{sh}, V = 0$
Open circuit voltage	$I = I_{sh} = 0, V = V_{OC,ref}$
Maximum power	$I = I_{max,ref}, V = V_{max,ref}$ $[d(IV)/dV]_{max}$

Based on the conditions mentioned in Table 3.4, the following Equations are derived to find the variables. From Equation 3.29 (Bahaidarah et al., 2013), the current (I) was found it depend on the light-generated current (I_L), the diode current (I_o), the series resistance (R_s), the short circuit resistance (R_{sh}), and the voltage (V).

$$I = I_L - I_O\left[exp\left(\frac{V + IR_S}{a}\right) - 1\right] - \frac{V + IR_S}{R_{Sh}} \qquad 3.29$$

A reference short circuit is calculated from Equation 3.30 (Bahaidarah et al., 2013), where it is calculated at Standard Test Conditions (STC).

$$\mathbf{I_{SC,ref}} = \mathbf{I_{L,ref}} - \mathbf{I_{0,ref}}\left[\mathbf{exp}\left(\frac{\mathbf{I_{sc,ref}R_{s,ref}}}{\mathbf{a_{ref}}}\right) - \mathbf{1}\right] - \left(\frac{\mathbf{I_{sc,ref}R_{s,ref}}}{\mathbf{R_{sh,ref}}}\right) \qquad 3.30$$

where $I_{SC,ref}$ is the reference short circuit, the diode reverses saturation current (Io), $I_{L,ref}$ is light generated current at STC (A). Based on Equation 3.31(Bahaidarah et al., 2013), calculate the maximum reference current.

$$I_{mp,ref} = I_{L,ref} - I_{O,ref}\left[exp\left(\frac{V_{mp,ref} + I_{mp,ref}R_{s,ref}}{a_{ref}}\right) - 1\right] - \left(\frac{V_{mp,ref} + I_{mp,ref}R_{s,ref}}{R_{sh,ref}}\right) \qquad 3.31$$

where series resistance at standard test conditions ($R_{s,ref}$), $I_{mp,ref}$ is reference maximum current, $V_{mp,ref}$ is reference maximum voltage, $R_{sh,ref}$ is reference shunt resistance, as shown in Equations 3.32 to 3.33 (Bahaidarah et al., 2013);

$$\frac{I_{mp,ref}}{V_{mp,ref}} = \frac{\left(\frac{I_{O,ref}}{a_{ref}}\right) exp\left(\frac{V_{mp,ref}+I_{mp,ref}R_{s,ref}}{a_{ref}}\right) + \frac{1}{R_{sh,ref}}}{1 + \left(\frac{I_{O,ref}R_{s,ref}}{a_{ref}}\right) exp\left(\frac{V_{mp,ref}+I_{mp,ref}R_{s,ref}}{a_{ref}}\right) + \frac{R_{s,ref}}{R_{sh,ref}}} \qquad 3.32$$

$$\frac{a}{a_{ref}} = \frac{T_C}{T_{c,ref}} \qquad 3.33$$

The light-generated current was calculated from Equation 3.34 based on the solar panel temperature and ambient temperature.

$$I_L = \frac{S}{S_{ref}}\left[I_{L,ref} + \mu I_{sc}(T_C - T_{C,ref})\right] \qquad 3.34$$

where the T_c is the current cell temperature and $T_{c,\,ref}$ is the reference cell temperature. The absorbed solar radiation can be estimated from Equation 3.35;

$$\frac{S}{S_{ref}} = M\left(\frac{G_b}{G_{ref}} R K_{\tau\alpha,b} + \frac{G_d}{G_{ref}} K_{\tau\alpha,d}\left(\frac{1+cos(\beta)}{2}\right) + \frac{G}{G_{ref}} \rho_g K_{\tau\alpha,g}\left(\frac{1-cos(\beta)}{2}\right)\right) \quad 3.35$$

where S_{ref} is absorbed solar radiation at STC (W/m^2), S is absorbed solar radiation, G_{ref} is solar intensity (W/m^2).

$$I_O = I_{oref}\left(\frac{T_C}{T_{C,ref}}\right)^3 exp\left(\frac{\varepsilon}{KT_{C,ref}} - \frac{\varepsilon}{KT_C}\right) \quad 3.36$$

Solving Equations 3.35 to 3.36 can get an optimum condition. Next, the operational values I_{mp} and V_{mp} can be found in Equations 3.37 and 38 (Bahaidarah et al., 2013).

$$\frac{I_{mp}}{V_{mp}} = \left[\frac{\frac{I_O}{a} exp\left(\frac{V_{mp}+I_{mp}R_s}{a}\right) + \frac{1}{R_{sh}}}{1 + \frac{R_s}{R_{sh}} + \frac{I_o R_s}{a} exp\left(\frac{V_{mp}+I_{mp}R_s}{a}\right)}\right] \quad 3.37$$

The maximum current capacity was calculated from Equation 3. 38.

$$I_{mp} = I_L - I_O\left[exp\left(\frac{V_{mp} + I_{mp}R_S}{a}\right) - 1\right] - \left[\frac{V_{mp} + I_{mp}R_S}{R_{sh}}\right] \quad 3.38$$

where the maximum power P_{max} and efficiency η_c can be found by Equations 3.39 and 3.40 (Bahaidarah et al., 2013).

$$P_{max} = I_{mp}V_{mp} \quad 3.39$$

$$\eta_c = \frac{I_{mp}V_{mp}}{AG} \quad 3.40$$

3.4.2 ANSYS simulation

The computational fluid dynamics software ANSYS was utilized to determine the temperature of the PV panel and understand the behaviour of water and porosity size during cooling. Figure 3.10a illustrates the flowchart depicting the analysis procedure. The components of the PV panel system were designed using the AutoCAD program. ANSYS analysis proved to be one of the most effective and straightforward methods to numerically comprehend the heat transfer behaviour for any model, especially regarding the cooling impact on the surface of the photovoltaic panel, which was not well understood. Several parameters, such as solar radiation intensity, ambient temperature, volume, flow rates, air velocity, and porosity size, were thoroughly investigated. The simulation is based on various hypotheses:

1. The flow through the cooling channel was assumed to be completely uniform and incompressible.
2. The effect of dust and moisture on the top of the photovoltaic panel is disregarded.
3. The thermophysical properties of the cooling duct and the PV panel remain constant with temperature changes.
4. Ethyl Vinyl Acetate (EVA) was treated as completely transparent with high transmissivity.
5. The walls of the cooling channel are considered adiabatic.

In the pursuit of comprehensive insights into photovoltaic cell cooling, a multi-layered heat transfer model was devised, encompassing critical components like glass, EVA, the solar cell, additional EVA, Tedlar, and the cooling water. To conduct this analysis, the ANSYS Fluent software was harnessed, employing a transient state condition with enabled energy analysis. The adoption of the k-epsilon RNG model proved instrumental in achieving accurate turbulence and swirling analysis, essential for capturing the intricacies of fluid behaviour.

To ensure a realistic representation of the system, the effect of gravity was incorporated, acting downward from the photovoltaic panel, mirroring real-world conditions. The choice of materials for the metals and the cooling liquid was accurately made, and the porous zone feature was activated, permitting the simulation of fluid flow through the porous media of the metal layers. Parameters such as metal porosity size were considered to accurately capture the porous flow characteristics. Boundary conditions played a pivotal role in shaping the simulation's accuracy. At the fluid domain's inlet, the velocity boundary condition was set to match the liquid's velocity upon entering the cooling channel, ensuring a seamless transition from the inlet. On the other hand, the outlet was treated with a pressure outlet condition set to zero, allowing the fluid to freely exit the domain. Additionally, the liquid wall boundary was defined as adiabatic, signifying no heat exchange with the surrounding walls.

The semi-implicit method for pressure-linked equations (Simplicity) was judiciously chosen as the solution method, accounting for the complexities of fluid flow and pressure variations. Furthermore, to maintain numerical stability and precision, a second-order upwind scheme was implemented for all relevant parameters. To guarantee the accuracy and reliability of the numerical analysis, accurate meshing, and convergence criteria were employed. A fine mesh with a size below $1e^{-4}$ was accurately created around the photovoltaic panel, ensuring details were adequately resolved. The simulation's residual convergence was monitored diligently, with Figure 3.10d indicating that the residuals converged to a commendable level between $1e^{-12}$ and $1e^{-14}$. This convergence signified the attainment of a well-converged numerical solution, instilling confidence in the credibility of the results.

Throughout the study, ANSYS was leveraged to scrutinize a range of influential parameters. The effect of porosity size, variations in volume flow rates, the impact of cooling channel height and shape, the selection of cooling fluid types, and porous media types were accurately investigated. These explorations aimed to unravel the most optimal configurations and conditions for efficient photovoltaic cell cooling.

In conclusion, the numerical analysis conducted using ANSYS has proven to be a valuable tool in shedding light on the complexities of photovoltaic cell cooling. By considering a comprehensive array of factors and employing advanced simulation techniques, researchers gained critical insights into the performance of various cooling strategies. These findings show more effective and sustainable cooling approaches, ultimately contributing to the advancement of photovoltaic technology and the global shift toward renewable energy solutions.

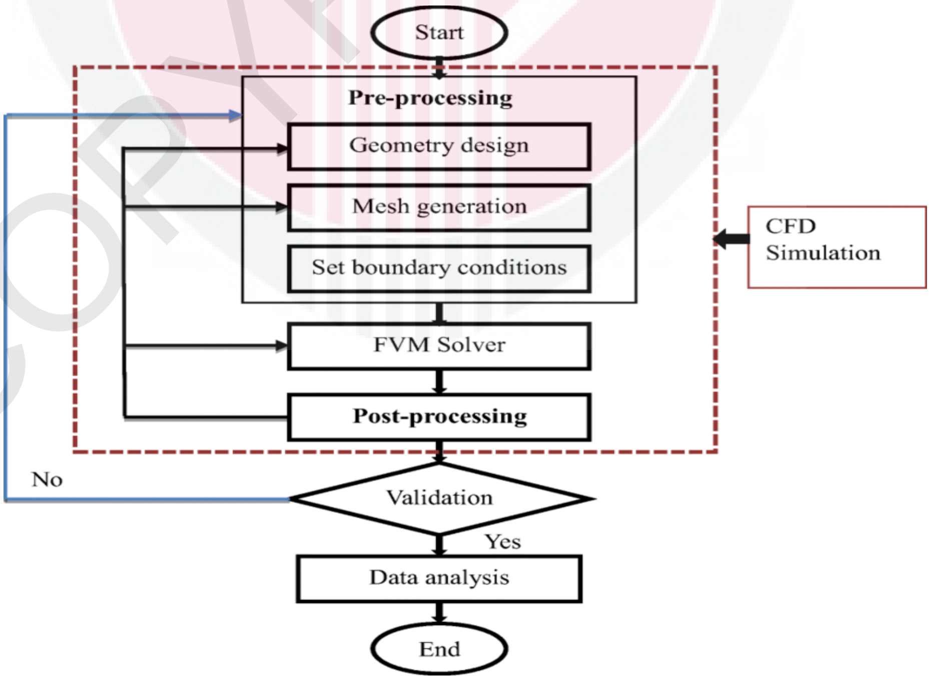

a) Flowchart of CFD analysis

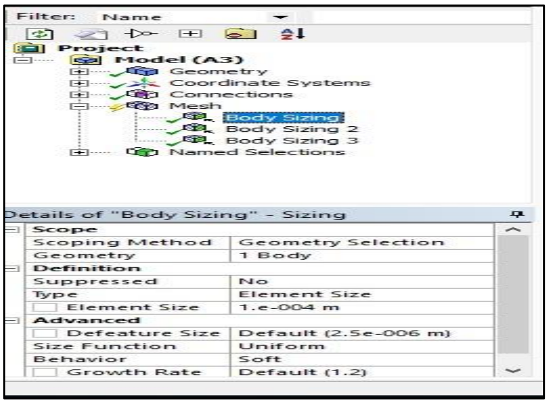

b) Mesh details

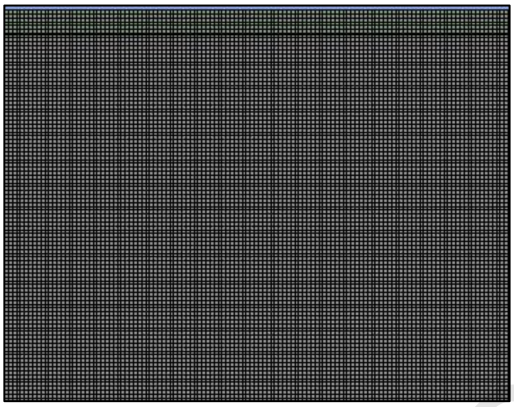

c) Mesh

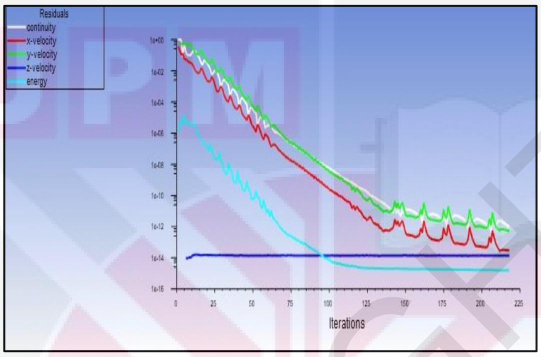

d) Residual

Figure 3.10: Flowchart and solution method

3.4.2.1 Governing Equations

The realm of numerical simulation was harnessed to unravel the three-dimensional equations that govern the temperature dynamics within the photovoltaic system. At the forefront of this computational endeavour stood the powerful ANSYS program, renowned for its prowess in seamlessly navigating the complex landscape of equation-based mathematical models.

The underpinning ethos of this simulation rested upon the ability of ANSYS to decipher and solve the equations that underlie thermal behaviour. This digital canvas became the virtual arena where thermal intricacies would unfold, paralleling the experimental experimentation in its understanding. As the numerical machinery churned through the equations, a digital tapestry of temperature distribution emerged, each pixel encapsulating a discrete element of thermal insight.

This computational was not conducted in isolation; rather, it stood as an illuminating companion to experimental inquiry. The numerical results generated by ANSYS were held in the experimental findings, each serving as a validating lens for the other. The marriage of experimental data and numerical simulations brought forth a symphony of validation, amplifying the confidence in the findings and enriching the tapestry of understanding. The simulation unfolded within the confines of a steady flow state, where the fluid dynamics were deemed incompressible a foundational assumption that streamlined the computational machinery. This calculated simplification, a testament to scientific rigor, enabled the computational prowess of ANSYS to unravel the temperature intricacies without undue encumbrance. Central to this computational odyssey were the equations themselves, eloquently encapsulating the mathematical foundation of the simulation. These equations, woven into the digital fabric, served as the guiding compass for ANSYS to traverse the landscape of thermal behaviour. Beneath the digital veneer lay an array of mathematical constructs, encompassing the behaviour of fluid dynamics, heat transfer, and energy conservation.

In summation, the ANSYS program emerged as a digital maestro, orchestrating the symphony of equations that governed the temperature dynamics. This computational overture unfolded in harmony with experimental exploration, enriching the scientific discourse through numerical insights. The equations, the bedrock of this simulation, formed the connective tissue between theory and practice, creating a bridge of understanding that spanned the realms of the virtual and the tangible.

The Continuity Equation, a cornerstone of fluid dynamics and mass conservation, stands as an elegant embodiment of the unbreakable link between the past, present, and future states of a flowing medium. This fundamental principle, steeped in mathematical elegance, asserts that within a closed system, the rate of mass entering a region is equal to the rate of mass exiting that same region.

Mathematically, the Continuity Equation takes shape as a precise expression, capturing the essence of fluid motion. It asserts that the product of fluid density, cross-sectional area, and velocity remains a constant along a streamline. This profound statement encapsulates the inextricable connection between fluid behaviour and spatial dynamics, with each infinitesimal element of the fluid's journey holding a piece of the overall puzzle.

In the context of the experimental and computational exploration within the realm of photovoltaic cooling, the Continuity Equation becomes a guiding beacon. As water courses through the cooling channels, its dynamic interplay with porous media and photovoltaic panels is choreographed by the tenets of continuity. The equation offers insights into how fluid dynamics respond to varying porosity sizes, flow rates, and thermal gradients, painting a comprehensive portrait of cooling efficiency.

The Continuity Equation, while a bedrock of fluid mechanics, finds its resonance extending beyond theoretical constructs. It materializes as a guiding principle in the experimental investigation, where water's journey through cooling channels echoes the mathematical underpinnings. Simultaneously, it forges the backbone of numerical simulations, dictating the fluid's behaviour as it courses through the virtual arena.

In the pursuit of enhanced photovoltaic cooling, the Continuity Equation stands as an eloquent bridge between mathematical abstraction and tangible reality. It weaves a tapestry that binds fluid motion, thermodynamics, and experimental observation, offering a profound insight into the interplay between forces that shape our world. As the experimental and computational endeavours unravel, the Continuity Equation remains an enduring companion, unravelling the symphony of fluid dynamics and guiding the optimized cooling strategies. Equation 3.41 is the Continuity Equation (Salman et al., 2022).

$$\frac{\partial u}{\partial x} + \frac{\partial v}{\partial y} + \frac{\partial w}{\partial z} = 0 \qquad \textbf{3-41}$$

Where $\frac{\partial u}{\partial x}$ is the change of velocity with concerning direction, $\frac{\partial v}{\partial y}$ is the change of velocity concerning the y direction and $\frac{\partial w}{\partial z}$ is the change of velocity concerning the z-direction.

The Momentum Equation, an embodiment of Newton's second law applied to fluid dynamics, stands as a powerful testament to the interplay of forces that shape the motion of fluids. This foundational principle asserts that the change in momentum of a fluid element is a direct result of the forces acting upon it. In essence, the Momentum Equation unveils the profound connection between the applied forces, fluid motion, and the resultant dynamic state. Mathematically, the Momentum Equation unfurls across various forms, each tailored to different scenarios and perspectives. The Navier-

Stokes equations, a cornerstone of fluid dynamics, encapsulate the Momentum Equation's essence and its translation into tangible equations. Within this mathematical symphony, velocity, pressure, density, and viscosity form the fluid's motion through the channel.

In the realm of experimental exploration within the photovoltaic cooling context, the Momentum Equation emerges as a guiding compass. As water traverses the cooling channels, its dynamic interaction with the porous media and photovoltaic panels becomes a manifestation of the Momentum Equation. Forces dictated by fluid velocity, pressure gradients, and channel geometries converge, shaping the fluid's trajectory and impacting the thermal equilibrium. The Momentum Equation assumes an equally prominent role within the realm of numerical simulations. It serves as a foundational pillar upon which the digital realm replicates the fluid's journey. Within this virtual arena, the mathematical constructs become avatars of fluid elements, and the Momentum Equation navigates their digital trajectory.

The experimental journey mirrors the mathematical and computational underpinnings. As water flows through the cooling channels, its path echoes the Momentum Equation's essence. The forces and motions become tangible manifestations of a mathematical principle, unfolding as experimental phenomena ripe for observation. In the pursuit of photovoltaic cooling, the Momentum Equations 3.42 to 3.44 (Salman et al., 2022), stands as a lodestar, guiding the exploration's trajectory. It unveils the forces that mould fluid dynamics, channelling them into the pursuit of enhanced energy efficiency. Whether in the laboratory or the virtual realm, the Momentum Equation reverberates as a foundational melody, dictating the fluid's motion and enabling cooling strategies.

$$\frac{\rho_f}{\phi}\left(u\frac{\partial u}{\partial x}+v\frac{\partial v}{\partial y}+w\frac{\partial w}{\partial z}\right) = -\frac{\partial p}{\partial x}+\mu_{eff}\left(\frac{\partial^2 u}{\partial x^2}+\frac{\partial^2 u}{\partial y^2}+\frac{\partial^2 u}{\partial z^2}\right)-\left(\frac{\mu_f}{k}+\frac{F\phi}{\sqrt{K}}u\right)u \quad \mathbf{3.42}$$

where ρ_f is the density of the fluid, ϕ is the porosity size of gravel, $\frac{\partial p}{\partial x}$ is the changes in pressure relative to the x direction, μ_f is water viscosity and k is the thermal conductivity of water.

The inclusion of the porosity volume within the momentum equation is a pivotal aspect of understanding and quantifying the porous media effect in the realm of solar simulation for photovoltaic testing. The momentum equation, a fundamental component of the governing equations, plays a crucial role in describing the fluid flow or transport phenomena within the porous material.

Incorporating the porosity volume directly into the momentum equation provides a tangible representation of how the porous structure influences the flow dynamics and transport processes. The porosity volume essentially acts as a modifier within the equation, signifying the fraction of the material that is permeable to the flow of fluid or other relevant entities. This representation makes the influence of porosity on the overall system behaviour explicitly clear, offering insights into how the presence of voids or pores affects the momentum transfer.

The momentum equation with the porosity volume term is particularly insightful when considering fluid flow through porous media. It delineates the spatial distribution of the porous structure, illustrating how fluid flows through interconnected voids and channels. The porosity volume becomes a key factor in determining the resistance that the fluid encounters as it traverses the porous material, influencing velocity profiles, pressure gradients, and other flow characteristics.

$$\frac{\rho_f}{\phi}\left(u\frac{\partial u}{\partial x}+v\frac{\partial v}{\partial y}+w\frac{\partial w}{\partial z}\right) = -\frac{\partial p}{\partial y}+\mu_{eff}\left(\frac{\partial^2 v}{\partial x^2}+\frac{\partial^2 v}{\partial y^2}+\frac{\partial^2 v}{\partial z^2}\right)-\left(\frac{\mu_f}{k}+\frac{F\phi}{\sqrt{K}}v\right)v \qquad 3.43$$

$$\frac{\rho_f}{\phi}\left(u\frac{\partial u}{\partial x}+v\frac{\partial v}{\partial y}+w\frac{\partial w}{\partial z}\right) = -\frac{\partial p}{\partial z}+\mu_{eff}\left(\frac{\partial^2 w}{\partial x^2}+\frac{\partial^2 w}{\partial y^2}+\frac{\partial^2 w}{\partial z^2}\right)-\left(\frac{\mu_f}{k}+\frac{F\phi}{\sqrt{K}}w\right)w \qquad 3.44$$

The Energy Equation, a keystone of thermodynamics and fluid dynamics, serves as a beacon illuminating the interplay between heat, work, and the dynamic flow of fluids. At its core, the Energy Equation embodies the principle of conservation of energy, asserting that the total energy within a fluid system remains constant unless acted upon by external forces. This fundamental tenet not only underpins the behaviour of fluids but also provides a window into the thermodynamic journey of energy transformations.

Mathematically, the Energy Equation takes on multifaceted forms, each a manifestation of energy's relentless metamorphosis within fluid dynamics. It encapsulates the exchange between kinetic and potential energy, the convective transport of thermal energy, and the conduction of energy through materials. In essence, the Energy Equation becomes a symphonic expression of the myriad ways energy is exchanged and transformed within the fluid's voyage. Within the web of photovoltaic cooling exploration, the Energy Equation emerges as a guiding compass, intertwined with the fluid's journey through the cooling channels. As water courses through these channels, its interaction with porous media, photovoltaic panels, and ambient surroundings embodies the dynamic essence of the Energy Equation. Thermal energy ebbs and flows exchanged and transformed in response to forces of convection, conduction, and radiation. In the realm of numerical simulations, the Energy Equation serves as the master conductor of the digital orchestra. the behaviour of energy transformations within the virtual realm, offering a digital canvas upon which thermal dynamics unfold. Here, fluid elements become vessels of energy exchange, their interactions, and transformations a digital embodiment of the Energy Equation's mathematical rigor. The experimental exploration, mirroring both theoretical and computational underpinnings, unveils the Energy Equation's essence within the laboratory setting. As water traverses the cooling channels, thermal energy shifts and transforms in response to the porous media's presence, fluid flow dynamics, and panel temperature differentials. The Energy Equation's impact becomes tangible as temperature gradients and fluid motion interweave in a dynamic choreography. The pursuit of optimized photovoltaic cooling is indelibly marked by the Energy Equation's guidance. It provides a roadmap for enhancing energy efficiency and unravelling the intricacies of heat transfer mechanisms and thermal equilibrium. The equation not only informs the experimental journey but also enriches the digital simulations, fostering a deeper understanding of energy's behaviour within complex fluid systems. Equation 3.45 represents the Energy Equation (Salman et al., 2022).

$$\rho_f\left(u\frac{\partial T_f}{\partial x}+v\frac{\partial T_f}{\partial y}+w\frac{\partial T_f}{\partial z}\right)=k_f\left(\frac{\partial^2 T_f}{\partial x^2}+\frac{\partial^2 T_f}{\partial y^2}+\frac{\partial^2 T_f}{\partial z^2}\right) \quad \textbf{3.45}$$

where T_f is the water temperature.

3.4.3 Machine learning

The primary goal of using the machine learning technique is to predict the main parameters that affect PV panel temperatures and the corresponding output power under cooling conditions involving water and porous media as weights. To achieve this goal, a solution employing six distinct algorithms was devised and the results were compared with experimental results. These algorithms encompass AdaBoost (AB), Random Forest (RF), Decision Tree (DT), Support Vector Machine (SVM), Gradient Boosting (GB), and Linear Regression (LR). The application of machine learning in this context serves two crucial purposes. Firstly, it can be used to validate the experimental results obtained, offering a reliable means of cross-verification. Secondly, it enables the identification of the most suitable algorithm or model for future heat transfer behaviour testing. This approach can be valuable because experimental investigations can be time-consuming and entail high operation and maintenance costs.

The expected results hinge on the consideration of several key parameters, which were previously employed in the experimental work. These parameters encompass solar radiation, air velocity surrounding the photovoltaic panel, ambient temperature, volume of flow rate, water temperature at the cooling channel inlet, and the level of porosity size. By incorporating these factors into the machine learning model, the predictions can be tailored to simulate real-world conditions accurately. To ensure the credibility of the predicted results, various evaluation metrics were employed, including the root square error (RMSE), absolute error (MAE), and R^2. These metrics play a pivotal role in assessing the accuracy and reliability of the machine learning model, instilling confidence in the validity of the predictions. Figure 3.11 provides a comprehensive illustration of the machine learning methodology adopted to forecast the PV panel performance's main parameters such as temperature and output power. By leveraging these advanced mathematical techniques, researchers can make informed decisions, optimize cooling strategies, and pave the way for more efficient and cost-effective heat transfer analysis in the realm of photovoltaic technology. Machine learning encompasses diverse methodologies that delineate how algorithms acquire knowledge and enhance their precision in prediction. Each model is meticulously tailored to particular data types, ensuring a seamless alignment between the algorithm's learning process and the inherent characteristics of the data it endeavours to predict. Let's delve into a comprehensive elucidation of each machine-learning model:

AdaBoost, an abbreviation for Adaptive Boosting, emerges as an ensemble learning technique that amalgamates weak learners into a potent classifier. Its proficiency lies in navigating diverse data types by iteratively adjusting the weights of misclassified instances, accentuating the significance of challenging data points throughout the learning process. Random Forest, operating through the construction of numerous decision trees during training, Random Forest culminates in predicting the mode of classes. This model excels in managing intricate relationships within the data, proving particularly advantageous in scenarios characterized by high-dimensional datasets (Fan et al., 2023). Decision trees, a foundational machine learning model, intricately partition data into subsets based on distinctive features. Renowned for its versatility and interpretability, this model finds applicability in both classification and regression tasks (Gao et al., 2023). A robust model for classification and regression endeavours, SVM establishes its effectiveness by pinpointing the hyperplane that optimally segregates data into distinct classes, maximizing the margin between them. SVM shines, especially in scenarios where data lacks linear separability (Gao et al., 2023). Embracing the principles of ensemble learning, Gradient Boosting orchestrates a sequence of weak learners, often decision trees, to rectify errors from preceding ones. Renowned for its prowess in predictive modelling, it consistently yields accurate results (Fan et al., 2023). Linear Regression, despite its simplicity, emerges as a potent model for predicting continuous outcomes. Rooted in the assumption of a linear relationship between input features and the target variable, it finds suitability in scenarios where data exhibits a linear trend (Fan et al., 2023). The selection of the most fitting machine learning model hinges on the nature of the data and the specifics of the prediction task at hand. A profound understanding of the unique characteristics and strengths inherent in each model empowers data, scientists and machine learning practitioners to make judicious choices, thereby optimizing the predictive prowess of their algorithms across a spectrum of diverse datasets.

3.4.3.1 Evaluation of performance

The assessment of machine learning models' performance is crucial for understanding the accuracy and reliability of their predictions. In this context, three essential statistical indicators were employed to quantitatively measure the errors and gauge the models' effectiveness. These indicators, namely the root mean squared error (RMSE), the mean absolute error (MAE), and the determination coefficient R^2 offer valuable insights into the models' ability to capture and predict the underlying patterns in the data. The root mean squared error (RMSE) is a widely used metric that evaluates the average magnitude of the errors between the predicted values and the actual observed values. By squaring the differences, computing the mean, and taking the square root, the RMSE provides a clear understanding of the overall accuracy of the machine learning model's predictions. A lower RMSE value signifies that the model's predictions are closer to the actual data, indicating better performance. The mean absolute error (MAE), another important indicator, calculates the average absolute difference between the predicted values and the observed data. Unlike RMSE, MAE does not involve squaring the errors, making it less sensitive to extreme outliers. A lower MAE value suggests that the model's predictions are more accurate and exhibit less bias. Additionally, the determination coefficient R^2, also known as the coefficient of determination, plays a crucial role in assessing the goodness of fit of the machine learning model. R^2 measures the proportion of the variance in the dependent variable that can be explained by the independent variables in the model. It ranges from 0 to 1, with a higher R^2 value indicating that the model explains a greater portion of the variability in the data. Moreover, the process of evaluating machine learning models using RMSE, MAE, and R^2 is an essential step in the iterative improvement of predictive capabilities and is calculated based on the Equations 3.46 to 3.48 (Fawaz et al., 2019). Researchers can fine-tune parameters, adjust algorithms, and optimize the model structure based on the insights gained from these evaluations. This iterative approach allows for continuous enhancements, resulting in more accurate and robust predictions over time.

$$\boldsymbol{RMSE} = \sqrt{\sum_{j=1}^{N} \frac{(P_{j} - \widehat{P}_{j})^2}{N}} \qquad \textbf{3.46}$$

$$MAE = \sqrt{\sum_{j=1}^{N} \frac{|P_{j-}\hat{P}_j|}{N}} \qquad 3.47$$

$$R^2 = 1 - \frac{\sum_{j=1}^{N}(\hat{P}_j - P_j)^2}{(\hat{P}_j - \hat{P}_{ave})^2} \qquad 3.48$$

where $P_j, \hat{P}_j, and\ \hat{P}_{ave}$ Predictive data, target data, and an average of the target data.

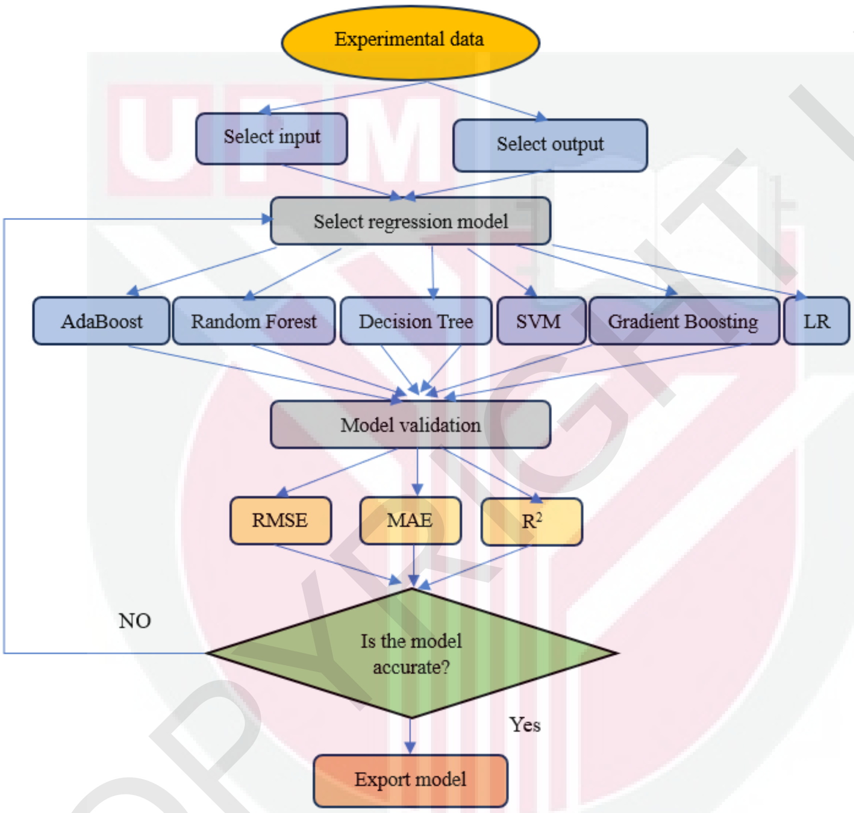

Figure 3.11: Machine learning methodology

3.4.4 Empirical correlation

In the context of the solar panel's electric power and temperature, an empirical correlation was developed based on a group of influential factors. These factors included solar radiation, water volume flow rate, porosity size, and water viscosity. By analysing and quantifying the relationships between these variables, the empirical correlation contributed to a better understanding of the impact of these factors on the solar panel's electrical performance and thermal behaviour. The empirical Correlation coefficient played a fundamental role in understanding variable relationships and facilitating accurate predictions. It was an invaluable tool in decision-making, model enhancement, and making meaningful connections between different factors. By applying this concept to the solar panel's electric power and temperature, researchers gained critical insights into the factors influencing its performance, paving the way for more efficient and effective solar energy utilization.

3.4.4.1 Output power and PV temperature empirical correlation

Through experimental work, a lot of evidence was collected on the effects of the output power PV temperature. Buckingham's theory was used to obtain the unknown to change the temperature. The basic dimensions are fundamental physical quantities used to describe all physical phenomena. The four basic dimensions in the International System of Units (SI) are Mass (M) - Measured in kilograms (kg), Length (L) - Measured in meters (m), Time (T) - Measured in seconds (s), Temperature (θ) - Measured in kelvin (K) These four basic dimensions form the foundation of dimensional analysis, which is used to derive non-dimensional groups or π groups to express physical relationships in terms of dimensionless quantities. Variables and dimensions are shown in Tables 3.6 and 3.7.

Table 3.6: Variants and dimensions for output power

variables	Dimensions	variables	Dimensions
G	$\frac{M}{T^3}$	$\frac{G}{\rho V^3}$	1
P	$\frac{ML^2}{T^3}$	$\frac{P}{\rho L^2 V^3}$	1
ρ	$\frac{M}{L^3}$	ρL^3	M
V	$\frac{L}{T}$	$\frac{V}{L}$	$\frac{1}{T}$
D_{hd}	L	L	L

Equation 3.49 represent the relationship of output power to a set of variables such as solar radiation, water velocity, water density, and the equivalent diameter of porous media.

$$\mathbf{P = f(G, D_{hd}, \rho, V)} \qquad \textbf{3.49}$$

Through Equation 3.49, it is clear that there are four independent variables, three of which include basic dimensions such as mass, length, time, and temperature. Accordingly, the analysis is as follows:

$$\Pi_1 = \frac{G}{\rho V^3} \qquad \textbf{3-50}$$

$$\Pi_2 = \frac{P}{\rho D_{hd}^2 V^3} \qquad \textbf{3.51}$$

$$\Pi_1 = c\Pi_2 \qquad \textbf{3-52}$$

$$\frac{\mathbf{P}}{\rho \mathbf{D_{hd}}^2 \mathbf{V}^3} = \mathbf{c}\frac{\mathbf{G}}{\rho \mathbf{V}^3} \qquad \mathbf{3.53}$$

$$V = \frac{\widehat{V}_w}{\phi} \qquad \mathbf{3.54}$$

Through Equations 3.50 to 3.54, can find the output power in its final form.

$$\mathbf{P = cGD_{hd}}^2 \qquad \mathbf{3\text{-}55}$$

where G expresses the solar radiation falling on the solar panel during the experiment, ϕ expresses the porosity size used, V the is water velocity during cooling, $\widehat{V}_w$ the water velocity without porous media, and c the correlation factor. The results of the correlation of electrical power for porosity have been found. It was compared with the experimental results and the error was found. All the results will be explained later.

Table 3.7: Variants and dimensions for temperature

variables	Dimensions	variables	Dimensions
G	$\frac{M}{T^3}$	$\frac{G}{\rho V^3}$	1
C_P	$\frac{L^2}{\theta T^2}$	$\frac{C_P \theta}{V^2}$	1
ρ	$\frac{M}{L^3}$	ρL^3	M
V	$\frac{L}{\mathrm{T}}$	$\frac{V}{\mathrm{L}}$	$\frac{1}{\mathrm{T}}$
θ	θ	θ	θ

where G expresses the solar radiation falling on the solar panel during the experiment, ε expresses the porosity size used, V is the water velocity during cooling, solar panel length L, while θ is PV temperature minus water inlet temperature.

$$\theta = f(G, C_p, \rho, V, L) \quad \textbf{3.56}$$

Through Equation 3.56, it is clear that there are 6 independent variables, four of which include basic dimensions such as mass, length, time, and temperature. Accordingly, the analysis is as follows:

$$\Pi_1 = \frac{G}{\rho V^3} \quad \textbf{3.57}$$

$$\Pi_2 = \frac{C_P \theta}{V^2} \quad \textbf{3.58}$$

The PV temperature correlation was developed based on some variables as mentioned earlier, including solar radiation, water velocity, porosity size, solar panel length, and inlet water temperature. Through Equations 3.57 to 3.60, can find the PV temperature in its final form. Based on Equations 3.61, it is possible to find the PV temperature.

$$\Pi_2 = a\ \Pi_2 \quad \textbf{3.59}$$

$$\frac{C_P \theta}{V^2} = a \frac{G}{\rho V^3} \quad \textbf{3.60}$$

$$\theta_c = \frac{aG}{C_P \rho V} + \theta_{in} \quad \textbf{3.61}$$

where G expresses the solar radiation falling on the solar panel during the experiment, ϕ expresses the porosity size used, V is the water velocity during cooling, $\hat{V}_w$ is the water velocity without porous media, C_p is the specific heat of water ρ is the density of water and a is the correlation factor. The results of the correlation of electrical power for porosity have been found. It was compared with the experimental results and the error was found. All the results will be explained later.

CHAPTER 4

RESULTS AND DISCUSSION

4.1 Overview

The primary objective of this research was to investigate the temperature reduction of the solar cells, thereby increasing both the electrical power and efficiency, while also ensuring the long-term preservation of the solar panels. To achieve this goal, the incorporation of a cooling system was deemed necessary, with the use of water and porous media being among the potential options to be explored. This chapter will show various results obtained from the experimentation processes, accompanied by in-depth discussions for each case. Consequently, the research work was bifurcated into two distinct components, namely experimental and numerical and the results are illustrated and discussed in this chapter.

4.2 Experimental work

During the indoor testing phase, the photovoltaic cells were subjected to controlled conditions in the solar energy laboratory. This enabled precise monitoring and analysis of the cooling system's impact on the temperature regulation of the cells. Various parameters, including solar radiation intensity, water velocity, and porosity size, were monitored and recorded to establish a clear correlation between the cooling system's performance and the photovoltaic cells' temperature. The outdoor experimental tests, on the other hand, emulated real-world conditions, providing valuable insights into the cooling system's effectiveness in practical applications. The outdoor testing scenario simulated the operating conditions encountered by photovoltaic cells in real-world installations, thus offering a more comprehensive understanding of the cooling system's performance. Throughout both the indoor and outdoor testing phases, data collection and rigorous analysis were carried out, adhering to scientific methodologies. The temperature of the photovoltaic cells was monitored under various cooling scenarios, while the electrical power output and efficiency were evaluated.

4.2.1 Indoor test

The indoor experimental setup allowed for precise control over ambient conditions, enabling a systematic exploration of the cooling system's performance under varying parameters. To ensure a comprehensive evaluation, a series of experiments were studied, encompassing four different porosity sizes: 0.35, 0.4, 0.48, and 0.5. For each porosity size, an investigation was carried out with five different volume flow rates of water: 1, 1.5, 2, 3, and 4 L/min. The aim was to identify the most optimal porosity size and volume flow rate combination for efficient PV cooling.

4.2.1.1 Enhanced photovoltaic panel temperature at porosity 0.35

In this experiment, the porosity size was fixed at 0.35 and the volume flow rate was changed. The aim was to find out the best amount of volume flow rate with fixed porosity size. Figure 4.1 shows the time in minutes with photovoltaic panel temperature of the experiments tested at different volume flow rates of 1, 1.5, 2, 3, and 4 L/min, for three continuous hours without any interruption. Based on Figure 4.1, the temperature increases gradually for the three cases; without cooling, cooling with water, and cooling with the porous size of 0.35, until it reaches stability and almost constant temperature. This increase in temperature was reasonable due to the amount of heat rejected by the photovoltaic panel. Based on this Figure 4.1a for a volume flow rate of 1 L/min the PV temperature without cooling was about 87.8^{o}C, and the temperature of the solar panel with water cooling was about 51^{o}C, while the cooling using the porous size of 0.35 reached 40.57^{o}C. The temperature of the solar panel without cooling was taken as a reference. This comparison was made through Equation 3.1, where the percentage of reduction in temperature was 51%. Based on Figure 4.1b, it is clear that the behaviour of the temperature of the solar panel when using a flow rate of 1.5 L/min was very similar to the behaviour when using 1 L/min, but with a difference in the temperature values, so that the temperature of the photovoltaic panel with water cooling reached 50.9^{o}C, while the temperature of cooling with porous media of 0.35 reached 40.16^{o}C. The percentage of reduction in temperature was 52.65%. Figure 4.1c shows the temperature behaviour at water volume flow rates of 2 L/min, where the PV panel temperature value reached 48.55^{o}C when cooling with water and 38.7^{o}C when using porous media. Figure 4.1d and e shows the temperature values for volume flow rates of 3 L/min, and 4 L/min, where they had the same behaviour but with different temperature values, where the temperature of cooling with porous media reached 39.7^{o}C and 39^{o}C respectively. These results highlight the effectiveness of cooling in reducing the temperature of the photovoltaic panels during operation. Water cooling and the use of porous media with a fixed porosity size of 0.35 were both successful in significantly reducing the panel temperature compared to the case without cooling.

4.2.1.2 Enhanced output power at porosity size 0.35

Figure 4.2 presents the change of output power with time for the three cases mentioned above, where the output power decreased with time due to the increase in temperature until it reached stability. Based on Figure 4.2a for a volume flow rate of 1 L/min, the output power from the solar panel for the three cases was as follows; without

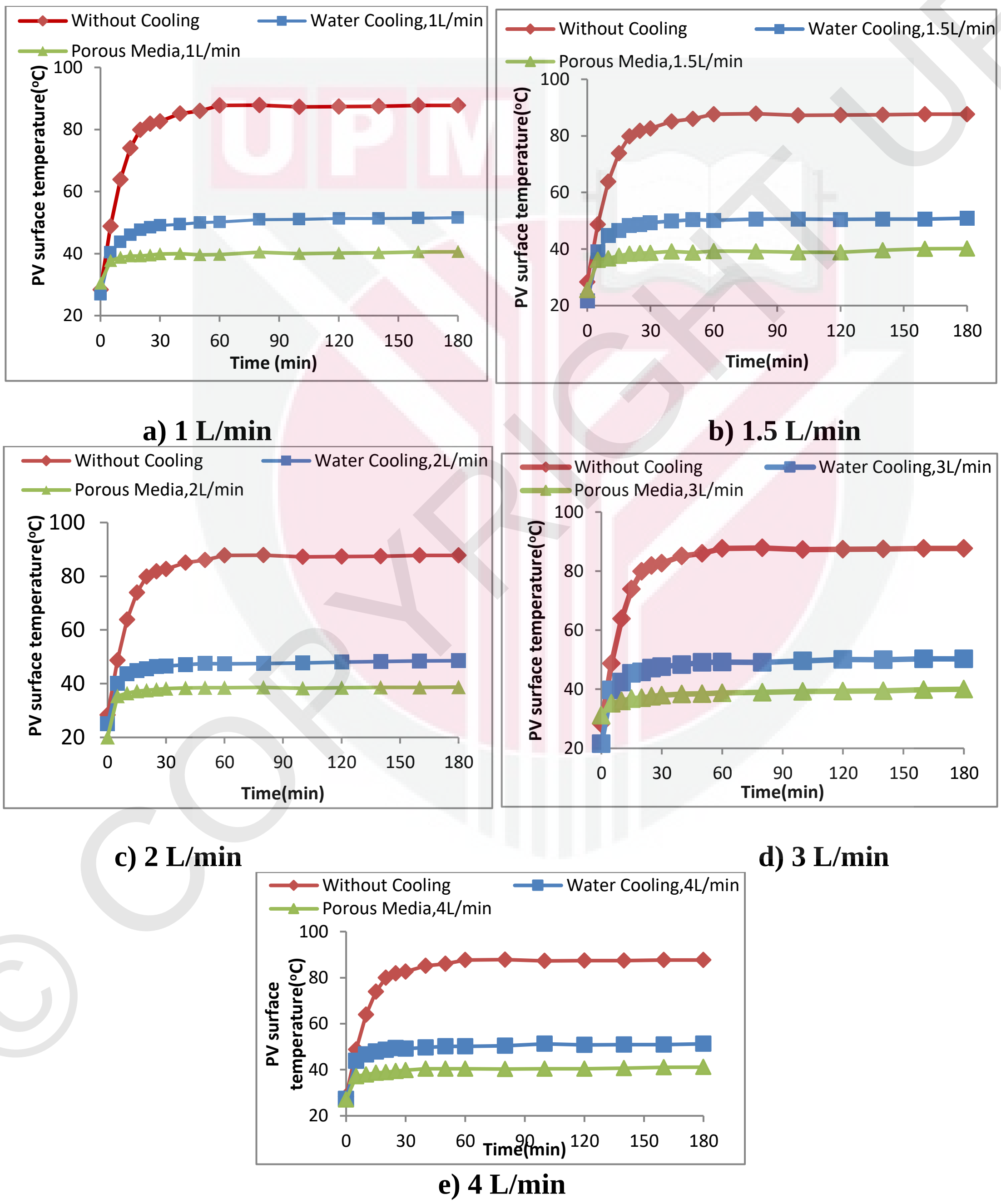

Figure 4.1: Experimental PV temperature results for porosity size 0.35 at different volume flow rates

cooling the power was reduced to 12.45 W, with water cooling reduced to 16.67 W, and cooling with porous media of 0.35 found to be the best among the three results, reaching a value of 18.01 W, while the percentage of increase was as follows: 34% for water cooling and 45% for porous cooling. From Figure 4.2b for volume flow rate at 1.5 L/min, the output power was as follows; for the water-cooling case reached 17.15 W, while the power reached 18.43 W for porous media cooling. Therefore, the percentage increase in power was as follows: 38% for water cooling and 48.39% for porous cooling.

Figure 4.2c shows the output power with time for a volume flow rate of 2 L/min. The results are as follows: Through cooling with water, the output power reduction was 17.3 W, but the output power reached 18.84 W due to cooling with the porous media of 0.35, so the percentage of increase was 51.69% for porous cooling. Through Figure 4.2d and 4.2e for the volume flow rate of 3 L/min and 4 L/min, the output power was as follows: water cooling reached 16.97 W and 17.3 W, while power for cooling by porous media reached 18.7 W and 18.73 W. Therefore, that the increase was as follows: 50.56% and 50.81% for porous cooling respectively.

4.2.1.3 Enhanced electrical efficiency at porosity size 0.35

From Figure 4.3, which illustrates the relationship between electrical efficiency and time, it becomes clear that efficiency has reduced over time for the no-cooling case. It was noticed also that the reduction in efficiency was greatest at no cooling, reaching the lowest value of 4.13%. However, with water cooling, it reached 5.54%. While cooling through porous media efficiency increased till it reached 6% based on Figure

4.3a. In Figure 4.3b, the electrical efficiency behaviour at a flow rate of 1.5 L/min, showed similar behaviour as a flow rate of 1 L/min, but with a difference in the electrical efficiency results, as it reached 5.82% with water cooling, while electrical efficiency reached 6.13% for the cooling with porous material of 0.35. Figure 4.3c shows the behaviour of the electrical efficiency at water volume flow rates of 2 L/min, reaching 5.75% for cooling with water and up to 6.26% for using porous material. Figures 4.3d and 4.3e showed the efficiency values for the 3 L/min and 4 L/min volume flow rates, where they had the same efficiency behaviour as at the previous volume flow rates of 1 L/m and 2 L/m but with different values, thence when cooling with porous material used the efficiency value reached 6.22% and 6.23% respectively.

4.2.1.4 Enhanced I-V curve at porosity size 0.35

Figure 4 -4a illustrates the relationship between current and voltage for the photovoltaic panel for all three cases mentioned above at a volume flow rate of 1 L/min. It is evident that as the temperature increases, there is a slight increase in current and a clear reduction in voltage. This emphasizes the importance of implementing a cooling system for the photovoltaic cells. The best case was cooling done through porous media, where the open voltage increased significantly and reached 22.54 V. While the water-cooled photovoltaic panel reached 21.41 V, thence the non-cooled solar panel showed a clear reduction in open voltage, reaching its lowest value of 18 V. Figure 4.4b expresses the voltage and current at a volume flow rate of 1.5 L/min, where the voltage reached 21.68V when cooled with water while cooling with porous media reached 22.65 V, and the lowest voltage of 18 V occurred for no cooling. Figures 4.4c, 4.4d, and 4.4e for volume flow rates of 2, 3, and 4 L/min. The values of the open voltages cooled with water were 21.47, 21.77, and 21.82 V. The coolant by porous media was 22.77, 22.75, and 22.67 V.

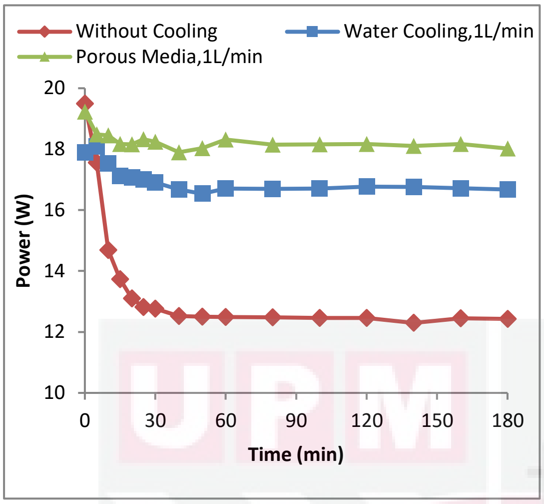

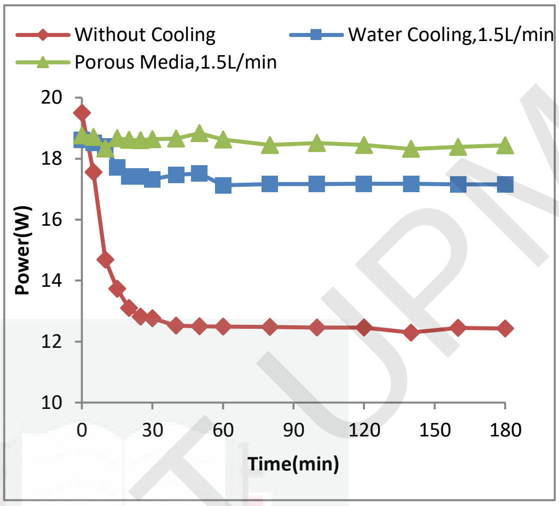

a) 1 L/min **b) 1.5 L/min**

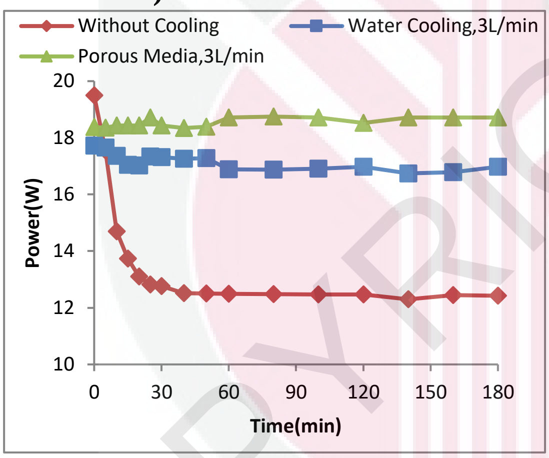

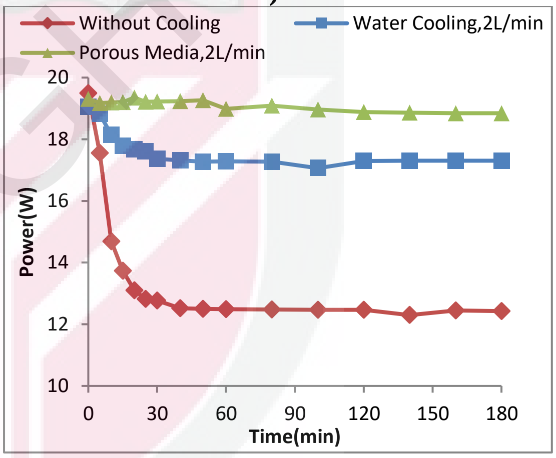

c) 2 L/min **d) 3 L/min**

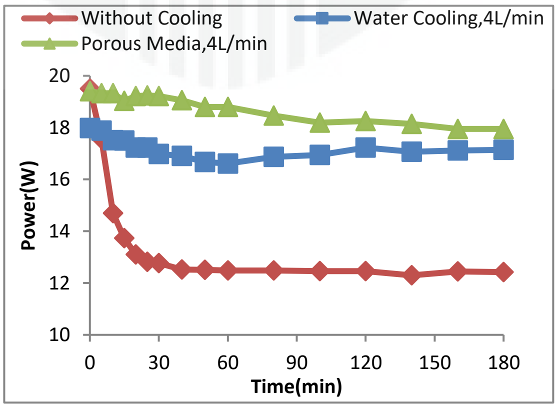

e) 4 L/min

Figure 4.2: Experimental output power results for porosity size 0.35 at different volume flow rates

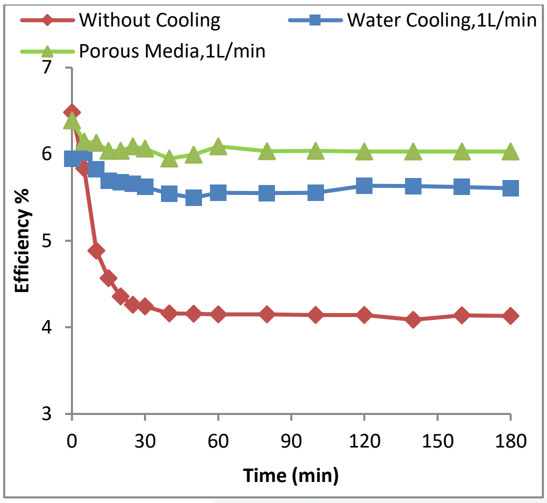

a) 1 L/min

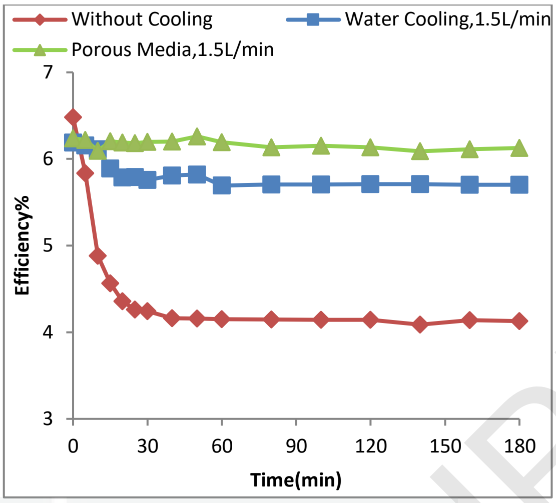

b) 1.5 L/min

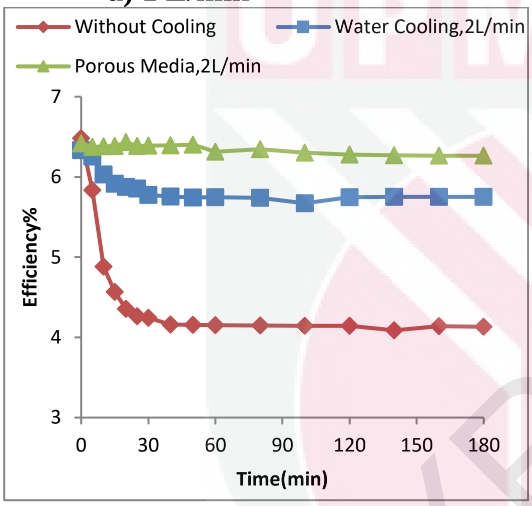

c) 2 L/min

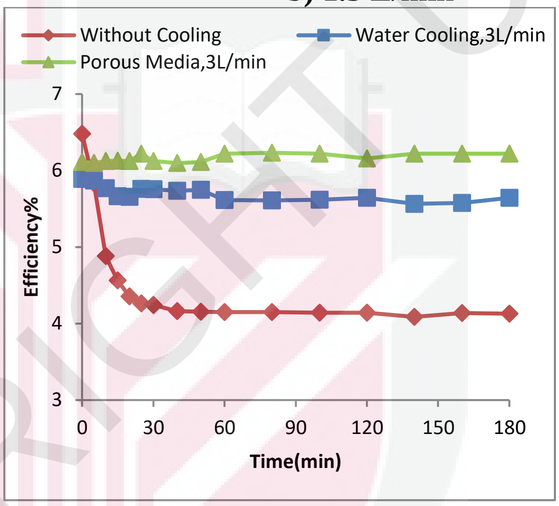

d) 3 L/min

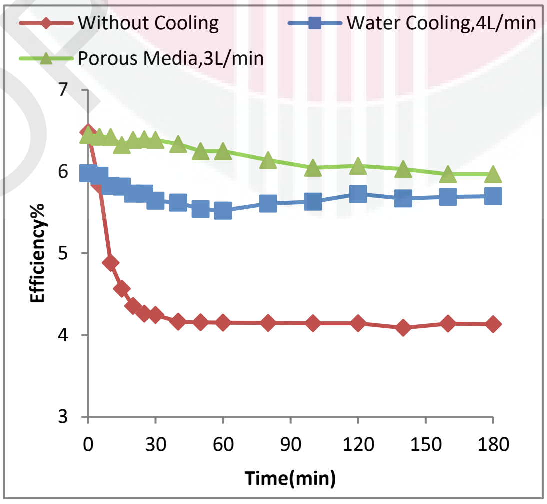

e) 4 L/min

Figure 4.3: Experimental efficiency for porosity size of 0.35 at different volume flow rates

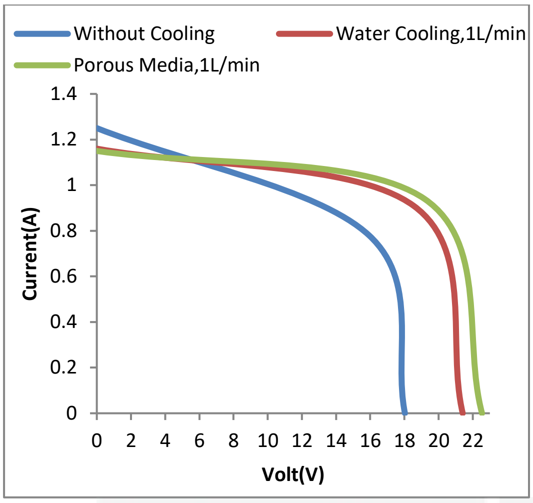

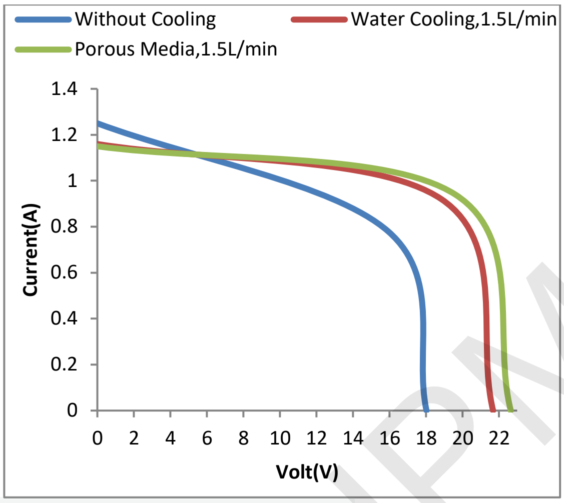

a) 1 L/min **b) 1.5L/min**

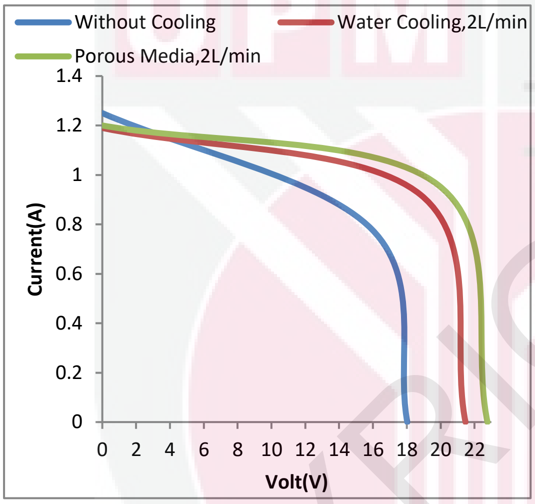

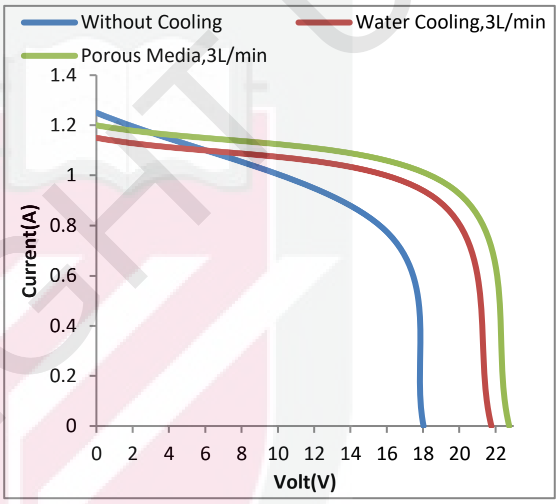

c) 2 L/min **d) 3 L/min**

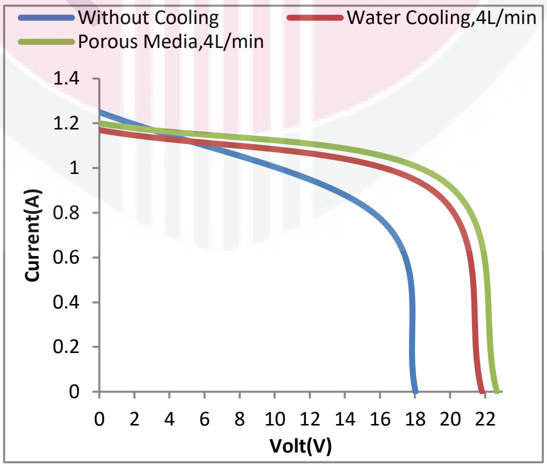

e) 4 L/min

Figure 4.4: Experimental I- V curve results for porosity size 0.35 at different volume flow rates

4.2.1.5 Enhanced photovoltaic panel temperature at porosity size 0.4

In this experiment, a porosity size of 0.4 was used as a coolant for photovoltaic cells at various flow rates. Figure 4.5 shows the change in the temperature of the photovoltaic panel with time due to the difference in volume flow rat, so the temperature gradually increases for the three cases until it reaches stability and constant temperature. In Figure 4.5a the cooling through the porous media reached 43°C when the volume flow rate was at 1L/min. Based on Figure 4.5b, the temperature of the PV panel at a volume flow rate of 1.5L/min reached 41.53°C. Figure 4.5c shows the temperature behaviour at water volume flow rates of 2 L/min, where the PV model temperature value reached 40.35°C when porous media was used. Figures 4.5d and 4.5e showed that the temperature values for the volume flow rates of 3 L/min and 4 L/min and the temperatures by cooling with porous media reach 40.20^{o}C and 40.00^{o}C respectively.

4.2.1.6 Enhanced output power at porosity size 0.40

Figure 4.6 presents the change of output power with time for the three cases it is found that the output power reduced with time due to the increase in temperature until it reached stability. Figure 4.6a shows that for a volume flow rate of 1 L/min, the output power of the solar panels cooled with porous media is the highest having a value of 17.63W, while Figure 4.6b showed that for a volume flow rate of 1.5 L/min, the output power of the solar panels cooled with porous media is about 18 W, and for a volume flow rate of 2 L/min, the power is 18.4 W. While in Figures 4.6d and 4.6e for the volume flow rate of 3 L/min and 4 L/min, the output power reached 18.4 W and 18.4 W respectively.

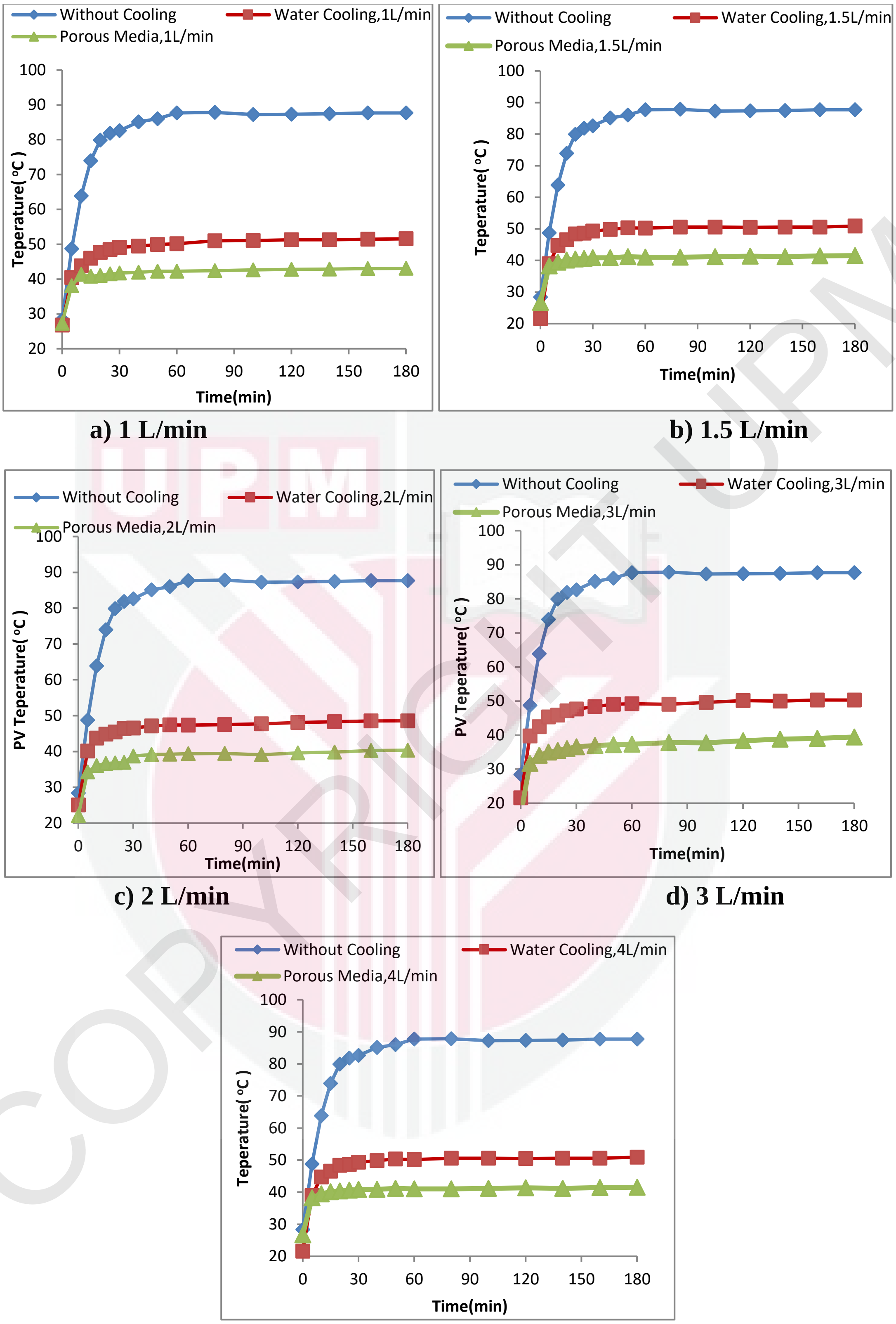

a) 1 L/min

b) 1.5 L/min

c) 2 L/min

d) 3 L/min

e) 4 L/min

Figure 4.5: Experimental PV temperature results for porosity size 0.40 at different volume flow rates

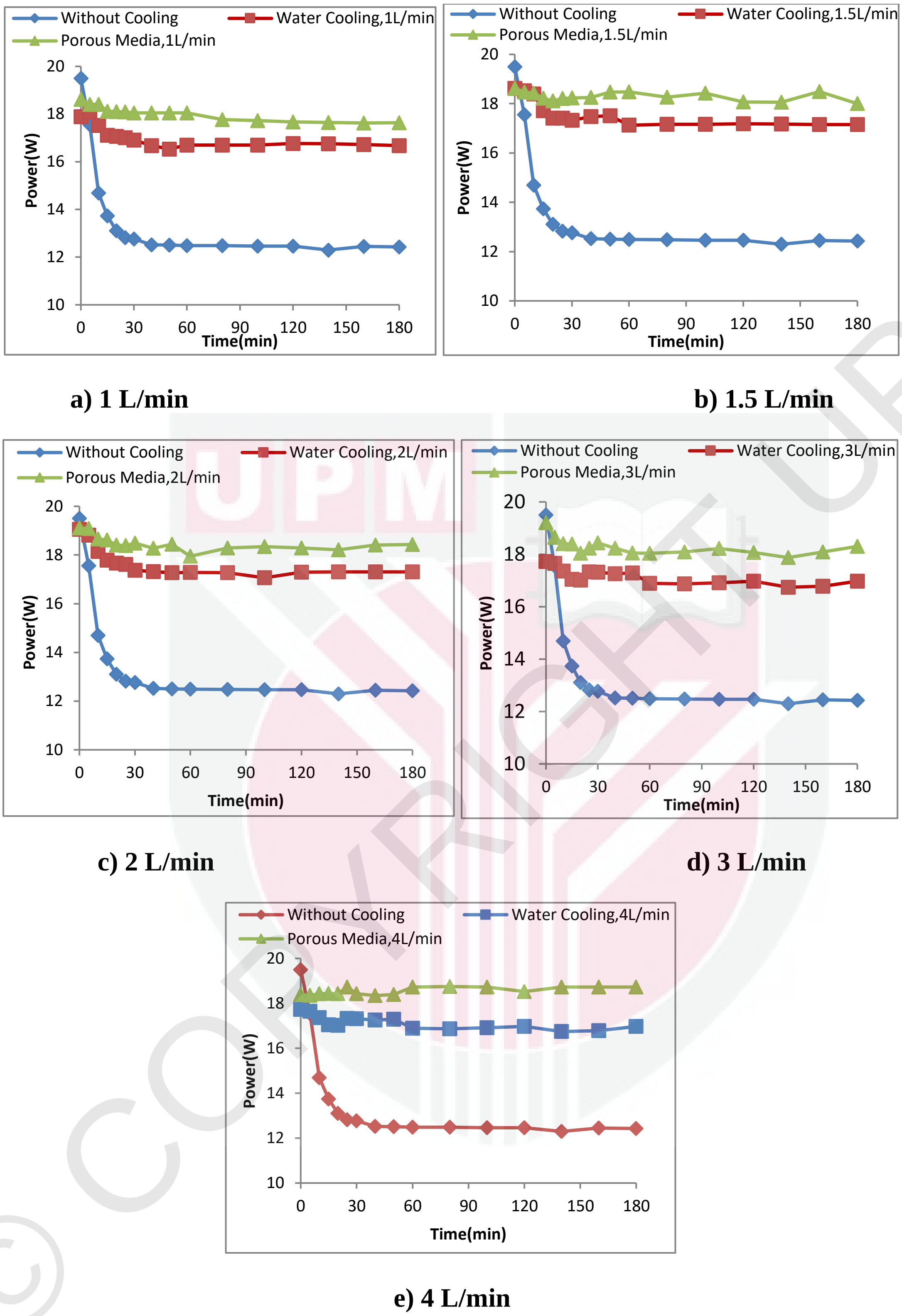

Figure 4.6: Experimental output power results for porosity size 0.4 and at different volume flow rates

4.2.1.7 Enhanced electrical efficiency at porosity size 0.40

From Figure 4.7a, which shows the relationship between electrical efficiency and time, at a flow volume of 1 L, the efficiency reached 5.86%. It is highlighted in Figure 4.7b that the efficiency at a flow rate of 1.5 L/min reached 5.98%. At water volume flow rates of 2 L/min, reached 6.12% Figure 4.7c. The volume flow rates of 3 L/min and 4 L/min reached 6.12%and 6.12%, respectively.

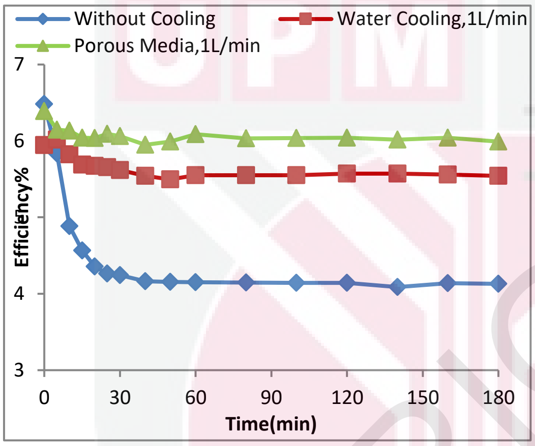

a) 1 L/min

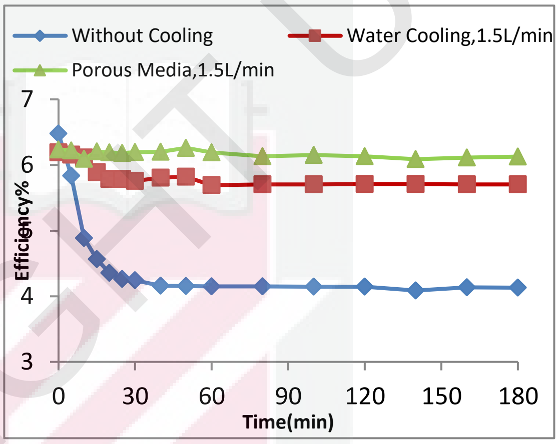

b) 1.5 L/min

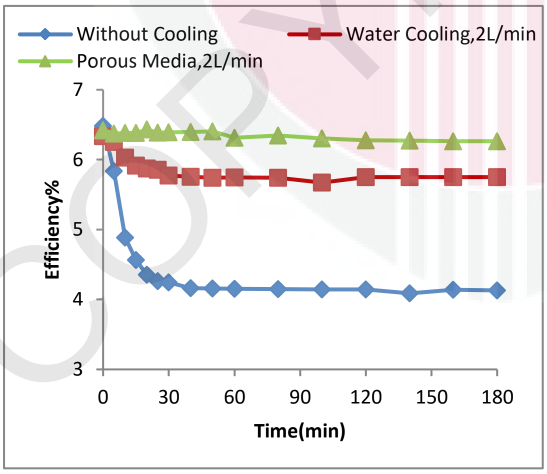

c) 2 L/min

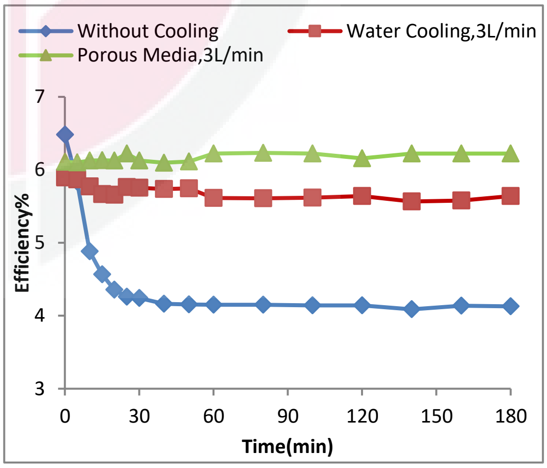

d) 3 L/min

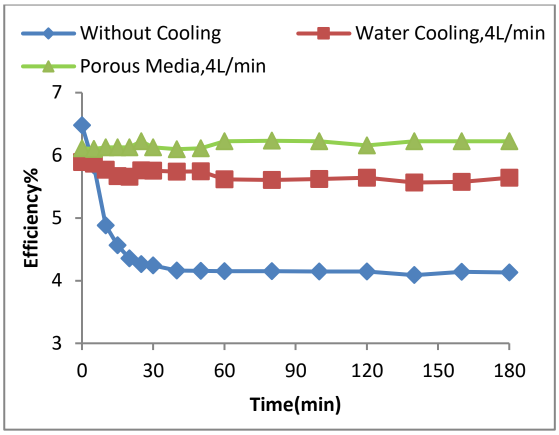

e) 4 L/min

Figure 4.7: Experimental efficiency results for porosity size 0.40 at different volume flow rates

4.2.1.8 Enhanced I-V curve at porosity size 0.40

Figure 4.8a shows the relationship between current and voltage for a PV panel with a flow rate of 1 L/min. It can be seen that the open voltage reached 22.54 V for porous media cooling. Figure 4.8b shows the voltage and current at a volume flow rate of 1.5 L/min, where the voltage reached 22.65V, and with volume flow rates of 2, 3, and 4 L/min, the value of the open voltages were 22.77, 22.75 and 22.67V, respectively, as shown in Figures 4.8c, 4.8d, and 4.8e.

4.2.1.9 Enhanced photovoltaic panel temperature at porosity 0.48

In this test, a porosity size of 0.48 was used to cool PV cells with different flow rates. From Figure 4.9, the PV temperature by cooling through the porous material reached 45°C when the volume flow rate was 1 L/min. While at volume flow rates of 1.5 L/min PV temperature reached 42.8°C and at water volume flow rates of 2 L/min, the temperature value of the PV model reached 42.36°C. At volume flow rates of 3 L/min and 4 L/min, the temperature reached 41.43^{o}C and 41.40^{o}C, respectively.

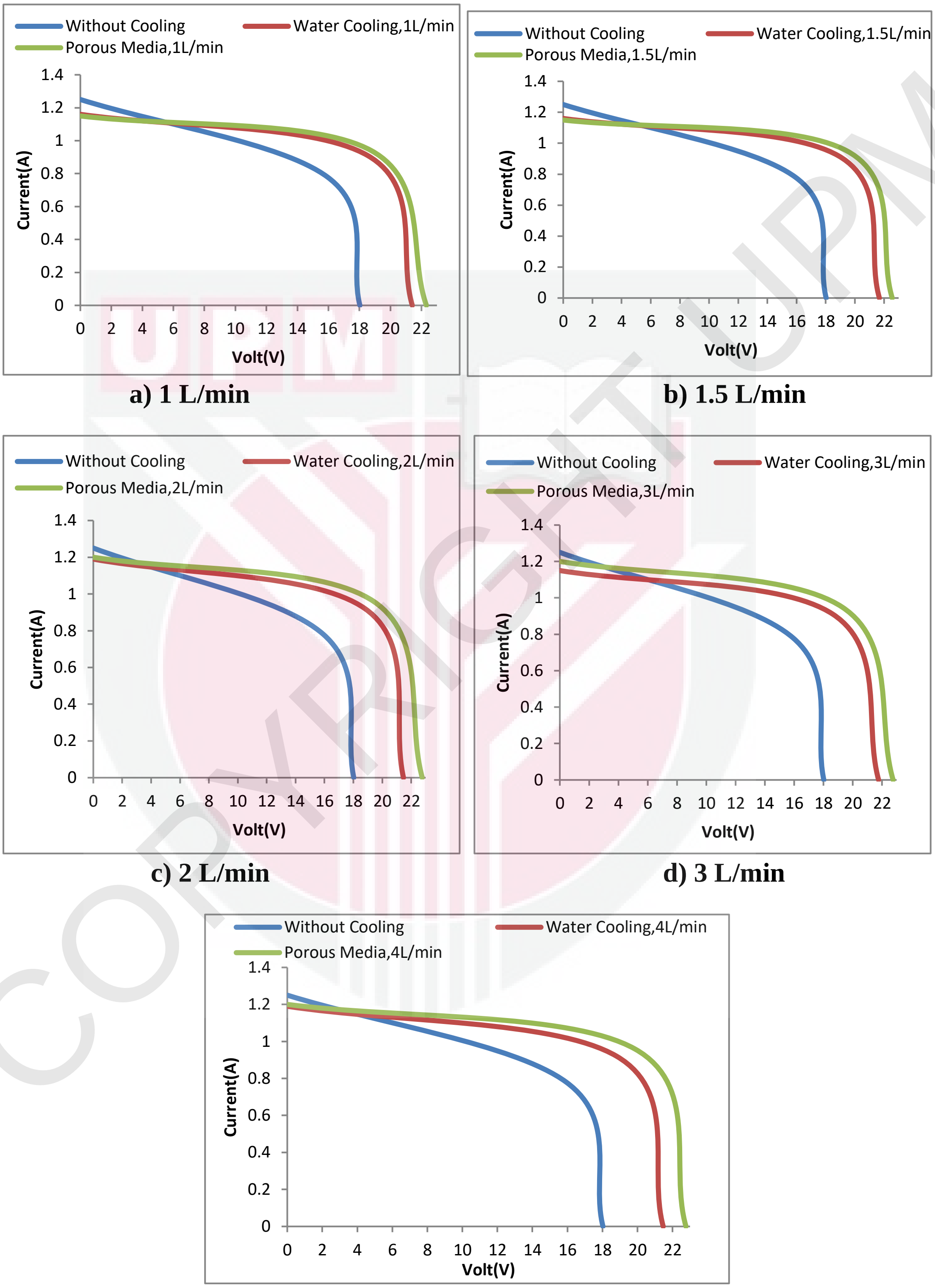

e) 4 L/min

Figure 4.8: Experimental I- V curve results for porosity size 0.40 at different volume flow rates

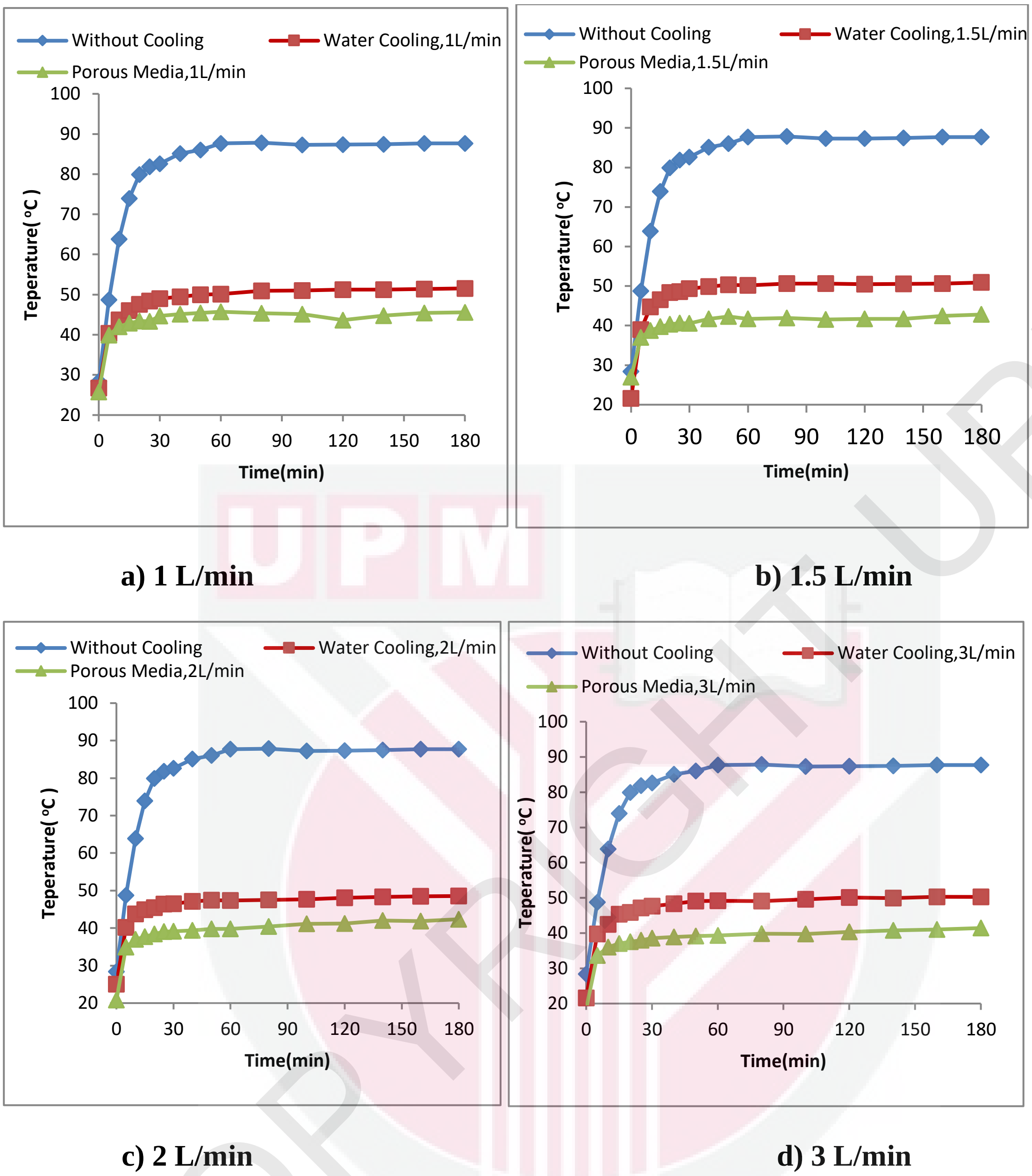

Figure 4.9: Experimental PV temperature results for porosity size 0.48 at different volume flow rates

4.2.1.10 Enhanced output power at porosity size 0.48

Figure 4.10 presents the variation of output power over time for different volume flow rates: 1 L/min, 1.5 L/min, 2 L/min, and 3 L/min. The solar panels in these tests were filled with porous material having a porosity size of 0.48. The corresponding output power values recorded for each flow rate were 16.9 W, 17.67 W, 17.8 W, and 18.16

W, respectively. The results from Figure 4.10 demonstrate how the volume flow rate impacts the output power of the solar panels. As the flow rate increases, there is a noticeable improvement in the output power, indicating that the cooling effect provided by the flow of fluid through the porous material enhances the performance of the photovoltaic system.

The highest output power of 18.16 W was achieved when the volume flow rate was set at 3 L/min, while the lowest output power of 16.9 W was observed at a flow rate of 1 L/min. This significant difference in output power between the two flow rates highlights the importance of efficient cooling mechanisms in photovoltaic systems.

The experiment's results suggest that employing the proper volume flow rate and utilizing the porous material with a porosity size of 0.48 can lead to substantial enhancements in the output power of solar panels. This information is valuable for designing and optimizing solar power systems to maximize energy generation and overall efficiency.

4.2.1.11 Enhanced electrical efficiency at porosity size 0.48

Figure 4.11 shows the relationship between electrical efficiency and time, at flow rates 1 L/min, 1.5 L/min, 2 L/min, and 3 L/min, where the efficiency at each flow rate reached 5.62%, 5.87%, 5.92%, and 6.04% respectively.

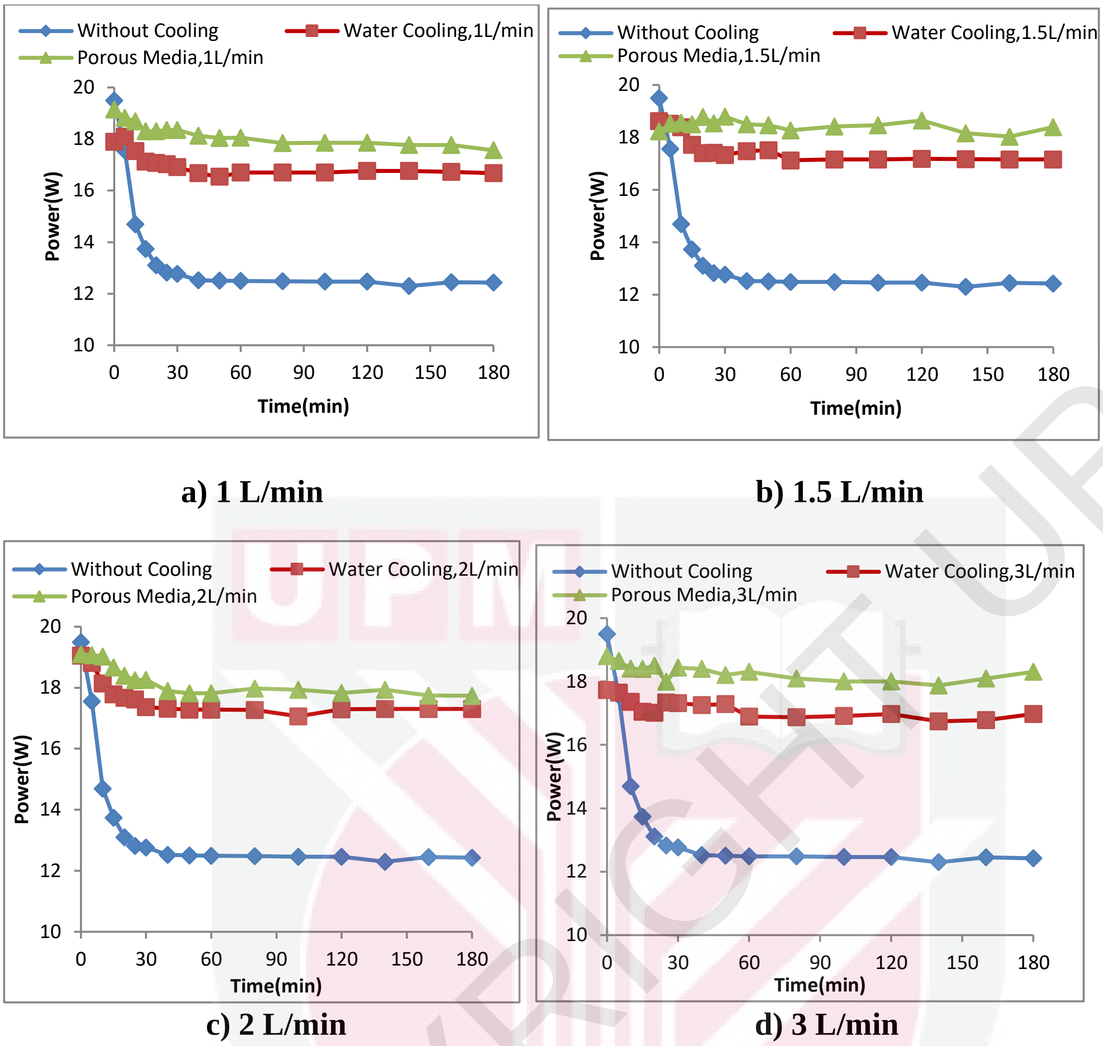

Figure 4.10: Experimental output power results for porosity size 0.48 at different volume flow rates

4.2.1.12 Enhanced I-V curve at porosity size 0.48

In Figure 4.12a, the graphical representation illustrates the correlation between current and voltage for a photovoltaic (PV) panel with a flow rate of 1 L/min. The open voltage, which refers to the voltage across the PV panel when no current flows through it, was recorded to be 22.5 V. This value provides valuable information about the panel's performance and its ability to generate electricity under specific flow conditions.

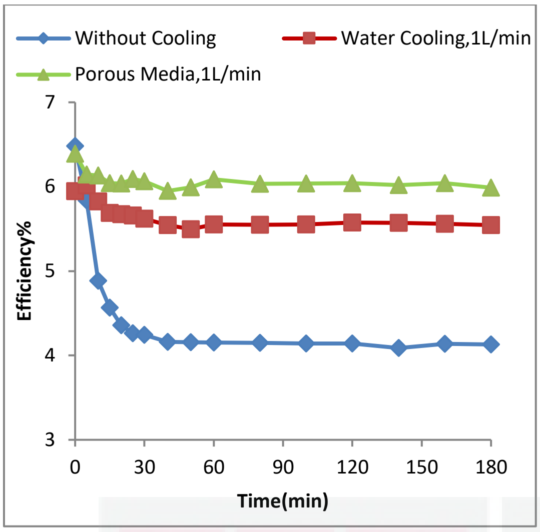

a) 1 L/min

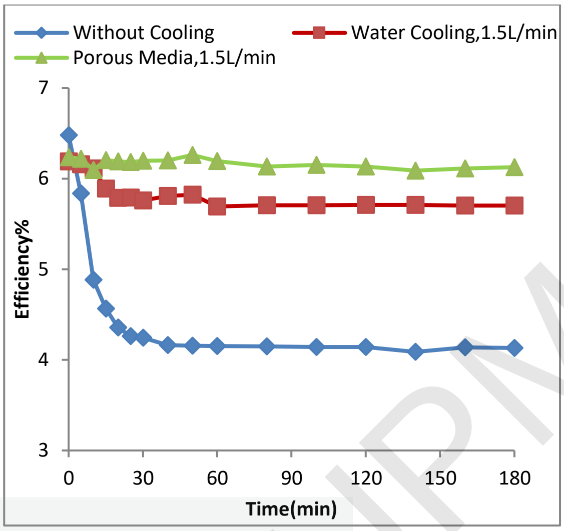

b) 1.5 L/min

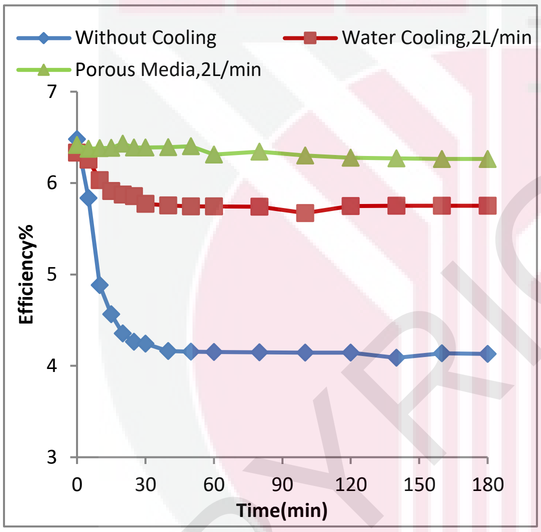

c) 2 L/min

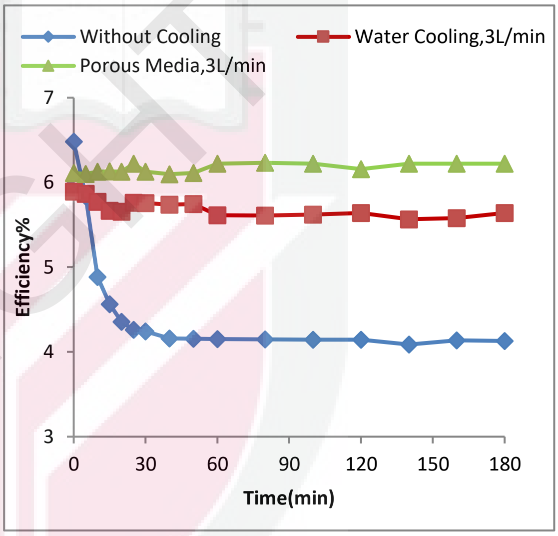

d) 3 L/min

Figure 4.11: Experimental efficiency results for porosity size 0.48 and different volume flow rates

Moving on to Figure 4.12b, the plot showcases the voltage and current behaviour at a volume flow rate of 1.5 L/min. At this flow rate, the voltage reading reached 22.6 V. As the volume flow rate increased to 2 L/min and 3 L/min, the open voltage values also experienced slight increments, measuring 22.68 V and 22.70 V, respectively.

The trends observed in Figures 4.12a and 4.12b reveal that the volume flow rate has a marginal influence on the open voltage of the PV panel. While the differences in voltage values are relatively small between the flow rates, they are still essential to consider when assessing the overall performance of the photovoltaic system.

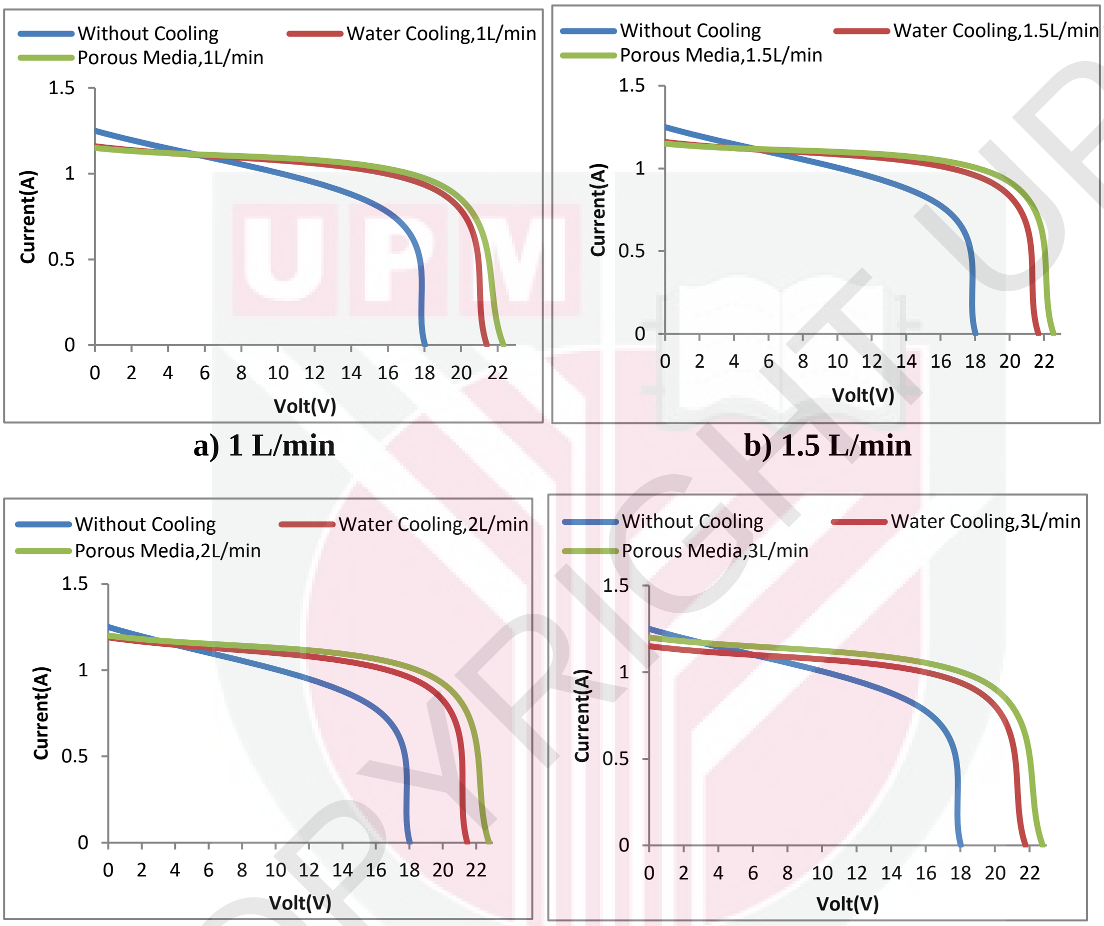

a) 1 L/min

b) 1.5 L/min

c) 2 L/min

d) 3 L/min

Figure 4.12: Experimental I- V curve results for porosity size 0.48 at different volume flow rates

4.2.1.13 PV temperature and output power at variable porosity size

Numerous experiments have been diligently conducted to investigate the cooling efficiency of photovoltaic cells, aiming to determine their temperature and output power under various conditions. These experiments involved testing different porosities, namely 0.35, 0.40, 0.48, and 0.5, and examining diverse volume flow rates, including 1, 1.5, 2, 3, and 4 L/min. By comparing the results obtained from these experiments, the experiment sought to identify the most favourable case and determine the optimum conditions for cooling photovoltaic panels effectively.

Remarkably, the outcomes of these experiments consistently revealed a significant reduction in temperature across all the tested porosity sizes and volume flow rates. As a direct consequence of this temperature reduction, there was an increase in the output power of the photovoltaic cells. This positive correlation between temperature decreases and output power enhancement further underscores the significance of efficient cooling strategies in maximizing the performance of photovoltaic systems.

The comprehensive results depicting the photovoltaic panel temperature and output power have been compiled and depicted in Figure 4.13. The graph demonstrates the substantial increase in output power observed across all experiments involving different porosity sizes and flow rates as the temperature was reduced. Notably, the most favourable case was identified when a porosity size of 0.35 was employed. The reason behind this optimal outcome could be attributed to the increased surface area of the porous media during the cooling process, resulting in superior heat convection absorbency.

The identification of the percentage of temperature reduction and the corresponding increase in output power through cooling photovoltaic cells is of utmost importance. To achieve this, Equations 3.1 and 3.2 were employed to calculate these percentages. Table 4.1 provides a comparison of the temperature reduction in a solar panel when compared to water cooling, while Table 4.2 presents a comparison of the temperature reduction when compared to the absence of cooling. Upon analysis, it was observed that the percentage decrease in the temperature of the photovoltaic (PV) panel, compared to the uncooled process, was found to be 55.87%. This substantial reduction highlights the significant impact of cooling measures in mitigating the detrimental effects of excessive heat on the PV panel's performance. On the other hand, the results showed that when compared to water-cooled PV panels, the temperature reduction reached only 20%. Accordingly, cooling with porous media yielded superior results in terms of temperature reduction and output power increase.

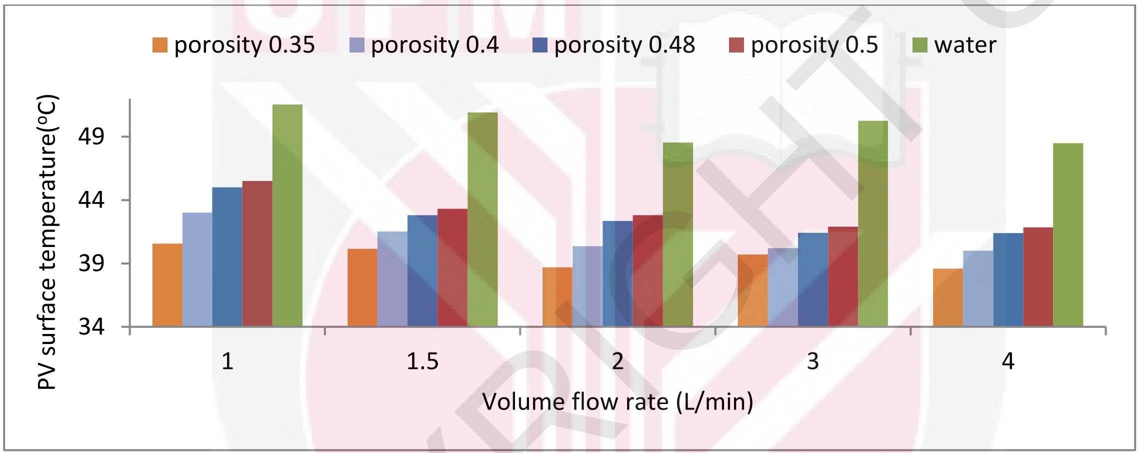

a) PV temperature

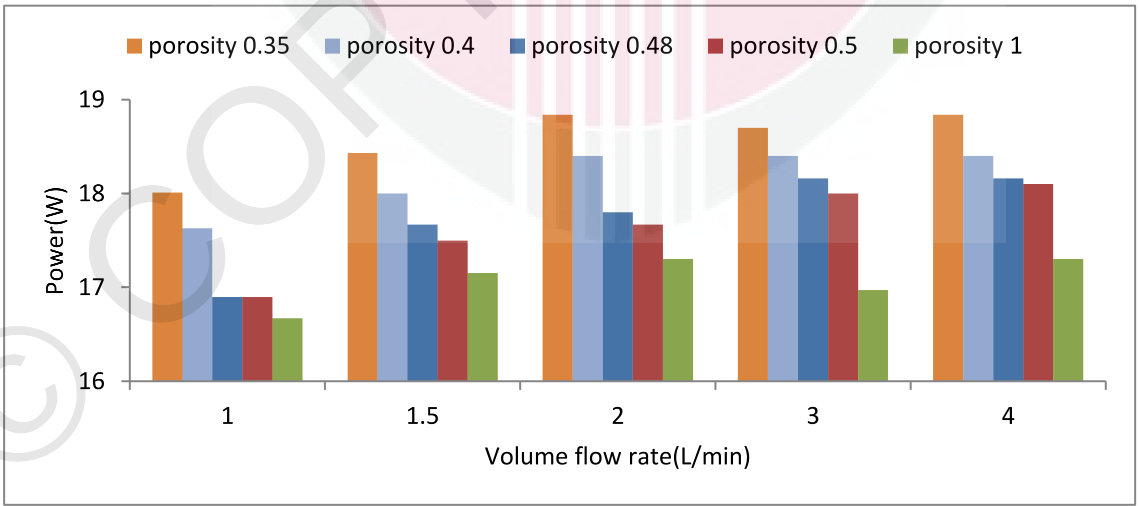

b) Output power

Figure 4.13: PV temperature and output power at different porosity sizes and different volume flow rates

The difference in temperature reduction between the water-cooled and porous media-cooled PV panels underscores the effectiveness of the latter. Cooling with porous media offers better heat dissipation and convection, ensuring that the PV cells operate at more favourable temperatures. As a result, the overall efficiency and performance of the photovoltaic system are enhanced, translating sunlight into electrical power with higher efficiency. Cooling photovoltaic cells is essential to achieve optimal performance and efficiency. The calculated percentages of temperature reduction and output power increase demonstrate the advantages of cooling with porous media. By incorporating such cooling techniques into photovoltaic system design and operation, can harness solar energy more efficiently.

Table 4.1: The percentage of temperature drop based on without cooling

Volume flow rate L/min	**PV cell surface temperature (ºC) with different porosity**				**Reduction (%) in cell surface temperature compared with uncooled**			
	0.35	**0.40**	**0.48**	**0.50**	**0.35**	**0.40**	**0.48**	**0.50**
1.0	40.57	43.00	45.00	45.50	53.74	50.97	48.69	48.12
1.5	40.16	41.53	42.80	43.30	54.21	52.65	51.20	50.63
2.0	38.70	40.35	42.36	42.80	55.87	53.99	51.70	51.20
3.0	39.70	40.20	41.43	41.90	54.73	54.16	52.76	52.22
4.0	39.60	40.00	41.40	41.85	54.84	54.39	52.79	52.28

Table 4.2: The percentage of temperature drop based on water-cooling

Volume flow rate (L/min)	**PV cell surface temperature (ºC) with different porosity**					**Reduction (%) in cell surface temperature compared with water cooling**			
	0.35	0.40	0.48	0.50	water	0.35	0.40	0.48	0.50
1.0	40.57	43.00	45.00	45.50	51.55	21.30	16.59	12.71	11.74
1.5	40.16	41.53	42.80	43.30	50.90	21.10	18.41	15.91	14.93
2.0	38.70	40.35	42.36	42.80	48.55	20.29	16.89	12.75	11.84
3.0	39.70	40.20	41.43	41.90	50.25	21.00	20.00	17.55	16.62
4.0	39.60	40.00	41.40	41.85	48.50	18.35	17.53	14.64	13.71

Table 4.3 provides a comparison of the increase in output power achieved through cooling with porous media. On the other hand, Table 4.4 presents the electrical efficiency and output power of the photovoltaic (PV) system when cooled with porous media and compares it with the uncooled case. Upon analysing the experimental results, it became evident that the most favourable outcome was achieved when the PV panel was cooled with porous media, particularly with a porosity size of 0.35. In this configuration, the output power reached an impressive 18.84 W and the highest efficiency attained was 6.26%. These results underscore the critical role played by porosity size in influencing the cooling process of photovoltaic cells, along with the significant impact of flow rates.

After comparing the cooled PV panel with porous media to the uncooled process, the percentage increase in output power was calculated to be 51.69%, and the efficiency was improved by 2.13%. These figures demonstrate the substantial benefits of implementing cooling measures, as they lead to a considerable enhancement in electrical efficiency and overall output power. In contrast, the results indicated that for the water-cooled PV panel, the increase in output power was 39.29%. The significant difference in the increase of output power between the porous media-cooled and water-cooled PV panels highlights the superior heat transfer exchange achieved through the former method. The cooling with porous media ensures efficient heat dissipation and temperature reduction in the PV cells, consequently resulting in a boost in output power.

In conclusion, the experimental findings indicate that cooling photovoltaic cells using porous media, especially with a porosity size of 0.35, yields the best results in terms of output power and electrical efficiency. The choice of porosity size and flow rates significantly affects the cooling process and, ultimately, the performance of the PV system. The considerable increase in output power and efficiency achieved through cooling with porous media emphasizes the importance of incorporating effective cooling techniques to optimize the performance of photovoltaic systems and maximize their energy conversion efficiency.

Table 4.3: The percentage of output power increase

Volume flow rate L/min	Output power (W) with different porosities					increase power (%) relative to uncooled			
	0.35	0.4	0.48	0.5	water	0.35	0.4	0.48	0.5
1.0	18.01	17.63	16.9	16.9	16.67	45.01	41.95	36.07	34.62
1.5	18.43	18	17.67	17.5	17.15	48.39	44.93	42.27	39.25
2.0	18.84	18.4	17.8	17.67	17.3	51.69	48.15	43.32	40.57
3.0	18.7	18.4	18.16	18	16.97	50.56	48.15	46.22	43.12
4.0	18.73	18.4	18.16	18.1	17.3	50.81	48.15	46.22	43.89

Table 4.4: The percentage of efficiency increase

Volume flow rate L/min	Efficiency (%) with different porosities					Enhancement (%) in efficiency compared uncooled			
	0.35	0.4	0.48	0.5	water	0.35	0.4	0.48	0.5
1.0	5.99	5.86	5.62	5.62	5.54	1.86	1.73	1.49	1.49
1.5	6.13	5.98	5.87	5.82	5.70	2.00	1.85	1.74	1.69
2.0	6.26	6.12	5.92	5.87	5.75	2.13	1.99	1.79	1.74
3.0	6.22	6.12	6.04	5.98	5.64	2.09	1.99	1.91	1.85
4.0	6.23	6.12	6.04	6.02	5.75	2.1	1.99	1.91	1.89

4.2.2 Outdoor test

This section presented the results of the external tests conducted at the Faculty of Engineering Technology on the roof of the Renewable Energy Laboratory. The tests took into account various ambient conditions, including solar radiation, ambient temperature, and air velocity, measured based on hourly daily conditions to ensure realistic outcomes. The study focused on two main aspects. Firstly, it investigated three different sizes of porosity sizes (0.35, 0.4, and 0.48) to assess their impact on the cooling process. Secondly, it examined five different flow volumes of water 1, 1.5, 2, 3, and 4 L/min to determine the most effective volume flow rate in conjunction with the chosen porosity size. To comprehensively address all factors influencing the cooling process, the study was divided into three distinct scenarios. Each scenario included all the relevant results that provided answers to the inquiries related to the factors affecting the cooling process. By conducting this thorough analysis under varying conditions, the main aim is to gain valuable insights into optimizing cooling efficiency and identifying the best combination of porosity size and volume flow rate for the specific system. These findings will contribute significantly to enhancing the overall performance and sustainability of the cooling process in renewable energy applications.

4.2.2.1 Comparisons between cooling with and without porous media

In this study, three photovoltaic cells were used, where the first was without cooling and the second was cooled with water, and the last photovoltaic cell was cooled with porous media having a porosity size of 0.35. Three flow rates of 1, 1.5, and 2 L/min were tested. Each experiment lasted seven consecutive hours, without interruption in cooling or solar radiation. Based on Figures 4.14a, 4.15a, and 4.16a comparison was made for the above three conditions, where it is observed that there is a temperature rise for all three cases, due to the exposure of the PV panel to sunlight, but the cooled panels are not as high as the uncooled panel, and this indicated that the cooling had a significant effect. The temperature of the PV without cooling increased to its highest value at 12:00 when it reached 49.1^{o}C, and the temperature of the water-cooled PV was 41.5^{o}C, while the temperature due to cooling with the porous media reached 39.4^{o}C and the best percentage of temperature reduction was at a flow rate of 2 L/min where the reduction in temperature reached to 19%. Based on the results, it is clear that the use of porous media gives better cooling than water alone.

4.2.2.2 The best possible porosity size for the best cooling

In this scenario, four PV panels were tested, three with channels filled with porous material (gravel) and one without cooling. This is to find out the optimum cooling condition of photovoltaic cells. These experiments aim to compare the porosity sizes to find out the best porosity size that can enhance the cooling process. The channels were filled as follows: the first channel with a porosity size of 0.35, the second channel 0.45, the third channel 0.48, and the fourth PV panel without cooling. All panels are tested under the same ambient conditions such as solar radiation, air velocity, air temperature, humidity, etc. In this experiment, three different volume flow rates 1 L/min, 1.5 L/min, and 2 L/min, respectively were tested. Based on Figures 4.17 to 4.19, it can be seen that the porosity size plays an important role in PV cooling. That is, the use of porous media with less porosity size gives better cooling results.

The reduction in temperature was 18.9%, 18.06%, and 17.24% when using a flow rate of 1 L/min and the increase in output power was 7.3%, 5.7%, and 4.1%. While when using a flow rate of 1.5 L/min, the temperature reduction for three porosity sizes was 24.44%, 22.5%, and 20.6%, respectively. The increases in electric power were 7.9%, 6.3%, and 4.7%. Experiment with a flow rate of 2 L/min, showed a reduction in temperature to 35.7%, 34.8%, and 34%, and an increase in power to 9.4%, 7.8%, and 6.2%, respectively. These results showed that the porosity size of 0.35 was the best size that can enhance the heat transfer absorptivity in cooling water. This can be assured by the homogenous distribution of the PV convective heat that occurred due to the small porosity size within the cooling water.

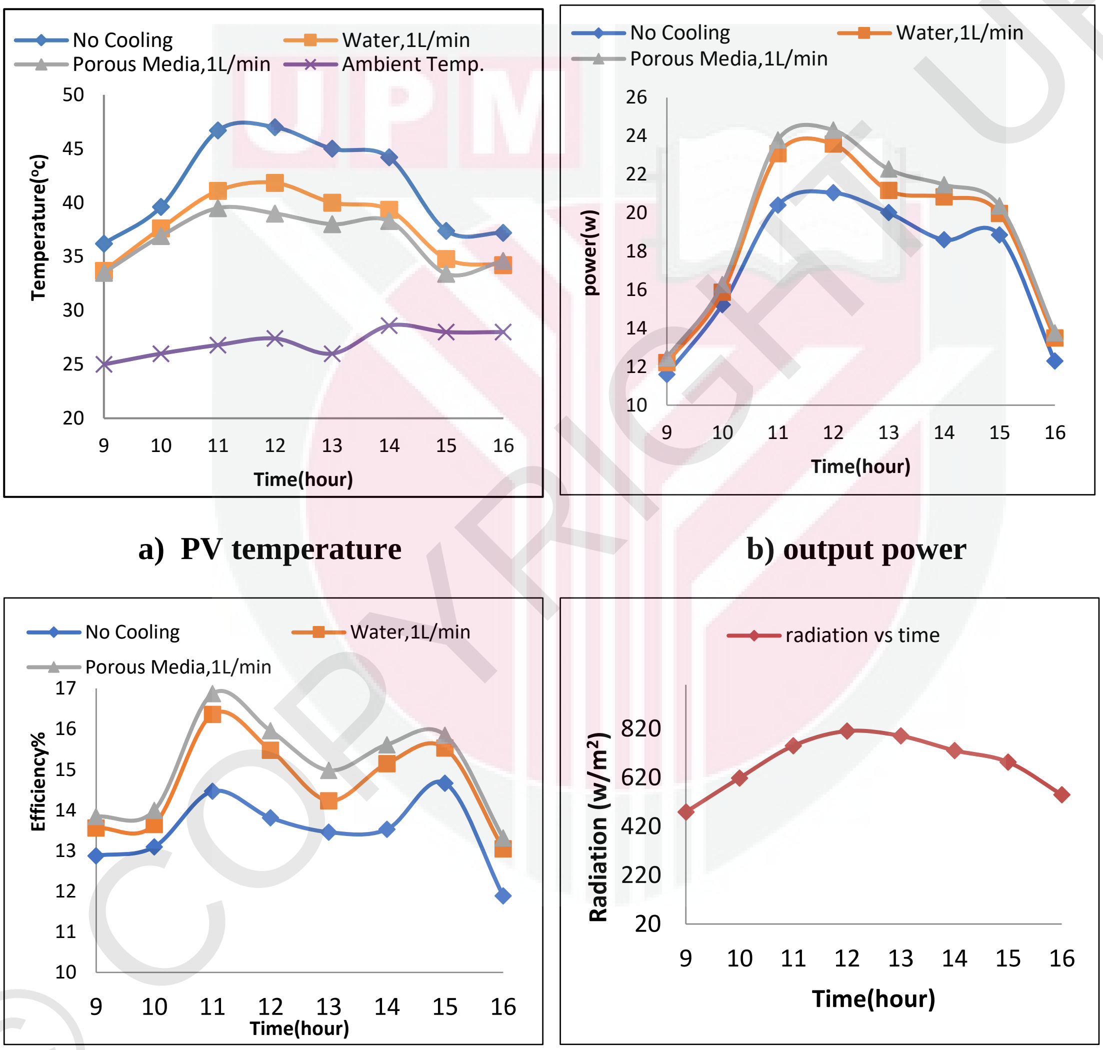

a) PV temperature **b) output power**

c) Efficiency **d) Solar radiation**

Figure 4.14: Experimental results for temperature, power output, efficiency, and solar radiation at a volume flow rate of 1 L/min

4.2.2.3 The best volume flow rate fit for the best cooling

In this section of the study, four photovoltaic (PV) panels were subjected to testing, with three of them equipped with cooling channels filled with porous media having a porosity size of 0.35. The fourth PV panel served as a reference and was left without any cooling. The primary focus was to compare the performance of the different flow rates under the same porosity size conditions. The experiments were conducted on the same day, ensuring uniform ambient conditions for accurate comparisons.

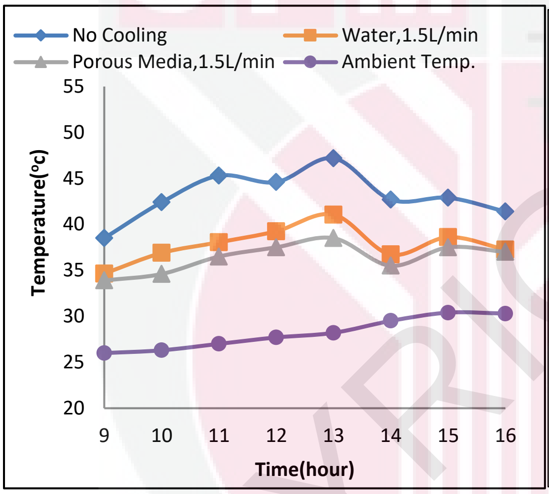

a) PV temperature

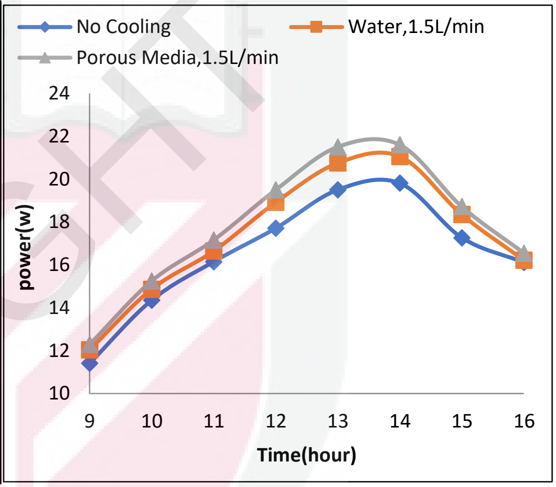

b) Output power

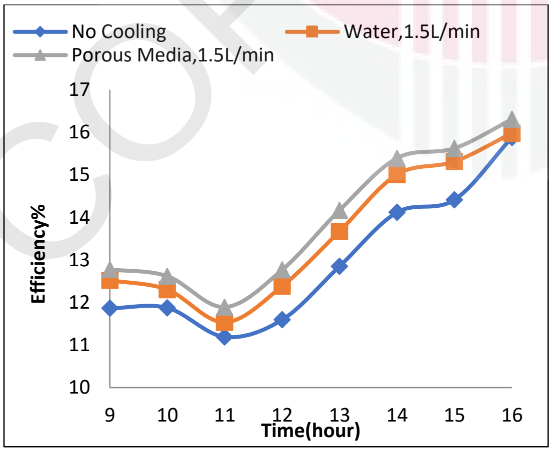

c) Efficiency

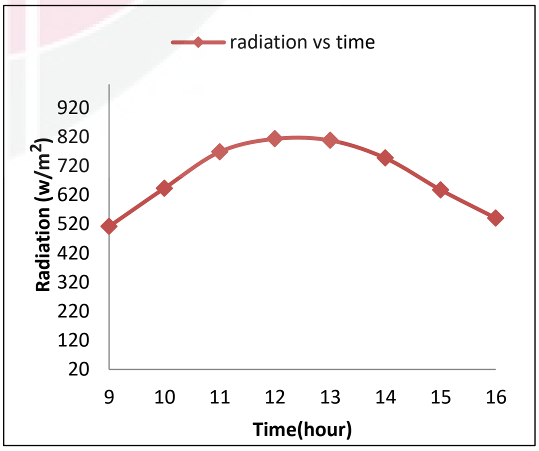

d) Solar radiation

Figure 4.15: Experimental results for temperature, power output, efficiency, and solar radiation at a volume flow rate of 1.5 L/min

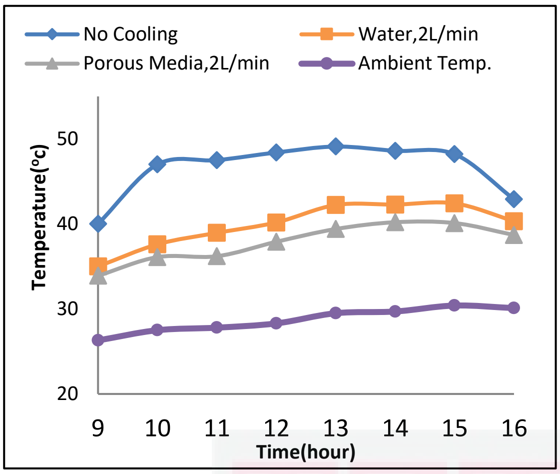

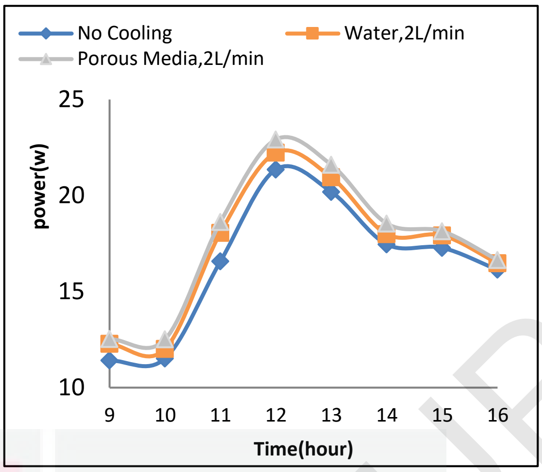

a) PV temperature b) Output power

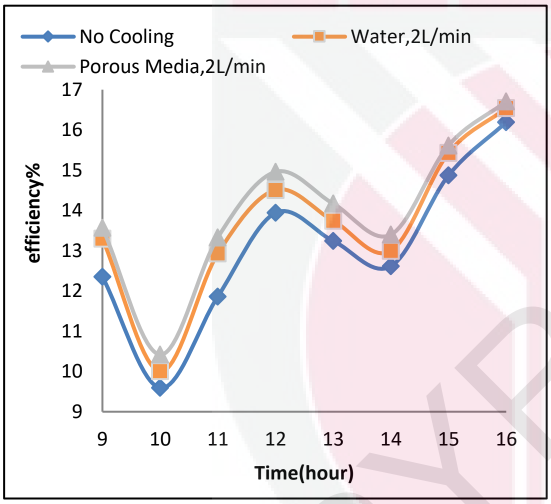

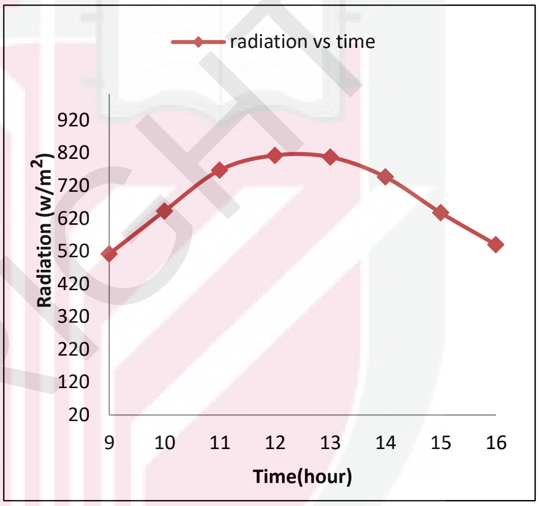

c) Efficiency d) Solar radiation

Figure 4.16: Experimental results for temperature, power output, efficiency, and solar radiation at a volume flow rate of 2 L/min

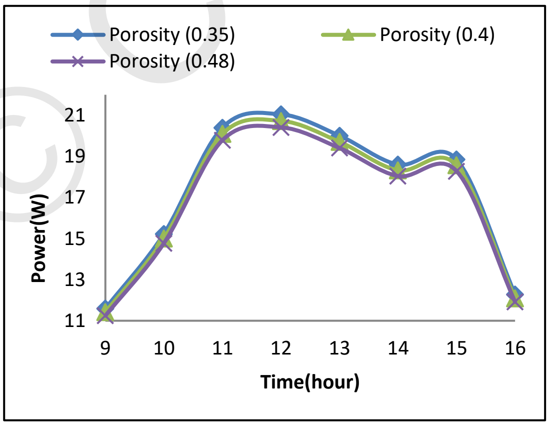

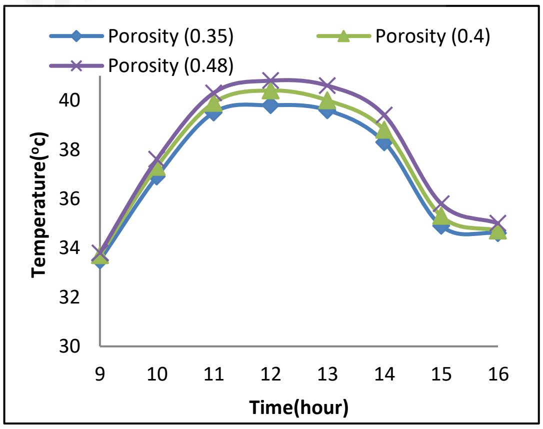

a) PV temperature b) output power

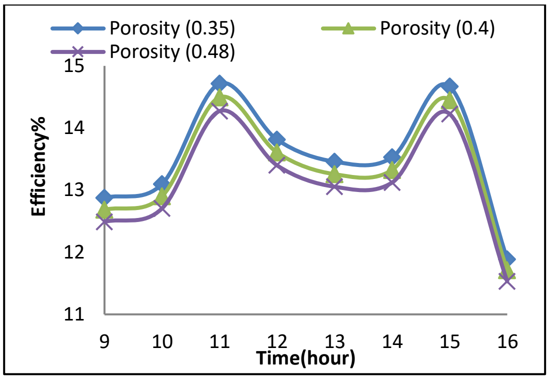

c) Efficiency

Figure 4.17: Experimental results for temperature, and power output, with different porosity sizes at a volume flow rate of 1 L/min

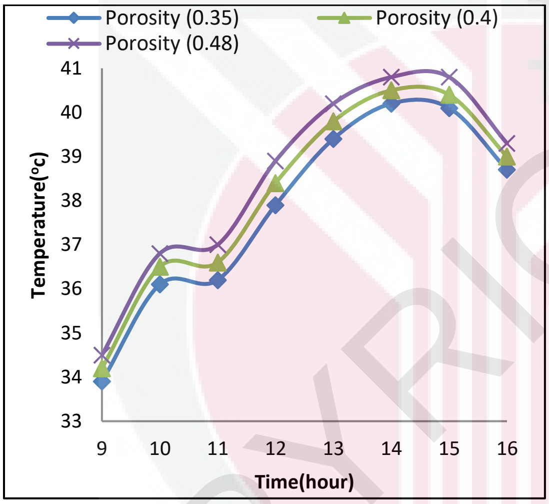

a) PV temperature

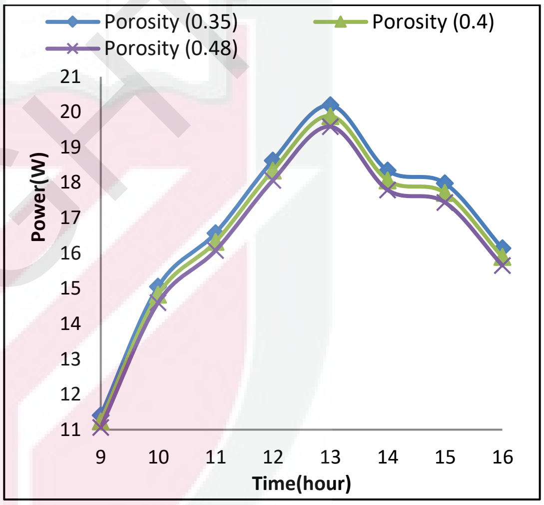

b) Output power

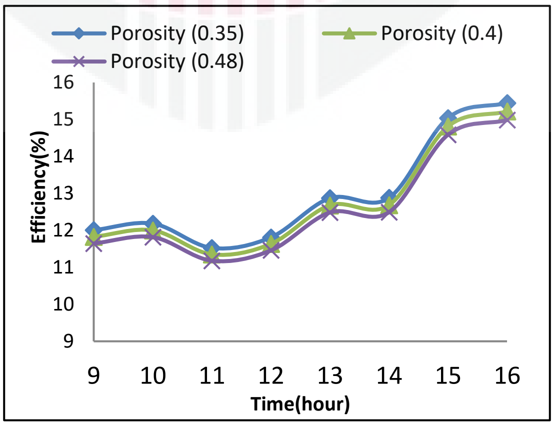

c) Efficiency

Figure 4.18: Experimental results for temperature, and power output, with different porosity sizes at a volume flow rate of 1.5 L/min

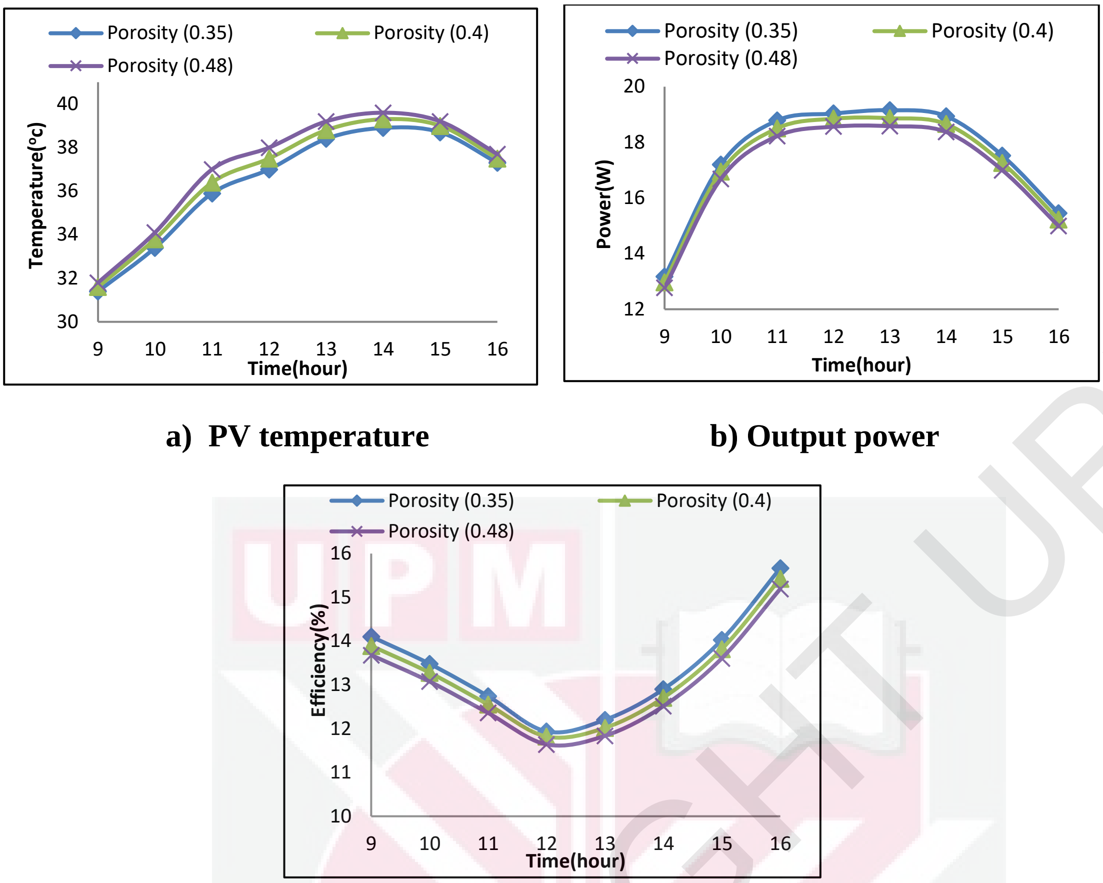

a) PV temperature

b) Output power

c) Efficiency

Figure 4.19: Experimental results for temperature, and power output, with different porosity size at a volume flow rate of 2 L/min

The three different volume flow rates tested were 1 L/min, 2 L/min, and 3 L/min. The objective was to investigate the impact of these flow rates on PV panel temperatures and determine the most effective cooling strategy. Figure 4.20 illustrates the effect of flow rates on PV temperatures. Upon analysing the results, it was observed that each flow rate led to a considerable reduction in temperature for the respective PV panels. The temperature reductions were approximately 18%, 20.6%, and 20.3% for the flow rates of 1 L/min, 2 L/min, and 3 L/min, respectively. These findings indicate that higher flow rates provided more efficient cooling and resulted in greater temperature reduction for the PV panels. The data obtained from this experiment highlights the significance of flow rates in the cooling process and their direct influence on the temperature regulation of PV panels. It is evident that increasing the volume flow rate positively impacts the cooling efficiency, leading to enhanced performance and improved temperature control of the PV system. These insights provide valuable information for designing effective cooling strategies to optimize the overall efficiency and longevity of photovoltaic panels in various operating conditions and environmental settings.

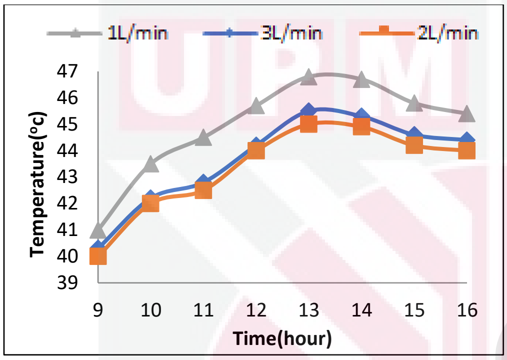

a) **PV temperature**

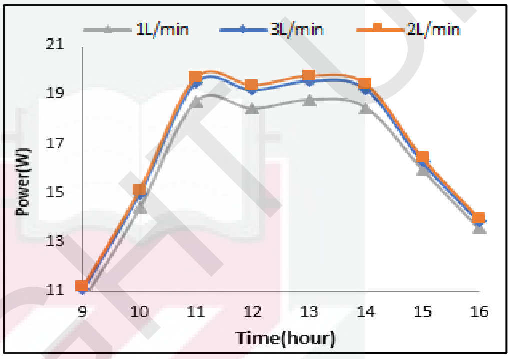

b) Output power

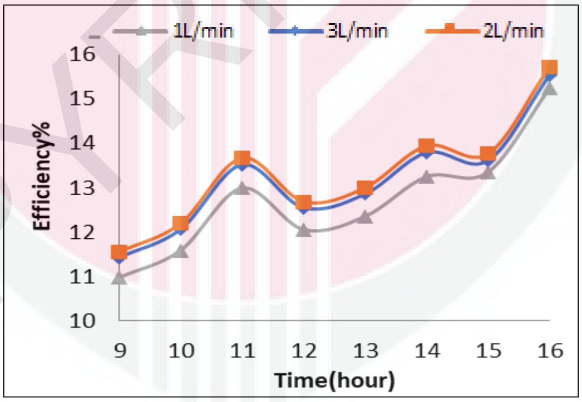

c) Efficiency

Figure 4.20: Experimental results for temperature, and power output, with different volume flow rates at a porosity size of 0.35

Based on comprehensive and accurate experimental research conducted in both controlled indoor environments and real-world outdoor conditions, the optimal porosity size value of 0.35 has emerged as the key to achieving superior results in various scenarios. This specific porosity size level has proven to be remarkably efficient in maximizing the performance of photovoltaic panels, ensuring that they deliver consistent and reliable energy output.

Furthermore, among the range of flow rates tested, the flow rate of 2 L/min has been identified as the most favourable choice. This flow rate plays a crucial role in mitigating temperature-related issues in photovoltaic panels, which are critical for their long-term performance and durability. Flow rates lower than 2 L/min tend to cause an undesirable rise in temperature, leading to potential overheating of the panels. On the other hand, flow rates higher than 2 L/min do not offer a significant improvement in temperature reduction compared to the optimal flow rate. Therefore, the flow rate of 2 liters per minute stands out as the perfect balance, effectively achieving the desired cooling effect without the need for excessive flow rates that might result in unnecessary costs.

The combination of the optimal porosity size value of 0.35 and the flow rate of 2 L/min represents a groundbreaking advancement in the field of photovoltaic technology. This discovery not only improves the performance and longevity of solar panels but also offers a practical and economical approach to harnessing renewable energy. The impact of porosity size on heat transfer is indeed crucial in various heat transfer processes. Understanding how porosity size influences convective heat transfer allows us to optimize cooling systems and enhance overall energy efficiency.

Equations 2.3 emphasize the direct correlation between the convective heat transfer coefficient and the actual heat transfer. When the convective heat transfer coefficient increases, it results in a corresponding increase in the overall heat transfer rate. This direct relationship highlights the importance of effectively managing the convective heat transfer coefficient to enhance heat dissipation in cooling applications.

Additionally, Equation 3.23 establishes that the convective heat transfer coefficient exhibits a direct correlation with the Nusselt number. Thus, an increase in the Nusselt number results in a corresponding increase in the convective heat transfer coefficient. This connection is essential in understanding the mechanisms governing the process. Interestingly, Equation 3.25 reveals an inverse effect of porosity size on the Nusselt number. This equation demonstrates that the product is divided by the porosity size, emphasizing an inverse relationship. Consequently, as the porosity size decreases, the Nusselt number increases. Consequently, this leads to an amplified convective heat transfer coefficient, thereby ultimately enhancing heat transfer by convection. By investigating these fundamental relationships, can gain deeper insights into the dynamics of the heat transfer process, particularly concerning the impact of porosity size, Nusselt number, and convective heat transfer coefficient. Understanding these factors helps us optimize cooling systems for photovoltaic panels and other applications, ensuring optimal energy efficiency and performance. Do not overlook the effect of porosity size on the velocity of the liquid, as the velocity of the fluid is calculated in the presence of porous media based on the velocity of the liquid without porous media divided by the porosity size, and thus the velocity increases. The effect of velocity will be explained in detail later. The influence of flow rates on heat transfer is a crucial aspect that significantly impacts the efficiency of various heat transfer processes. By delving into the equations, particularly Equation 3.26, we can gain valuable insights into how the magnitude of flow rates affects convective heat transfer, thereby facilitating the optimization of cooling systems. Equation 3.26, which relies on the Reynolds number, unveils a direct correlation between the volume flow rate and the Reynolds number. When the volume of the flow rate increases, the velocity of the fluid also rises, leading to a corresponding increase in the Reynolds number. This heightened Reynolds number, in turn, contributes to the elevation of the Nusselt number since they are directly related. As a result, the convective heat transfer coefficient is amplified, as previously mentioned, leading to enhanced heat transfer.

It becomes evident that manipulating flow rates has an impact on the overall heat transfer process. Through optimizing flow rates, cooling systems can be fine-tuned to achieve efficient heat dissipation, which is particularly crucial in applications involving solar cells and photovoltaic systems. This study showcases a consistent pattern of behaviour while yielding distinct results compared to previous studies on photovoltaic cooling (Ebaid et, al. 2018). The findings of this research align with the trends observed in prior investigations, yet they also bring forth novel insights and outcomes that contribute to understanding the cooling dynamics in photovoltaic systems. The increase in power and electrical efficiency occurs through a decrease in the temperature of the photovoltaic panels. Based on this, and what was mentioned previously, as the porosity decreases, the temperature decreases. Exploring the technical reasons behind the increased power and electrical efficiency in photovoltaic (PV) systems at lower temperatures reveals several fundamental principles. Lower temperatures widen the semiconductor bandgap, enabling more effective absorption of higher-energy photons by PV materials (Laabab et al., 2022). This stems from the temperature-dependent energy required for electron transitions. Additionally, lower temperatures result in longer carrier lifetimes due to reduced thermal generation and recombination rates, enhancing charge extraction and electrical efficiency. The intrinsic carrier concentration in the semiconductor decreases at lower temperatures, minimizing parasitic conduction paths and improving overall PV cell efficiency. Furthermore, the internal resistance of PV cells diminishes, facilitating a more efficient flow of charge carriers and reducing losses for higher electrical efficiency. Lower temperatures also impact voltage and current characteristics, with a general increase in voltage and a potential decrease in current output, contributing to an overall rise in power output within specific temperature ranges. Understanding these technical intricacies is crucial for optimizing PV operation in colder climates or during cooler periods, ultimately enhancing energy conversion efficiency and overall system performance.

4.3 Numerical results

A comprehensive numerical investigation was carried out to analyse the cooling of PV panels, aiming to determine the panel temperature and output power under various conditions. The primary purpose of this numerical study was to identify the optimal conditions, which could later be compared with the experimental data for validation. One of the significant advantages of numerical studies is their relatively short time and low financial cost, allowing for numerous simulations with various factors under investigation, such as solar radiation, air velocity, ambient temperature, water flow rates, porosity size, and other relevant parameters. The numerical simulation provides a versatile platform to explore different scenarios and study the effects of changing variables on PV panel performance. It enables us to assess the impact of multiple factors on the cooling process without the constraints of time and resources associated with experimental work. Moreover, the numerical results can be cross-validated by comparing them with the experimental findings, thereby ensuring the accuracy and reliability of the simulations.

For indoor conditions, the numerical study is divided into four distinct scenarios. The first scenario involves a mathematical approach, where analytical equations and calculations are used to model the cooling process. In the second scenario, a numerical simulation is employed, leveraging computational fluid dynamics (CFD) techniques to simulate the fluid flow and heat transfer within the cooling system. The third scenario adopts machine learning algorithms, which use experimental results to predict the panel temperature and output power under specific conditions. Finally, the fourth scenario involves establishing empirical correlations based on empirical data to describe the cooling behaviour, similar to the outdoor study. By conducting this comprehensive numerical investigation, a deeper understanding of the cooling process and its influencing factors can be obtained. The insights gained from these simulations will serve as a valuable reference for designing efficient cooling strategies for PV panels under different indoor and outdoor conditions. Furthermore, the correlation between the numerical and experimental results will enhance the credibility of the findings and contribute to the development of more effective and sustainable photovoltaic cooling techniques.

4.3.1 Analytical results of a mathematical model

The accuracy of the temperature predictions for the photovoltaic panel cooled by porous media was validated through model analyses using mathematical equations.

This thermal and electrical model took into account various important variables, including solar radiation, air temperature, and air velocity, among others. The main objective was to compare all the experimental results with the corresponding mathematical results obtained under different flow rates and porosity size levels.

In this section, the thermal and electrical model was accurately formulated, considering the influence of multiple variables as mentioned earlier. To ensure the credibility of the numerical results, they were compared with the experimental data once the photovoltaic cells' temperatures had reached a stable state under different flow rate conditions of 1, 1.5, and 2 L/min, as well as porosity size values of 0.35, 0.40, and 0.48. The focus of this presentation is primarily on the results obtained for the porosity size value of 0.35.

To obtain the results and conduct the analysis, Equations 3.15 and 3.39 were employed. These equations served as essential tools in determining the temperature behaviour and outlet power of the photovoltaic panel when subjected to porous media cooling. By comparing the numerical outcomes with the experimental findings, the reliability and accuracy of the mathematical model were validated, ensuring that it accurately captures the cooling process under varying conditions.

The careful examination and comparison of both experimental and numerical results will shed light on the effectiveness of cooling with porous media and the impact of different flow rates and porosities on the photovoltaic panel's performance. This in-depth analysis will contribute to the development of efficient and reliable cooling strategies for photovoltaic systems, further promoting the adoption of sustainable and energy-efficient technologies in the field of solar energy.

4.3.1.1 Indoor test

Figure 4.21 provides valuable insights into the comparison between the experimental and mathematical results for different flow rates. The analysis revealed that for a flow rate of 1 L/min, there was a minor discrepancy of 3.2% between the experimental and mathematical temperature readings and an even smaller deviation of 1% for the power output.

Similarly, at a flow rate of 1.5 L/min, the error between the mathematical and experimental temperature values was 3.6%, while the power output exhibited a mere 0.5% discrepancy. Moving on to the flow rate of 2 L/min, the temperature comparison resulted in a somewhat higher error of 5.6%, while the power output showed a slightly larger deviation of 1.5%. These results are consistent with a study carried out by Ahmed et al. (2019) and Bahaidarah et al. (2013).

These findings indicate that the mathematical model is generally in good agreement with the experimental data, as the errors observed are relatively small. Such validation of the model's accuracy is crucial for its practical application in predicting the behaviour of photovoltaic panels under various cooling conditions. It ensures that the model can reliably inform decision-making processes and aid in the optimization of cooling strategies for enhanced photovoltaic performance and energy efficiency.

4.3.1.2 Outdoor test

To determine the temperature of the photovoltaic panel at various flow rates, Equations 3.15 to 3.21 were employed and their results were compared with the experimental data. The analysis, as depicted in Figure 4.22, showcased that the maximum discrepancy between the experimental and mathematical results was approximately 4%. These results are consistent with a study carried out by Ahmed et al. (2019) and Bahaidarah et al. (2013).

This level of accuracy demonstrated by the mathematical model in predicting the photovoltaic panel's temperature is of great significance. It validates the model's reliability and its potential applicability to a wide range of conditions. With such a precise prediction capability, the mathematical model emerges as a robust and versatile tool for further investigations into photovoltaic system cooling under varying scenarios.

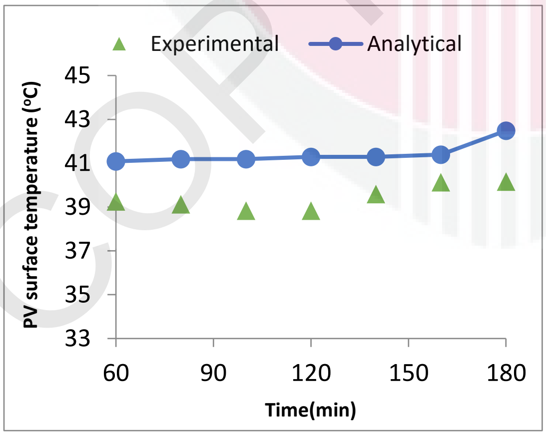

a) 1 L/min

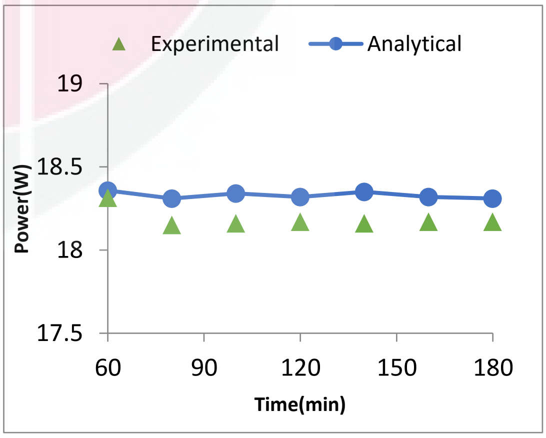

b) 1 L/min

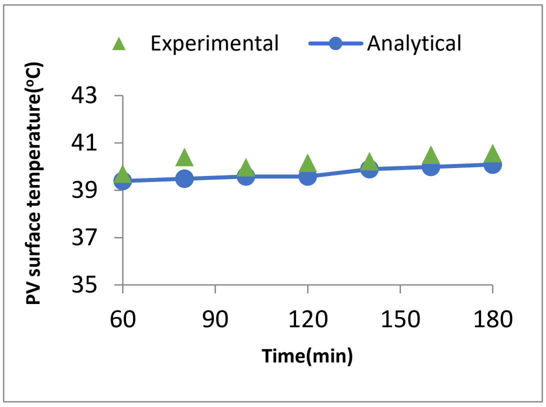

c) 1.5 L/min

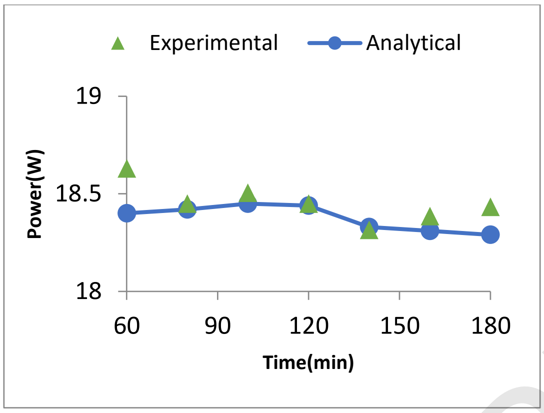

d) 1.5 L/min

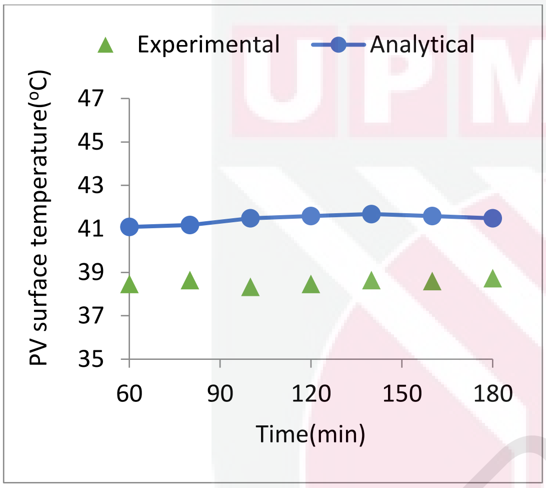

e) 2 L/min

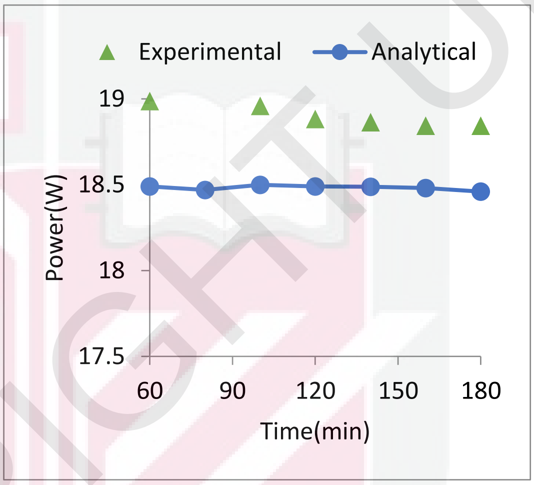

f) 2 L/min

Figure 4.21: Comparison between experimental results and analytical results

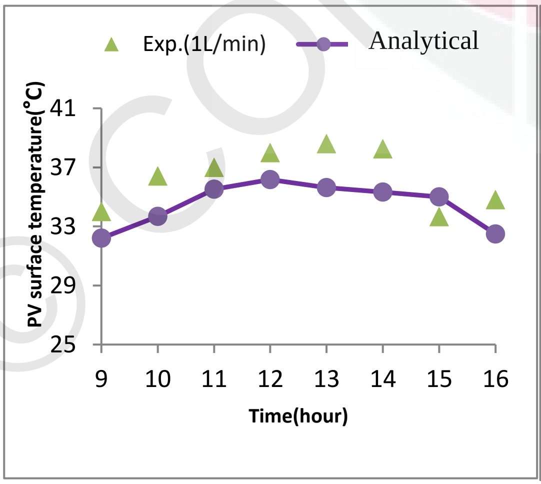

a) 1 L/min

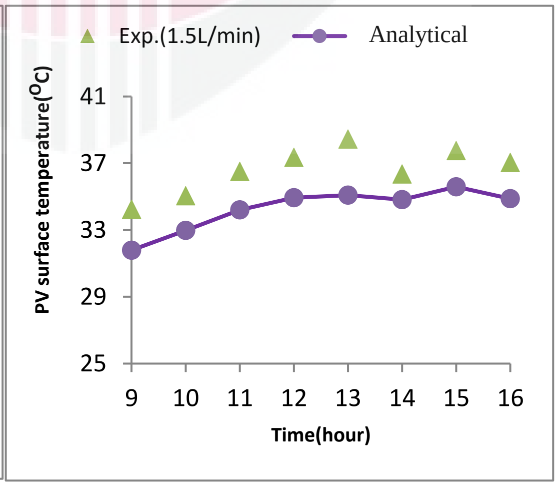

b) 1.5 L/min

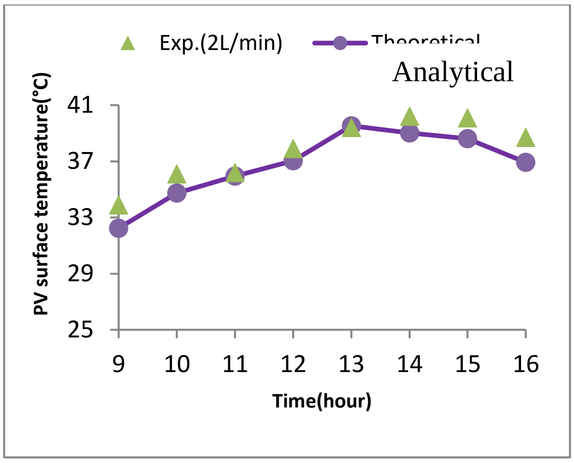

c) 2 L/min

Figure 4.22: Comparison between experimental and mathematical results

Figure 4.23 presents the effect of the Reynolds, Prandtl number, and porosity size on the Nusselt number, and the effect of the Prandtl number on the Nusselt number at porosity size 0.35. The Prandtl number had a direct influence on the Nusselt number. Whenever the Prandtl number reduces, the Nusslet number reduces, and vice versa. It is clear that the Reynolds number has an effect on the Nusselt number, and that with an increase in the Reynolds number, the Nusselt number increases at 0.35 porosity size. This is due to the effect of porosity size on the fluid velocity. Moreover, porosity size affects the Nusselt number. Figure 4.23c shows the change in porosity size with the Nusselt number at Reynolds 1.5 and the Prandtl number at 5.87. The results showed that porosity size has an inverse relationship with the Nusselt number, which means that when porosity size increases, the Nusselt number reduces.

Figures 4.23d and 4.23e showed the effect of velocity and porosity size on pressure drop, the relationship between the velocity of the fluid passing through the porous media on the pressure, as with the increase in velocity, the pressure difference increases, and this is due to the narrowness of the crossing area. it is clear that with the increase in porosity size, the pressure difference reductions, and this is due to the increase in the gap between the pebbles, and the diameter of the pebbles has an effect on the pressure difference similar to porosity size, and this is because the porosity size depends on the diameter of the pebbles, that is, the porosity size increases with the increase in the diameter of the pebbles.

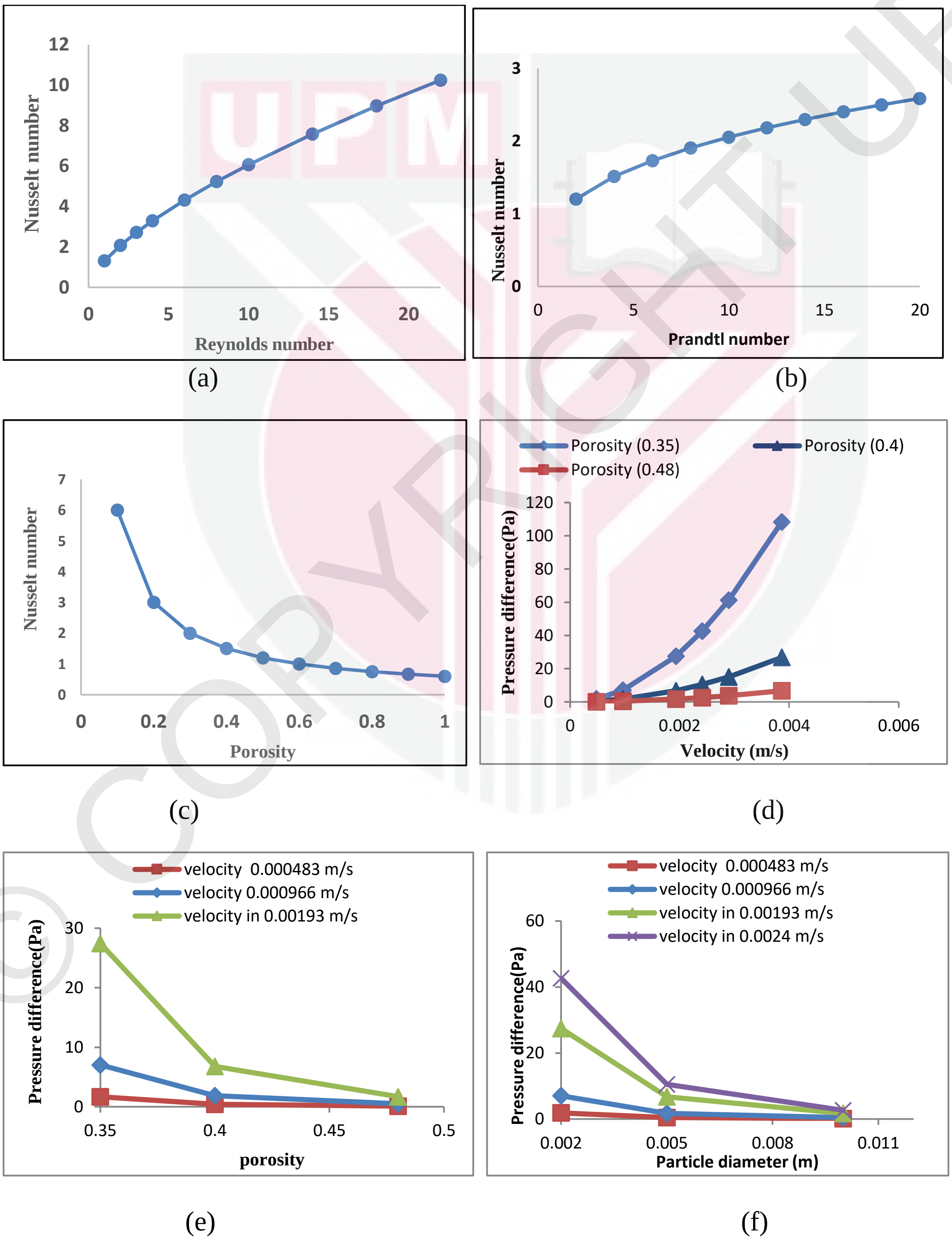

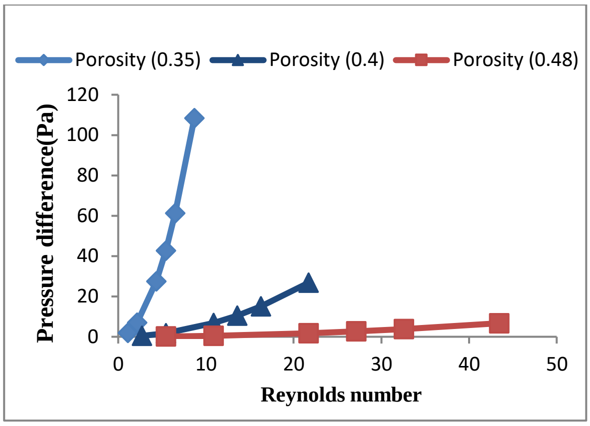

(g)

Figure 4.23: Effect of the Reynolds, Prandtl number, and porosity size on the Nusselt number and difference of pressure

4.3.2 Simulation results of ANSYS

It is worth noting that one of the best ways to understand the behaviour of heat transfer from the photovoltaic panel to the cooling water is through numerical analysis because it does not require a long time or a high financial cost to find results, just needs well-known software and correct boundary conditions of the model under study.

4.3.3 Validation

Before starting to use ANSYS there are need for experimental results for comparison purposes. At the beginning of the simulation, a test on the effect of the mesh size on the results was done. In this test, it was essential to find the error rate such as convergence, therefore, this test is necessary to determine the appropriate size of the mesh to have a proper time limit for the simulation.

The input boundary conditions assumed such as; the volume flow rate of 2 L/min, the solar radiation of 814 W/m^2, and the temperature of the water entering the channel at 24^{o}C, were used for the simulation. Based on Figure 4.24 and 4.25, the results showed that when the number of nodes in the mesh is more than 285420, it will not affect the results, so the number of nodes stayed at 285420 for all simulations. The rectangular grid in mesh was used to provide a good distribution around the photocell model. A comparison was made between the numerical and experimental results as shown in Figures 4.26a, 4.26b, and 4.26c, the figures showed that the deviation in the readings between the numerical and the experimental results for the PV temperature was 2.3%, 2.3%, and 1.8% for flow rates of 1 L/min, 1.5 L/min, and 2 L/min, respectively, and for fixed porosity size of 0.35.

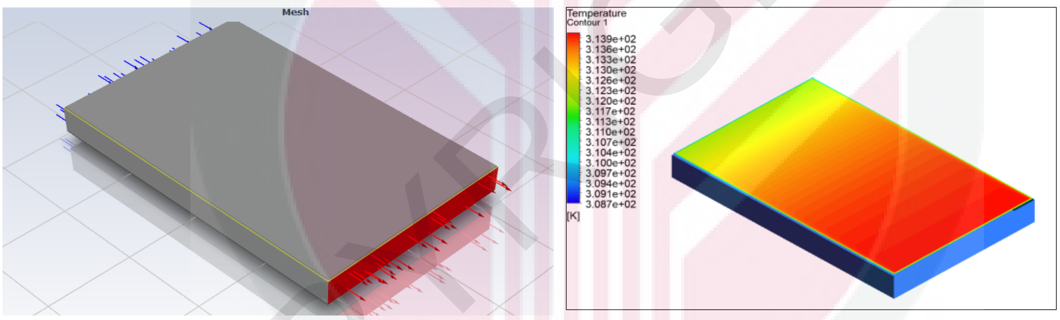

a) Geometry **b) Temperature distribution**

Figure 4.24: Geometry and Temperature distribution

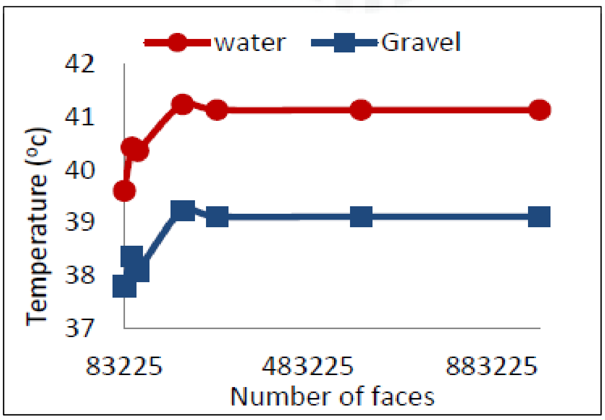

Figure 4.25: PV temperature with number of faces

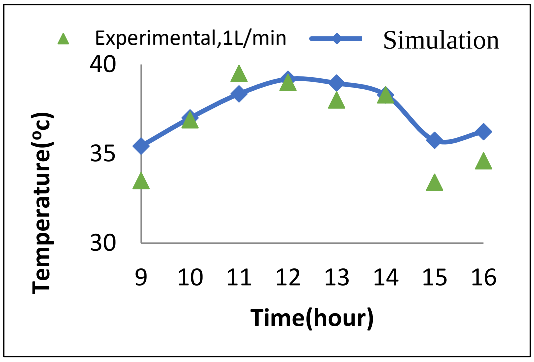

a)1 L/min

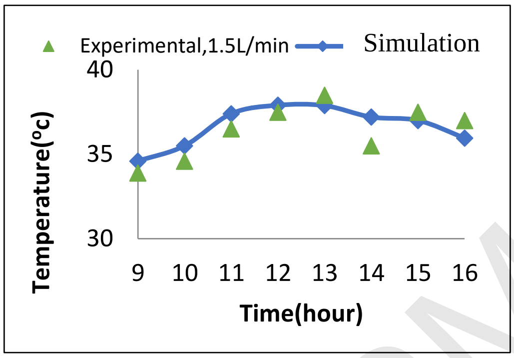

b) 1.5 L/min

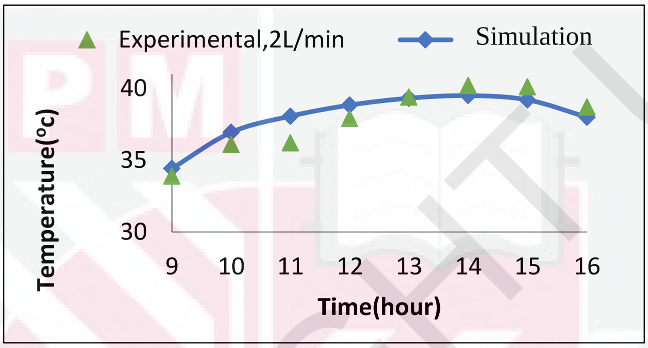

c) 2 L/min

Figure 4.26: Comparison between experimental results and numerical results

4.3.3.1 Parameters studies

In the study to investigate the effect of various other parameters involved in PV cooling by porous media. These parameters include the cooling channel height, as well as the shape of the cooling channel, types of coolants, and types of porous media.

4.3.3.1.1 The effect of the cooling channel height

Figure 4.27 presents an analysis of the temperature difference observed in the photovoltaic panel, considering different heights of the cooling channel: 50mm, 30mm, 10mm, and 5mm. In these analyses, porous media with a porosity size of 0.35

was utilized, along with a constant volume flow rate of 2 L/min, and solar radiation ranging from 350 to 1000W/m^2 was applied to all cooling channels. The results indicated that the temperature of the photovoltaic panel exhibited a gradual increase in response to higher solar radiation levels. According to the data in Figure 4.27a to 4.27d, the maximum temperature recorded for the photovoltaic panel occurred at a solar radiation level of 1000W/m^2, with corresponding temperatures of 42^{o}C, 41.7^{o}C, 39.3°C, and 27.3^{o}C, for cooling channel heights of 50mm, 30mm, 10mm, and 5mm, respectively, when porous media was used.

The findings from this analysis shed light on the significant impact of the cooling channel's height on the photovoltaic panel's temperature. As the height of the cooling channel decreases, the velocity of the liquid within the channel increases, resulting in a more efficient heat transfer process and a subsequent reduction in the temperature of the photovoltaic panel, Figure 4.28 represents the PV temperature with the radiation difference for all cooling channels. This outcome underscores the critical importance of optimizing the design of cooling systems for photovoltaic panels. By carefully selecting the appropriate cooling channel height, can effectively enhance the panel's thermal performance and ensure its stable operation even under high solar radiation conditions. The research findings present a crucial revelation: reducing the height of the cooling duct has a positive impact on lowering the temperature of PV panels. This phenomenon can be comprehended by referring to a fundamental formula in fluid mechanics, which relates the volume flow rate (Q) to the fluid velocity (V) multiplied by the cross-sectional area (A) of the channel. The cross-sectional area (A) of the channel is determined by its height (h) multiplied by its width (w), as represented by the equation (A = wh). Notably, this equation establishes a direct relationship between the channel's height and its cross-sectional area, implying that a decrease in height results in a reduction in the cross-sectional area.

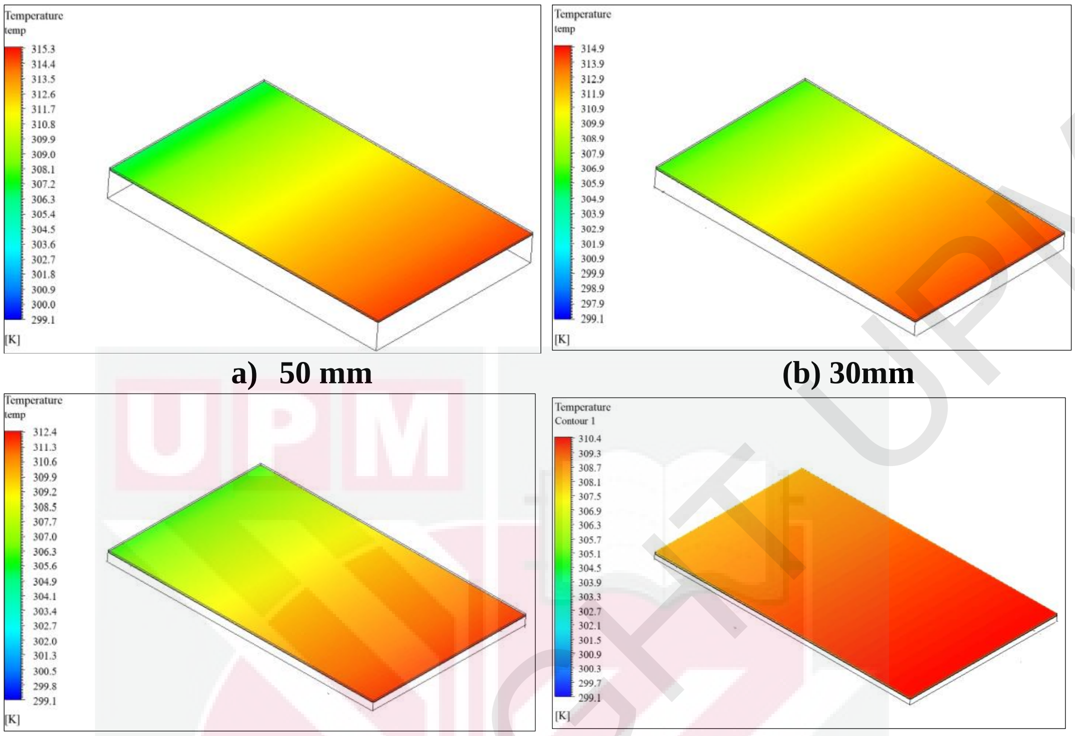

a) 50 mm (b) 30mm

c) 10 mm (d) 5 mm

Figure 4.27: PV temperature distribution with different cooling channel height

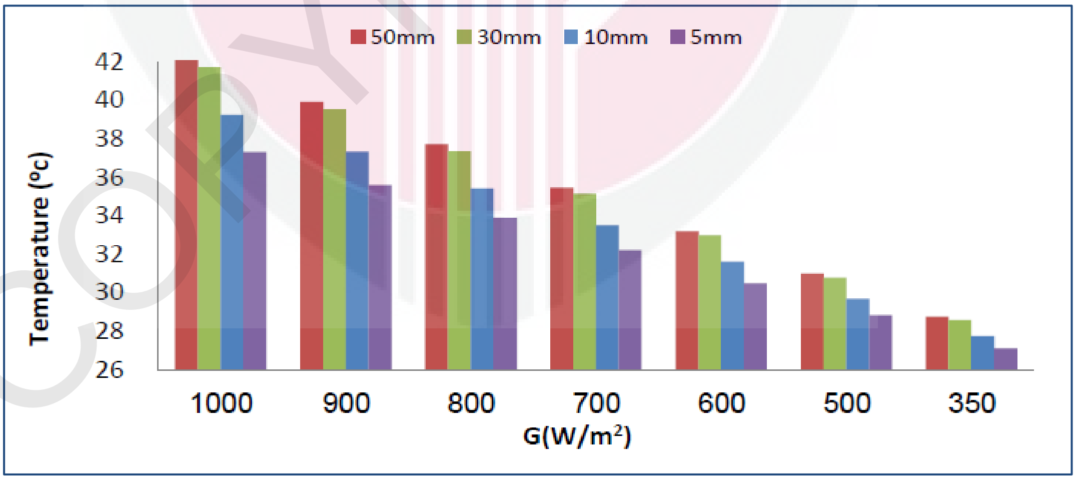

Figure 4.28: PV temperature with different solar radiation at different cooling channel heights

Assuming the volume of the flow rate remains constant, the equation (V = Q / A) (Bahaidarah et al., 2013) reveals that the fluid velocity (V) increases in response. This leads to an interesting inverse relationship between the height of the cooling channel and the velocity of the fluid. By reducing the height of the cooling channel, the fluid velocity escalates. As a result, the convective heat transfer coefficient is enhanced, leading to more efficient heat dissipation from the PV panels. The consequence is a noticeable decrease in the panels' temperatures, significantly improving their overall performance.

4.3.3.1.2 The effect of the cooling channel shape

Solar panels are composed of a group of solar cells that serve as receivers, absorbing sunlight and converting it into usable electricity. These solar cells were connected within a specific framework, often arranged in series or parallel to optimize their performance. As we previously discussed, solar panels are susceptible to the effects of temperature, which can impact their efficiency and overall longevity. Nevertheless, they remain the backbone of any solar energy system, as they are the primary components responsible for generating clean and sustainable electricity.

Upon closer examination of Figure 4.29 and a thorough analysis of the results, a noticeable disparity in temperatures among the solar cells on a single photovoltaic panel becomes evident. This disparity implies that certain cells experience higher temperatures than others, and this variance in temperature distribution occurs directly on the photovoltaic panel's surface. Regrettably, this temperature difference can lead to accelerated deterioration of the affected cells, potentially limiting the solar panel's overall efficiency and lifespan.

The origin of this undesirable phenomenon lies in the increased temperature of the liquid circulating along the photovoltaic panel. To address this issue effectively, a promising solution has been proposed: the implementation of a cooling channel with an inhomogeneous height. This ingenious design entails setting the inlet height of the cooling channel higher than the outlet height.

The concept behind this cooling mechanism is based on the principle that an increase in liquid velocity translates to a corresponding rise in the rate of heat transfer. By engineering the cooling channel with a difference in height between the inlet and outlet, the liquid's speed is accelerated as it traverses through the channel. This heightened velocity facilitates a more efficient absorption of excess heat from the solar cells, thereby mitigating the temperature differences and ensuring a more uniform and optimal thermal environment for the entire photovoltaic panel. This innovative cooling approach not only guards against premature cell degradation but also significantly improves the overall energy output and performance of the solar panel system.

The analysis conducted on the cooling channels for the solar panel system yielded valuable insights into the impact of different channel heights on the temperature of the photovoltaic (PV) panel. The main cooling channel, with a height of 5 mm from both the water inlet and outlet (A), served as the reference point for comparison. Subsequently, three alternative cooling channels were proposed: channel B with a height of 4 mm at the outlet, channel C with a height of 3 mm at the outlet, and channel D with a height of 2 mm at the outlet. All channels had a consistent width of 340 mm.

To evaluate the cooling channels' effectiveness, a porous media with a volume flow rate of 2 L/min, along with solar radiation ranging from 350 to 1000W/m^2 for all configurations. As expected, the PV panel's temperature increased gradually with increasing solar radiation. Figures 4.29a, 4.29b, 4.29c, and 4.29d presented crucial data on the maximum temperature of the PV panel at 1000W/m^2 solar irradiation for channels A, B, C, and D, respectively. The temperatures recorded were 37.29°C, 36.9°C, 36.6°C, and 36.2°C, indicating that the choice of a cooling channel significantly influenced the PV panel's temperature.

Analysing the results revealed a direct relationship between the decrease in channel height at the outlet and the reduction in PV panel temperature. However, it was evident that excessively lowering the height at the outlet could compromise temperature uniformity. Such a scenario would lead to higher temperatures at the beginning of the PV panel compared to its end, potentially causing uneven heating and impacting overall efficiency.

To address this issue, the study investigated different heights for the cooling channels, specifically 5 mm, 4 mm, 3 mm, and 2 mm. Upon analysing Figure 4.30, also based on Figure 4.31 the temperature differences between the photovoltaic panels were measured at 1.3°C, 0.92°C, 0.45°C, and 0.6°C, respectively, for the mentioned heights. The comparison made it clear that the optimal height at the outlet was 3 mm, striking a balance between effective cooling and temperature uniformity.

The research findings conclusively highlighted the critical importance of the cooling channel's shape and dimensions in maintaining a consistent and controlled temperature for the PV panel. A height of 3 mm at the outlet emerged as the most suitable configuration, ensuring efficient heat dissipation while preserving temperature homogeneity across the entire solar panel.

These results hold great significance for the design and implementation of solar energy systems. By utilizing the most effective cooling channel configuration, solar panels can operate at their peak efficiency, contributing to the wider adoption of sustainable and eco-friendly energy solutions. Figure 4.32 shows the behaviour of the fluid velocity inside the cooling channel. The fluid velocity remains constant when the channel height is uniform at the inlet and outlet, while Figure 4.32b shows an increase in the fluid velocity at the outlet due to the decrease in height.

In photovoltaic cooling in general, this cooling system aim is to reduce the temperature of the photovoltaic cells to improve their efficiency in converting light into electrical energy. However, it was found that the photovoltaic panel has an uneven temperature on all the cells in the panel, as we mentioned earlier. This undesirable phenomenon can be explained as follows;

As the coolant passes through the cooling channel, the liquid absorbs heat from the photovoltaic cells and turns into a warmer liquid as it goes towards the exit of the cooling channel or the end of the PV panel. This heated liquid then goes to the other end of the cooling channel installed on the back side of the PV panel.

At the starting point of the cooling channel or the first part of the photovoltaic panel, the coolant is colder; this is because it has not yet been exposed to the heat of the photovoltaic cells. Therefore, at the start, the liquid has the ability to draw more heat from the photovoltaic cells and cool them down due to the difference between the temperature of the photovoltaic panel and the temperature of the liquid.

On the other hand, at the end of the last plate or section, the coolant is warmer; this is because it has been exposed to the heat of the photovoltaic cells along the cooling channel. Thus, the liquid becomes warmer and thus the temperature difference between the PV panel and the cooling liquid decreases. In this way, the photovoltaic has a higher temperature at its end than at its beginning, as a result of the coolant flow and its response to the heat produced in the photovoltaics along the channel.

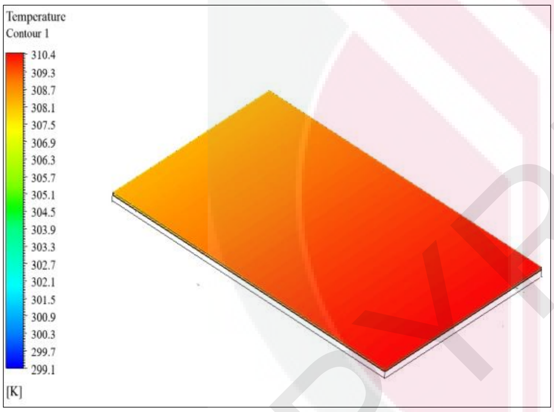

a) 5 mm-5 mm

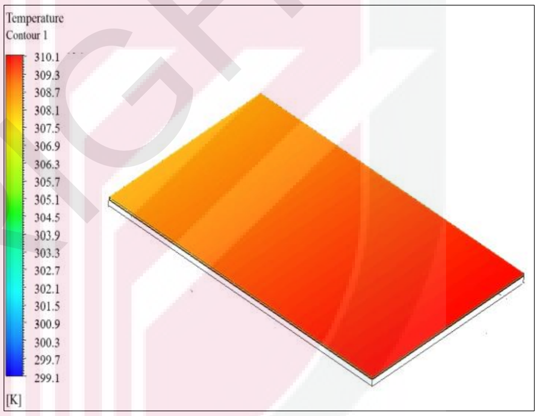

(b) 5 mm-4mm

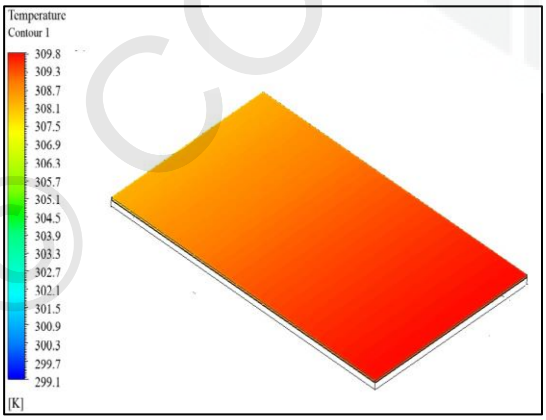

c) 5 mm-3 mm

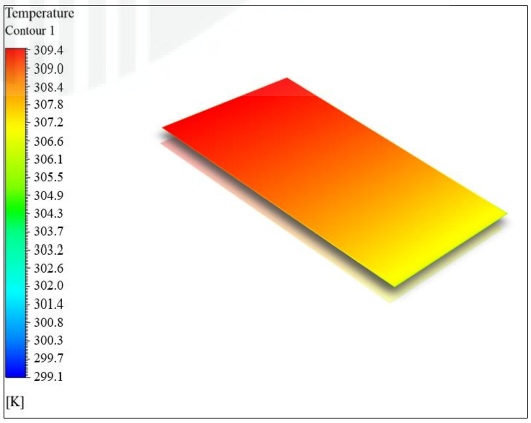

(d) 5mm-2 mm

Figure 4.29: PV temperature distribution with different cooling channel shapes

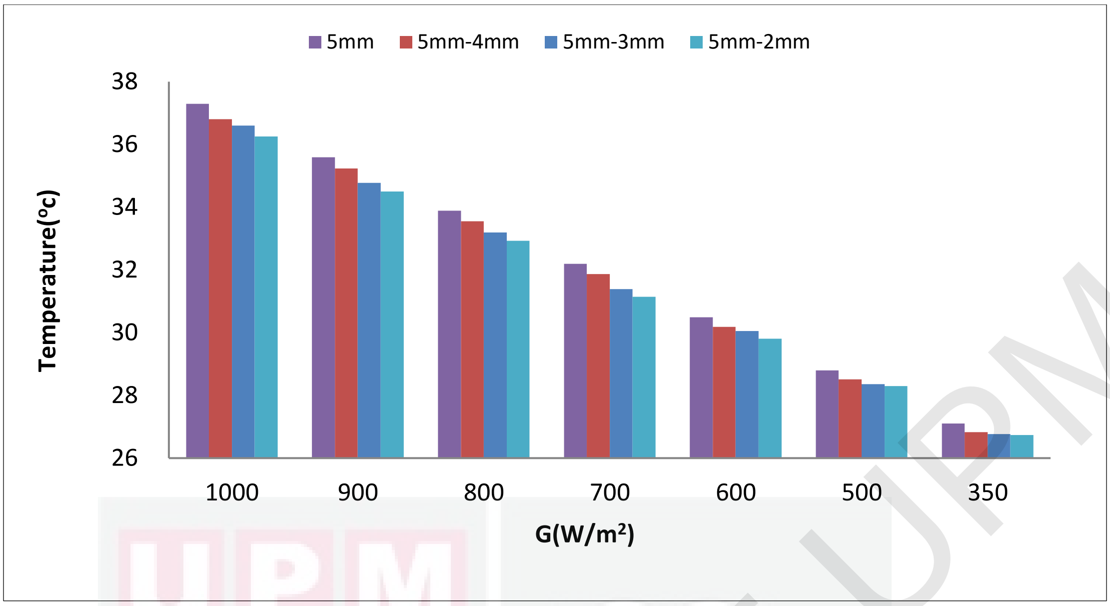

Figure 4.30: PV temperature with different solar radiation at different cooling channel heights

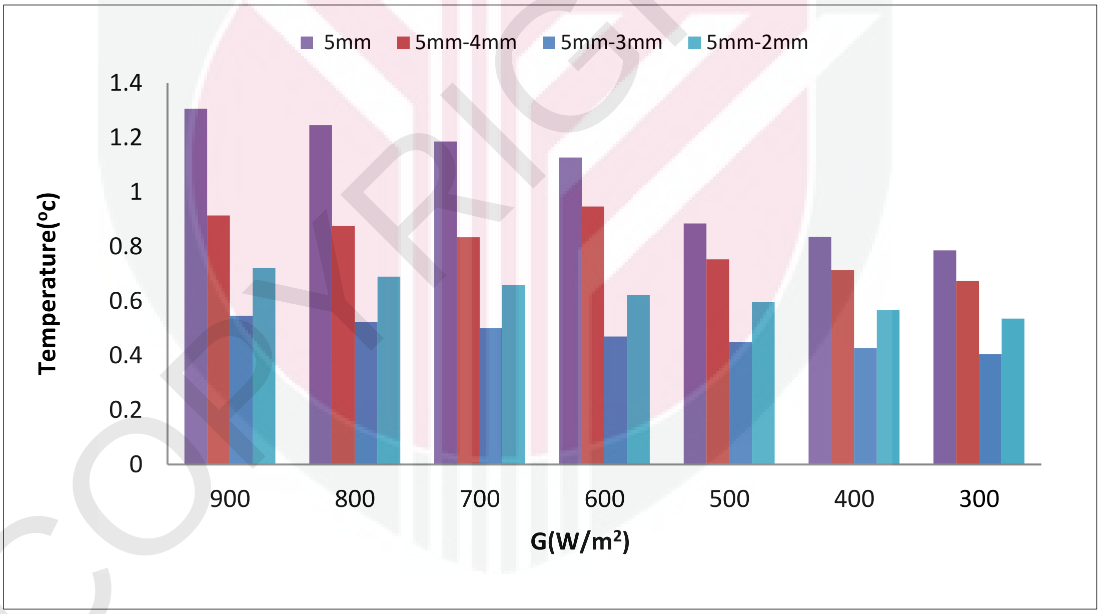

Figure 4.31: The difference in PV temperature with the difference in solar radiation at different outlet heights

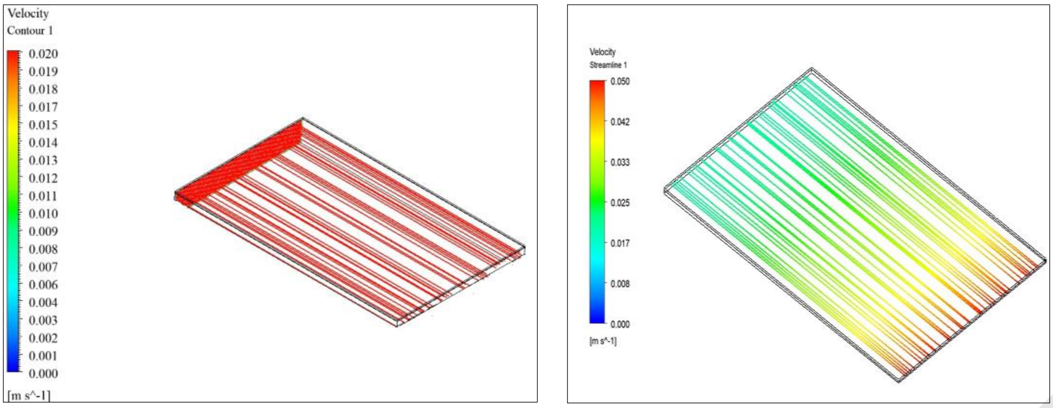

a) 5 mm-5 mm **(b) 5mm-2 mm**

Figure 4.32: Liquid Velocity distribution

To address this phenomenon, a new approach was adopted by designing a heterogeneous cooling channel with a varying height profile. This ingenious design incorporates a higher starting height, gradually transitioning to lower heights toward the end of the cooling channel. As a result, an intriguing fluid dynamics phenomenon called "liquid acceleration" or "liquid flow enhancement" occurs within these heterogeneous cooling channels.

The underlying principle behind this acceleration phenomenon can be attributed to Bernoulli's law, a fundamental concept in hydraulics that governs fluid behaviour during flow. According to Bernoulli's law, as a fluid traverses a narrow channel, its velocity increases, while in a wider channel, its speed decreases. Based on the continuity equation is a fundamental principle in fluid mechanics and hydrodynamics, used to describe the behaviour of fluids during flow. The continuity equation expresses the conservation of fluid quantity between two points during flow. The continuity equation further highlights the disparity in heights along the channel, resulting in a boost in velocity.

The continuity equation is written as follows: Cross-sectional area at inlet point (Ain) × inlet Velocity (Vin) = Cross-sectional area at outlet point (Aout) × outlet Velocity (Vout). This equation highlights the effect of changing the area, which comprises both height and width. As the width of the channel remains constant, the variable becomes the height (h). Consequently, the continuity equation becomes Vout = Vin * (hin / hout). Consequently, the fluid velocity at the channel's outlet surpasses that at its inlet.

In the context of a heterogeneous cooling channel, the initial higher height leading to a lower height at the end induces an acceleration in the liquid as it enters the narrower section (at the outlet point). Consequently, the liquid experiences a continuous acceleration along the PV panel's length until it reaches the channel's end. Importantly, the change in height and velocity remains linear throughout this passage.

This ingenious design has profound implications for the cooling process, particularly in terms of heat transfer. As discussed earlier, the Reynolds-Winslet equation and convective heat transfer coefficient play crucial roles in this context. With the liquid's accelerated velocity, the heat transfer from the PV cells to the liquid intensifies during the cooling process. This leads to a substantial improvement in cooling efficiency and a marked reduction in the temperature of the PV panel at its end.

4.3.3.1.3 The effect of the coolant types

In Figure 4.33, a comprehensive study was conducted to analyse the temperature difference in the PV panel when various coolants, including water, chemical alcohol, and engine oil, were employed. The experiment was carried out with a porosity size of

0.35, a volume flow rate of 2 L/min, and solar radiation ranging from 350 to 1000W/m^2, consistently applied to all coolant types. As expected, the temperature of the PV panel gradually increased with the escalation of solar radiation levels. The results from Figure 4.34 provided valuable insights into the impact of coolant selection on the maximum PV temperature, specifically at a solar irradiation level of 1000W/m^2. Among the coolants tested, water exhibited the lowest maximum PV temperature, recording 36.6°C, followed by chemical alcohol with a slightly higher maximum temperature of 37.8°C. Engine oil showed the highest maximum PV temperature at 39°C.

This data unequivocally highlights the significance of the choice of coolant in the cooling process for PV panels. The type of coolant used plays a critical role in regulating the temperature and overall efficiency of the solar panel system. Different coolants possess distinct thermal properties, such as thermal conductivity and heat capacity, which directly influence their ability to absorb and dissipate heat effectively. Chemical alcohol, for instance, has specific heat transfer characteristics, which result in a marginally higher maximum PV temperature when compared to water. On the other hand, water, being a commonly used coolant, demonstrated efficient cooling properties, leading to a lower maximum PV temperature. Engine oil, with its unique thermal properties, exhibited the highest maximum PV temperature among the tested coolants.

The variation in PV panel temperatures is directly linked to the dissimilarities in the cooling efficiency of each coolant. Coolants with higher thermal conductivity and heat capacity are better equipped to dissipate heat, leading to lower PV temperatures and improved energy conversion efficiency. Figure 4.34 displays the difference in PV temperature with the difference in solar radiation at a different type of coolant. Equations 2.3 shed light on the crucial link between the convective heat transfer coefficient and the actual heat transfer. The direct relationship indicates that an increase in the convective heat transfer coefficient results in a proportional rise in the overall heat transfer rate. This underscores the effective management of the convection heat transfer coefficient to optimize heat dissipation in cooling applications.

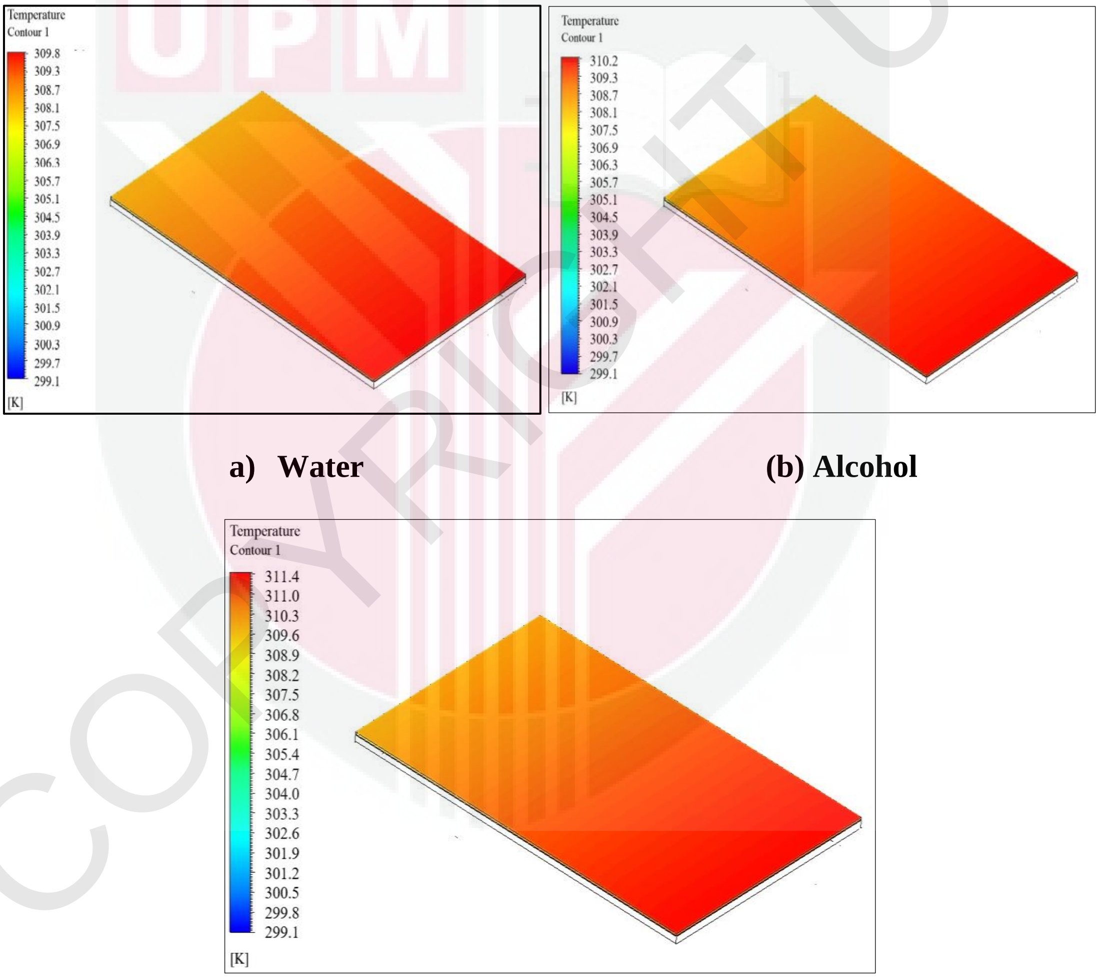

a) Water **(b) Alcohol**

c) Engine oil

Figure 4.33: PV temperature distribution with the difference in the coolant types

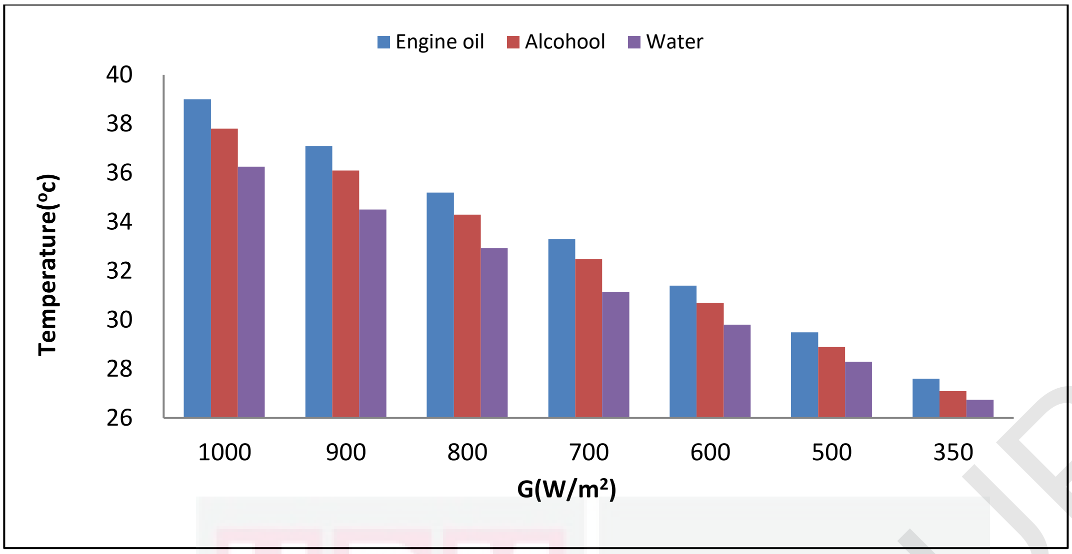

Figure 4.34: The difference in PV temperature with the differences in solar radiation at different coolant types

Moreover, Equation 3.23 highlights that the convective heat transfer coefficient is directly influenced by the thermal conductivity of the fluid. Hence, higher thermal conductivity leads to an enhanced convective heat transfer coefficient, facilitating more efficient heat transfer. Furthermore, according to Equation 3.26, the density of the liquid shows a direct relationship with the Reynolds number. Understanding the impact of density on the Reynolds number is vital in comprehending the fluid flow behaviour and how it affects the cooling process.

In the context of heat capacity, the equation ($Q = mC_p \Delta T$) (Bahaidarah et al., 2013) underscores the importance of specific heat capacity (C_p), which denotes the amount of heat a material can absorb per unit mass to achieve a certain temperature change. Heat capacity plays a crucial role in controlling temperatures and regulating heat flow within thermal systems. Its significance in cooling processes cannot be underestimated, as it determines the ability of a fluid to store and release heat, thereby affecting overall cooling efficiency.

It is crucial to recognize that these properties, including thermal conductivity, density, and heat capacity, vary from one fluid to another. As a result, understanding these interconnections is fundamental to comprehending the mechanisms that govern cooling processes.

4.3.3.1.4 The effect of the porous media types

The insights gained from Figure 4.35 shed light on the significant influence of porous media type selection on the maximum PV temperature, specifically under a solar irradiation level of 1000 W/m^2. The study compared various media types, including sandstone, Flint, Marble, and Gravel. Each type of porous media demonstrated distinct cooling performances, resulting in different maximum PV temperatures.

Based on Figure 4.36, it is clear that among the media types tested, sandstone proved to be the most effective coolant, yielding the lowest maximum PV temperature at 35.66°C. Flint followed closely with a slightly higher maximum temperature of 35.89°C. Similarly, Marble also recorded a temperature of 35.94°C. On the other hand, Gravel showed the highest maximum PV temperature of 36.6°C.

The variation in maximum PV temperatures when using different types of porous media can be attributed to the unique properties of each material, with thermal conductivity playing a crucial role. The media with higher thermal conductivity efficiently transfer heat away from the PV panel, resulting in lower temperatures. Conversely, media with lower thermal conductivity exhibited reduced cooling efficiency, leading to relatively higher PV temperatures.

The findings highlight the critical importance of selecting the most appropriate porous media to optimize the cooling performance of solar panels. Understanding the thermal properties of the media enables system designers to make informed decisions, ensuring effective heat dissipation and temperature regulation.

The impact of the type of porous media on reducing the temperature of photovoltaic panels has become evident. Equations 2.2 reveal the critical connection between heat transfer by conduction and the thermal conductivity of porous media. The direct correlation clearly indicates that as thermal conductivity increases, so does the heat transfer efficiency. This underscores the vital role of effectively managing thermal conductivity to enhance heat dissipation in photovoltaic cooling applications.

Selecting the right porous media with higher thermal conductivity can significantly improve the cooling performance of photovoltaic panels. The higher thermal conductivity ensures a more efficient transfer of heat away from the panels, thereby helping to maintain lower operating temperatures. This, in turn, has a positive impact on the overall performance and lifespan of the photovoltaic system.

4.3.4 Prediction results of machine learning

Machine learning was an easy and inexpensive way to predict the results of future studies, therefore to predict the temperature of the photovoltaic panel and its output power, six algorithms' models have been used. The aim of using these six algorithms was to find out the accurate algorithm model that can be used in future studies. The predictive results from machine learning techniques based on the parameters that affect the performance of the photovoltaic panel are investigated. These algorithms encompass AdaBoost (AB), Random Forest (RF), Decision Tree (DT), Support Vector Machine (SVM), Gradient Boosting (GB), and Linear Regression (LR), were used taking into account the previously mentioned factors for experimental work such as, solar radiation, air velocity surrounding the PV panel, ambient temperature, volume flow rate, and water temperature leaving the cooling channel, temperature entering the cooling channel, and porosity size. Moreover, to ensure the validity of the results, root mean square error (RMSE), absolute error (MAE), and R^2 were found.

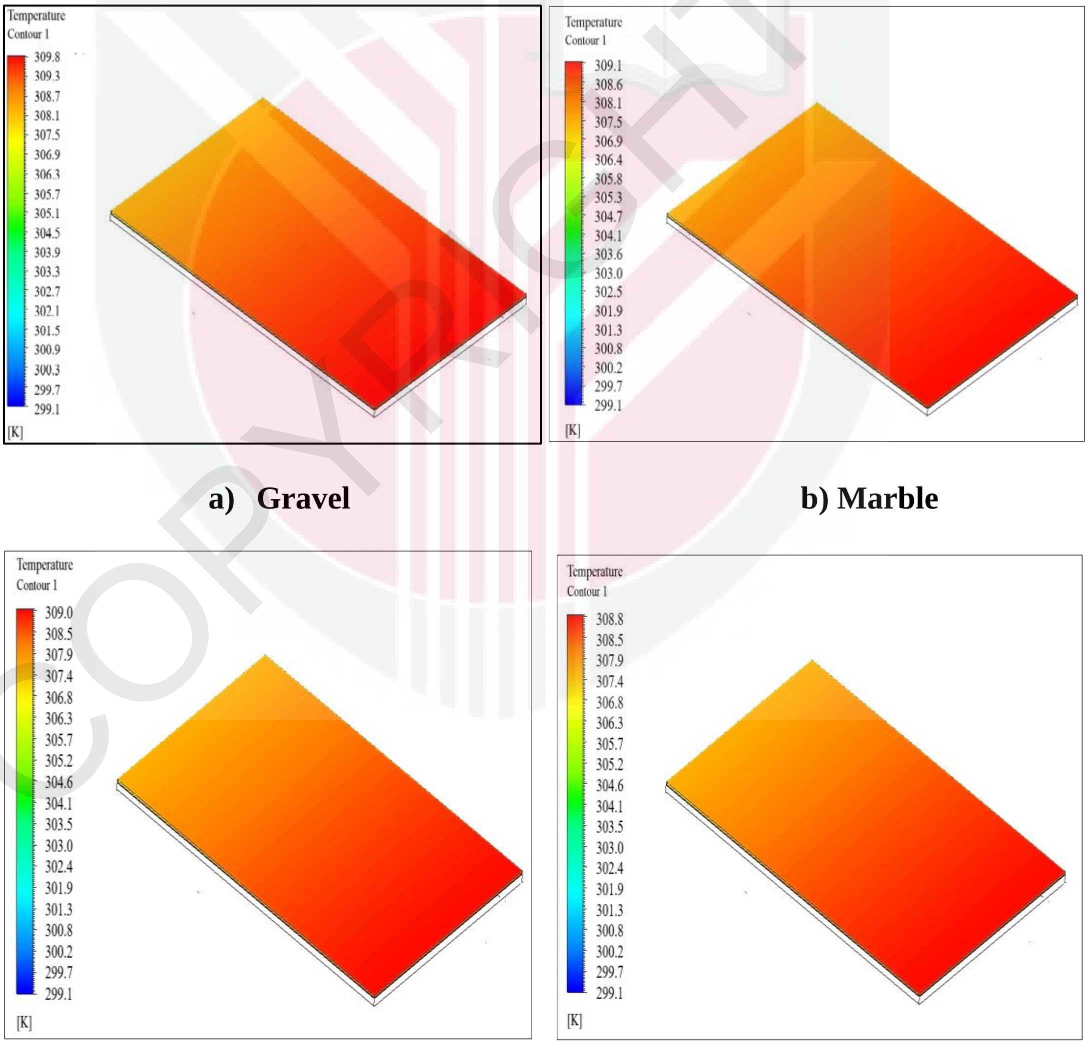

a) Gravel **b) Marble**

c) Flint **d) Sandstone**

Figure 4.35: PV temperature distribution with differences in the coolant types

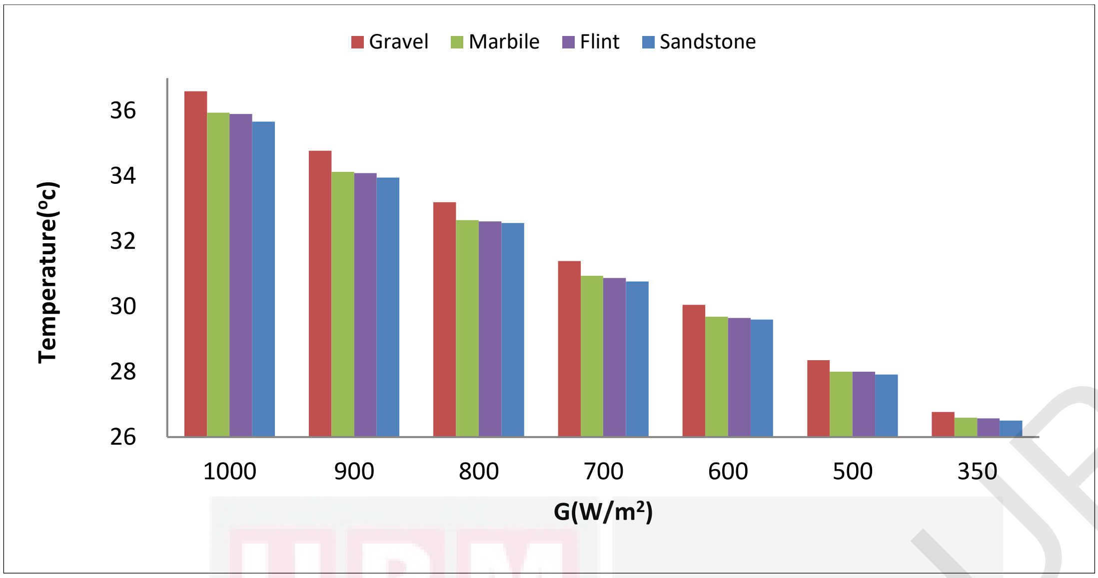

Figure 4.36: The temperature of the photovoltaic panel varies with the difference in solar radiation and the difference in the type of porous media PV average surface temperature

The accuracy of the results was checked and presented in Table 4.5, where it was clear from this table the value of the plan. Accordingly, it was possible to notice that the performance of the AdaBoost algorithm was the best among all other algorithms. The error value was as follows: RMSE 0.5135, MAE 0.3829, and R^2 0.986. In addition, the linear regression algorithm was the worst among them all, as follows: RMSE 1.1756, MAE 0.8673, and R^2 0.929, respectively. Figure 4.37 presents the six algorithms AdaBoost, Random Forest, Decision Tree, Support Vector Machine (SVM), and Gradient Boosting that were used in comparison with the experimental results, to find the PV panel temperature results. Based on the results similarity it was found that the predictive results were close to the experimental results. Accordingly, it was possible to use machine learning techniques to check future scientific cases for similar research without the need for laborious experimental work.

Table 4.5: Machine learning results for PV average surface temperature

Algorithm	RMSE	MAE	R^2
AdaBoost	0.5135	0.3829	0.9866
Random Forest	0.5824	0.41009	0.9827
Decision Tree	0.7006	0.5127	0.9750
SVM	0.7360	0.4504	0.9725
Gradient Boosting	0.7892	0.5622	0.9683
Linear Regression	1.1756	0.8673	0.9298

4.3.4.1 PV output power

The accuracy of the predicted logarithmic results for PV power out has been validated and presented in Table 4.6. Accordingly, it can be seen that the performance of the SVM algorithm was the best among all other algorithms. The error value is as follows: RMSE 0.1057, MAE 0.0889, and R^2 0.9892. In addition, the linear regression algorithm was the worst among them all, as follows: RMSE 0.1543, MAE 0.1221, and R^2 0.9770, respectively. It is clear from Figure 4.38 that there is a clear agreement between the six prediction results that were mentioned previously and the experimental results of the output power, but the best of these results were when using the SVM algorithm.

Table 4.6: Machine learning results for output power

Algorithm	RMSE	MAE	R^2
SVM	0.1057	0.0889	0.9892
Linear Regression	0.1156	0.0946	0.9871
Random Forest	0.1208	0.0975	0.9859
Gradient Boosting	0.1264	0.0992	0.9846
AdaBoost	0.1342	0.1010	0.9826
Decision Tree	0.1543	0.1221	0.9770

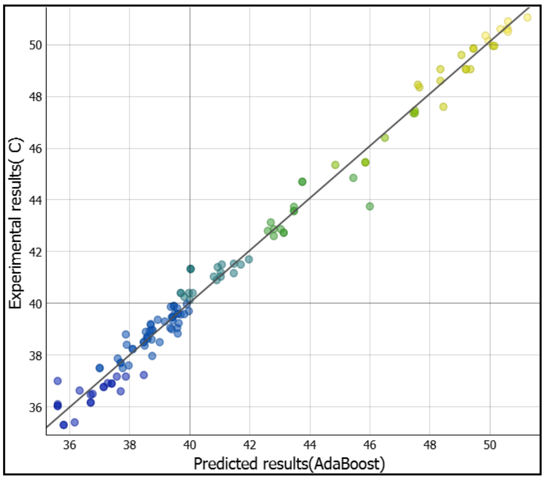

(a)

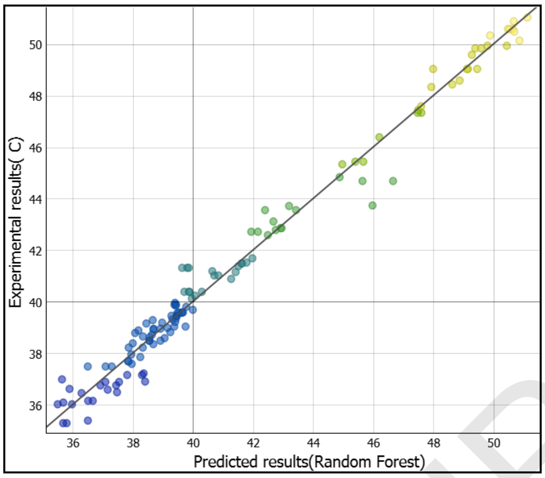

(b)

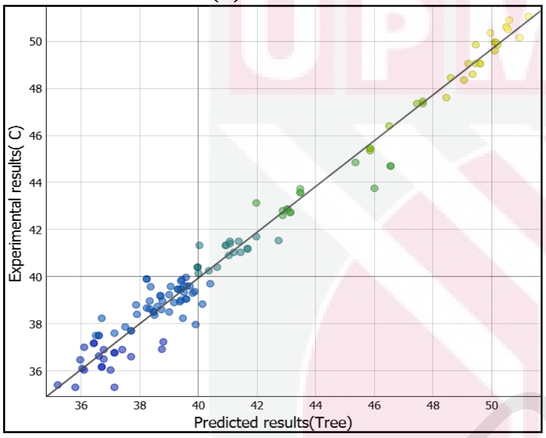

(c)

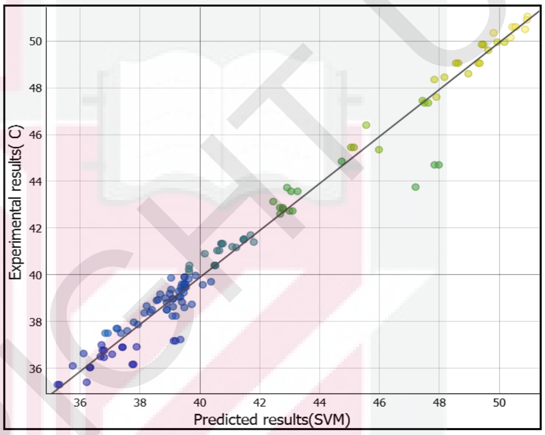

(d)

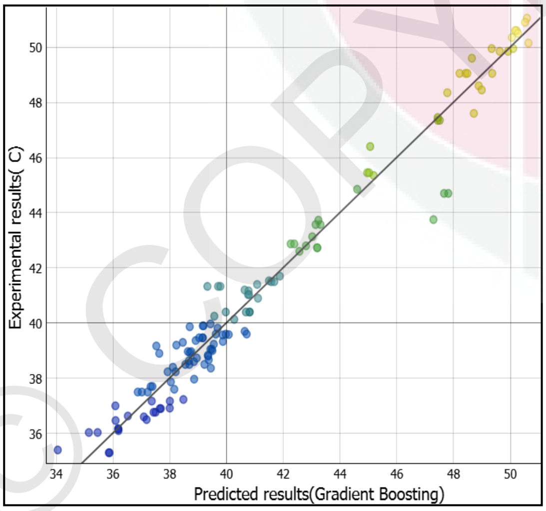

(e)

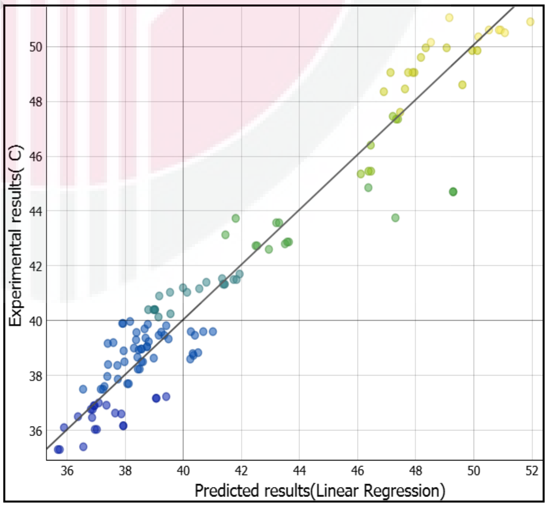

(f)

Figure 4.37: Predict PV average surface temperature with different machine learning algorithms

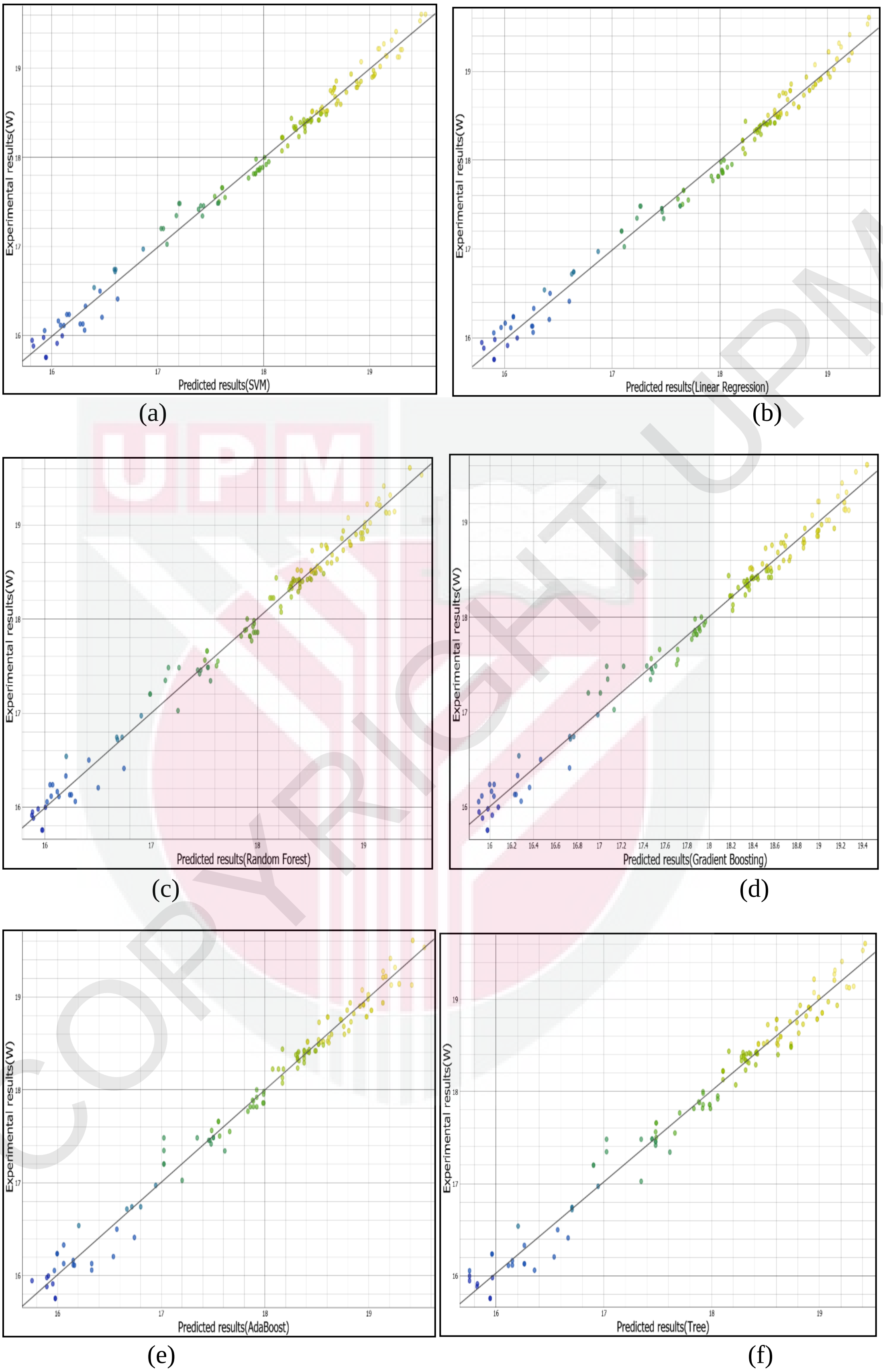

Figure 4.38: PV output power Prediction with different machine learning algorithms

4.3.4.2 Parameter's weight

For the cooling of photovoltaic cells, there are many parameters affecting the process, including solar radiation, the volume of flow rate, the temperature of the water inlet to the channel, the air temperature, the wind speed, and the porosity size. From Table 4.7, it was found that porosity size has the greatest effect on the cooling process followed by the low volume flow rate, and this result is consistent with the experimental results conducted indoors and outdoors. It was found also that the flow rate has a lesser effect than the porosity size, and accordingly, if the flow rates and the porosity size are reduced, the performance will be in the best condition which will save the cost of water pumping and enhance the PV power output.

Table 47.: PV cooling parameter's weight

Parameters	Parameters weight%
Porosity size	25.80
Time	15.07
Inlet temperature	13.65
Volume flow rate	12.29
Ambient temperature	0.983

4.3.5 Empirical correlation results

The advent of the empirical correlation linking the output power of photovoltaic panels to their operating temperature marks a pivotal milestone, propelling the field toward greater efficiency and sustainability. This groundbreaking correlation not only deepens our comprehension of photovoltaic systems but also serves as a powerful and indispensable tool for future research endeavours, streamlining the investigative process and alleviating the need for laborious and time-consuming experimental work.

However, the performance of these panels is inextricably linked to the fluctuations in operating temperature they experience under diverse environmental conditions. This temperature dependency poses a significant challenge in maximizing their efficiency and output power, necessitating a comprehensive understanding of the relationship between temperature variations and panel performance, as mentioned in Chapter Three.

4.3.5.1 Empirical correlation of power

The experimental results were compared with the results of the developed correlation based on Equations 3.55 to ensure the validity and accuracy of the results. Figures 4.39, 4.40, and 4.41 show the comparison results for the output power at variable porosities of 0.35, 0.4, and 0.48 and different flow volume rates of 1, 1.5, and 2 L/min. The results of the errors analysis found that the error for the volumetric flow rates of 1 L/min and different porosities of 0.35, 0.4, and 0.48 was as follows: 0.7%, 1.6%, and 1.9%, respectively. Hence, the volume flow rate of 1.5 L/min was 1.1%, 1.5%, and 2.5%, respectively. Furthermore, at a flow rate of 2 L/min, the errors were 2.2%, 2%, and 2.3%, respectively.

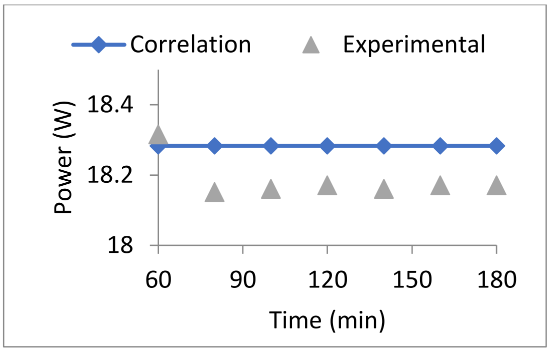

(a) 0.35

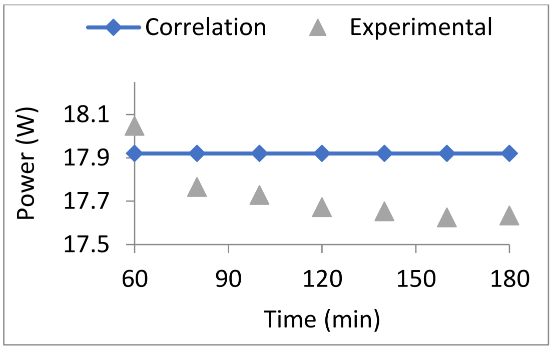

(b) 0.4

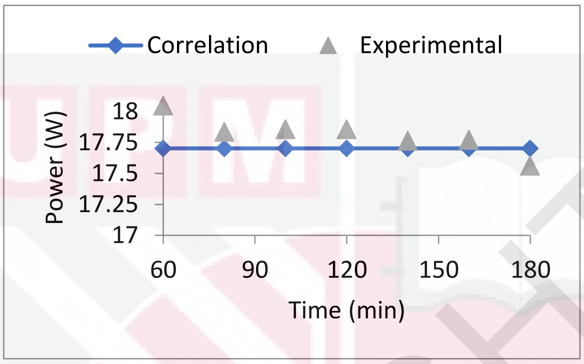

(c) 0.48

Figure 4.39: Comparison between experimental results and correlation results for a volume flow rate of 1 L/min

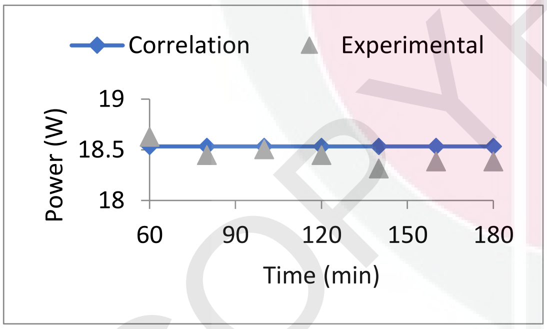

(a) 0.35

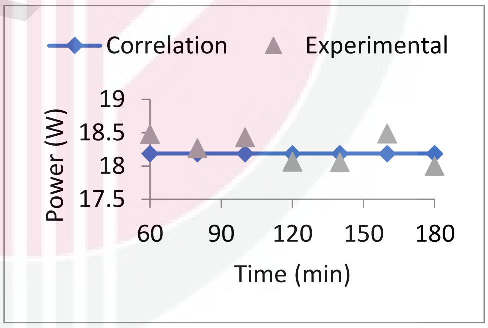

(b) 0.4

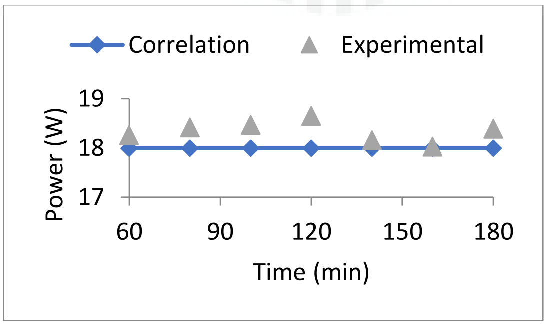

(c) 0.48

Figure 4.40: Comparison between experimental results and correlation results for a volume flow rate of 1.5 L/min

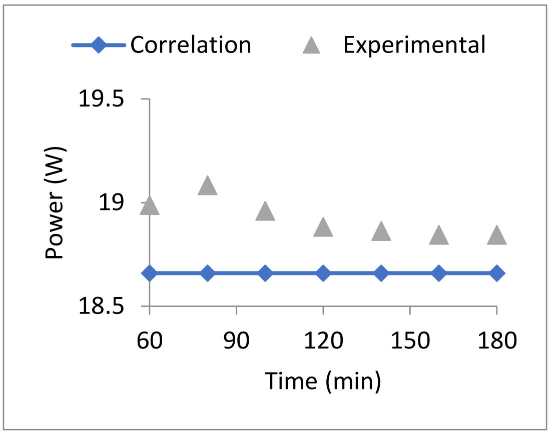

(a) 0.35

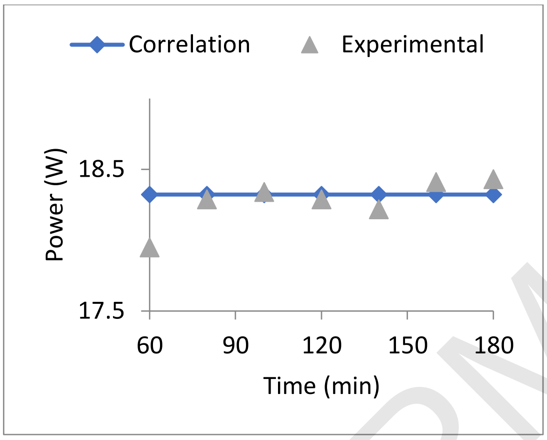

(b) 0.4

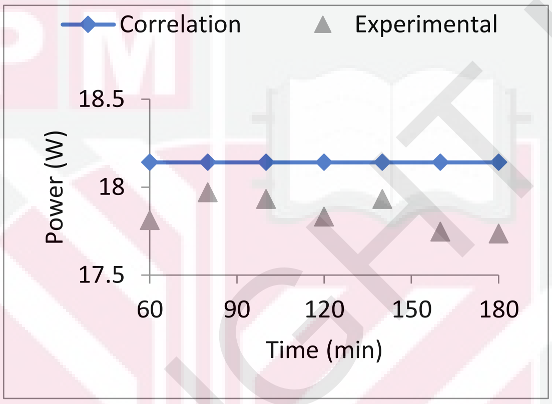

(c) 0.48

Figure 4.41: Comparison between experimental results and correlation results for a volume flow rate of 2 L/min

To find the power output, three different porosities were used, and accordingly, the correlation formula was developed, and the coefficient that affects the results when the porosities differed was found, and it was introduced and displayed in Table 4.8 for each porosity size that was used to cool.

Table 4.8: Correlation coefficient

Porosity size	Correlation factor (c)
0.35	22500
0.4	2292
0.48	292

4.3.5.2 Empirical correlation of PV temperature

To further verify the results the developed correlation based on Equation 3.61 was used to find the temperature of the PV panel. The results compared with the experimental study are shown in Figures 4.42, 4.43, and 4.44 at variable porosity size for each flow rate, and the error analysis of these results was found when using the flow is 1 L /min with a porosity size of 0.35, 0.4 and 0.48. The error was 2.6%, 4.5%, and 4.7%. At a volume flow rate of 1.5 L/min and 4.3%, 1.3%, and 4.7%, and a volume flow rate of 2 L/min were found to be 3.2%, 5%, and 4.1%, respectively.

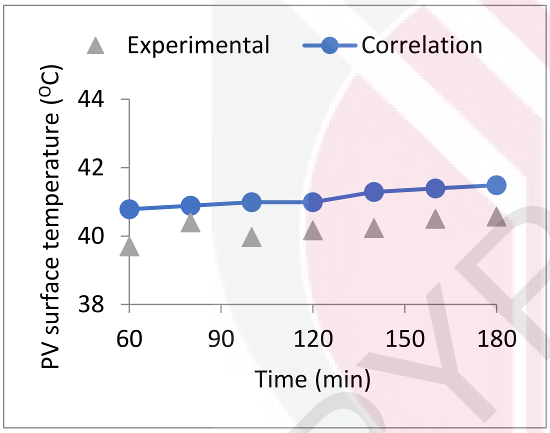

(a) 0.35

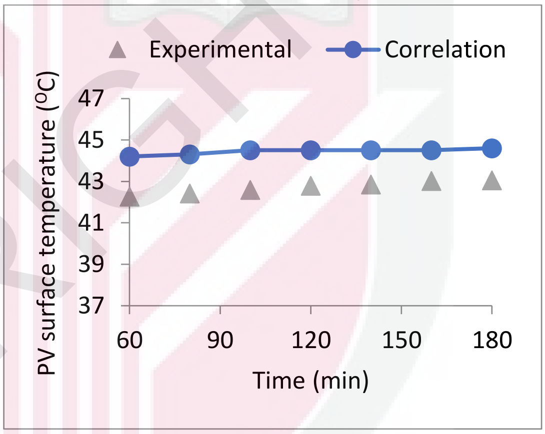

(b) 0.4

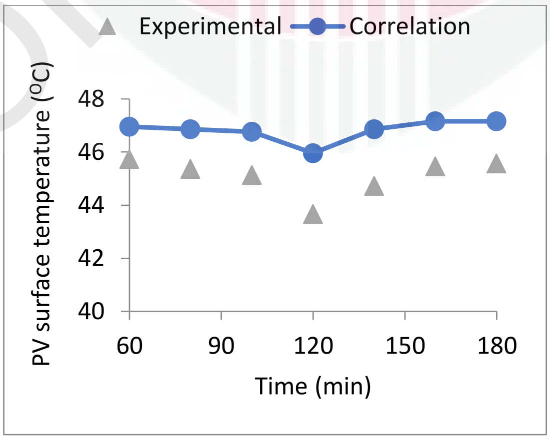

(c) 0.48

Figure 4.42: Comparison between experimental results and correlation results for a volume flow rate of 1 L/min

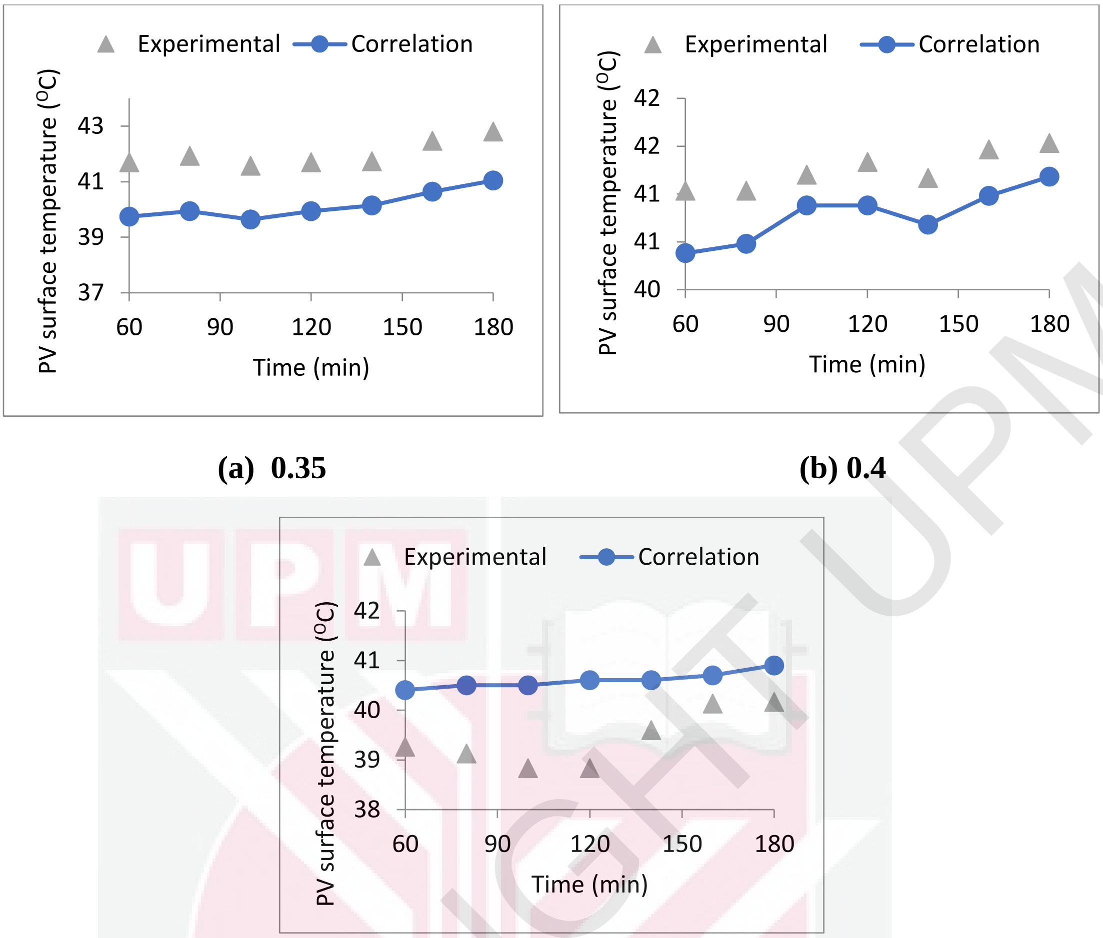

(a) 0.35 **(b) 0.4**

(c) 0.48

Figure 4.43: Comparison between experimental results and correlation results for a volume flow rate of 1.5 L/min

In the pursuit of determining the temperature of the PV panel, the correlation method was employed, incorporating three distinct porosities. Through accurate analysis, an empirical correlation equation was devised, specifically tailored to account for the variations in porosity size. This equation serves as a powerful tool in predicting the temperature of the PV panel under different porosity size conditions.

Notably, the coefficient that exerts a significant influence on the results when the porosities differ was thoroughly examined. The impact of this coefficient on temperature reduction was accurately charted and presented in Figure 4.45, providing valuable insights into the cooling efficiency for each porosity size utilized.

The correlation method employed in this research, incorporating different porosities, has yielded invaluable insights into predicting PV panel temperatures accurately. The coefficient analysis presented in Figure 4.45, serves as a key resource for optimizing cooling strategies based on varying porosity size conditions. By customizing cooling designs to match specific porosity size parameters, the potential for enhanced energy efficiency and improved performance of photovoltaic cells becomes apparent. This advancement in the field of renewable energy research holds great promise for a greener and more sustainable energy future.

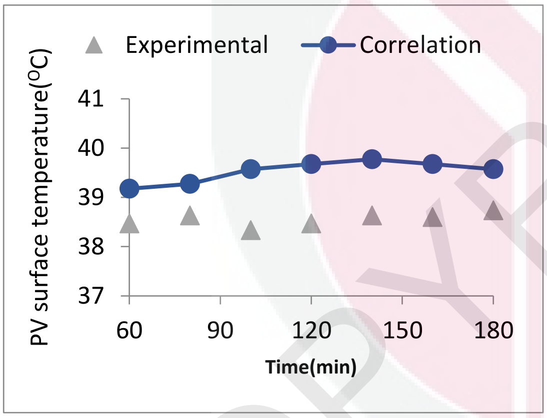

(a) 0.35

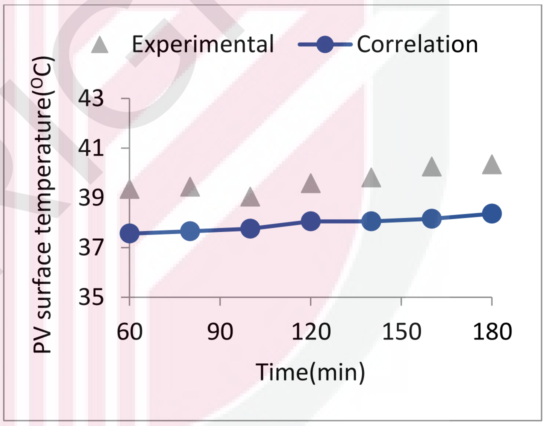

(b) 0.4

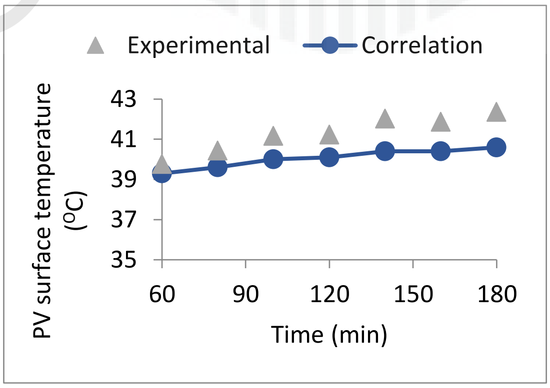

(c) 0.48

Figure 4.44: Comparison between experimental results and correlation results for a volume flow rate of 2 L/min

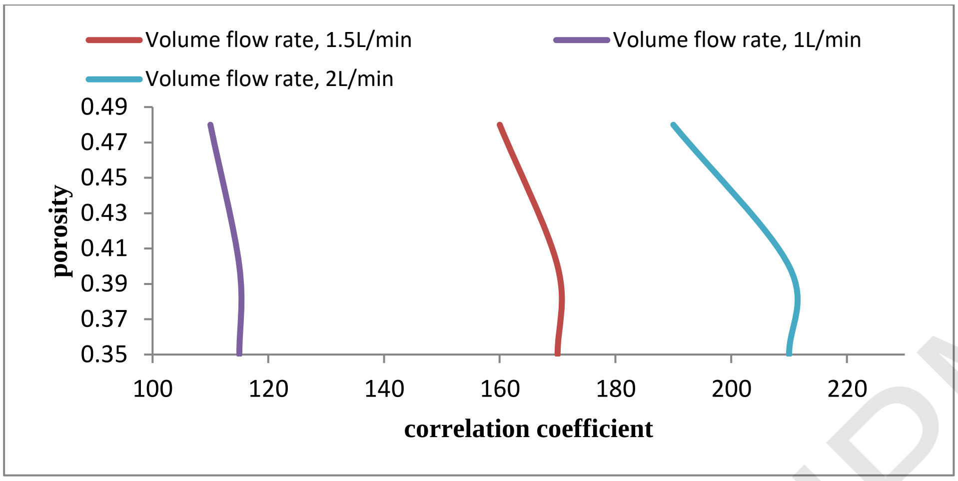

Figure 4.45: Correlation coefficient values for different porosities

4.4 Comparison between previous studies and the current work

Based on Table 4.9, a comprehensive comparison between the findings of previous studies and the outcomes of the current work is presented. The results unequivocally indicate that the current research has achieved superior performance in two crucial aspects: temperature reduction and output power enhancement. Regarding temperature reduction which dropped 22°C, while the best decrease in temperature in previous studies ranged between15-19°C, the current work surpasses the previous studies by implementing innovative cooling techniques that effectively mitigate the temperature rise in photovoltaic cells. The efficient cooling strategy applied in this research has led to significantly lower PV temperatures, ensuring that the photovoltaic cells operate under optimal conditions. By minimizing heat accumulation, the risk of performance degradation and efficiency loss is effectively mitigated, resulting in more stable and reliable electrical output.

Furthermore, the current work excels in increasing the output power of the photovoltaic panels. By implementing advanced technologies and precise thermal management, the research has successfully boosted the power output of solar panels. This enhancement in power generation is of paramount importance as it directly translates into improved energy efficiency and more productive utilization of solar energy.

The superiority of the current research findings has far-reaching implications in various applications, including solar energy systems for residential, commercial, and industrial use. The enhanced temperature regulation and increased power output contribute to greater energy yields, making solar technologies even more attractive and viable for widespread adoption. It is important to acknowledge that advancements in technology, accurate experimental techniques, and comprehensive data analysis have all contributed to the outcomes of the current work. The comparison with previous studies has enabled us to identify areas for improvement and implement novel strategies to overcome previous limitations.

Table 4.9: Comparison between previous work and current work

Authors	Coolant	Reduction of temperature (°C)	Increase in output power%
Current work	Porous media	22	14.4
Lin et al. (2019)	Air	4	7
Micheli et al. (2015)	Air	13	7.7
Moradgholi et al. (2014)	Methanol	13	5
Smith et al. (2014)	Water	11	6
Hasan et al. (2016)	PCM	10	6.6
Tang et al. (2010)	Air	4.7	8
Ebaid et al. (2018)	Nanofluied	20	9

CHAPTER 5

CONCLUSIONS AND RECOMMENDATION

5.1 Conclusions

Based on a thorough analysis of the results obtained from the photovoltaic cooling experiments and numerical analysis conducted in indoor and outdoor conditions, utilizing water and in combination with various porous mediums, several significant conclusions can be drawn as follows;

Objective 1

Indoor and outdoor experiments demonstrated that adding porous materials to water enhances cooling for photovoltaic cells. Porous mediums improve heat dissipation, lowering PV panel temperatures more effectively than water alone. Indoor tests revealed improved power and efficiency across cooling methods. Optimal outcomes occurred at 0.35 porosity size and 2 L/min flow, resulting in reduced temperature and increased power and efficiency. Without cooling, the PV panel reached 87.7°C, while water cooling lowered it to 48°C, and porous media cooled it to 38.7°C, yielding higher output power (12.8W vs. 19W). Porous media also excelled in electrical efficiency, with a peak open voltage of 22.5V. In the outdoor experiments, three scenarios were tested. Scenario one: Uncooled PV panel peaked at 49.1°C by noon, water-cooled at 41.5°C, while porous media-cooled hit 39.4°C, the most effective. At 2 L/min and 0.35 porosity size, a 19% temperature drop was noted – the best result. In scenario two, 0.35 porosity size offered optimal cooling, reducing temperatures by 35.7°C, 34.8°C, and 34°C for 0.35, 0.4, and 0.48 porosities, respectively. Power gains were 9.4%, 7.8%, and 6.2%. Scenario three explored flow rates: 1 L/min, 2 L/min, and 3 L/min. higher flow rates led to 18%, 20.3%, and 21% PV temperature reductions. Mathematical models have proven to have the ability to give results that are close to experimental results, offering a systematic and systematic approach to understanding complex phenomena. These models undergo rigorous verification processes, ensuring the accuracy and reliability of their results. In this study, these mathematical models showed a low average error rate of less than 5.6%.

Objective 2

ANSYS software was used in the study to investigate the effect of various other parameters involved in PV cooling by porous media. These parameters include the cooling channel height, which ranged from 50 mm to 5 mm, as well as the shape of the cooling channel which was achieved by varying the channel height at the liquid outlet from 4 mm to 2 mm while maintaining a fixed channel inlet height of 5 mm. Moreover, various types of coolants, which were water, chemical alcohol, engine oil, and different types of porous media, including gravel, marble, flint, and sandstone were further considered in this study. For the study using ANSYS, the PV temperature was found to be 36.6°C, which was achieved with a cooling channel height of 5 mm at the inlet and 3 mm at the outlet, employing water as the coolant and sandstone as the porous media with the optimization porosity size and volume flow rate are 0.35 and 2 L/min.

Objective3

The formulation of the empirical correlations was crafted, taking into account the coefficients that influence the behaviour of the photovoltaic panel. By incorporating these essential factors, the correlation provides a reliable and accurate estimation of the panel's output power and PV temperature with an error of less than 5%.

5.2 Recommendation

Recommendations are vital aspects of any research, as they offer valuable insights for future investigations and potential improvements. In the context of photovoltaic cooling, several noteworthy recommendations can be made to further enhance the efficiency and effectiveness of the cooling process:

1. Exploration of Passive Cooling Techniques: While active cooling methods have proven effective, another area worth exploring is the implementation of passive cooling techniques. Passive cooling systems rely on natural heat dissipation mechanisms, eliminating the need for external power sources. Such systems are generally simpler, more cost-effective, and require minimal maintenance. By harnessing the principles of natural convection and radiation, researchers can design innovative passive cooling solutions that enhance energy efficiency and promote sustainability.

2. Integration of Advanced Control Systems: Incorporating advanced control systems and intelligent algorithms can further optimize the cooling process. These systems can continuously monitor the PV panel's temperature and adjust the cooling mechanisms in real-time to ensure optimal performance. Through automated control, researchers can achieve a fine balance between temperature regulation and energy consumption, ultimately leading to enhanced overall system efficiency.

3. Comprehensive experimental study on the effect of different forms of cooling channels.

These recommendations present exciting opportunities for further advancement in photovoltaic cooling technology. By exploring alternative porous media, considering different cooling fluids, and exploring passive cooling approaches, researchers can optimize the efficiency and sustainability of photovoltaic systems. Additionally, integrating advanced control systems and conducting long-term reliability assessments will pave the way for more robust and reliable photovoltaic cooling solutions, contributing to the continuous growth of renewable energy technologies.

5.3 Novelty of this study

The novel aspects of this research lie in the comprehensive exploration and optimization of porous media cooling techniques for photovoltaic panels. The key innovations can be outlined as follows:

1. Integrated Approach for Temperature Reduction and Optimization:

Unlike conventional cooling methods, our approach integrates the reduction of the operating temperature of photovoltaic (PV) panels with the simultaneous optimization of porosity size and volume flow rates within the porous media. This dual focus ensures a holistic and efficient cooling strategy tailored to the unique characteristics of the PV system. Rapid Assessment of Temperature and Power Output: The emphasis on obtaining quick results for PV temperature and output power sets our research apart. This accelerated assessment not only expedites the evaluation process but also allows for swift adjustments, providing practical insights for real-time applications and operational adjustments.

2. Comprehensive Investigation of Cooling Parameters:

Our study goes beyond the conventional by conducting an in-depth investigation into various parameters influencing PV cooling through porous media. This includes a systematic exploration of cooling channel height, channel geometry, coolant types, and diverse porous media. The broad scope of these parameters ensures a nuanced understanding of their individual and collective impacts on the cooling efficiency of the PV system. Weighted Analysis for Parameter Significance: In an innovative step, our research aims to determine the weights assigned to different parameters in the PV cooling process. This unique approach involves assessing the relative significance of porosity size, volume flow rate, time, Inlet temperature, and ambient temperature. The determination of parameter weights contributes to a nuanced understanding of their respective impacts on the overall cooling performance.

3. Development of Empirical Correlation:

The formulation of an empirical correlation for temperature and output power under various cooling conditions using porous media stands out as a significant contribution. This correlation provides a quantitative framework for predicting the relationship between cooling parameters and PV performance, facilitating the design and optimization of porous media cooling systems.

In essence, the novelty of this research lies in its multifaceted approach that combines optimization, rapid assessment, comprehensive parameter investigation, weighted analysis, and the development of an empirical correlation. These elements collectively contribute to advancing the current understanding of porous media cooling for photovoltaic panels, offering valuable insights for practical implementation and future research endeavours.

REFERENCES

Abdulgafar, S. A. Omar, O. S. Yousif, K. M. (2007). Improving The Efficiency of Polycrystalline Solar Panel Via Water Immersion Method. In International Journal of Innovative Research in Science, Engineering and Technology (An ISO) 3, 8127 – 8132.

Ahmed, O. K. Hamada, K. I. & Salih, A. M. (2019). Enhancement of the performance of Photovoltaic/Trombe wall system using the porous medium: Experimental and theoretical study. Energy, 171, 14–26.

Ahmed, O. K. & Mohammed, Z. A. (2017). Influence of porous media on the performance of hybrid PV/Thermal collector. Renewable Energy, 112, 378–387.

Aldihani, A. Aldossary, A. Mahmoud, S. & Al-Dadaha, R. K. (2014). The effect of cooling on the performance of photovoltaic cells under dusty environmental conditions. Energy Procedia, 61, 2383–2386.

Aldossary, A. Mahmoud, S. & Al-Dadah, R. (2016). Technical feasibility study of passive and active cooling for concentrator PV in harsh environment. Applied Thermal Engineering, 100, 490–500.

Alizadeh, H. Ghasempour, R. Shafii, M. B. Ahmadi, M. H. Yan, W.-M. & Nazari, M. A. (2018). Numerical simulation of PV cooling by using single turn pulsating heat pipe. International Journal of Heat and Mass Transfer, 127, 203–208.

AL-Musawi, A. I. A. Taheri, A. Farzanehnia, A. Sardarabadi, M. & Passandideh-Fard, M. (2019). Numerical study of the effects of nanofluids and phase-change materials in photovoltaic thermal (PVT) systems. Journal of Thermal Analysis and Calorimetry, 137, 623–636.

Amelia, A. R. Irwan, Y. M. Irwanto, M. Leow, W. Z. Gomesh, N. Safwati, I. & Anuar, M. A. M. (2016). Cooling on Photovoltaic Panel Using Forced Air Convection Induced by DC Fan. International Journal of Electrical and Computer Engineering (IJECE), 6(2), 526.

Amori, K. E. & Taqi Al-Najjar, H. M. (2012). Analysis of thermal and electrical performance of a hybrid (PV/T) air based solar collector for Iraq. Applied Energy, 98, 384–395.

Badran, O. Abdulhadi, E. & Mamlook, R. (2010). Evaluation of Solar Electric Power Technologies in Jordan. Journal of Mechanical and Industrial Engineering,4, (1) 121-128.

Bahaidarah, H. M. S. (2016). Experimental performance evaluation and modeling of jet impingement cooling for thermal management of photovoltaics. Solar Energy, 135, 605–617.

Bahaidarah, H. Subhan, A. Gandhidasan, P. & Rehman, S. (2013). Performance evaluation of a PV (photovoltaic) module by back surface water cooling for hot climatic conditions. Energy, 59, 445–453.

Bai, A. Popp, J. Balogh, P. Gabnai, Z. Pályi, B. Farkas, I. Pintér, G. & Zsiborács, H. (2016). Technical and economic effects of cooling of monocrystalline photovoltaic modules under Hungarian conditions. In Renewable and Sustainable Energy Reviews, 60, 1086–1099).

Baloch, A. A. B. Bahaidarah, H. M. S. Gandhidasan, P. & Al-Sulaiman, F. A. (2015). Experimental and numerical performance analysis of a converging channel heat exchanger for PV cooling. Energy Conversion and Management, 103, 14–27.

Barrau, J. Rosell, J. Chemisana, D. Tadrist, L. & Ibañez, M. (2011). Effect of a hybrid jet impingement/micro-channel cooling device on the performance of densely packed PV cells under high concentration. Solar Energy, 85(11), 2655–2665.

Bayrak, F. Oztop, H. F. & Selimefendigil, F. (2020). Experimental study for the application of different cooling techniques in photovoltaic (PV) panels. Energy Conversion and Management, 212, 112789.

Beccali, M. Finocchiaro, P. & Nocke, B. (2009). Energy and economic assessment of desiccant cooling systems coupled with single glazed air and hybrid PV/thermal solar collectors for applications in hot and humid climate. Solar Energy, 83(10), 1828–1846.

Bongiorno, V. Gibbon, S. Michailidou, E. & Curioni, M. (2022). Exploring the use of machine learning for interpreting electrochemical impedance spectroscopy data: evaluation of the training dataset size. Corrosion Science, 198, 110119.

Bilen, K. & Erdoğan, İ. (2023). Effects of cooling on performance of photovoltaic/thermal (PV/T) solar panels: A comprehensive review. Solar Energy, 262, 111829.

Buker, M. S. Mempouo, B. & Riffat, S. B. (2015). Experimental investigation of a building integrated photovoltaic/thermal roof collector combined with a liquid desiccant enhanced indirect evaporative cooling system. Energy Conversion and Management, 101, 239–254.

Čáchová, M. Koňáková, D. Vejmelková, E. Keppert, M. & Černý, R. (2016). Mechanical and thermal properties of the Czech marbles. International conference of numerical analysis and applied mathematics, 1738, 280010.

Carriere, T. Vernay, C. Pitaval, S. Kariniotakis, G. (2019) a Novel Approach for Seamless Probabilistic Photovoltaic Power Forecasting Covering Multiple Time Frames. IEEE Trans-Actions on Smart Grid, 2019(3).

Chandrasekar, M. & Senthilkumar, T. (2015). Experimental demonstration of enhanced solar energy utilization in flat PV (photovoltaic) modules cooled by heat spreaders in conjunction with cotton wick structures. Energy, 90, 1401–1410.

Chandrasekar, M. Suresh, S. Senthilkumar, T. & Ganesh Karthikeyan, M. (2013). Passive cooling of standalone flat PV module with cotton wick structures. Energy Conversion and Management, 71, 43–50.

Ebaid, M. S. Y. Ghrair, A. M. & Al-Busoul, M. (2018). Experimental investigation of cooling photovoltaic (PV) panels using (TiO2) nanofluid in water - polyethylene glycol mixture and (Al2O3) nanofluid in water-cetyltrimethylammonium bromide mixture. Energy Conversion and Management, 155, 324–343.

Ebrahimi, M. Rahimi, M. & Rahimi, A. (2015). An experimental study on using natural vaporization for cooling of a photovoltaic solar cell. International Communications in Heat and Mass Transfer, 65, 22–30.

Eitner, U. Kontges, M. & Brendel, R. (2009). Measuring thermomechanical displacements of solar cells in laminates using digital image correlation. 2009 34th IEEE Photovoltaic Specialists Conference (PVSC), 001280–001284.

El Mays, A. Ammar, R. Hawa, M. Akroush, M. A. Hachem, F. Khaled, M. & Ramadan, M. (2017). Improving Photovoltaic Panel Using Finned Plate of Aluminum. Energy Procedia, 119, 812–817.

Elminshawy, N. A. S. El Ghandour, M. Gad, H. M. El-Damhogi, D. G. El-Nahhas, K. & Addas, M. F. (2019). The performance of a buried heat exchanger system for PV panel cooling under elevated air temperatures. Geothermics, 82, 7–15.

Elminshawy, N. A. S. El-Ghandour, M. Elhenawy, Y. Bassyouni, M. El-Damhogi, D. G. & Addas, M. F. (2019). Experimental investigation of a V-trough PV concentrator integrated with a buried water heat exchanger cooling system. Solar Energy, 193, 706–714.

Elnozahy, A. Rahman, A. K. A. Ali, A. H. H. Abdel-Salam, M. & Ookawara, S. (2015). Performance of a PV module integrated with standalone building in hot arid areas as enhanced by surface cooling and cleaning. Energy and Buildings, 88, 100–109.

Eseye, A. T. Zhang, J. & Zheng, D. (2018). Short-term photovoltaic solar power forecasting using a hybrid Wavelet-PSO-SVM model based on SCADA and Meteorological information. Renewable Energy, 118, 357–367.

Fan, M. Feng, G. Xu, J. Yang, H. Kong, X. & Li, H. (2023). Simulation of air-cooled PV/T air conditioning system for cooling and power cogeneration. Applied Thermal Engineering, 224, 119971.

Incropera, F. & DeWitt, D. (2007). Fundamentals of heat and mass transfer (6th ed.). J. Wiley & Sons.

Gao, Y. Wu, D. Dai, Z. Wang, C. Zhu, L. Zhang, J. Xu, G. & Zhang, X. (2023). A passive evaporative cooling strategy to enhance the electricity production of hybrid PV-STEG system. Applied Energy, 349, 121689.

Gholami, A. Ameri, M. Zandi, M. Gavagsaz Ghoachani, R. & Kazem, H. A. (2022). Predicting solar photovoltaic electrical output under variable environmental conditions: Modified semi-empirical correlations for dust. Energy for Sustainable Development, 71, 389–405.

Golzari, S. Kasaeian, A. Amidpour, M. Nasirivatan, S. & Mousavi, S. (2018). Experimental investigation of the effects of corona wind on the performance of an air-cooled PV/T. Renewable Energy, 127, 284–297.

Gomaa, M. R. Hammad, W. Al-Dhaifallah, M. & Rezk, H. (2020). Performance enhancement of grid-tied PV system through proposed design cooling techniques: An experimental study and comparative analysis. Solar Energy, 211, 1110–1127.

Guo, W. Xu, L. Wang, T. Zhao, D. & Tang, X. (2024). Photovoltaic Power Prediction Based on Hybrid Deep Learning Networks and Meteorological Data. Sensors, 24(5), 1593.

Hachicha, A. A. Ghenai, C. & Hamid, A.-K. (2015). Enhancing the Performance of a Photovoltaic Module Using Different Cooling Methods. International Journal of Environmental, Chemical, Ecological, Geological and Geophysical Engineering ,9, 999-1002.

Hafith, S. A. Mohd Eltous, Y. Eltous, Y. & Abdelhafith, S. (2013). Feasibility of residential grid connected PV system under the Jordanian net metering renewable energy law. Journal of Energy Technologies and Policy, 3(7) 34-37.

Harmailil, I. O. Sultan, S. M. Tso, C. P. Fudholi, A. Mohammad, M. & Ibrahim, A. (2024). A review on recent photovoltaic module cooling techniques: Types and assessment methods. Results in Engineering, 22, 102225.

Hasan, A. Alnoman, H. & Shah, A. (2016). Energy Efficiency Enhancement of Photovoltaics by Phase Change Materials through Thermal Energy Recovery. Energies, 9(10), 782.

Herez, A. El Hage, H. Lemenand, T. Ramadan, M. & Khaled, M. (2020). Review on photovoltaic/thermal hybrid solar collectors: Classifications, applications and new systems. Solar Energy, 207, 1321–1347.

Hussien, A. Eltayesh, A. & El-Batsh, H. M. (2023). Experimental and numerical investigation for PV cooling by forced convection. Alexandria Engineering Journal, 64, 427–440.

Hamdan, M. A. & Kardasi, K. K. (2017). Improvement of Photovoltaic Panel Efficiency using Nanofluid. International Journal of Thermal and Environmental Engineering, 14(2), 143-151.

Ibrahim, T. Hachem, F. Ramadan, M. Faraj, J. El Achkar, G. & Khaled, M. (2023). Cooling PV panels by free and forced convections: Experiments and comparative study. AIMS Energy, 11(5), 774–794.

Idoko, L. Anaya-Lara, O. & McDonald, A. (2018). Enhancing PV modules efficiency and power output using multi-concept cooling technique. Energy Reports, 4, 357–369.

Irwan, Y. M. Leow, W. Z. Irwanto, M. Fareq, M. Amelia, A. R. Gomesh, N. & Safwati, I. (2015). Indoor Test Performance of PV Panel through Water Cooling Method. Energy Procedia, 79, 604–611.

Fawaz, H. Forestier, G. Weber, J. Idoumghar, L. & Muller, P. A. (2019). Deep learning for time series classification: a review. Data Mining and Knowledge Discovery, 33(4), 917–963.

Jakhrani, A. Q. Samo, S. R. Kamboh, S. A. Labadin, J. & Rigit, A. R. H. (2014). An Improved Mathematical Model for Computing Power Output of Solar Photovoltaic Modules. International Journal of Photoenergy, 2014, 1–9.

Jamali, S. Yari, M. & Mahmoudi, S. M. S. (2018). Enhanced power generation through cooling a semi-transparent PV power plant with a solar chimney. Energy Conversion and Management, 175, 227–235.

Kabeel, A. E. Abdelgaied, M. & Sathyamurthy, R. (2019). A comprehensive investigation of the optimization cooling technique for improving the performance of PV module with reflectors under Egyptian conditions. Solar Energy, 186, 257–263.

Karami, N. & Rahimi, M. (2014). Heat transfer enhancement in a PV cell using Boehmite nanofluid. Energy Conversion and Management, 86, 275–285.

Kong, R. Deethayat, T. Asanakham, A. & Kiatsiriroat, T. (2020). Performance and economic evaluation of a photovoltaic/thermal (PV/T)-cascade heat pump for combined cooling, heat and power in tropical climate area. Journal of Energy Storage, 30,101507.

Kordzadeh, A. (2010). The effects of nominal power of array and system head on the operation of photovoltaic water pumping set with array surface covered by a film of water. Renewable Energy, 35(5), 1098–1102.

Krauter, S. (2004). Increased electrical yield via water flow over the front of photovoltaic panels. Solar Energy Materials and Solar Cells, 82(1–2), 131–137.

Panjwani, M. & Narejo, G. (2014). Effect of humidity on the efficiency of solar cell (photovoltaic). International Journal of Engineering Research and General Science, 2(4), 499.

Laabab, I. Ziani, S. & Benami, A. (2022). Solar panels overheating protection: a review. Indonesian Journal of Electrical Engineering and Computer Science, 29(1), 49-55.

Lin, Y. Adilbekova, B. Firdaus, Y. Yengel, E. Faber, H. Sajjad, M. Zheng, X. Yarali, E. Seitkhan, A. Bakr, O. M. El-Labban, A. Schwingenschlögl, U. Tung, V. McCulloch, I. Laquai, F. & Anthopoulos, T. D. (2019). 17% Efficient Organic Solar Cells Based on Liquid Exfoliated WS 2 as a Replacement for PEDOT:PSS. Advanced Materials, 31(46), 1-42.

Liu, Y. Chen, Y. Wang, D. Liu, J. Luo, X. Wang, Y. Liu, H. & Liu, J. (2021). Experimental and numerical analyses of parameter optimization of photovoltaic cooling system. Energy, 215, 119159.

Ma, T. Yang, H. Zhang, Y. Lu, L. & Wang, X. (2015). Using phase change materials in photovoltaic systems for thermal regulation and electrical efficiency improvement: A review and outlook. In Renewable and Sustainable Energy Reviews, 43, 1273–1284.

Marion, B. Schaefer, R. Caine, H. & Sanchez, G. (2013). Measured and modeled photovoltaic system energy losses from snow for Colorado and Wisconsin locations. Solar Energy, 97, 112–121.

Markovics, D. & Mayer, M. J. (2022). Comparison of machine learning methods for photovoltaic power forecasting based on numerical weather prediction. Renewable and Sustainable Energy Reviews, 161, 112364.

Mazón-Hernández, R. García-Cascales, J. R. Vera-García, F. Káiser, A. S. & Zamora, B. (2013). Improving the Electrical Parameters of a Photovoltaic Panel by Means of an Induced or Forced Air Stream. International Journal of Photoenergy, 2013, 1–10.

Meng, Q. Wang, Y. & Zhang, L. (2011). Irradiance characteristics and optimization design of a large-scale solar simulator. Solar Energy, 85(9), 1758–1767.

Micheli, L. Reddy, K. S. & Mallick, T. K. (2015). Plate micro-fins in natural convection: An opportunity for passive concentrating photovoltaic cooling. Energy Procedia, 82, 301–308.

Mojumder, J. C. Chong, W. T. Ong, H. C. Leong, K. Y. & Abdullah-Al-Mamoon. (2016). An experimental investigation on performance analysis of air type photovoltaic thermal collector system integrated with cooling fins design. Energy and Buildings, 130, 272–285.

Moradgholi, M. Nowee, S. M. & Abrishamchi, I. (2014). Application of heat pipe in an experimental investigation on a novel photovoltaic/thermal (PV/T) system. Solar Energy, 107, 82–88.

Najafi, H. & Woodbury, K. A. (2013). Optimization of a cooling system based on Peltier effect for photovoltaic cells. Solar Energy, 91, 152–160.

Nižetić, S. Čoko, D. Yadav, A. & Grubišić-Čabo, F. (2016). Water spray cooling technique applied on a photovoltaic panel: The performance response. Energy Conversion and Management, 108, 287–296.

Odeh, S. & Behnia, M. (2009). Improving Photovoltaic Module Efficiency Using Water Cooling. Heat Transfer Engineering, 30(6), 499–505.

Olalla, C. Hasan, Md. Deline, C. & Maksimović, D. (2018). Mitigation of Hot-Spots in Photovoltaic Systems Using Distributed Power Electronics. Energies, 11(4), 726.

Olmuş, U. Güzelel, Y. E. & Büyükalaca, O. (2023). Seasonal analysis of a desiccant air-conditioning system supported by water-cooled PV/T units. Energy and Buildings, 291, 113101.

Özakin, A. N. & Kaya, F. (2019). Effect on the exergy of the PVT system of fins added to an air-cooled channel: A study on temperature and air velocity with ANSYS Fluent. Solar Energy, 184, 561–569.

Patil, M. Sidramappa, A. Shetty, S. K. & Hebbale, A. M. (2023). Experimental study of solar PV/T panel to increase the energy conversion efficiency by air cooling. Materials Today: Proceedings, 92, 309–313.

Popovici, C. G. Hudişteanu, S. V. Mateescu, T. D. & Chereches, N. C. (2016). Efficiency Improvement of Photovoltaic Panels by Using Air Cooled Heat Sinks. Energy Procedia, 85, 425–432.

Radwan, A. Ahmed, M. & Ookawara, S. (2016). Performance enhancement of concentrated photovoltaic systems using a microchannel heat sink with nanofluids. Energy Conversion and Management, 119, 289–303.

Rahimi, M. Asadi, M. Karami, N. & Karimi, E. (2015). A comparative study on using single and multi header microchannels in a hybrid PV cell cooling. Energy Conversion and Management, 101, 1–8.

Rahimi, M. Valeh-e-Sheyda, P. Parsamoghadam, M. A. Masahi, M. M. & Alsairafi, A. A. (2014). Design of a self-adjusted jet impingement system for cooling of photovoltaic cells. Energy Conversion and Management, 83, 48–57.

Rajput, U. J. & Yang, J. (2018). Comparison of heat sink and water type PV/T collector for polycrystalline photovoltaic panel cooling. Renewable Energy, 116, 479–491.

Ramadan, M. R. I. El-Sebaii, A. A. Aboul-Enein, S. & El-Bialy, E. (2007). Thermal performance of a packed bed double-pass solar air heater. Energy, 32(8), 1524–1535.

Royne, A. & Dey, C. J. (2007). Design of a jet impingement cooling device for densely packed PV cells under high concentration. Solar Energy, 81(8), 1014–1024.

Sahay, A. Sethi, V. K. Tiwari, A. C. & Pandey, M. (2015). A review of solar photovoltaic panel cooling systems with special reference to Ground coupled central panel cooling system (GC-CPCS). In Renewable and Sustainable Energy Reviews, 42, 306–312.

Saidan, M. Albaali, A. G. Alasis, E. & Kaldellis, J. K. (2016). Experimental study on the effect of dust deposition on solar photovoltaic panels in desert environment. Renewable Energy, 92, 499–505.

Salman, A. H. A. Hilal, K. H. & Ghadhban, S. A. (2022). Enhancing performance of PV module using water flow through porous media. Case Studies in Thermal Engineering, 34, 102000.

Sivaraj, S. Rathanasamy, R. Kaliyannan, G. V. Panchal, H. Jawad Alrubaie, A. Musa Jaber, M. Said, Z. & Memon, S. (2022). A Comprehensive Review on Current Performance, Challenges and Progress in Thin-Film Solar Cells. Energies, 15(22), 8688.

Smets, A.H.M. Jäger, K. Isabella, O. Van Swaaij, R.A.C.M.M. & Zeman, M. (2016). Solar Energy: The Physics and Engineering of Photovoltaic Conversion Technologies and Systems. Cambridge: UIT.

Smith, M. K. Selbak, H. Wamser, C. C. Day, N. U. Krieske, M. Sailor, D. J. & Rosenstiel, T. N. (2014). Water Cooling Method to Improve the Performance of Field-Mounted, Insulated, and Concentrating Photovoltaic Modules. Journal of Solar Energy Engineering, 136(3), SOL-13-1159.

Soliman, A. M. A. & Hassan, H. (2019). Effect of heat spreader size, microchannel configuration and nanoparticles on the performance of PV-heat spreader-microchannels system. Solar Energy, 182, 286–297.

Stropnik, R. & Stritih, U. (2016). Increasing the efficiency of PV panel with the use of PCM. Renewable Energy, 97, 671–679.

Sun, Q. (2017). Analyses of the factors influencing sandstone thermal conductivity. Acta Geodynamica et Geomaterialia,14(2), 173–180.

Tang, X. Quan, Z. & Zhao, Y. (2010). Experimental Investigation of Solar Panel Cooling by a Novel Micro Heat Pipe Array. Energy and Power Engineering, 2(03), 171–174.

Tonui, J. K. & Tripanagnostopoulos, Y. (2007). Air-cooled PV/T solar collectors with low cost performance improvements. Solar Energy, 81(4), 498–511.

Wu, S. & Xiong, C. (2014). Passive cooling technology for photovoltaic panels for domestic houses. International Journal of Low-Carbon Technologies, 9(2), 118–126.

Wu, S.-Y. Chen, C. & Xiao, L. (2018). Heat transfer characteristics and performance evaluation of water-cooled PV/T system with cooling channel above PV panel. Renewable Energy, 125, 936–946.

Xu, Z. & Kleinstreuer, C. (2014). Concentration photovoltaic–thermal energy co-generation system using nanofluids for cooling and heating. Energy Conversion and Management, 87, 504–512.

Zhang, Q. He, S. Song, T. Wang, M. Liu, Z. Zhao, J. Gao, Q. Huang, X. Han, K. Qi, J. Gao, M. & Shi, Y. (2023). Modeling of a PV system by a back-mounted spray cooling section for performance improvement. Applied Energy, 332, 120532

Zhang, Y. Shen, C. Zhang, C. Pu, J. Yang, Q. & Sun, C. (2022). A novel porous channel to optimize the cooling performance of PV modules. Energy and Built Environment, 3(2), 210–225.

Zhao, D. & Tan, G. (2014). A review of thermoelectric cooling: Materials, modeling and applications. Applied Thermal Engineering, 66(1–2), 15–24.

Zhu, L. Boehm, R. F. Wang, Y. Halford, C. & Sun, Y. (2011). Water immersion cooling of PV cells in a high concentration system. Solar Energy Materials and Solar Cells, 95(2), 538–545.

APPENDICES

Appendix A

Sample indoor experimental results with porosity size 0.35 at different volume flow rates.

Table 1: PV temperature and output power at a volume flow rate of 1L/min

Time	PV temp. (ºC)	P (W)
0	30.37	19.2254
5	37.67	18.487
10	38.70	18.449
15	39.17	18.1702
20	39.20	18.1608
25	39.47	18.3255
30	39.90	18.24
40	39.97	17.8976
50	39.57	18.0292
60	39.70	18.316
80	40.40	18.1514
100	39.97	18.1608
120	40.17	18.1702
140	40.23	18.1044
160	40.50	18.1702
180	40.57	18.0198

Table 2: PV temperature and output power at a volume flow rate of 1.5 L/min

Time	PV temp. (ºC)	P (W)
0	25.5	18.7598
5	36.16	18.7104
10	36.7	18.335
15	37.66	18.6675
20	38.36	18.62
25	38.56	18.601
30	38.66	18.639
40	39.13	18.658
50	38.73	18.8352
60	39.26	18.6295
80	39.13	18.449
100	38.83	18.506
120	38.83	18.449
140	39.6	18.316
160	40.13	18.3864
180	40.16	18.4334

Table 3: PV temperature and output power at a volume flow rate of 2 L/min

Time	PV temp. (ºC)	P (W)
0	20	19.303
5	35.4	19.1769
10	36.46	19.1963
15	37.26	19.206
20	37.50	19.3515
25	37.86	19.2157
30	38.23	19.2254
40	38.4	19.2351
50	38.5	19.2642
60	38.46	18.9888
80	38.63	19.0848
100	38.33	18.96
120	38.46	18.8832
140	38.63	18.864
160	38.60	18.8448
180	38.73	18.8448

Appendix B

Sample outdoor experimental results with porosity size 0.35 and different volume flow rate

Table 4: PV temperature and output power at a volume flow rate of 1L/min

Time	PV temp. (ºC)	P (W)
9	33.5	13.0356
10	36.9	19.4355
11	39.5	24.245
12	39	24.349
13	33.3	21.4092
14	38.3	21.0858
15	33.4	19.5615
16	34.6	14.736

Table 5: PV temperature and output power at a volume flow rate of 1.5L/min

Time	PV temp. (ºC)	P (W)
9	33.9	12.9717
10	34.6	19.488
11	36.5	24.336
12	37.5	24.388
13	38.5	21.318
14	35.5	21.0745
15	37.5	19.3725
16	37	14.68

Appendix C

Table 6: Sample machine learning results for PV temperature

Time	Ambient temp.	porosity size	Q(L/min)	Experimental results (oC)	Linear Regression	(SVM)	Decision Tree	kNN	(Random Forest)	AdaBoost	Gradient Boosting
5	21.9	0.35	2	35.4	36.56	36.2	35.20	37.67	36.49	36.17	34.05
5	27.2	0.35	1.5	36.2	37.93	37.7	36.70	36.70	36.50	36.70	36.19
5	21.6	0.4	1.5	38.2	38.43	39.1	39.47	37.90	37.85	38.10	38.21
5	27.2	0.35	1.5	36.2	37.93	37.8	36.70	36.70	36.66	36.70	36.18
5	21.6	0.4	1.5	38.2	38.50	39.2	36.70	37.90	38.32	38.10	37.93
10	15.6	0.48	3	36.0	37.02	36.3	37.00	34.63	35.96	35.60	35.46
10	21	0.4	1	41.3	41.37	40.7	40.03	44.70	39.85	40.03	39.33
10	15.6	0.48	3	36.0	36.95	36.3	36.10	34.63	35.49	35.60	35.15
10	21	0.4	1	41.3	41.41	40.8	40.93	40.03	39.63	40.03	39.70
10	21.3	1	1.5	44.7	49.28	48.0	46.55	40.03	45.63	43.75	47.67
10	21	0.4	1	41.3	41.43	40.7	40.93	40.03	39.79	40.03	39.78
10	21.3	1	1.5	44.7	49.30	47.8	46.55	40.03	46.64	43.75	47.81
10	21.7	1	1	43.8	47.30	47.2	46.00	38.70	45.96	46.00	47.29
10	22.3	0.35	2	36.5	36.86	36.8	35.97	43.75	36.28	36.70	36.09
15	20.8	0.35	3	36.8	36.82	36.8	37.13	45.35	36.91	37.13	37.50
15	15.8	0.48	3	37.0	37.09	36.7	36.10	35.60	35.63	35.60	36.08
15	20.4	1	2	44.9	46.37	44.7	45.35	45.35	44.87	45.45	44.60
15	20.9	0.35	1	39.2	37.40	38.7	38.70	46.00	38.44	38.70	37.53
15	20.8	1	3	45.4	46.11	46.0	45.85	44.85	44.96	44.85	45.18
15	20.8	0.35	3	36.8	36.88	36.7	37.13	45.35	37.43	37.13	37.43
20	21.9	1	1	47.6	47.46	47.9	48.45	39.20	47.58	48.45	48.71
20	20.6	1	2	45.5	46.37	45.1	45.85	45.85	45.66	45.85	45.02
20	23.1	0.35	4	38.9	38.47	38.6	39.37	48.35	38.67	38.67	38.70
20	15.9	0.48	3	37.5	37.16	36.9	36.60	36.10	37.08	37.00	37.02
20	15.9	0.4	4	35.3	35.68	35.2	35.80	36.10	35.67	35.80	35.85
20	21.1	0.35	1	39.2	37.59	39.0	38.70	47.60	38.96	38.70	38.23

Table 6: Continued

20	21.1	0.48	1	41.4	40.79	41.8	41.07	40.40	41.51	40.93	41.08
20	20.6	1	2	45.5	46.46	45.0	45.85	45.85	45.39	45.85	44.96
20	15.9	0.4	4	35.3	35.74	35.3	37.13	37.50	35.79	35.80	35.88
20	21.5	0.4	1.5	40.4	38.79	39.6	40.63	39.20	40.29	40.10	39.97
20	15.9	0.4	3	36.1	35.89	35.8	36.03	35.30	35.67	35.60	36.19
20	15.9	0.48	3	37.5	37.23	36.8	36.60	35.30	36.49	37.00	36.87
25	21.9	0.4	1	41.5	41.73	41.5	41.07	48.60	41.61	41.70	41.57
25	20.8	1	2	46.4	46.45	45.6	46.50	47.10	46.19	46.50	45.06
25	23.1	0.35	2	37.9	37.74	37.9	37.50	40.63	38.24	37.60	38.04
25	22	1	1	48.5	47.63	48.2	48.60	39.47	48.62	47.60	48.99
25	21.9	0.4	1	41.5	41.83	41.5	41.37	48.60	41.61	41.07	41.68
25	19.6	0.4	2	36.9	37.35	37.9	38.75	46.40	38.40	37.27	38.00
25	18.3	0.48	1.5	36.6	37.65	36.1	36.60	35.07	35.88	36.33	36.52
25	21	0.35	3	37.6	37.28	37.6	37.13	47.10	37.95	37.97	38.16
25	23.3	0.35	4	39.4	38.70	39.0	39.87	48.60	39.42	38.93	38.91
25	21.8	1	1.5	48.6	49.61	49.0	49.35	41.37	48.86	48.35	48.88
30	18.7	0.48	1.5	36.6	37.86	37.1	37.70	35.13	37.15	37.70	37.09
30	23.3	0.35	4	39.9	38.78	39.0	39.43	49.35	39.41	39.37	38.70
30	22.2	1	1	49.1	47.95	48.6	49.45	40.90	49.44	49.35	49.36
30	21.4	0.35	1	39.9	37.93	39.5	38.23	40.90	39.37	39.47	39.19
30	27.9	0.35	1.5	38.7	38.42	38.2	38.23	38.23	38.32	38.57	39.37
30	21.1	0.35	3	38.0	37.38	37.8	39.90	47.65	37.94	38.75	38.86
30	21.4	0.35	1	39.9	37.90	39.5	38.23	49.05	39.43	39.47	39.16
30	22	0.4	1	41.7	41.94	41.7	41.97	49.35	41.97	41.97	41.88
40	17	0.48	3	38.9	37.95	38.6	39.17	37.50	38.17	38.53	37.63
40	21.5	0.35	1	40.0	38.16	39.9	39.57	49.45	39.39	39.90	39.43
40	21.5	1	3	48.4	46.90	47.8	49.05	47.10	47.92	47.65	47.78
40	22.2	1	1.5	49.9	49.94	49.4	49.45	43.13	49.58	49.45	49.63
40	17	0.4	3	37.5	36.55	37.4	36.50	38.90	37.29	37.77	37.22
40	17	0.4	4	36.5	36.37	36.7	36.77	38.90	37.46	36.77	37.18
40	21.5	0.35	3	38.4	37.73	38.1	38.50	48.35	38.67	38.50	39.45

Table 6: Continued

40	22.1	0.48	1	43.1	41.45	42.5	41.97	49.85	42.66	42.70	43.02
40	22.3	0.4	1.5	40.9	39.17	40.2	41.03	49.45	41.26	40.90	41.11
50	22.7	1	1	50.0	48.34	50.2	50.15	39.57	50.43	50.15	50.10
50	21.6	1	3	49.1	47.13	48.6	49.20	47.45	47.98	48.35	48.21
50	23.8	0.35	2	38.5	38.56	38.9	38.47	49.95	38.54	38.47	38.55
50	21.7	0.35	1	39.6	38.39	40.1	38.37	41.20	39.46	39.70	39.86
50	23.3	0.35	4	39.5	39.15	39.5	39.30	50.35	39.44	39.43	39.16
50	23.8	0.35	2	38.5	38.61	38.9	38.47	49.95	38.53	38.47	38.69
50	21.3	1	2	47.5	47.21	47.4	47.65	49.05	47.48	47.50	47.44
50	22.4	1	1.5	50.4	50.16	49.8	49.95	43.47	49.87	49.85	50.05
60	19.5	0.48	1.5	37.7	38.12	37.2	37.70	35.77	37.85	37.70	37.39
60	17.9	0.4	4	36.9	36.95	37.4	36.77	39.30	37.53	37.40	37.65
60	22.3	0.48	1	43.7	41.80	42.9	43.47	50.20	43.19	43.47	43.24
60	17.9	0.48	3	39.3	38.37	39.3	39.80	37.90	38.65	39.17	38.46
60	21.3	1	2	47.4	47.39	47.5	47.45	39.35	47.59	47.45	47.51
60	17.9	0.4	4	36.9	36.92	37.4	37.40	39.30	37.07	37.40	37.69
60	23.5	0.35	4	39.5	39.34	39.5	39.30	50.20	39.45	39.43	39.16
60	21.3	1	2	47.4	47.32	47.6	47.65	39.35	47.46	47.50	47.44
60	19.5	0.48	1.5	37.7	38.07	37.2	37.70	35.77	37.83	37.70	37.33
60	22.8	1	1	50.2	48.52	50.4	50.95	38.47	50.85	49.95	50.64
60	21.8	0.35	1	39.7	38.66	40.4	40.40	41.03	39.98	39.97	40.64
80	22.1	0.35	1	40.4	38.98	40.5	39.97	50.95	39.85	39.70	40.68
80	22.7	1	1.5	50.6	50.52	50.4	50.50	43.37	50.47	50.35	50.22
80	22.1	0.35	1	40.4	39.02	40.5	39.97	50.95	39.87	39.97	40.81
80	21.7	0.35	3	39.0	38.54	39.1	38.33	49.05	38.68	38.73	38.76
80	23.9	0.35	2	38.6	38.98	39.1	38.33	50.95	38.54	38.60	38.68
80	20.5	0.4	1.5	41.0	39.54	40.6	41.20	40.40	40.84	41.03	40.79
80	21.8	1	3	49.1	47.74	49.3	49.60	47.50	49.10	49.20	48.48
80	21.8	1	3	49.1	47.89	49.3	49.60	47.50	49.14	49.20	48.42
80	21.7	0.35	3	39.0	38.57	39.1	38.77	49.05	38.90	38.77	38.64
80	18.7	0.4	3	38.4	37.41	38.3	37.90	39.80	37.99	37.90	38.11

Table 6: Continued

100	18.6	0.48	2	37.2	39.08	39.1	36.43	38.33	37.80	37.57	37.36
100	22.8	1	1.5	50.6	50.86	50.6	50.50	42.60	50.52	50.55	50.17
100	22.8	1	1.5	50.6	50.92	50.5	50.50	43.13	50.63	50.60	50.19
100	21.4	0.4	2	39.1	38.75	39.3	39.58	47.70	39.37	39.35	39.48
100	22.8	0.4	1	42.6	42.94	42.7	42.87	43.13	42.48	42.80	42.57
100	22.8	1	1	51.1	49.15	50.9	51.25	39.97	51.12	51.25	50.58
100	21.9	1	3	49.6	48.18	49.6	50.10	47.70	49.27	49.05	48.64
100	21.4	0.4	2	39.1	38.75	39.3	39.57	47.70	39.74	39.58	39.43
100	20	0.4	1.5	41.2	39.99	41.1	41.67	43.13	40.63	41.03	40.64
100	18.6	0.48	2	37.2	39.06	39.2	36.43	38.33	38.29	37.87	38.00
120	23.7	0.35	4	39.5	40.40	39.4	39.40	39.33	39.27	39.40	39.04
120	23.1	1	1.5	50.5	51.07	50.9	50.55	42.80	50.68	50.60	50.27
120	21.9	0.4	2	39.6	39.24	39.5	39.05	48.05	39.61	39.82	40.08
120	28.9	0.35	1.5	38.8	40.51	39.4	40.13	38.47	39.23	39.60	39.34
120	19.3	0.48	2	37.2	39.41	39.3	38.80	38.90	38.35	38.47	38.48
120	19.7	0.4	4	38.5	37.97	38.4	39.00	40.30	38.90	39.00	39.22
120	22.2	0.35	3	39.3	39.49	39.4	39.50	50.10	39.30	39.43	39.87
120	22.9	0.4	1	42.8	43.50	42.8	42.87	50.50	42.74	42.60	42.80
140	21.4	0.4	2	39.8	39.41	39.6	39.40	48.30	39.76	39.58	39.69
140	23.8	0.4	1	42.9	43.63	42.7	43.03	50.55	42.91	43.03	42.26
140	23.5	0.35	4	39.6	40.69	39.4	39.50	39.50	39.51	39.60	39.62
140	22.3	1	3	50.0	49.06	49.9	50.10	39.50	49.79	50.10	49.34
140	23.8	0.4	1	42.9	43.58	42.8	43.03	50.55	42.94	42.80	42.39
140	20.1	0.48	1	42.7	42.54	43.1	43.13	41.17	42.15	43.13	43.20
140	20.3	0.4	4	39.0	38.30	38.8	39.40	39.40	39.14	39.40	39.50
140	20.1	0.48	1	42.7	42.49	43.0	43.13	40.23	41.93	43.13	43.19
140	19.5	0.4	1.5	41.2	40.55	41.2	41.67	39.82	41.41	41.47	40.78
160	21.2	0.4	4	39.2	38.81	39.5	39.00	39.63	39.40	39.63	39.55
160	21.6	0.4	2	40.3	39.56	39.6	40.35	48.50	40.05	39.82	39.57
160	24.4	0.35	2	38.6	40.24	39.5	38.73	50.30	39.04	38.73	38.85
160	21.2	0.48	3	41.0	40.13	40.6	41.43	39.63	40.70	40.80	40.76

Table 6: Continued

160	23.4	0.35	4	39.6	41.02	39.5	39.60	50.60	39.66	39.60	39.97
180	19.2	0.48	1.5	38.8	40.32	38.9	37.87	38.37	38.06	37.87	39.35
180	20.8	0.48	1	43.6	43.29	43.0	43.47	41.53	43.42	43.47	43.14
180	23.5	1	1.5	50.9	51.95	50.9	50.60	43.07	50.66	50.60	50.52
180	24.2	0.35	2	38.7	40.35	39.7	38.60	40.57	38.62	38.60	38.95
180	19.6	0.4	1.5	41.5	41.33	41.5	42.73	43.57	41.77	41.47	41.50
180	20.8	0.48	1	43.6	43.20	43.3	43.47	41.53	42.39	43.47	43.31
180	21.6	0.4	3	40.1	39.14	39.6	40.00	41.43	39.95	40.00	40.27

Appendix D

Samples of calculation

The temperature of the photovoltaic cell can be calculated using Equation 3.15 as follow;

$$T_g = \frac{800 * 0.64 - 111 + 18.6 * 27 + 9.82 * 25}{18.6 + 9.82} = 40.41^oC$$

$U_{c,r}$is the coefficient of heat transfer between the PV glass and the surrounding environment, and can be calculated using Equation 3.16 as follow:

$$U_{c,r} = \left[\frac{1}{13.3 + 5.3}\right]^{-1} = 18.6\ W/m^2k$$

Convective heat transfer coefficient, and radiation heat transfer coefficient, the values of the coefficients can be found in Equations 3.17 and 3.18 respectively.

$$h_c = 5.7 + 3.8 * 2 = 13.3\ W/m^2k$$

where V is the velocity of the surrounding air around the PV cells

$$h_r = 0.82\ 5.68\text{^}(-8)((40 + 273)^2 + (27 + 273)^2)(40 + 27 + 2 * 273) = 5.3W/m^2k$$

$U_1$is the coefficient of heat transfer between the PV glass and water, and can be calculated using Equation 3.19 as follow:

$$U_1 = \left[\frac{0.003}{1.8} + \frac{0.0002}{0.34} + \frac{0.0002}{0.34} + \frac{0.001}{0.2} + \frac{1}{5.03 + 4.85}\right]^{-1} = 9.82W/m^2k$$

$$G.\alpha_c = U_2(T_T - T_a) + h_{c,f}(T_T - T_f) + h_{r,pm}(T_T - T_{pm})$$

Through Equation 3.21, the temperature of the solar panel from the back

$$T_T = \frac{800 * 0.64 + 555 * 27 + 4.85 * 25 + 5.03 * 25}{4.85 + 5.03 + 555} = 27.8^oC$$

$U_2$is the coefficient of heat transfer from glass to bottom Tedlar, and can be calculated using Equation 3.22 as follow:

$$\boldsymbol{U_2} = \left[\frac{\mathbf{0.003}}{\mathbf{1.8}} + \frac{\mathbf{0.0002}}{\mathbf{0.34}} + \frac{\mathbf{0.0002}}{\mathbf{0.34}} + \frac{\mathbf{0.001}}{\mathbf{0.2}}\right]^{-1} = \mathbf{555W}/\boldsymbol{m}^{\mathbf{2}}\mathbf{k}$$

$h_{c,f}$ is the convective heat transfer coefficient for water flowing channel filled with porous medium can be calculated from Equation 3.23.

$$\boldsymbol{h_{c,f}} = \left[\frac{\mathbf{0.8}}{\mathbf{4.74 * 083}}\right]^{-1} = \mathbf{4.85\ W}/\boldsymbol{m}^{\mathbf{2}}\mathbf{k}$$

where ke is the thermal conductivity calculated using Equation 3.24 as follow:

$$\boldsymbol{k_e} = \mathbf{0.351.19_{+}\ (1 - 0.35)64} = \mathbf{0.83W/m\ k}$$

Nu_{pm-f} is Nusselt number calculated using Equation 3.25 as follow:

$$\boldsymbol{Nu_{pm-f}} = \left(\frac{\mathbf{0.255}}{\mathbf{0.35}}\right)\mathbf{7.3^{2/3}*5.18^{1/3}} = \mathbf{4.74}$$

Re_{pm} is Reynolds number calculated using Equation 3.26 as follow:

$$\boldsymbol{Re_{pm}} = \frac{\mathbf{1000 * 0.0019 * 0.002}}{\mathbf{0.00089((1 - 0.35)}} = \mathbf{7.3}$$

$h_{r,pm}$ is the radiation heat transfer coefficient from Tedlar to the porous medium, which can be calculated using Equation 3.27 as follow:

$$\boldsymbol{h_{r,pm}} = \mathbf{0.82\ 5.68\hat{}(-8)((29 + 273)^2 + (25 + 273)^2)(29 + 27 + 2 * 273)} = \mathbf{5.02W}/\boldsymbol{m}^{\mathbf{2}}\mathbf{k}$$

Appendix E

Description of the machine learning algorithms that were used

AdaBoost

AdaBoost, an abbreviation for Adaptive Boosting, emerges as an ensemble learning technique that amalgamates weak learners into a potent classifier. Its proficiency lies in navigating diverse data types by iteratively adjusting the weights of misclassified instances, accentuating the significance of challenging data points throughout the learning process. AdaBoost (Adaptive Boosting) is a machine learning ensemble method that combines multiple weak learners (often decision trees) to create a strong learner. It was introduced by Yoav Freund and Robert Schapire in 1996. Here's a detailed description of how AdaBoost works:

1. Initialization: Initially, each data point is assigned an equal weight. 2. Train weak learners: AdaBoost sequentially trains a series of weak learners, typically decision trees, on the training data. A weak learner is a model that performs slightly better than random guessing, often referred to as a "weak" classifier. 3. Weighted error calculation: After each weak learner is trained, AdaBoost evaluates its performance on the training data. Data points that are misclassified by the weak learner are assigned higher weights, while correctly classified points are assigned lower weights. 4. Classifier weight calculation: AdaBoost assigns a weight to each weak learner based on its performance. More accurate weak learners are given higher weights, indicating their importance in the final ensemble. 5. Ensemble combination: AdaBoost combines the weak learners into a strong learner by assigning weights to their predictions based

on their individual performance. The final prediction is a weighted sum of the predictions of all weak learners.

6. Iterative Process: AdaBoost iteratively repeats the process of training weak learners, adjusting weights, and combining them into a strong learner until a specified number of iterations (or until a desired level of accuracy is achieved).

Random Forest

Random Forest is a powerful ensemble learning technique used for classification and regression tasks. It is based on the concept of decision trees and combines the predictions of multiple individual trees to improve the overall performance and robustness of the model. Here's a detailed description of how Random Forest works:

1. Bootstrap Sampling (Random Sampling with Replacement): Random Forest begins by creating multiple decision trees, each trained on a random subset of the training data. This random sampling with replacement technique, known as bootstrap sampling, ensures diversity among the trees. 2. Feature randomization: In addition to using random subsets of the training data, Random Forest also introduces randomness in feature selection. At each node of the decision tree, instead of considering all features, only a random subset of features is considered for splitting. This helps to decorrelate the trees and reduce overfitting. 3. Construction of Decision Trees: Each decision tree in the Random Forest is constructed recursively by selecting the best split at each node based on a criterion such as Gini impurity for classification tasks or mean squared error for regression tasks. The process continues until the tree reaches a specified maximum depth or another stopping criterion is met. 4. Ensemble prediction: Once all decision trees are constructed, predictions are made by aggregating the

predictions of individual trees. For classification tasks, the class with the most votes (mode) among all trees is chosen as the final prediction. For regression tasks, the average (mean or median) of the predicted values from all trees is taken as the final prediction. 5. Out-of-Bag (OOB) evaluation: Random Forest utilizes out-of-bag samples, which are data points not included in the bootstrap sample used to train each tree. These samples can be used to estimate the performance of the model without the need for a separate validation set. 6. Hyperparameter tuning: Random Forest has several hyperparameters that can be tuned to optimize performance, such as the number of trees (n_estimators), maximum depth of the trees, minimum samples required to split a node, and maximum number of features to consider for each split.

Decision Tree (T)

A decision tree (T) is a fundamental machine learning model used for both classification and regression tasks. It is a tree-like structure composed of nodes and directed edges that represent decisions and their consequences. Here's a detailed description of the components of a decision tree:

1. Root node: At the top of the tree is the root node, which represents the entire dataset or subset of data being split into different branches. 2. Internal nodes (Decision Nodes): Internal nodes represent features or attributes of the dataset. Each internal node contains a decision rule that determines how the data should be split based on the value of the feature associated with that node. 3. Branches (Edges): Branches emanate from internal nodes and represent the possible outcomes or decisions based on the value of the feature being evaluated. Each branch leads to another internal node or a leaf node. 4. Leaf nodes: Leaf nodes are the terminal nodes of the tree and represent

the final outcome or prediction. In classification tasks, each leaf node corresponds to a class label, while in regression tasks, each leaf node contains a predicted numerical value. 5. Splitting criteria: The decision tree algorithm determines the optimal feature and value to split the data at each internal node based on a splitting criterion. Common splitting criteria include Gini impurity for classification tasks and mean squared error (MSE) for regression tasks. 6. Recursive partitioning: The process of building a decision tree involves recursively partitioning the dataset into smaller subsets based on the selected features and splitting criteria until certain stopping conditions are met. These conditions could include reaching a maximum tree depth, minimum number of samples per leaf node, or no further improvement in impurity or error reduction. 7. Pruning: After the tree is fully grown, pruning techniques may be applied to reduce its size and complexity, thus improving its generalization performance and reducing the risk of overfitting.

Support Vector Machine (SVM):

Support Vector Machine (SVM) is a powerful supervised learning algorithm used for classification and regression tasks. It works by finding the hyperplane that best separates the data points into different classes while maximizing the margin between the classes. Here's a detailed description of SVM:

1. Hyperplane: In SVM, a hyperplane is a decision boundary that separates the data points into different classes. For binary classification, the hyperplane is a line in two dimensions and a plane in three dimensions. In higher dimensions, it's referred to as a hyperplane.

2. Support Vectors: Support vectors are the data points that lie closest to the hyperplane. These points are crucial in determining the optimal hyperplane because they influence its position and orientation. 3. Margin: The margin is the distance between the hyperplane and the closest data points (support vectors). SVM aims to maximize this margin, as it indicates a robust separation between classes and improves the model's generalization performance. 4. Kernel trick: SVM can efficiently handle nonlinear decision boundaries by transforming the input features into a higher-dimensional space using kernel functions (e.g. polynomial kernel, radial basis function kernel). This allows SVM to capture complex patterns and achieve better separation between classes. 5. Regularization parameter (C): The regularization parameter (C) in SVM controls the trade-off between maximizing the margin and minimizing the classification error. A smaller value of C allows for a wider margin but may lead to misclassification errors, while a larger value of C reduces the margin but may result in overfitting. 6. Kernel parameters: In addition to the regularization parameter, kernel functions in SVM may have additional parameters (e.g. gamma for RBF kernel, degree for polynomial kernel) that need to be tuned for optimal performance.

Gradient Boosting (GB):

Gradient Boosting is a powerful ensemble learning technique used for both regression and classification tasks. It builds a strong predictive model by combining multiple weak learners (typically decision trees) sequentially in a stage-wise fashion. Here's how Gradient Boosting works:

1.Weak learners (Decision Trees): Gradient Boosting builds an ensemble of weak learners, usually decision trees, where each tree is trained on the residuals (errors) of the previous tree. Unlike bagging techniques like Random Forest, which train each tree independently, Gradient Boosting trains the trees sequentially, with each subsequent tree focusing on reducing the errors made by the previous trees. 2. Loss function: Gradient Boosting minimizes a loss function, such as mean squared error (MSE) for regression or cross-entropy loss for classification, by adding weak learners that correct the errors made by the previous learners. At each stage of training, the algorithm calculates the negative gradient of the loss function with respect to the predicted values, and fits the next weak learner to this gradient. 3. Gradient descent: Gradient Boosting uses gradient descent optimization to iteratively fit the weak learners to the negative gradient of the loss function. This process gradually improves the model's predictions by moving in the direction that minimizes the loss. By sequentially adding trees that target the residual errors, Gradient Boosting builds a strong ensemble model that can capture complex patterns in the data. 4. Learning rate: Gradient Boosting introduces a learning rate parameter (also known as shrinkage) to control the contribution of each tree to the ensemble. A smaller learning rate makes the model more robust to overfitting but requires more trees to achieve the same performance. By tuning the learning rate, practitioners can strike a balance between model complexity and generalization performance. 5. Regularization: Gradient Boosting can also employ regularization techniques like tree pruning, limiting the maximum depth of trees, or adding penalties to the loss function to prevent overfitting. Regularization helps prevent the model from memorizing the training data and encourages it to learn more generalizable patterns.

Appendix F

An example of machine learning for AdaBoost

```
In [10]: import pandas as pd
         import numpy as np
         import matplotlib.pyplot as plt
         from sklearn.ensemble import AdaBoostRegressor
         from sklearn.model_selection import train_test_split
         from sklearn.metrics import mean_squared_error, mean_absolute_error, r2_score

          # Read data from Excel file
         data = pd.read_excel('M8.xlsx')

         # # Divide the data into screening and target variables
         X = data.iloc[:, :-1]
         y = data.iloc[:, -1]

         # Split the data into training and test sets
         X_train, X_test, y_train, y_test = train_test_split(X, y, test_size=0.2, rando

         # Training the AdaBoost model
         adaboost = AdaBoostRegressor(n_estimators=50, learning_rate=1, random_state=42
         adaboost.fit(X_train, y_train)

         # Predicting values
         y_pred = adaboost.predict(X_test)

         # Performance calculation
         r2 = r2_score(y_test, y_pred)
         mae = mean_absolute_error(y_test, y_pred)
         rmse = mean_squared_error(y_test, y_pred, squared=False)

         # Print performance results
         print("R squared:", r2)
         print("MAE:", mae)
         print("RMSE:", rmse)

         # Draw the curve
         plt.figure(figsize=(10, 6))
         plt.scatter(y_test, y_pred, color='blue', label='Actual vs Predicted')
         plt.plot([min(y_test), max(y_test)], [min(y_test), max(y_test)], color='red',
         plt.xlabel('Actual Temperature')
         plt.ylabel('Predicted Temperature')
         plt.title('Actual vs Predicted Temperature (AdaBoost)')
         plt.legend()
         plt.grid(True)
         plt.show()

         R squared: 0.9541747142984391
         MAE: 0.6511089418106283
         RMSE: 0.7962528414122494
```

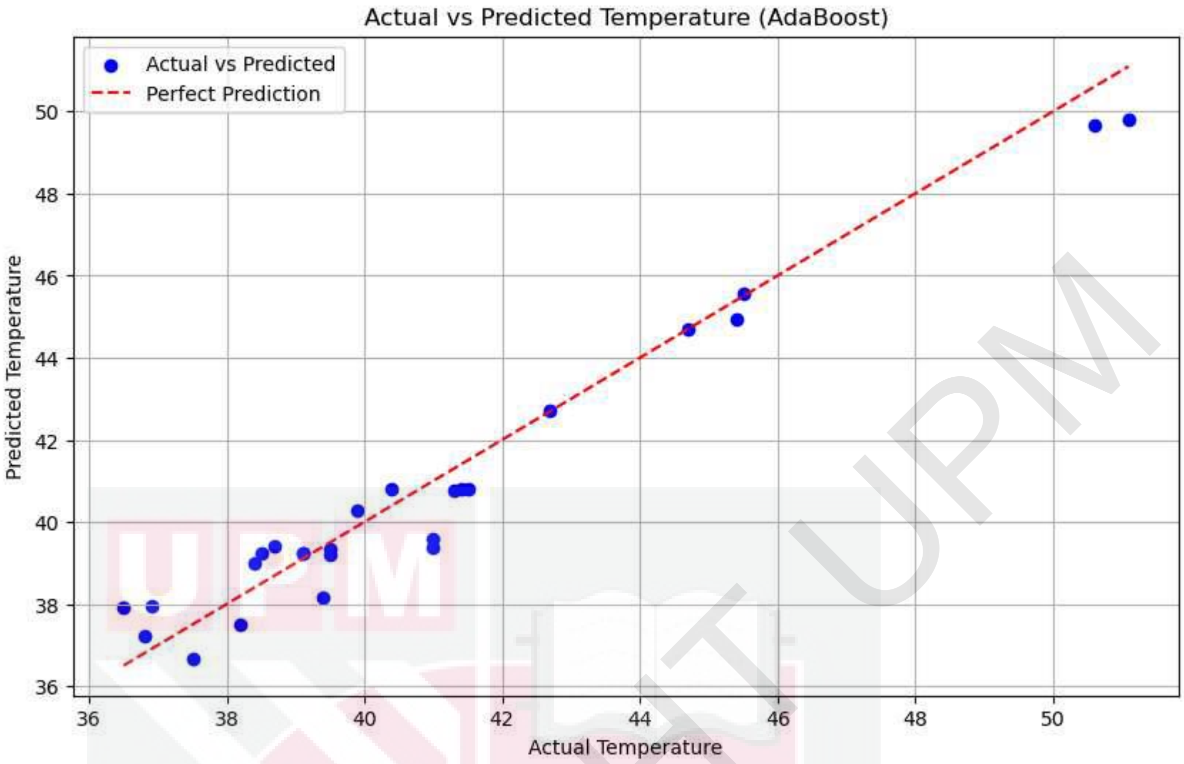

In [4]:
```
# Draw the curve
plt.figure(figsize=(10, 6))

plt.scatter(y_train, adaboost.predict(X_train), color='green', label='Train',
plt.scatter(y_test, y_pred, color='blue', label='Test', marker='o')
plt.plot([min(y_test), max(y_test)], [min(y_test), max(y_test)], color='red',
plt.xlabel('Actual Temperature')
plt.ylabel('Predicted Temperature')
plt.title('Actual vs Predicted Temperature (AdaBoost)')
plt.legend()
plt.grid(True)
plt.show()
```

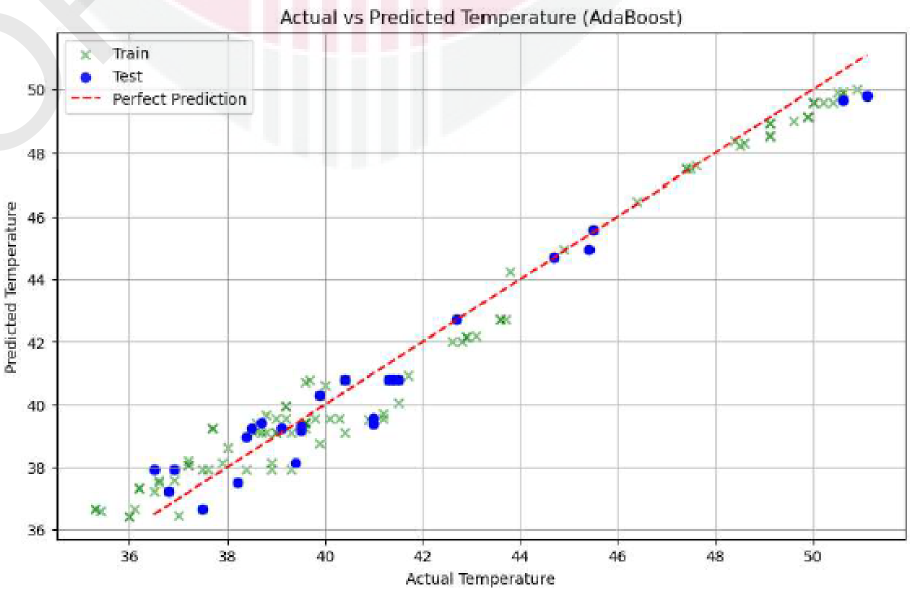

In [18]:
```
#  Prediction of temperature values
predicted_temperatures = adaboost.predict(X_test)

# Calculate absolute error
errors = abs(predicted_temperatures - y_test)

# Calculate the error rate
error_percentage = (errors / y_test) * 100

# Display actual and predicted temperature with percentage line
results = pd.DataFrame({'Actual Temperature': y_test, 'Predicted Temperature':
print(results)
```

```
    Actual Temperature  Predicted Temperature  Error Percentage
0                 36.5              37.920000          3.890411
1                 39.4              38.145714          3.183466
2                 36.8              37.228205          1.163601
3                 37.5              36.657895          2.245614
4                 42.7              42.711111          0.026021
5                 38.4              38.976923          1.502404
6                 36.9              37.937500          2.811653
7                 38.5              39.250877          1.950330
8                 40.4              40.792857          0.972419
9                 41.4              40.809677          1.425900
10                51.1              49.800000          2.544031
11                45.5              45.575000          0.164835
12                39.5              39.200000          0.759494
13                38.2              37.510345          1.805380
14                39.1              39.250877          0.385875
15                39.5              39.328571          0.433996
16                41.5              40.792857          1.703959
17                50.6              49.675000          1.828063
18                39.1              39.250877          0.385875
19                41.0              39.570588          3.486370
20                45.4              44.933333          1.027900
21                41.3              40.780000          1.259080
22                41.0              39.380000          3.951220
23                44.7              44.700000          0.000000
24                38.7              39.422222          1.866207
25                39.9              40.296364          0.993393
```

In [19]:
```
feature_importances = adaboost.feature_importances_
print("Feature Importances:")
for i, importance in enumerate(feature_importances):
    print(f"Feature {i+1}: {importance}")
```

```
Feature Importances:
Feature 1: 0.14689846423448463
Feature 2: 0.06090452829725444
Feature 3: 0.5907734774569217
Feature 4: 0.20142353001133917
```

In [5]:
```
import pandas as pd
import matplotlib.pyplot as plt
from sklearn.ensemble import AdaBoostRegressor
from sklearn.metrics import mean_squared_error, mean_absolute_error, r2_score


data = pd.read_excel('M8.xlsx')

# # Divide the data into screening and target variables
X = data.iloc[:, :-1]
y = data.iloc[:, -1]

# Training the AdaBoost model
adaboost = AdaBoostRegressor(n_estimators=50, learning_rate=1, random_state=42
adaboost.fit(X, y)


new_data = pd.read_excel('M10.xlsx')

X_new = new_data.iloc[:, :-1]


predicted_temperatures_new = adaboost.predict(X_new)


new_data['Predicted Temperature'] = predicted_temperatures_new
new_data['Actual Temperature'] = data.iloc[:, -1]  # Adding actual temperature

mse = mean_squared_error(new_data['Actual Temperature'], new_data['Predicted T
mae = mean_absolute_error(new_data['Actual Temperature'], new_data['Predicted
r2 = r2_score(new_data['Actual Temperature'], new_data['Predicted Temperature'

print("Mean Squared Error:", mse)
print("Mean Absolute Error:", mae)
print("R-squared:", r2)

plt.figure(figsize=(8, 6))
plt.scatter(new_data['Predicted Temperature'], new_data['Actual Temperature'],
plt.plot([min(new_data['Predicted Temperature']), max(new_data['Predicted Temp
         [min(new_data['Actual Temperature']), max(new_data['Actual Temperatur
         color='red', linestyle='--', label='Perfect Prediction')
plt.xlabel('Predicted Temperature')
plt.ylabel('Actual Temperature')
plt.title('Actual vs Predicted Temperature')
plt.legend()
plt.grid(True)
plt.show()
```

```
Mean Squared Error: 0.5741973231231761
Mean Absolute Error: 0.6278714607700836
R-squared: 0.9710017678737421
```

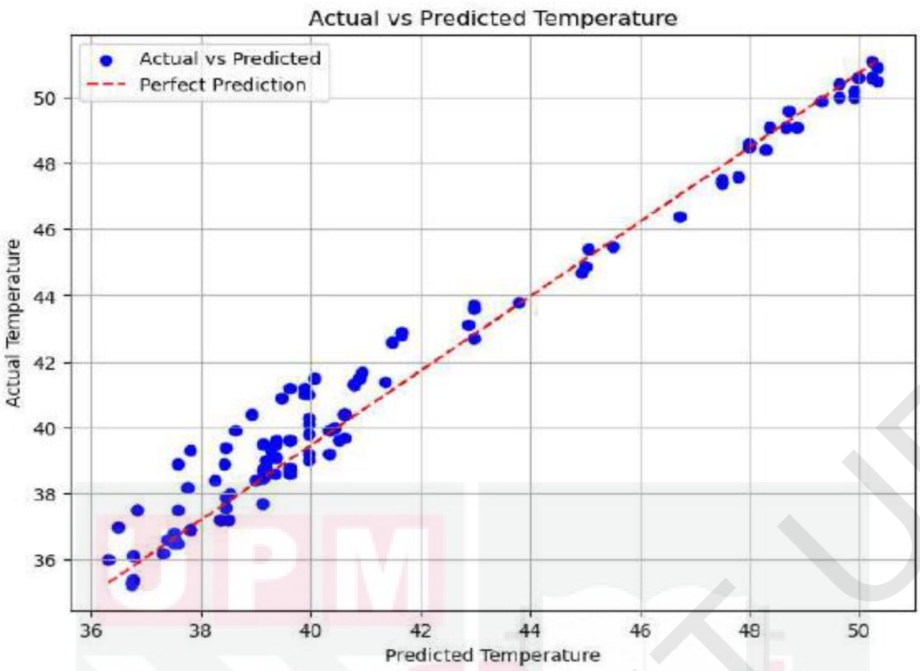

In [7]:
```
import pandas as pd
import matplotlib.pyplot as plt
from sklearn.ensemble import AdaBoostRegressor
from sklearn.metrics import mean_absolute_error

data = pd.read_excel('M8.xlsx')

# # Divide the data into screening and target variables
X = data.iloc[:, :-1]
y = data.iloc[:, -1]

# Training the AdaBoost model
adaboost = AdaBoostRegressor(n_estimators=50, learning_rate=1, random_state=42
adaboost.fit(X, y)

new_data = pd.read_excel('M10.xlsx')

X_new = new_data.iloc[:, :-1]

predicted_temperatures_new = adaboost.predict(X_new)

new_data['Predicted Temperature'] = predicted_temperatures_new
new_data['Actual Temperature'] = data.iloc[:, -1]  # Adding actual temperature

new_data['Error (%)'] = ((new_data['Actual Temperature'] - new_data['Predicted


print(new_data[['Actual Temperature', 'Predicted Temperature', 'Error (%)']].h
```

```
    Actual Temperature  Predicted Temperature  Error (%)
0                 35.4              36.752941  -3.821868
1                 36.2              37.293333  -3.020258
2                 38.2              37.750685   1.176217
3                 36.2              37.293333  -3.020258
4                 38.2              37.750685   1.176217
5                 36.0              36.316667  -0.879630
6                 41.3              40.773846   1.273980
7                 36.0              36.316667  -0.879630
8                 41.3              40.773846   1.273980
9                 44.7              44.933333  -0.521999
10                41.3              40.773846   1.273980
11                44.7              44.933333  -0.521999
12                43.8              43.800000   0.000000
13                36.5              37.506667  -2.757991
14                36.8              37.506667  -1.920290
15                37.0              36.496970   1.359541
16                44.9              45.000000  -0.222717
17                39.2              40.336842  -2.900107
18                45.4              45.050000   0.770925
19                36.8              37.506667  -1.920290
```

Appendix G

Experimental instruments

Solar power meter specifications

Display	LCD display, 4 digit LCD reading
Range	200.0 W/m^2 ,2000 W/m^2 63.4 Btu/(ft^2 x h) , 634 Btu / (ft^2 x h)
Resolution	0.1 W/m^2 ,1 W/m^2 0.1 Btu/(ft^2 x h) , 1 Btu / (ft^2 x h)
Spectral response	400 to 1000nm
Accuracy	Typically within ±10 W/m^2 [±3 Btu / (ft^2 x h)] or ±5%, whichever is greater in sunlight ; Additional temperature induced error ±0.38 W/m^2/°C [±0.12 Btu / (ft^2 x h)/°C] from 25°C
Angular accuracy	Cosine corrected <5% for angles < 60°
Drift	< ±2% per year
Calibration	User recalibration available
Over-Input	Display shows "OL"
Sampling Rate	1 times/sec
Manual Data Memory and Read	99 sets
Auto Data Memory	microSD CARD 2GB
Battery	6 pcs 1.5V size AAA
Battery Life	Approx. 50 hours
Operating Temp and Humidity	0°**C** to 50°**C** (32°**F** to 122°**F**) below 80%RH
Storage Temp and Humidity	-10°**C** to 60°**C** below 70%RH
Dimension & Weight	150(L)x72(W)x35(H) mm / Approx. 320g
Accessories Included	Operation Manual, 6 pcs 1.5V size AAA, USB Cable, CD software

Voltmeter specifications

Function	**Range**	**Resolution**	**Accuracy** ± ([% of Reading] + [Counts])		**Model**
DC millivolts	600.0 mV	0.1 mV	0.5 % + 2		114, 115, 117
DC Volts	6.000 V 60.00 V 600.0 V	0.001 V 0.01 V 0.1 V	0.5 % + 2		114, 115, 117
			DC, 45 to 500 Hz	500 Hz to 1 kHz	
Auto-V LoZ[1] True-rms	600.0 V	0.1 V	2.0 % + 3	4.0 % + 3	114, 117
			45 to 500 Hz	500 Hz to 1 kHz	
AC millivolts[1] True-rms	600.0 mV	0.1 mV	1.0 % + 3	2.0 % + 3	114, 115, 117
AC Volts[1] True-rms	6.000 V 60.00 V 600.0 V	0.001 V 0.01 V 0.1 V	1.0 % + 3	2.0 % + 3	114, 115, 117

Ammeter specifications

Function	Range	Resolution	Accuracy ± ([% of Reading] + [Counts])	Model
AC Amps True-rms[1] (45 Hz to 500 Hz)	6.000 A 10.00 A[3] 20 A for 30 seconds max., 10 minutes rest min.	0.001 A 0.01 A	1.5 % + 3	115, 117
DC Amps	6.000 A 10.00 A[3] 20 A for 30 seconds max., 10 minutes rest min.	0.001 A 0.01 A	1.0 % + 3	115, 117
Hz (V or A input)[2]	99.99 Hz 999.9 Hz 9.999 kHz 50.00 kHz	0.01 Hz 0.1 Hz 0.001 kHz 0.01 kHz	0.1 % + 2	115, 117

LIST OF PUBLICATIONS

Published

Masalha, I. Binti Masuri, S. U. Badran, O. Bin Mohd Ariffin, M. K. A. Abi Talib, A. R. & Alfaqs, F. (2023). Theoretical and Experimental Study on the Performance of Photovoltaic using Porous Media Cooling under Indoor Condition. International Journal of Renewable Energy Development, 12(2), 313–327.

Masalha, I. Masuri, S. U. Badran, O. O. Ariffin, M. K. A. M. Abu Talib, A. R. & Alfaqs, F. (2023). Outdoor experimental and numerical simulation of photovoltaic cooling using porous media. Case Studies in Thermal Engineering, 42(December 2022), 102748.

Under review

Masalha, I. Binti Masuri, S. U. Badran, O. Bin Mohd Ariffin, M. K. A. and Abi Talib, A. R. Experimental and Machine learning techniques for predicting average surface temperature and output power of photovoltaic panel cooled by porous media under the indoor condition. International Review of Energy.

Masalha, I. Binti Masuri, S. U. Badran, O. Bin Mohd Ariffin, M. K. A. and Abi Talib, A. R. Cooling photovoltaic modules for power and efficiency enhancement. International Review of Mechanical Engineering.